

Iron(II) pyridine-2-carbaldehyde-2-pyridylhydrazone complexes modified with Fréchet type dendritic wedges for scanning tunneling microscopy

Inauguraldissertation

zur

Erlangung der Würde eines Doktors der Philosophie

vorgelegt der

Philosophisch-Naturwissenschaftlichen Fakultät

der Universität Basel

von

Marc Häusler

aus

Unterägeri (Zug)

Basel, 2010

Originaldokument gespeichert auf dem Dokumentenserver der Universität Basel
edoc.unibas.ch



Dieses Werk ist unter dem Vertrag „Creative Commons Namensnennung-Keine kommerzielle Nutzung-Keine Bearbeitung 2.5 Schweiz“ lizenziert. Die vollständige Lizenz kann unter creativecommons.org/licences/by-nc-nd/2.5/ch eingesehen werden.



Namensnennung-Keine kommerzielle Nutzung-Keine Bearbeitung 2.5 Schweiz

Sie dürfen:



das Werk vervielfältigen, verbreiten und öffentlich zugänglich machen

Zu den folgenden Bedingungen:



Namensnennung. Sie müssen den Namen des Autors/Rechteinhabers in der von ihm festgelegten Weise nennen (wodurch aber nicht der Eindruck entstehen darf, Sie oder die Nutzung des Werkes durch Sie würden entlohnt).



Keine kommerzielle Nutzung. Dieses Werk darf nicht für kommerzielle Zwecke verwendet werden.



Keine Bearbeitung. Dieses Werk darf nicht bearbeitet oder in anderer Weise verändert werden.

- Im Falle einer Verbreitung müssen Sie anderen die Lizenzbedingungen, unter welche dieses Werk fällt, mitteilen. Am Einfachsten ist es, einen Link auf diese Seite einzubinden.
- Jede der vorgenannten Bedingungen kann aufgehoben werden, sofern Sie die Einwilligung des Rechteinhabers dazu erhalten.
- Diese Lizenz lässt die Urheberpersönlichkeitsrechte unberührt.

Die gesetzlichen Schranken des Urheberrechts bleiben hiervon unberührt.

Die Commons Deed ist eine Zusammenfassung des Lizenzvertrags in allgemeinverständlicher Sprache: <http://creativecommons.org/licenses/by-nc-nd/2.5/ch/legalcode.de>

Haftungsausschluss:

Die Commons Deed ist kein Lizenzvertrag. Sie ist lediglich ein Referenztext, der den zugrundeliegenden Lizenzvertrag übersichtlich und in allgemeinverständlicher Sprache wiedergibt. Die Deed selbst entfaltet keine juristische Wirkung und erscheint im eigentlichen Lizenzvertrag nicht. Creative Commons ist keine Rechtsanwalts-gesellschaft und leistet keine Rechtsberatung. Die Weitergabe und Verlinkung des Commons Deeds führt zu keinem Mandatsverhältnis.

Genehmigt von der Philosophisch-Naturwissenschaftlichen Fakultät
auf Antrag von

Edwin C. Constable und Marcel Mayor

Basel, den 22. 6. 2010

Prof. Dr. Eberhard Parlow

Some random thoughts

"Science is a wonderful thing if one does not have to earn one's living at it."

Albert Einstein

"In physics, you don't have to go around making trouble for yourself - nature does it for you."

Frank Wilczek

"That theory is worthless. It isn't even wrong!"

Wolfgang Pauli

"Research is the process of going up alleys to see if they are blind."

Marston Bates

"In all science, error precedes the truth, and it is better it should go first than last."

Hugh Walpole

"Leave the atom alone."

E. Y. Harburg

"Science is simply common sense at its best, that is, rigidly accurate in observation, and merciless to fallacy in logic."

Thomas Huxley

"Take young researchers, put them together in virtual seclusion, give them an unprecedented degree of freedom and turn up the pressure by fostering competitiveness."

James D. Watson

"The distance between insanity and genius is measured only by success."

Bruce Feirstein

"Your theory is crazy, but it's not crazy enough to be true."

Niels Bohr

Acknowledgments

I've got so many people to whom I owe gratitude that compiling a list can never be complete.

First of all I'm grateful for my parents that have allowed me and made it possible for me to follow my own path and my sister for her encouragements.

I'm in deep debt to my supervisors Ed Constable and Catherine Housecroft who have welcomed me into their group and were always there for me with knowledge and tips when I ran out of one of them.

I'd like to thank the whole of the Constable-Housecroft group for being so nice and friendly people. They're all fabulous persons but I'd like to name a few that I'm in deep debt to. First Jason Price for the interesting talks we had and his endless patience with me. The same goes for Emma Dunphy and Kate Harris who always listened when I came babbling to them.

Special thanks go to Serena Belegriou and Agnieszka Jagoda for helping me with the Langmuir-Blodgett measurements.

The staff of the department, our administrator Beatrice Erismann who keeps the whole administration side running, Markus Hauri, Alois Schäuble and Roy Lips who keep us supplied with all the things we'd never thought we'd need them.

The analytical staff with Daniel Häussinger who takes care of the NMR machines, Heinz Nadig who is in charge of the mass spectrometry and Werner Kirsch in charge of the microanalysis.

Last but not least I'd like to thank the University of Basel and the Swiss Science Foundation for financing my expedition into chemistry.

Abbreviations

Å	Ångström (10^{-10} m)
BAM	Brewster angle microscope
bipy	2,2'-bipyridine
CSP	crystal structure prediction
d	doublet
DMF	dimethylformamide
EI	electron ionisation
eq	equivalents
ESI	electrospray ionisation
eV	electronvolt (energy, $1 \text{ eV} \approx 1.60 \cdot 10^{-19} \text{ J}$)
FAB	fast atom bombardment
g	mass unit
HOPG	highly oriented pyrolytic graphite
Hpaphy	pyridine-2-carbaldehyde-2-pyridylhydrazone (protonated)
Hz	Hertz [s^{-1}]
IR	infrared
k	kilo (10^3)
K	Kelvin (temperature unit)
L	liter [m^{-3}]
LB	Langmuir-Blodgett
m	milli (10^{-3})
m	meter (length unit)
M	mega (10^6)
μ	micro (10^{-6})
m/z	mass over charge
MeOH	methanol
MeCN	acetonitrile
m. p.	melting point
n	nano (10^{-9})
Nd:YAG	neodymium-doped yttrium aluminium garnet
NMR	nuclear magnetic resonance

p	pico (10^{-12})
paphy	pyridine-2-carbaldehyde-2-pyridylhydrazone (deprotonated)
ppm	parts per million
q	quartet
s	singlet
SAM	self-assembled monolayer
STM	scanning tunneling microscopy
t	triplett
terpy	2,2':6',2''-terpyridine
TFA	trifluoroacetic acid
THF	tetrahydrofuran
TLC	thin layer chromatography
UV	ultraviolet
vis	visible

Index

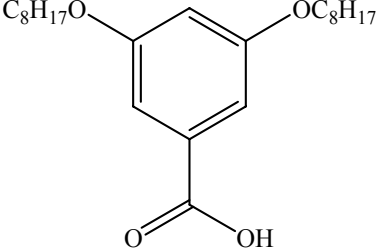
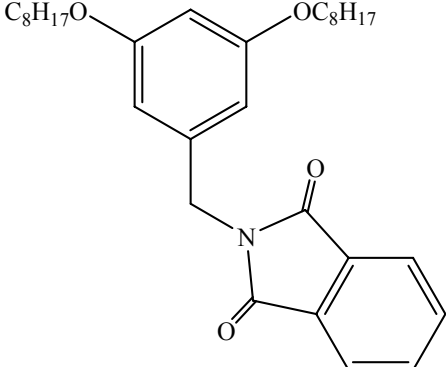
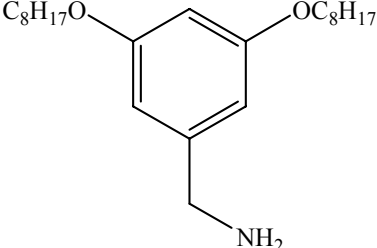
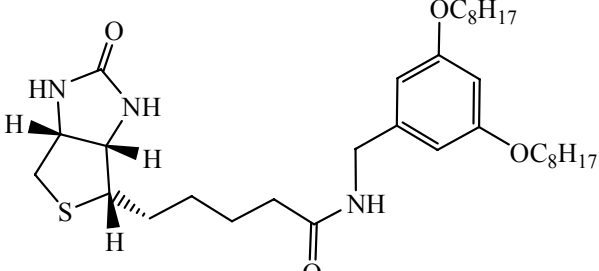
Compounds.....	3
1. Introduction.....	13
1.1 Supramolecular Chemistry.....	13
1.2 Complexes.....	15
1.3 Dendrimers.....	18
1.4 Scanning Tunneling Microscopy.....	21
1.5 Project Aims.....	23
1.6 References.....	24
2. Methods and Instruments.....	25
2.1 General Experimental.....	25
2.2 Analytical Instruments.....	25
3. Dendritic wedges, their properties and Synthesis.....	27
3.1 Introduction.....	27
3.2 Aims.....	34
3.3 Synthesis.....	35
3.4 Didendritic wedge compounds.....	40
3.5 Results and Concluions.....	45
3.6 Experimental section.....	54
3.6.1 G1 derivatives.....	54
3.6.2 G2 derivatives.....	60
3.6.3 Didendritic wedge compounds.....	66
3.7 References.....	71
4. Pyridine-2-carbaldehyde-2-pyridylhydrazone and its iron(II) complexes.....	73
4.1 Introduction.....	73
4.1.1 History.....	73
4.1.2 Analytical Applications.....	76
4.1.3 Practical Applications.....	77
4.1.4 Properties.....	77
4.1.5 Stereochemistry.....	79
4.1.6 Toxicity.....	80
4.1.7 Summary.....	81
4.2 Aims.....	82
4.3 Synthesis.....	82
4.4 Titration experiments.....	87
4.5 Hindered Rotation.....	90
4.6 Conclusions.....	93
4.7 Experimental Section.....	94
4.8 References.....	104

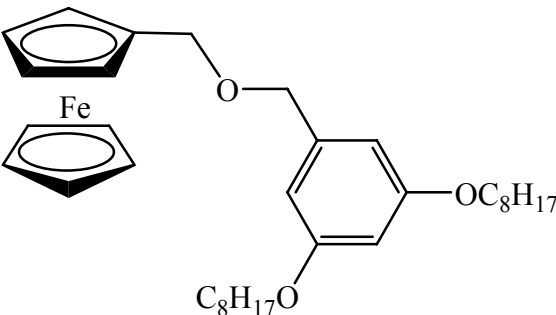
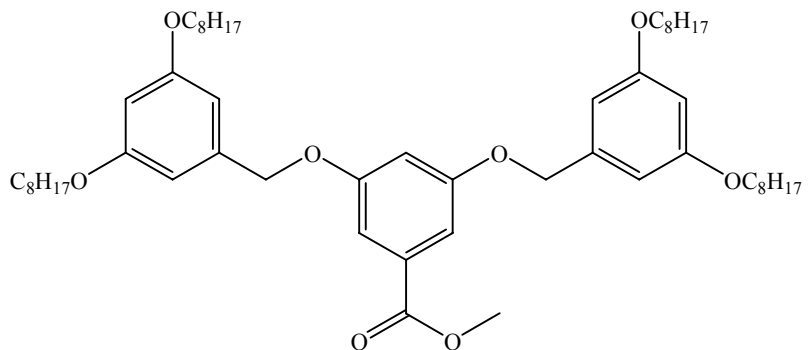
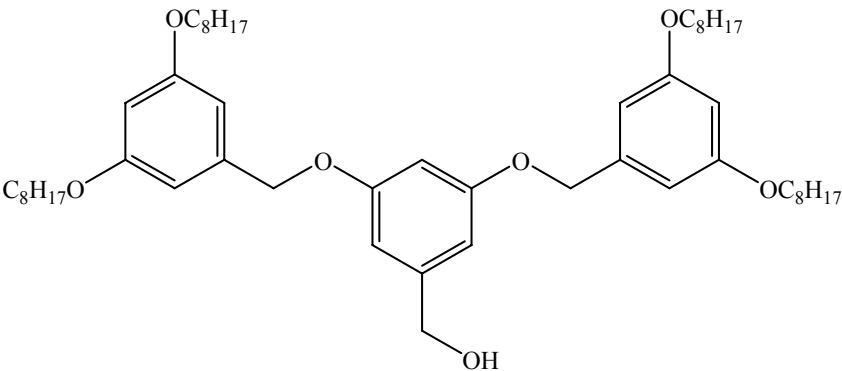
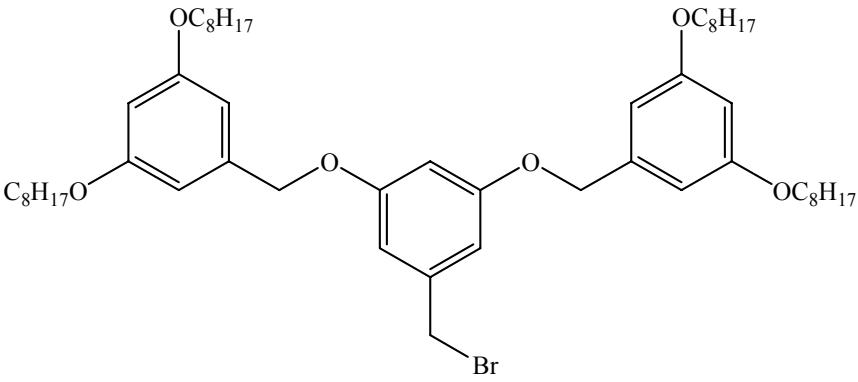
5.	Monolayer formation and STM analysis.....	107
5.1	Introduction	107
5.1.1	History.....	107
5.1.2	Working Principle	108
5.2	Aims	109
5.3	Procedures and Techniques.....	110
5.3.1	General information	110
5.3.2	Substrate preparation.....	111
5.3.3	Tip preparation	111
5.3.4	Sample preparation.....	112
5.3.5	Data analysis	113
5.4	Practical considerations during measurements	113
5.4.1	Artefacts	113
5.4.2	Plane group assignment.....	116
5.5	Results	117
5.5.1	STM.....	117
5.6	Langmuir-Blodgett techniques	123
5.6.1	Introduction	123
5.6.2	Aims	125
5.6.3	Methods and procedures.....	125
5.6.4	Results	126
5.6.5	LB deposition	133
5.6.6	STM measurements.....	135
5.7	Conclusions	138
5.8	References	139
6.	Conclusions	140
	Appendix - Crystallographic data	141

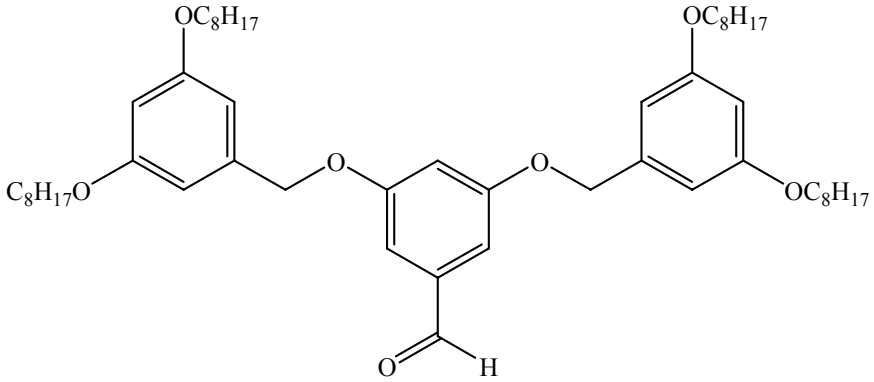
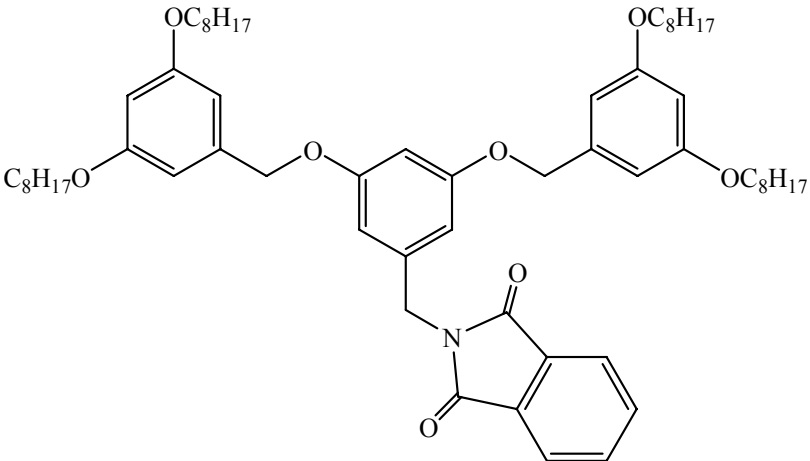
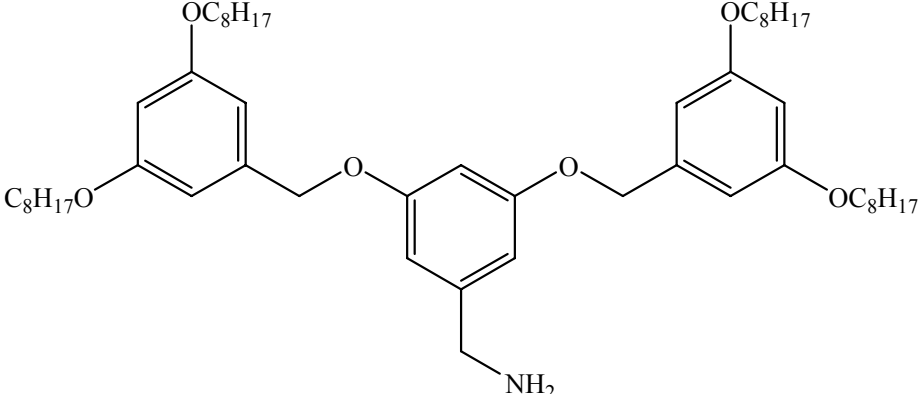
Compounds

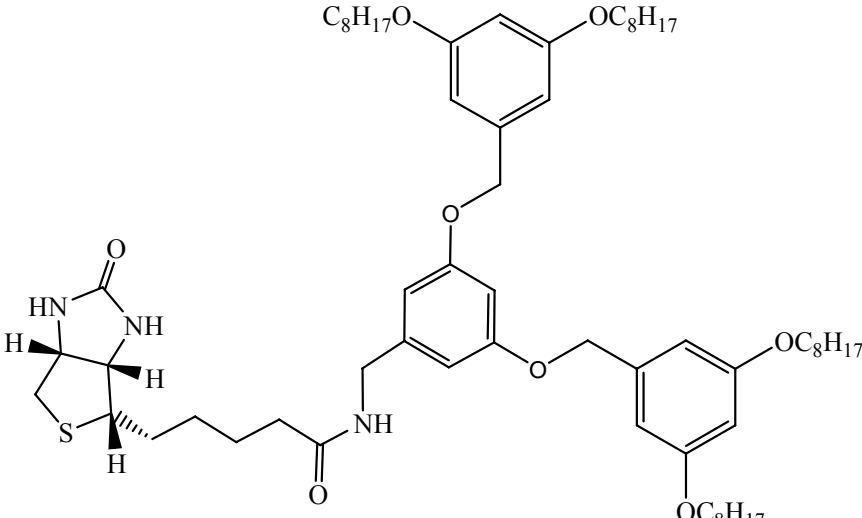
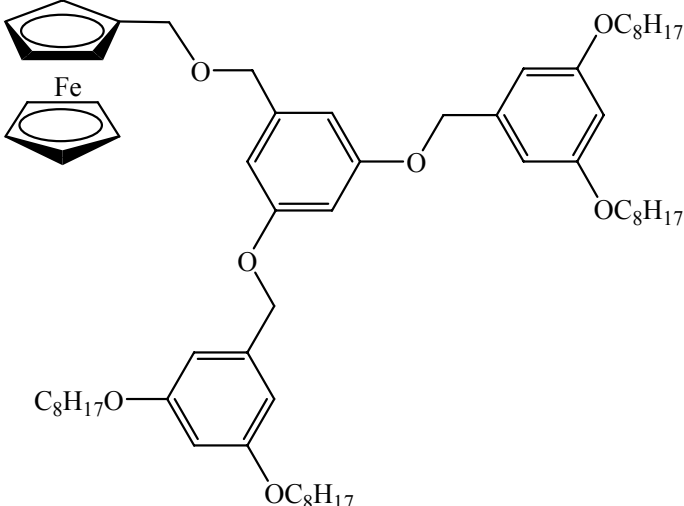
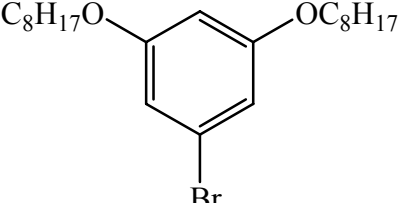
Methyl 3,5-bis(octyloxy)benzoate	1
3,5-Bis(octyloxy)benzyl alcohol	2
3,5-Bis(octyloxy)benzyl bromide	3
3,5-Bis(octyloxy)benzaldehyde	4
3,5-Bis(octyloxy)benzyl mesylate	5

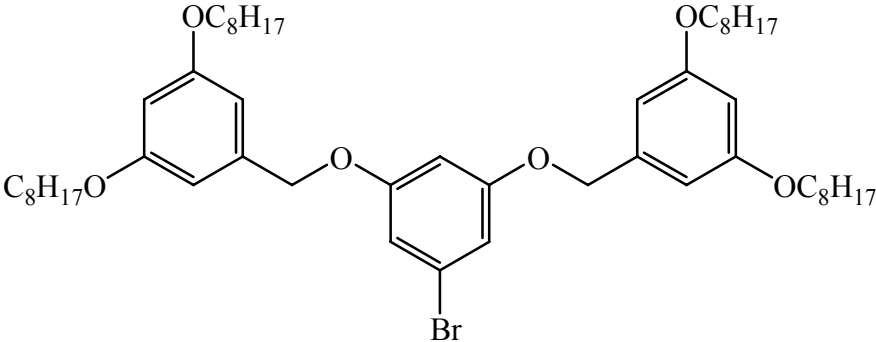
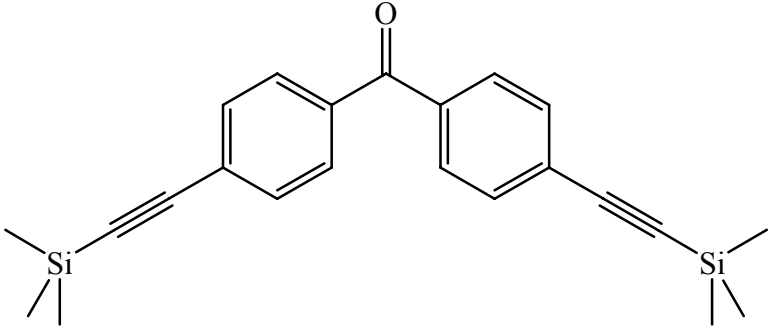
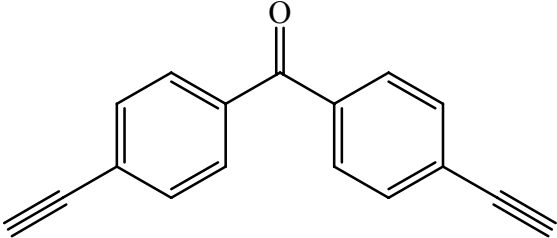
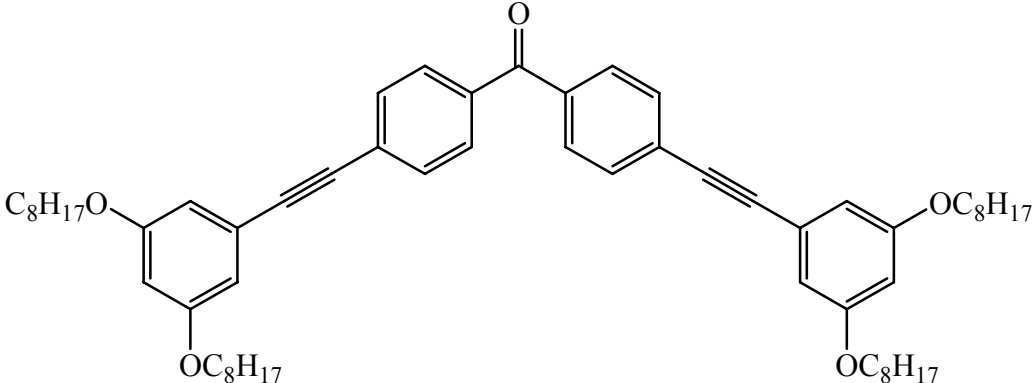
Compounds

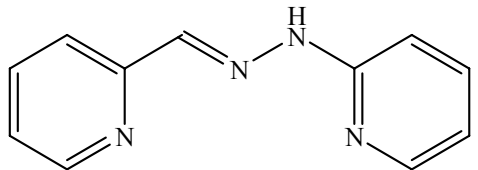
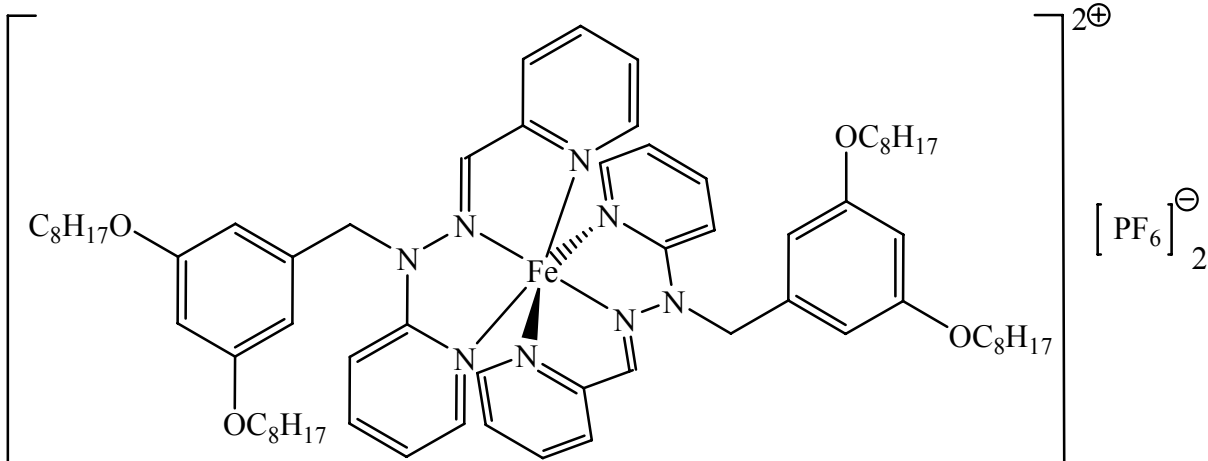
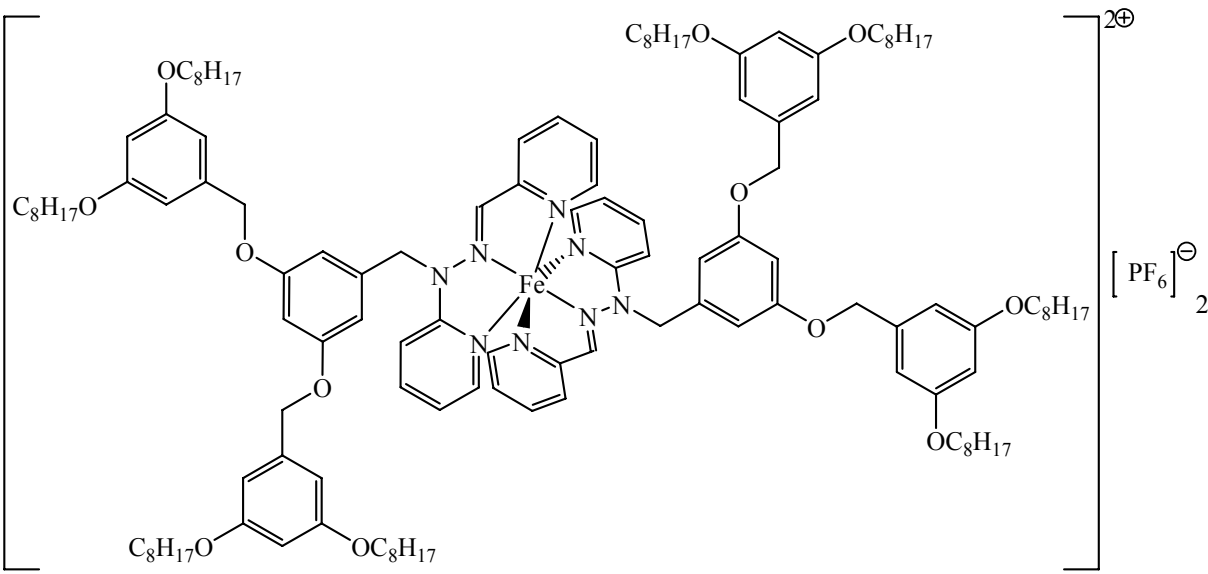
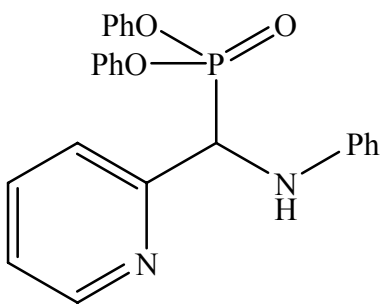
3,5-Bis(octyloxy)benzoic acid	6
	
<i>N</i> -{3,5-Bis(octyloxy)benzyl}phthalimide	7
	
3,5-Bis(octyloxy)benzylamine	8
	
	9
	

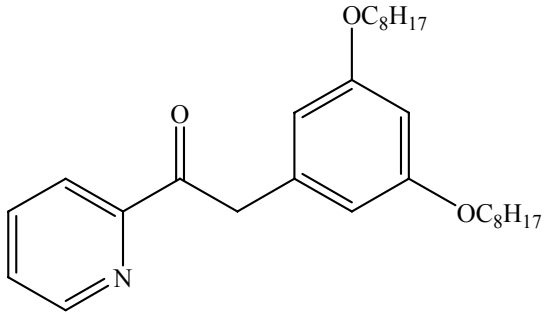
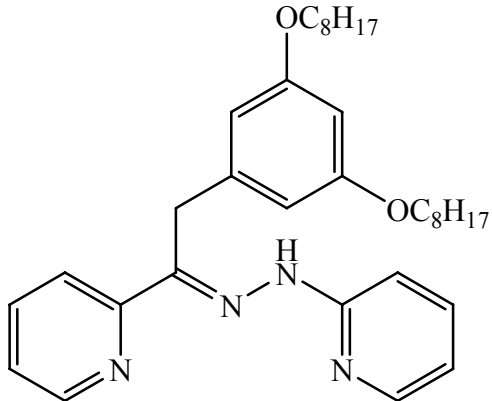
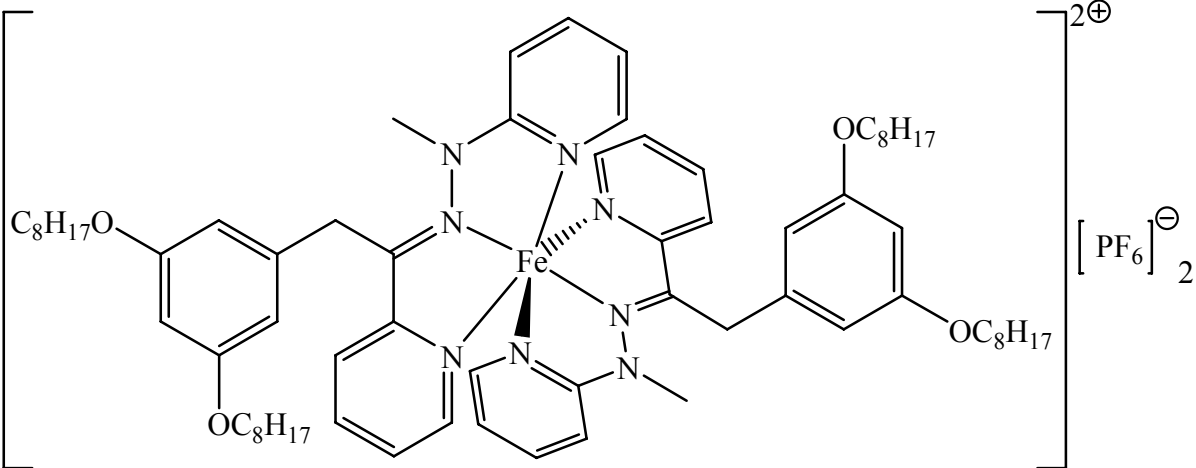
	10
<p>Methyl 3,5-bis(3,5-dioctyloxybenzyloxy)benzoate</p> 	11
<p>3,5-Bis(3,5-dioctyloxybenzyloxy)benzyl alcohol</p> 	12
<p>3,5-Bis(3,5-dioctyloxybenzyloxy)benzyl bromide</p> 	13

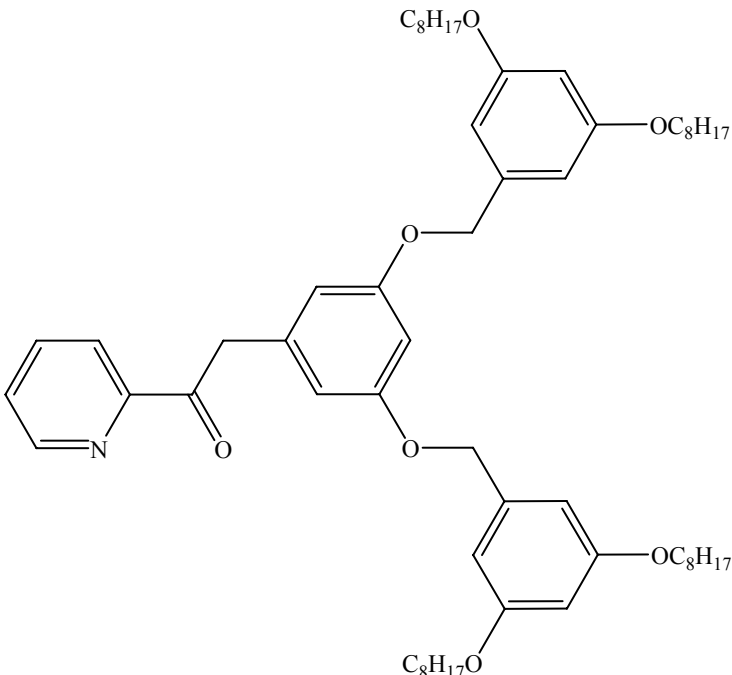
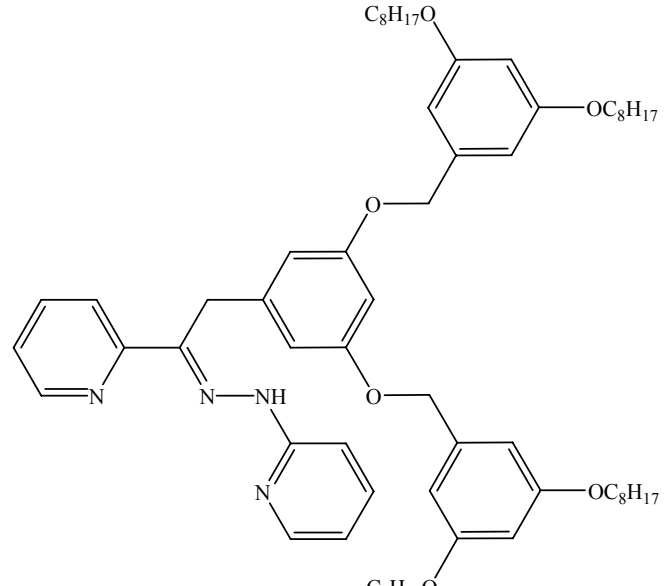
3,5-Bis(3,5-dioctyloxybenzyloxy)benzaldehyde	14
 <p>The structure shows a central benzene ring with an aldehyde group (-CHO) at the para position. Two benzyloxy groups are attached to the central ring at the 3 and 5 positions. Each benzyloxy group consists of a methylene group (-CH₂-) connected to a benzene ring. This benzene ring has two octyloxy groups (-OC₈H₁₇) at the 3 and 5 positions.</p>	
<i>N</i> -{3,5-Bis(3,5-dioctyloxybenzyloxy)benzyl}-phthalimide	15
 <p>The structure is similar to compound 14, but the aldehyde group is replaced by a benzyl group (-CH₂-) which is connected to the nitrogen atom of a phthalimide ring system.</p>	
3,5-Bis(3,5-dioctyloxybenzyloxy)benzylamine	16
 <p>The structure is similar to compound 14, but the aldehyde group is replaced by a primary amine group (-CH₂NH₂) at the para position of the central benzene ring.</p>	

	<p>17</p>
	<p>18</p>
<p>Bromo-3,5-(bis(octyloxy))benzene</p>	<p>19</p>
	

Bromo-3,5-bis(3,5-dioctyloxybenzyloxy)benzene	20
	
4,4'-Bis(trimethylsilylethynyl)acetophenone	21
	
4,4'-Bis(ethynyl)acetophenone	22
	
(3,5-Bis(octyloxy)phenylethynyl)acetophenone	23
	

Pyridine-2-carbaldehyde-2-pyridylhydrazone	24
	
25	
	
26	
	
Diphenyl-1-(phenylamino)-1-(2-pyridyl) methylphosphonate	27
	

2-(3,5-Bis(octyloxy)phenyl)(2-pyridyl)ethanone	28
	
2-(3,5-bis(octyloxy)phenyl)(2-pyridyl)ethanone-2-pyridylhydrazone	29
	
	30
	

<p>2-(3,5-Bis(3,5-dioctyloxybenzyloxy)phenyl)(2-pyridyl)ethanone</p>	<p>31</p>
	
<p>2-(3,5-Bis(3,5-bis(octyloxybenzyl)oxy)phenyl)-2-(2-pyridyl)ethanone-2'-pyridylhydrazone</p>	<p>32</p>
	

1. Introduction

1.1 Supramolecular chemistry

Supramolecular chemistry is a relatively new concept in chemistry¹. Non-covalent bonds are used to assemble small subunits into big arrays. One of the pioneers in this field is J.-M. Lehn. He was awarded the Nobel Prize in 1987 for his work. The two most often used non-covalent forces are hydrogen bonds and metal-ligand interactions. Hydrogen bond strengths vary strongly depending on the involved hetero atoms. Beginning with the weakest interaction for $\text{CH}_4 \cdots \text{F}-\text{CH}_3$ which shows 48 J/mol up to 9.3 kJ/mol for $\text{F} \cdots \text{H}-\text{F}$ ². Metal-ligand interactions can easily have 100 kJ/mol energy. Considering the relative energies it is understandable that more commonly metal-ligand interactions are used for the assemblies. The much higher energies make these bonds not only stronger but the well defined geometry of the metal-ligand interaction allows for reliable predictions and excellent control¹.

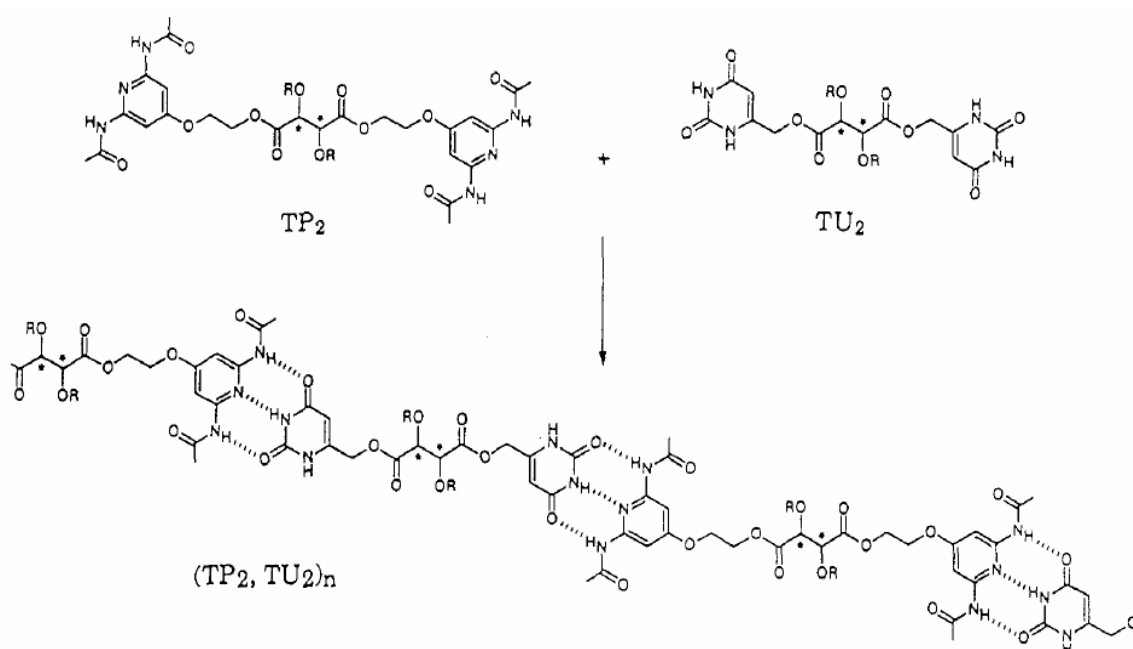


Fig. 1.1.1 Example for a supramolecular assembly using hydrogen bonds³

Fig. 1.1.1 gives an example for such a non-covalent assembly. Using hydrogen bonds a linear polymer is made³. This is a very elegant approach to the synthesis of this polymer. But the problem of this compound is that the individual interactions are not very strong. Polar solvents like methanol that can form hydrogen bonds themselves can destroy this polymer. An alternative to the hydrogen bonds are metal-ligand interactions. A famous experiment

conducted by Lehn was the synthesis of chains of 2,2'-bipyridines connected through different linkers.

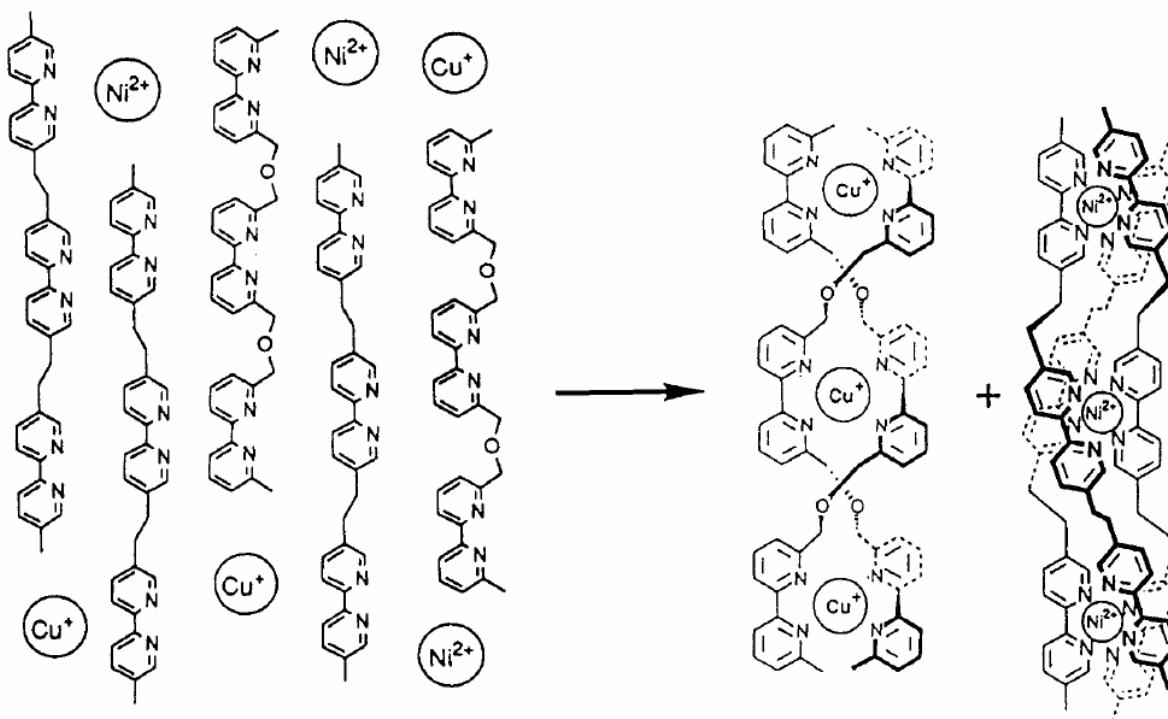


Fig. 1.1.2 Experiment conducted by Lehn. Through selective interactions the mixture of the four starting materials (left) produces two distinct products (right)³.

This experiment works because copper(I) prefers a tetrahedral and nickel(II) an octahedral coordination sphere. The linker between the 2,2'-bipyridines are in one chain at the 5,5' and in the other chain at the 6,6' positions. The 5,5'-linked chain therefore favours a more linear geometry while the 6,6' chain is already quite bent. When these chains are now mixed with metal ions that have a different coordination sphere, like nickel(II) and copper(I), it was observed that the mixture of the four compounds yielded two distinct products³ (fig. 1.1.2).

Molecular recognition, as shown in the experiments in fig. 1.1.1 and 1.1.2, is a very important principle of nanotechnology. Direct manipulation at the molecular level is only possible in a limited fashion and even in the cases where it is possible, it is hard and tedious work. Letting the materials themselves do the desired arrangement is a very elegant way. This self-assembly as demonstrated in the examples above is a solution for the lack of direct control on the molecular level. By planning compounds accordingly, intermolecular forces can be used to force the desired assembly.

Templated reactions are part of this topic. Ligand binding sites are included in molecules that then form complexes with another molecule and a metal. This ensures the right

conformation of the two molecules towards each other in the next synthetic steps. Usually, after completion of the synthetic part the templating metal is removed again.

Some of the more prominent examples are the catenanes and molecular knots. Initial attempts to prepare these molecular knots, interwoven loops, were without templating, leaving it to statistical occurrences that the target molecule was made. Obviously the yields on these syntheses were very low. By using templates, the synthesis of catenanes was greatly improved⁴. Two reviews on the topic can be found here^{5,6}.

Hydrogen bonds and the metal-ligand bond are only two of many possible intermolecular forces. The reason why almost exclusively these two are used in self-assembly and templated syntheses is their strength. As pointed out earlier the hydrogen bond brings in average about 10 kJ/mol and the metal-ligand bond in the area of 100 kJ/mol. The London and dipole-dipole interactions are on the scale the next. They are again weaker by an order of magnitude than the hydrogen bonds⁷. This makes the prediction of the probable self-assembly product based on them very difficult.

This can also be seen in the theoretical field of crystal structure prediction. On the frontier in this field is S. Price. Today's models are able to predict intermolecular interaction of hydrogen bonds and the resulting crystal structures of small and rigid molecules with some success⁸. An additional problem in this field is polymorphism. Molecules can crystallize in different lattices and under different conditions different lattices might be favoured, giving rise to many different possibilities and probabilities. While small rigid molecules with intermolecular hydrogen bonds start to become almost predictable, more flexible molecules even with hydrogen bonds are already beyond current capabilities. If the intermolecular interactions do not show any hydrogen or metal-ligand bonds predictions become most difficult. To take self-assembly to the next level, the understanding and prediction of these weak interactions would be necessary.

1.2 Complexes

The metal-ligand interaction is one of the strongest non-covalent bonds. Many self-assemblies use the metal-ligand interaction for directing syntheses. This is called templating. Usually after completion of the synthesis, the metal ion is removed.

Ligands are defined through many parameters. One very important one is their coordination number, beginning at 1 for a monodentate ligand to bi- and tri- dentate ligands. Higher coordination numbers are possible but are not commonly used in supramolecular and

template chemistry. This is because many metals used have a coordination number of six. Two tri dentate ligands will fill the coordination sphere of such a metal.

Two very often used ligands for supramolecular chemistry are 2,2'-bipyridine (bipy) and 2,2':6',2''-terpyridine (terpy). Their easy synthesis and the numerous possibilities for modifications makes them the primary choice for many applications⁹⁻¹¹.

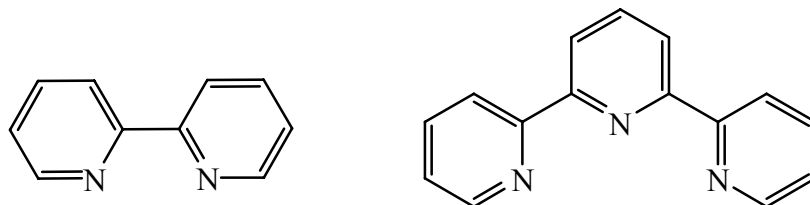


Fig. 1.2.1 2,2'-Bipyridine (left) and 2,2':6',2''-terpyridine (right)

Very often the terpy is modified at the 4'-position. This yields with two ligands and a octahedral metal ion an achiral complex.

Complexes of an octahedral metal with bipy are enantiomeric, even with a symmetrical substitution on bipy.

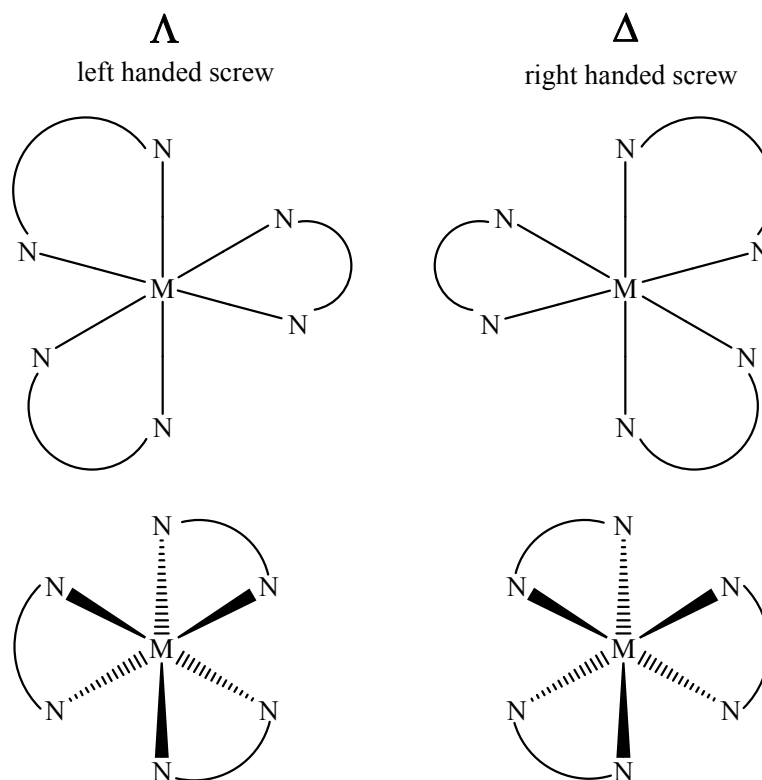


Fig. 1.2.2 Λ (left) and Δ (right) configuration of a bidentate ligand complex

Fig. 1.2.2 shows the two possible enantiomeric forms for an octahedral complex with three bidentate ligands. As shown, the two ligands are image and mirror image towards each other. On the left is the left handed screw shown, on the right the right handed screw.

Usually the stereochemistry of these compounds is irrelevant since in an achiral environment both compounds behave the same. But under certain conditions the stereochemistry starts to matter. For example an octahedral complex formed with three bidentate ligands containing a chiral centre. Assuming the ligand is symmetrical and enantiopure the products formed are the Δ and Λ forms of the complex. These two compounds show even in an achiral environment different behaviour and can for example be separated on a column. This is why, when possible, 4'-substituted terpy ligands are used. With two symmetrical tri dentate ligands an octahedral complex is achiral.

Another tridentate ligand is pyridine-2-carbaldehyde-2-pyridylhydrazone (Hpaphy) (fig. 1.2.3). This ligand was first synthesised by Lions and Martin¹². Hpaphy is quite a remarkable ligand and it was proposed for many applications (also see chapter 4 for an exhaustive review) but did not achieve large scale usage. Among other things Hpaphy is able to adopt two conformations, the Z and the E form. In the E form once a complex is formed the proton at the position 2 (fig. 1.2.4) can easily be removed. With a doubly charged metal ion a charge neutral complex is then formed. In the Z form the amine proton is used for an intramolecular hydrogen bond (fig. 1.2.3). This also blocks the third coordination site, making Hpaphy a bidentate ligand.

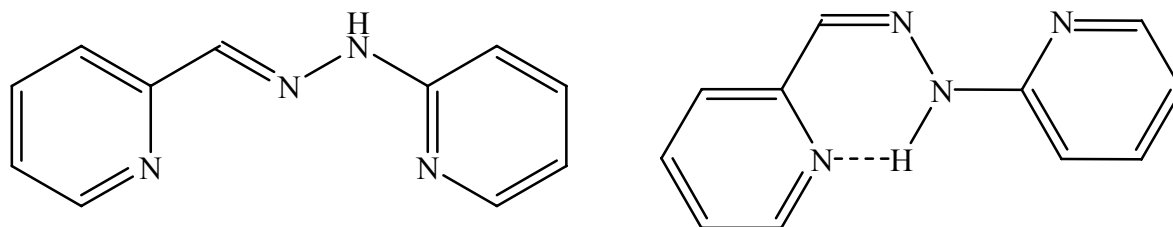


Fig. 1.2.3 The two forms of pyridine-2-carbaldehyde-2-pyridylhydrazone (Hpaphy). *E*-Hpaphy (left); *Z*-Hpaphy (right) with the intramolecular H-bond.

Hpaphy also offers two easy accessible points for modification (fig. 1.2.4 1 and 2) on the backbone. Of course the aromatic rings can be modified as in bipy or terpy. It is the two positions on the backbone that make Hpaphy so special. These two positions become available at different stages of the synthesis and can so be easily modified differently.

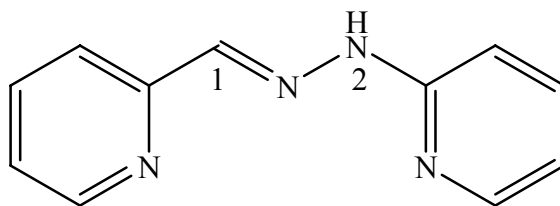


Fig. 1.2.4 Structure of pyridine-2-carbaldehyde-2-pyridylhydrazone (Hpaphy)

1.3 Dendrimers

Polymers are an essential part in today's material sciences. Polymers are usually long chains of monomers that were covalently coupled together through a chemical reaction. Due to the synthesis pathway, a polymer is actually a mixture of compounds that differ mainly through their molecular weight. The building block, the monomer, is the same in all of them but the number of the coupled monomers is differing. This makes an exact characterisation difficult for the broad distribution of molecular weight. The molecular weight given for a polymer is only an average value. This polydiversity is a big problem in polymers when a high uniformity is required. Different methods for purification have been developed but they work only in limited fashion, only allowing the separation of molecules much bigger or much smaller than the average.

A further step in the control of the molecular weight of polymers are dendrimers. The name is derived from the Greek word for tree, for their structures show an increasing number of branches going away from the centre. These polymer-related molecules usually have a much better defined shape and size than polymers, but their synthesis is also much more difficult.

The last few years showed a constant increase in scientific interest in dendrimers and with this interest, new fields for applications were expanded. Dendrimers are now studied for encapsulation experiments, liquid crystals, self-assembled monolayers, surface patterning, bio sensors and drug delivery systems. A review written by Astruc¹³ is an excellent starting point for further reading.

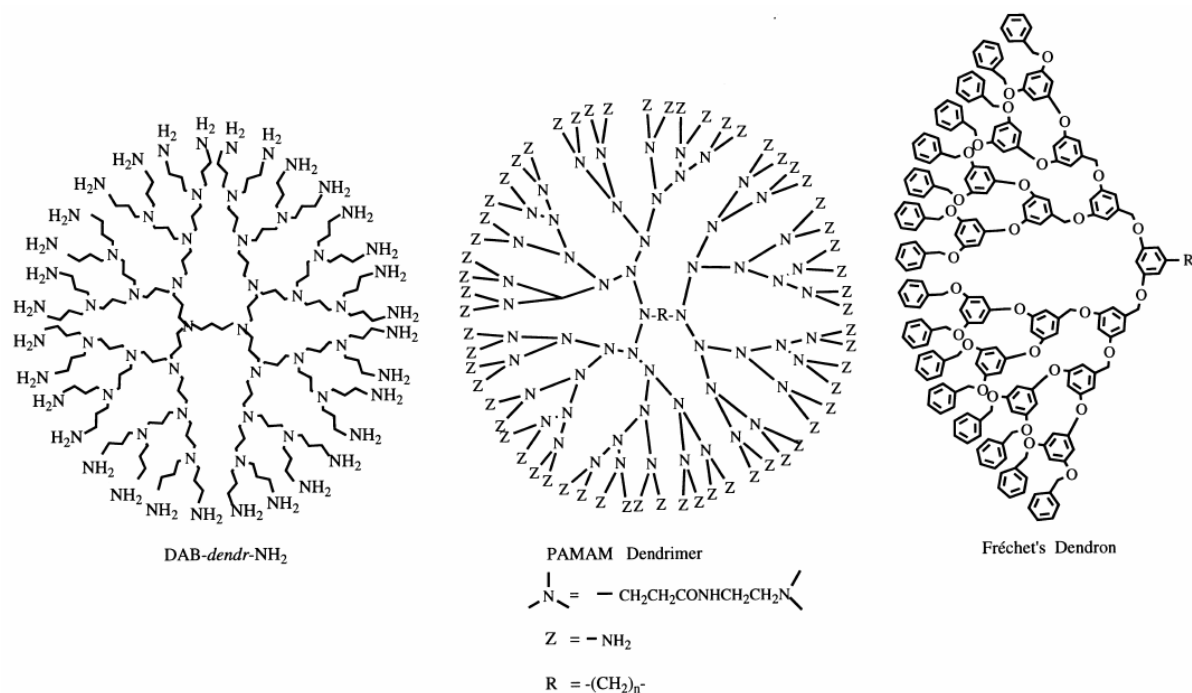


Fig. 1.3.1 Some of the most used dendrimers¹⁴

Fig. 1.3.1 shows some of the most used dendrimers. The big synthetic difference between polymers and dendrimers is that dendrimers are composed of two different monomers while polymers are often only composed out of one monomer type. The synthesis is achieved by switching between the two different monomers from step to step. This gives direct and immediate control over how long the branches will become. But despite best efforts and a much reduced polydiversity, a complete homogeneity is not achievable. The polydiversity in dendrimers has mostly steric reasons. With increasing branch number the density on the outer shell is increasing. At some point it is simply no longer possible to react all functional groups of the outer shell with the next monomer unit. This leads to defects in the structure and polydiversity.

Fréchet noticed this and developed a new approach for the synthesis of dendrimers¹⁵. The convergent approach practically eliminates polydiversity from the conventional synthesis respectively the polydiversity is so strong between the different forms that classical purification methods work again. Fréchet began his synthesis with the outer shell and moved inwards, synthesising whole dendritic wedges. These wedges were then coupled to the core unit. Since all synthetic steps of the wedges are followed by purification in which incompletely reacted parts and excess starting materials are removed, the wedges are very clean and homogenous materials.

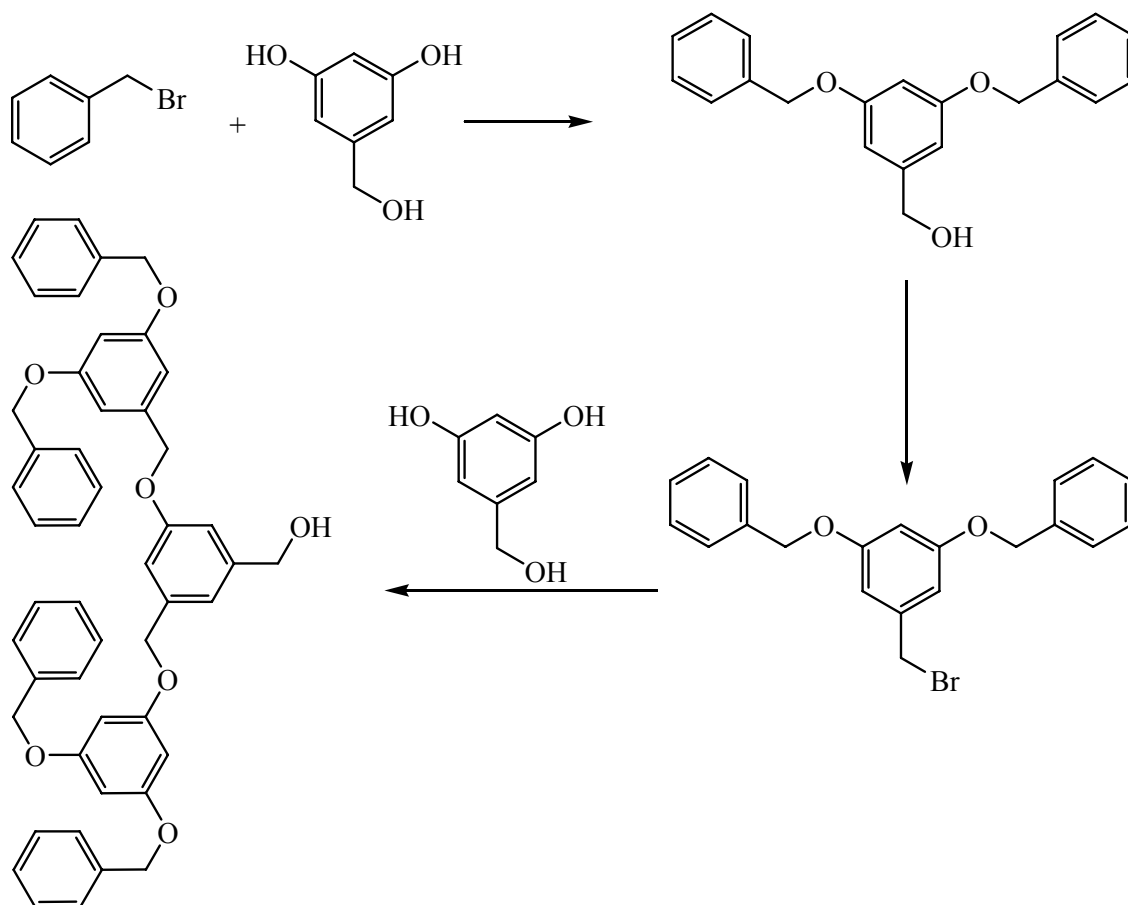


Fig. 1.3.2 Schematic dendrimer synthesis by Fréchet

Through repeating the steps shown in fig. 1.3.2 a dendritic wedge with no polydiversity is formed.

This purity is generally a desired feature, but the more complex synthesis makes it often not worthwhile, but is of paramount importance for some applications. A good example for the need of pure compounds is crystal growth. Growing crystals can be a means of purification. In a solution of different compounds, the component with the lowest solubility will crystallize first. By establishing a long range order, the rest of the same component will aggregate on these first crystallites, selectively removing this component from the solution. Or put the other way round, if a compound shows a very high homogeneity, crystallisation becomes easier.

1.4 Scanning tunnelling microscopy

Scanning tunneling microscopy (STM) was developed by Binnig and Rohrer at the IBM labs in Zürich in the early 1980s. Originally the inventors just wanted to study oxide thin films on metal surfaces. The lack of a useful tool for this task led to the development of the STM machine. Binnig and Rohrer very soon realised the value of the tool they had developed. Both were awarded the Nobel Prize in Physics 1986. STM and x-ray crystallography are the two only methods that show a resolution on the molecular and even atomic scale. X-ray crystallography requires a single crystal and temperatures of about 180 K. STM allows for much broader measuring conditions and even measurements in dynamic environments, a feat that x-ray crystallography does not show since in the crystal lattice most of the structure is locked into place.

STM conditions can be high vacuum and close to 0 K up to measurements in air at ambient temperature. As much as the measurement parameters differ so can also the substrate be varied. The two most commonly used ones are gold and graphite. The main requirements are an atomically flat surface and conductance. One of the major downsides of STM is that monolayers are required. Another is that the substrates pose requirements on the analyte. Gold substrates are in general used with thiols. The favourable sulfur-gold interaction is used to chemisorb the analyte on the surface. This vastly increases the probability for monolayers on the surface with the additional insurance that the analyte is not able to move since the sulfur is bound covalently to the gold. Graphite substrates are usually used in connection with organic molecules. It has been shown that alkyl chains show a surprisingly strong affinity towards graphite with about 1 kJ/mol per methylene unit¹⁶. Varying the length of the alkyl chains allows tweaking the adsorption strength as desired. Increasing the length of the alkyl chains makes the adsorption stronger, shortening the chains weakens the bond. A weaker bond is not necessarily a disadvantage. The weaker bond usually allows for desorption and readsorption of molecules maximising the interactions not only between the surface but also between the single molecules. This gives rise to very homogeneous and defect free monolayers (fig. 1.4.1). A downside of this setup is that when no monolayer should form, no STM observation can be made. This is due to the thermal movement that is too strong as well as the electric field of the tip can simply push the molecules away.

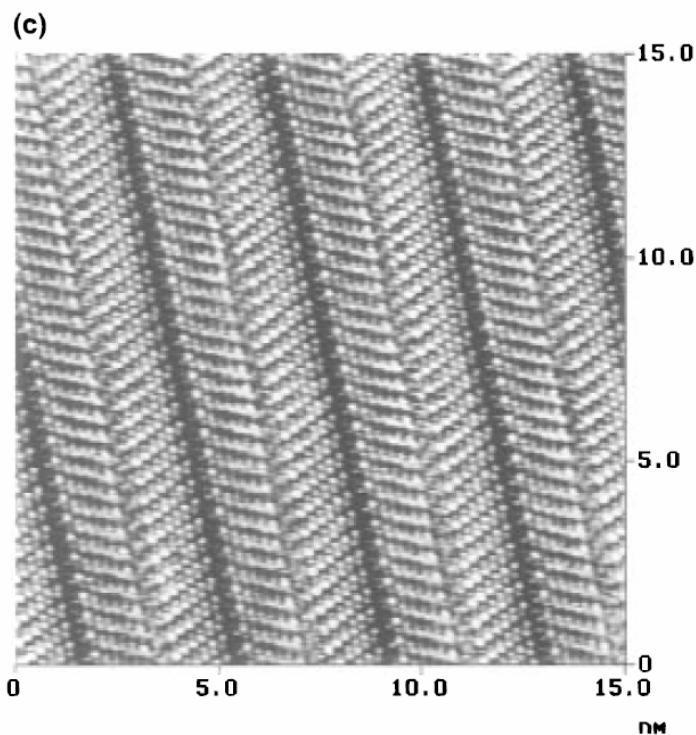


Fig. 1.4.1 Tetradecanol on graphite (reproduced from¹⁶)

STM has become an important analytical tool for surface chemistry. Especially the atomic resolution allows analysis of single molecules. This is of big importance since the behaviour of a single molecule or atom can differ strongly from the properties of the bulk material¹⁷. This is caused by the averaging that is always happening in bulk materials. This can help examining and understanding quantum mechanical problems.

Over the recent years STM has become much more than just an analytical imaging tool. So were methods developed for nanolithography and the direct manipulation of atoms¹⁸. Nanotechnology and supramolecular chemistry are two closely related fields that make ample use of the new technologies.

Supramolecular chemistry is a field of growing importance. Through self-assembly by non-covalent forces large superstructures are generated. These structures have different applications like coatings. Of a growing importance are porous materials for hydrogen storage. Nanotechnology is a wide term that includes molecular machines for example. Scaling a macroscopic function down to the molecular level is a big synthetic challenge. Molecular switches, muscles and rotors have been synthesised¹⁹⁻²¹, even molecular cars (fig. 1.4.2). STM enables imaging of these systems but more important it gives the possibility for direct manipulation.

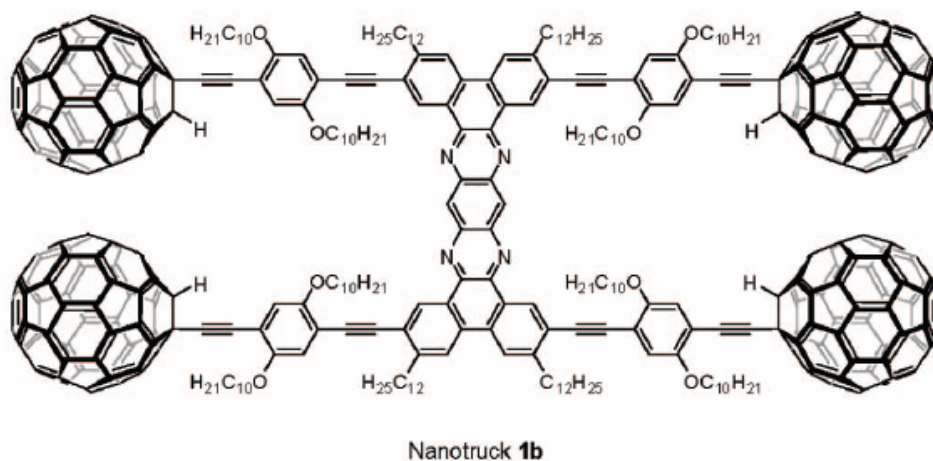


Fig. 1.4.2 Nanotruck (reproduced from²¹)

Today's silicon based electronics will soon hit the limits of miniaturisation possible. Molecular electronics offer further downscaling. Intensive research on this field is currently being undertaken^{17,18,22,23}. To advance molecular electronics STM has shown to be of great value. The examination of the conductance of single molecules is important because the quantum mechanical properties of single molecules can vary from those of the bulk material.

All these applications make STM a very versatile method that is continuously improved and adapted to new tasks.

1.5 Project Aims

Through combination of previously mentioned aspects we wished to gain further insights into the self-organisation of organometallic compounds on graphite. Iron(II) complexes of paphy, modified with Fréchet type dendritic wedges were selected as target molecules. For maximisation of the interaction between the compounds and the graphite substrate used for STM analysis, the terminal groups for the dendritic wedges were selected to be n-octyl chains. Also the free ligand with the dendritic wedge and the final complex would be compared.

1.6 References

- (1) Lehn, J.-M. *Supramolecular Chemistry - Concepts and Perspectives*; VCH, 1995.
- (2) Steiner, T. *Angew Chem Int Edit* **2002**, *41*, 48-76.
- (3) Lehn, J. M. *Pure Appl. Chem.* **1994**, *66*, 1961-1966.
- (4) Collin, J. P.; Heitz, V.; Bonnet, S.; Sauvage, J. P. *Inorg. Chem. Commun.* **2005**, *8*, 1063-1074.
- (5) Stoddart, J. F. *Chem. Soc. Rev.* **2009**, *38*, 1802-1820.
- (6) Faiz, J. A.; Heitz, V.; Sauvage, J. P. *Chem. Soc. Rev.* **2009**, *38*, 422-442.
- (7) Jones, L.; Atkins, P. *Chemistry - Molecules, Matter, and Change*; 4th ed.; W. H. Freeman, 2000.
- (8) Price, S. L. *Phys. Chem. Chem. Phys.* **2008**, *10*, 1996-2009.
- (9) Pettinari, C.; Masciocchi, N.; Pandolfo, L.; Pucci, D. *Chem.-Eur. J.* **2010**, *16*, 1106-1123.
- (10) Constable, E. C. *Chem. Soc. Rev.* **2007**, *36*, 246-253.
- (11) Concepcion, J. J.; Jurss, J. W.; Brennaman, M. K.; Hoertz, P. G.; Patrocinio, A. O. T.; Iha, N. Y. M.; Templeton, J. L.; Meyer, T. J. *Acc. Chem. Res.* **2009**, *42*, 1954-1965.
- (12) Lions, F.; Martin, K. V. *J. Am. Chem. Soc.* **1958**, *80*, 3858-3865.
- (13) Astruc, D.; Boisselier, E.; Ornelas, C. *Chem. Rev. (Washington, DC, U. S.)* **2010**, *110*, 1857-1959.
- (14) Inoue, K. *Prog. Polym. Sci.* **2000**, *25*, 453-571.
- (15) Hawker, C. J.; Frechet, J. M. J. *J. Am. Chem. Soc.* **1990**, *112*, 7638-7647.
- (16) Claypool, C. L.; Faglioni, F.; Goddard, W. A.; Gray, H. B.; Lewis, N. S.; Marcus, R. A. *J. Phys. Chem. B* **1997**, *101*, 5978-5995.
- (17) Kroger, J.; Neel, N.; Limot, L. *J. Phys.: Condens. Matter* **2008**, *20*.
- (18) Samori, P. *Scanning probe microscopies beyond imaging manipulation of molecules and nanostructures*; WILEY-VCH: Weinheim, 2006.
- (19) Kay, E. R.; Leigh, D. A.; Zerbetto, F. *Angew. Chem., Int. Ed.* **2007**, *46*, 72-191.
- (20) Balzani, V.; Credi, A.; Venturi, M. *Chem. Soc. Rev.* **2009**, *38*, 1542-1550.
- (21) Vives, G.; Tour, J. M. *Acc. Chem. Res.* **2009**, *42*, 473-487.
- (22) Hermann, B. A.; Scherer, L. J.; Housecroft, C. E.; Constable, E. C. *Adv. Funct. Mater.* **2006**, *16*, 221-235.
- (23) Johannes, A. A. W. E.; Shengbin, L.; Steven, De F. *Angew. Chem., Int. Ed.* **2009**, *48*, 7298-7332.

2. Methods and Instruments

2.1 General Experimental

Chemicals were used as delivered by the supplier unless stated otherwise. For reactions under nitrogen, standard Schlenk techniques were employed.

2.2 Analytical Instruments

NMR measurements were conducted with a Bruker AM250, a Bruker DRX400 and a Bruker DRX500 spectrometers for the 250 MHz, 400 MHz and 500 MHz experiments respectively. For the signal assignment COSY, HMQC and HMBC spectra were used. The 500 MHz NMR spectra were recorded by K. Harris, V. Jullien, J. Beves or J. Price.

The residual solvent peak was used for referencing (CDCl_3 : ^1H – 7.26 ppm, ^{13}C – 77.23 ppm; C_6D_6 : ^1H – 7.16 ppm, ^{13}C – 128.39 ppm; CD_3CN : ^1H – 1.94 ppm, ^{13}C – 118.69 ppm).

FAB mass spectra were measured with a Finnigan MAT 312 mass spectrometer with 3-nitrobenzylalcohol as supporting matrix. EI mass spectra were recorded with a Finnigan MAT 95Q mass spectrometer. Ion source strength is given in the individual experimental parts. FAB and EI measurements were executed by H. Nadig.

ESI mass spectroscopy was conducted on a Bruker Esquire 3000 plus instrument. The measurements were done by P. Rösel.

IR measurements were done on a Shimadzu FTIR-8400S spectrometer modified with a Golden Gate attachment to handle neat samples.

UV-vis spectra were recorded on a Perkin-Elmer Carey 5000 spectrophotometer. The solvent used was CH_2Cl_2 .

Microanalyses were done on a Leco CHN-900 microanalyser. The measurements were performed by W. Kirsch.

X-ray diffraction measurements for single crystal analysis were conducted with a Enraf-Nonius Kappa CCP diffractometer with graphite monochromated Mo K_{α} radiation source. The measurements were done by M. Neuburger. The structures were solved by M. Neuburger, S. Schaffner or J. Zampese.

3. Dendritic wedges, their properties and synthesis

3.1 Introduction

Dendrimers are a steadily growing field in chemistry. Their often quite simple synthesis is countered by difficult purification. Also it is common for dendrimers to have imperfections due to incomplete conversions in synthetic steps¹. This leads with the traditional dendrimers always to polydiversity as known from unbranched polymers².

The synthetic approach developed by Hawker and Fréchet¹ offers cleaner and very homogenous dendrimers (fig. 3.1.1) (also see chapter 1).

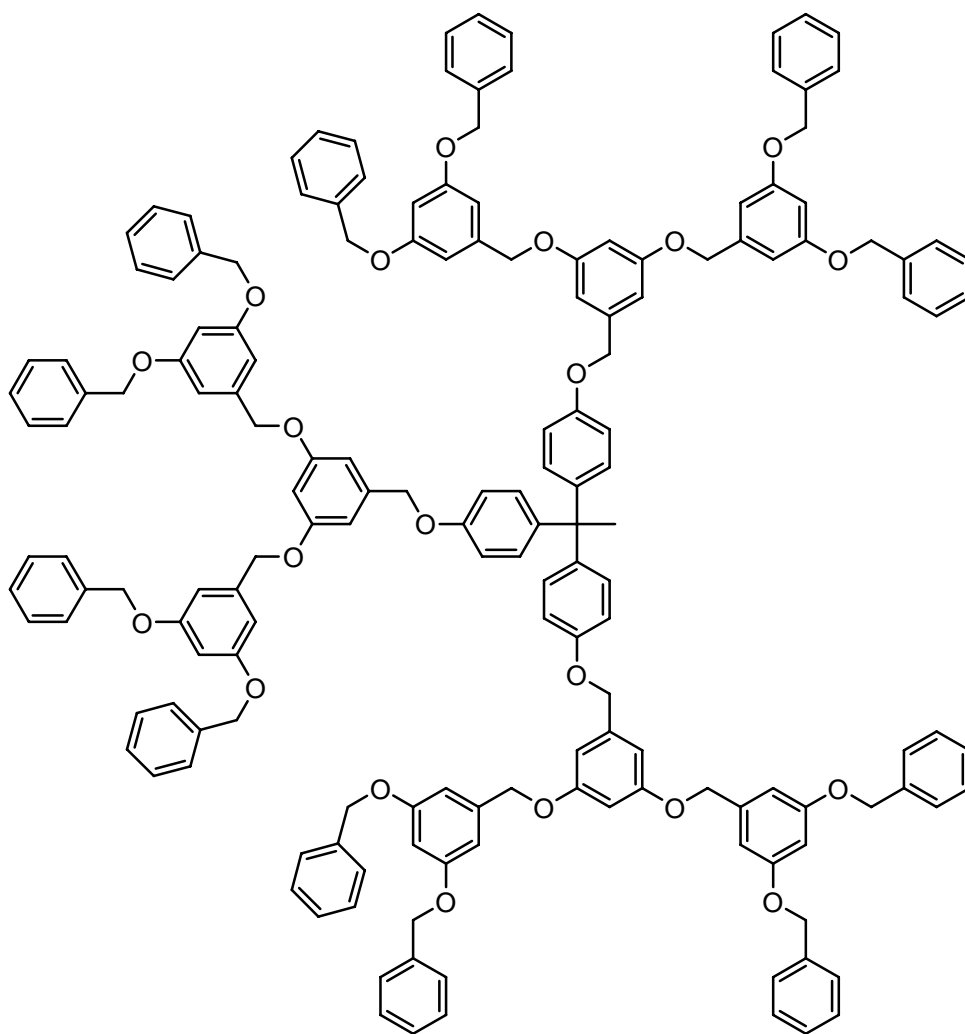


Fig. 3.1.1 Example of a Fréchet type dendrimer

Long hydrocarbon chains are known to adsorb on highly ordered pyrolytic graphite (HOPG) surfaces³⁻⁶ in an ordered fashion allowing analysis of the monolayers so formed by scanning tunnelling microscopy (STM). By switching the benzyl terminal groups of the

Fréchet type dendritic wedges¹ for n-octyl chains, dendritic wedges with high adsorption affinity to HOPG have been generated⁷.

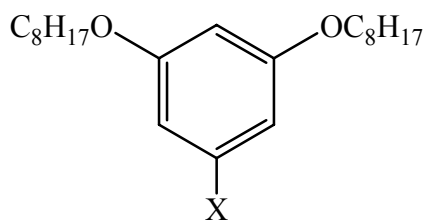


Fig. 3.1.2 The G1 dendritic wedge. The 1-position on the aromatic ring marking the place for modifications

The structure in fig. 3.1.2 is referred to as generation 1 (**G1**). The second generation dendritic wedge (**G2**) is shown in fig. 3.1.3.

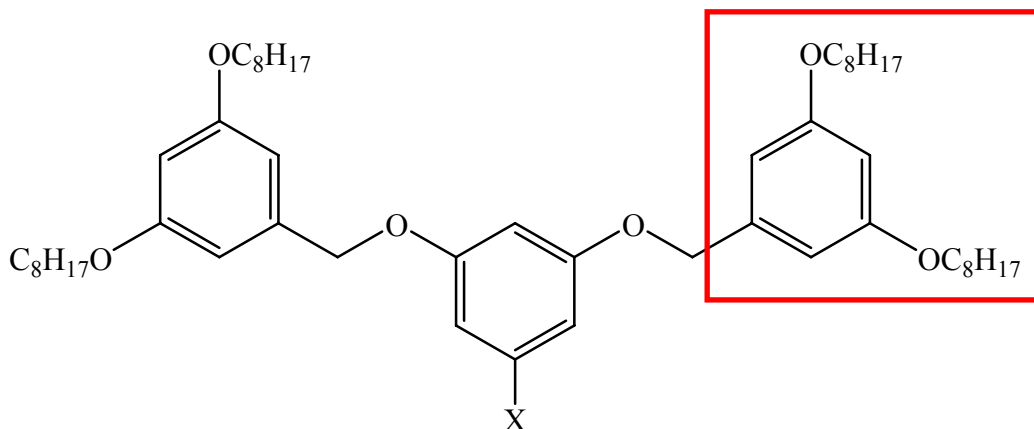


Fig. 3.1.3 The G2 dendritic wedge. The red rectangle marking the G1 unit

These dendritic wedges are very homogenous and have almost no polydiversity. These two properties make the dendritic wedges excellent model compounds for studying the driving forces for monolayer arrangement. The minimization of imperfections is very important in supporting the long range ordering.

Type of interaction	Typical energy (kJ/mol)
Ion – Ion	250
Hydrogen bonding	20
Dipole - dipole	2 - 0.3 (strongly molecule depending)
London forces	2

Table 3.1.1 Intermolecular forces and the average energy in kJ/mol (reproduced from ⁸)

Further insights into these mechanisms are important because the forces responsible for the final arrangement are weak dipole-dipole and London forces. Average energies for intermolecular interactions are given in table 3.1.1. Today's force fields for computational chemistry work quite well for ion-ion interactions and hydrogen bonds. The London and dipole-dipole interactions (which are an order of magnitude weaker than hydrogen bonds) are too weak to allow for an accurate prediction with current models and force fields. The degrees of freedom accompanying the long alkyl chains turn the situation from bad to worse. The interaction with the substrate is another point that is not easy to quantify by calculations since most methods do not allow for such parameters.

One of the frontier fields of computational chemistry is the area of crystal structure prediction (CSP). The excellent review by S. Price⁹ explains many of the key issues. Due to the frontier position of CSP, there is still a lot of basic research being conducted to gain further insights into the governing principles. To test the available systems for reliability, model compounds with known crystal structures are calculated to see if the computational structures are in agreement with the experimental data. The available models for calculations are still very rough though. They are only applicable to quite small and rigid organic molecules which interact with one another through hydrogen bonding. Compounds like the dendritic wedges with flexible n-octyl chains are beyond the scope of current calculations.

The strong interest in CSP comes from industry, especially the pharmaceutical industry. Many compounds show polymorphism. Polymorphs of one compound are chemically the same compound but crystallize in different forms. Different polymorphs can show very different physical behaviour. A prime example for this is diamond vs. graphite. While diamonds are the hardest natural material known to man, one of the biggest industrial applications for graphite is its use as a lubricant.

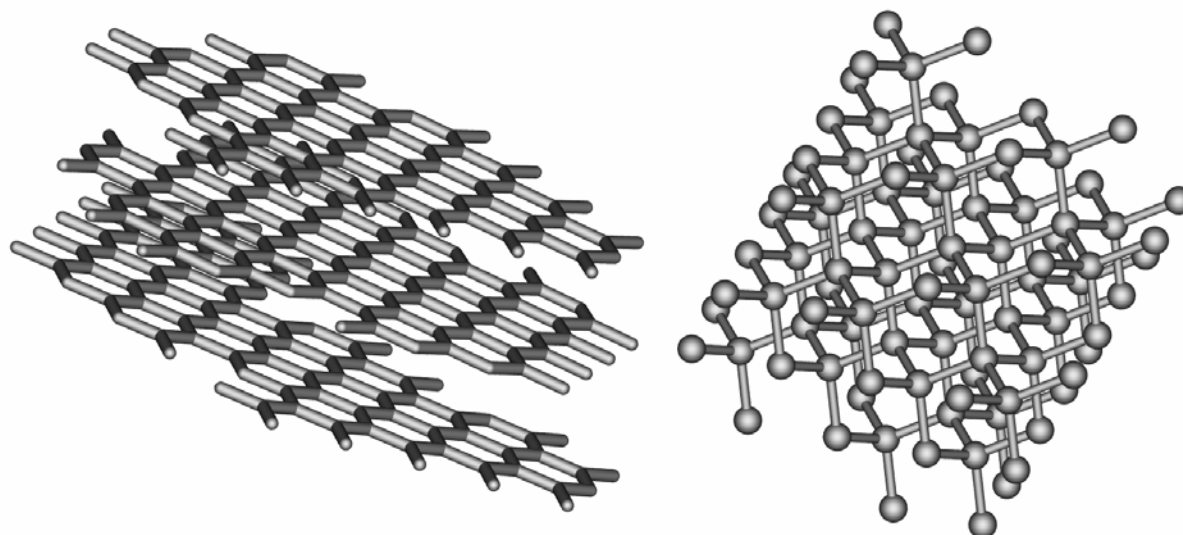


Fig. 3.1.4 The graphite form (left) and diamond form (right) of carbon. In graphite the planes are easily moved against each other due to the weak van-der-Waals forces between them. In the diamond lattice no such weak interactions are present; all carbon atoms are connected through strong covalent σ -bonds.

In pharmaceutical compounds, the biggest issue is the different solubilities of different polymorphs of the same compound. It is possible that through the solubilities, big differences in bioavailability and activity are expressed. Additionally each polymorph of the same compound is legally treated as a new compound. If a rival pharmaceutical company manages to find a previously unreported polymorph, the patent on that compound can be broken legally. Therefore, for a company that is applying for a patent on a compound, it is paramount to have found and characterised all possible polymorphs. CSP is a very promising technique towards polymorph prediction⁹. Some progress on polymorph prediction has been made but still many questions remain unanswered. It is observable that CSP returns too many possible polymorphs. An explanation for this is that the calculations are conducted at simulated 0 K. This leads actually to many different possible polymorphs⁹. Most of these polymorphs are not observable in experiments since the very small energy differences between some of the forms make them merge into one form at higher temperatures due to thermal motion of the atoms.

Since the models and force fields used are approximations to the quantum mechanically correct description of nature, they have to be constantly revised to check if they give a correct representation of reality. The approximations that cause errors in the calculations are, unfortunately, necessary to cut down on the time needed for the calculations. The correct quantum mechanical calculations are currently not solvable within a useful timeframe.

Obtaining empirical data is therefore of paramount importance to increase the number of examples to test the models against.

The available crystallographic data on the dendritic wedges in this present work is, unfortunately, very limited. The first generation wedges (fig. 3.1.2) are usually oils at room temperature but the second generation wedges (fig. 3.1.3) can be crystallised and structures for the alcohol, aldehyde and amine are known¹⁰. Since all three structures are very similar the functional group seems to be of only minor importance in the crystal lattice arrangement.

The possible formation of monolayers of these dendritic wedges on HOPG and analysis of the arrangements offers access to two dimensional crystallographic data. The restriction to two dimensions for the molecules offers easier analysis and interpretation of arrangements and lattices. Surprisingly, little modelling work is being done in this area. No publication could be found where the STM analysis followed the modelling. When modelling is being conducted, it is in most cases to get arguments for a proposed arrangement coming from an observed pattern.

An unanswered question that might explain some of the lack of modelling work is how much the substrate surface (HOPG in our case) templates the monolayer arrangements¹¹. An influence on the surface arrangement by the substrate has to be expected but the intermolecular forces should also not be neglected. If STM measurements at the liquid-solid interface are conducted the solvent is expected to have an additional influence. All these factors pose for today's modelling and computational systems problems that are nearly impossible to solve.

The structures shown with the figures 3.1.2 and 3.1.3 are the **G1** respectively **G2** dendritic wedges. To avoid generating polydiversity the **G1** wedge is synthesised first, cleaned and then used for the generation of the **G2** wedge.

The iterative divergent synthesis of these compounds can make the synthesis of sufficient quantities of generations beyond **G2** very costly for an only marginal improved chemical behaviour in respect to the formation of monolayers. This is known from a previous coworker in our research group who has been experimenting with **G3** compounds for the same intended purposes as the ones here in this work. His experiences with the **G3** compounds were disappointing and so the **G3** compounds were abandoned.

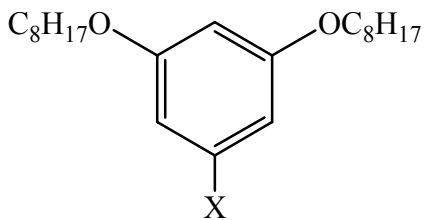
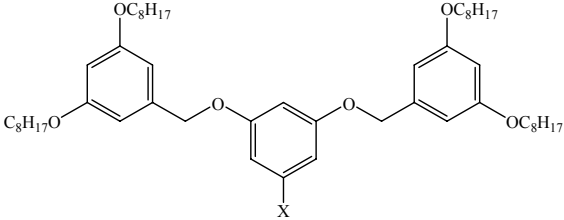
X	G1	G2
		
COOCH ₃	1	11
CH ₂ OH	2	12
CHO	4	14
CH ₂ Br	3	13
CH ₂ OSO ₂ CH ₃	5	

Table 3.1.2 Overview over the different **G1** and **G2** compounds and the assigned compound numbers

For the **G1** and **G2**, a wide variety of different functional groups in the 1 position of the aromatic ring are available; The methyl ester (**1**) / (**11**) ($X = \text{COOCH}_3$)¹², benzyl alcohol (**2**) / (**12**) ($X = \text{CH}_2\text{OH}$)¹², benzaldehyde (**4**) / (**14**) ($X = \text{CHO}$)⁷, benzyl bromide (**3**) / (**13**) ($X = \text{CH}_2\text{Br}$)¹⁰ and benzyl mesylate (**5**) ($X = \text{CH}_2\text{OSO}_2\text{CH}_3$)¹³ are reported and known. From these compounds many others are accessible, for example the carboxylic acid (**6**) as the ester hydrolysis product.

From the synthetic pathway the benzyl alcohol and carboxylic acid are readily available. The other derivatives require additional synthetic steps that reduce the overall yields. Scheme 3.1.5 gives an overview of the different syntheses for the derivatives, starting from the methyl ester.

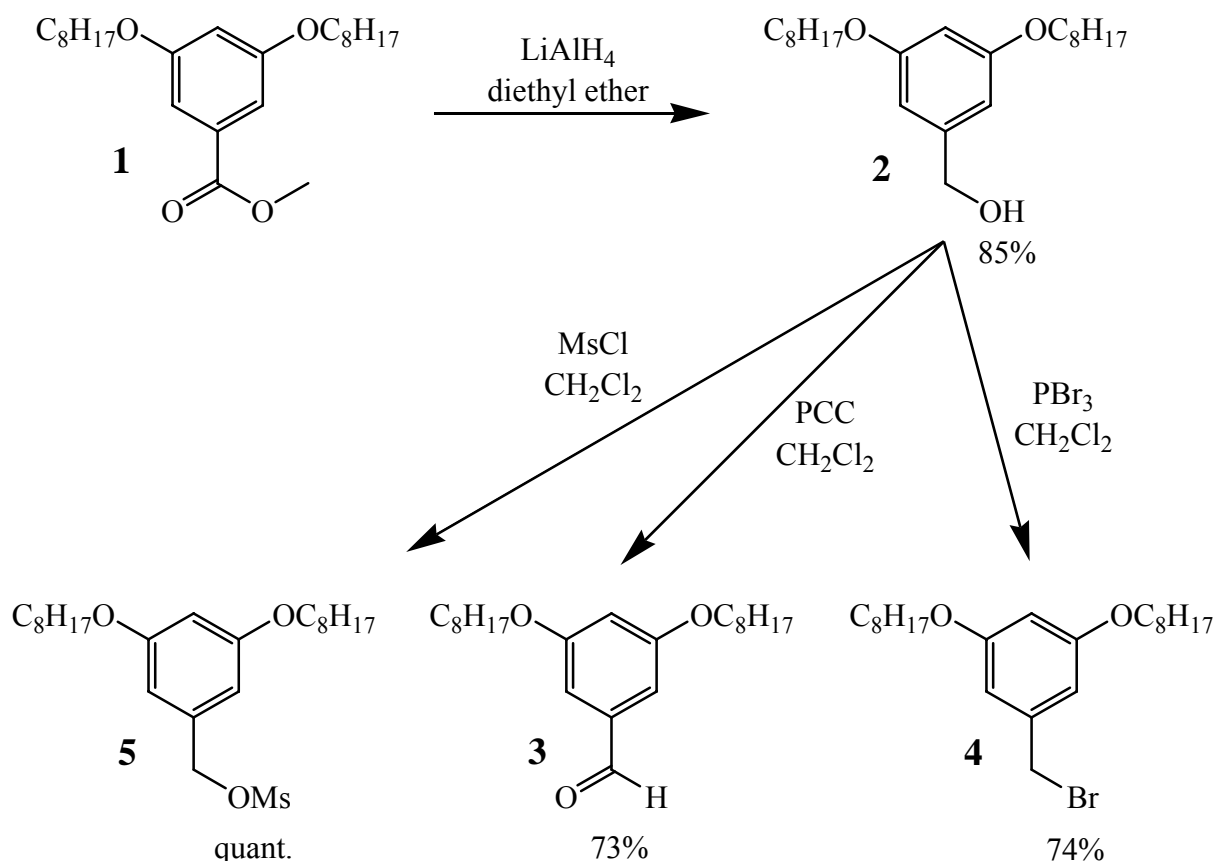


Fig. 3.1.5. Overview over the different terminal functional groups of the dendritic wedges.

($\text{Ms} = \text{CH}_3\text{SO}_2$, $\text{PCC} = \text{pyridinium chlorochromate}$)

Of the presented compounds, all have been reported in the literature. The **G1** carboxylic acid (**6**) has been synthesised but was not reported.

As also outlined in the STM chapter (see chapter 5), the octyl modified dendritic wedges are excellent candidates for adsorption on HOPG. Due to the surprisingly strong hydrocarbon-carbon interaction (each methylene group in the chains adds to the total force) the alkyl chains will adsorb onto a HOPG surface. Another big advantage of the selected system is that although the interactions of the compounds with the substrate are surprisingly strong, the adsorption strength is not so high that it could not be broken again. This reversibility allows for monolayers to rearrange, for example, from one polymorph to another⁷ but the aim was to allow the monolayer to repair defects that occurred during the formation. This would then give rise to large area, defect free, homogenous monolayers.

The 3,5-bis-RO- $\text{C}_6\text{H}_3\text{X}$ dendritic wedge has been chosen to increase the electron density in the aromatic rings. STM measurements record the tunnelling current between sample/substrate and tip. To generate a contrast, the sample needs to have a higher or lower electron density than the graphite surface. Since the alkyl chains already have a much lower electron density than the graphite substrate, they show up in the STM measurements as darker

areas. Similarly, the electron rich aromatic rings show as bright spots and a recognisable pattern is generated.

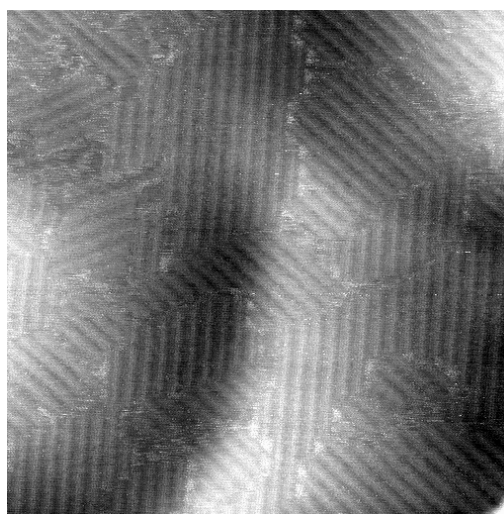


Fig. 3.1.6 STM image of G1-phthalimide (7) (150 x 150 nm). Clearly visible are the bright stripes of the aromatic systems and the darker stripes of the alkyl chains. Note the different arrangement domains of the sample on the surface.

An example for this is given in fig. 3.1.6. We can easily see the dark and bright stripes resulting from the alkyl chain respectively aromatic rings.

3.2 Aims

As outlined in the introduction, the Fréchet-type dendritic wedges are a very promising target for the formation of monolayers on HOPG. The easy and reasonably yielding syntheses that can be scaled up readily making the 3,5-bis(octyloxy)benzene compounds an obvious choice as primary building blocks. An extension to the known functionalisations of the dendritic wedges was targeted, especially the synthesis of the amino derivatives, and special functionalisations of the dendritic wedges.

Additionally, the synthesis of didendritic wedges was proposed to gain further insights into surface arrangements and offered a strong binding unit for surface adsorption that would offer in situ surface modification possibilities.

3.3 Synthesis

The syntheses of many of the dendritic wedges have been reported and will therefore not be discussed here in detail (see fig. 3.1.5). Starting from the commercially available 3,5-dihydroxybenzoic acid the methyl ester is generated¹⁴. This compound is the core unit for the **G1** as well as any further generation. It is convenient that this synthesis is easy to scale up to a 100 g scale or more. The next step is the formation of the ether linkage in the chains. This is done by a relatively mild reaction of methyl 3,5-dihydroxybenzoate and 1-bromooctane. As a base, potassium carbonate is used¹⁵. This mild method has the advantage that the ester group is stable under these conditions. The use of not overly reactive reagents in the reaction allows for very easy scale up of the reaction. The most important practical consideration is that the stirring of the reaction has to be optimised since the heterogeneous conditions require efficient stirring of the reactants.

The biggest concern regarding the homogeneity of the dendritic wedges arises from the use of 1-bromooctane. Even though the starting material was bought in the highest purity, contaminations with branched bromooctane isomers are likely to occur. These undesired compounds cannot be removed before the reaction as their physical properties are too similar.

The crystallisation of the ester allows removal of such undesired side products and so one can continue on with the compound containing purely n-octyl chains. The homogeneity of the n-octyl chains has been confirmed by several crystal structures of follow up compounds.

The reduction of the ester group with lithium aluminium hydride was done as described in by P. B. Rheiner and D. Seebach¹².

The central group does not necessarily have to be the methyl ester. A direct coupling of the chains to 3,5-dihydroxybenzyl alcohol is possible due to the much higher pK_a of the benzyl alcohol (≈ 15) compared to the aromatic hydroxyl groups (≈ 10). But purification of the first generation ester is much easier since it can be done by crystallisation. The first generation benzyl alcohol is liquid at room temperature. Even though the **G2** alcohol (**12**) would be a solid at room temperature purification by crystallisation is not an option for this compound due to the long crystallization times. Chromatography on the other hand allows relatively large amounts of compound to be purified at once with excellent resolution.

The stationary phase for chromatography is silica. The interaction of the silica OH groups with the compound OH group leads to unnecessary broadening of the chromatography band reducing the effectiveness of the separation method. This is avoided by using the **G2** ester (**11**) instead.

The reductions of the ester compounds **(1)** / **(11)** with lithium aluminium hydride work quantitatively and are reliable.

The benzyl alcohol is the basis for most of the further modifications. By mesylation of the alcohol¹³ a very reactive electrophile (fig. 3.3.1) is generated that is then for example, used to form the second generation dendritic wedge.

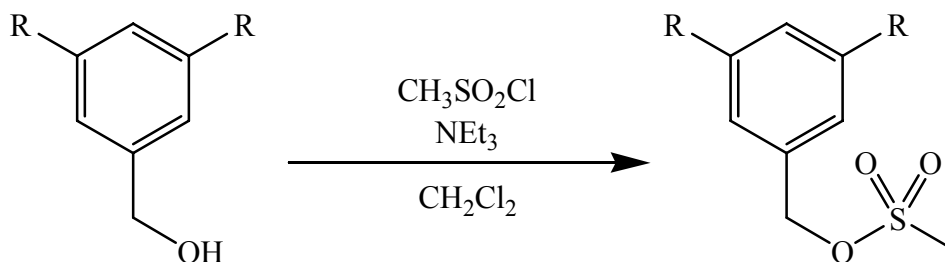


Fig. 3.3.1 Mesylation reaction (valid for first and second generations)

The same product could also be obtained by turning the benzyl alcohol into the benzyl bromide but the yields for the bromide formation were unsatisfactory considering the large amounts of compound needed for the second generation formation. However, the bromide has the big advantage that it can be purified and is storable. The mesylate is too reactive and has a tendency to decompose. The second generation dendritic wedge is formed by the same reaction as the coupling of the alkyl chains to the aromatic core unit. The mesylate is reacted with methyl 3,5-dihydroxy benzoic ester in the presence of potassium carbonate. To enhance the basicity of the potassium carbonate, small amounts of 18-crown-6 are added to the reaction¹.

The aldehyde **(4)** / **(14)** (see table 3.1.2) is synthesised by an oxidation with pyridiniumchlorochromate (PCC)⁷. This method has proven to be reliable and is high yielding. Precautions have to be taken to ensure that the reaction conditions are water free. In the presence of water, the oxidation continues and the acid is formed.

The bromide **(3)** / **(13)** is formed by a reaction of the benzyl alcohol with phosphorus tribromide¹⁶.

Following the concept of F. Vögtle et al.¹⁷ the benzyl amine **(8)** / **(16)** was synthesised in two steps via the phthalimide derivatives **(7)** / **(15)**. The benzyl bromide is reacted with potassium phthalimide as shown in fig. 3.3.2.

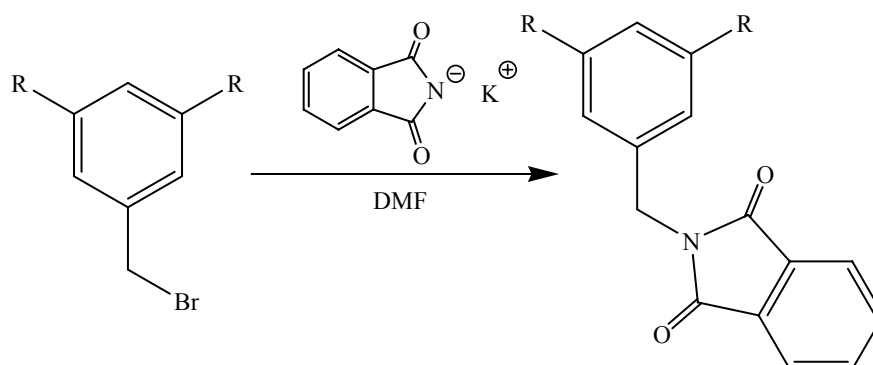


Fig. 3.3.2 Formation of the dendritic phthalimide derivate

This product is then converted to the benzylamine by reaction with hydrazine.

The same reactions also work for the second generation dendritic wedges. Sometimes smaller yields have to be accepted. The reason for this is not always clear, but the most likely reason is that the higher steric demand of the bigger wedge reduces the availability of the functional group at the core unit.

Compound functional group	G1 yield	G2 yield
Aldehyde	73%	80%
Bromide	74%	53%
Phthalimide	83%	95%
Amine	95%	77%

Table 3.3.1 Average yields for the conversions of the functional groups.

Table 3.3.1 contains the average yields for some of the functional group conversions. In general, the conversions are comparable between the generations concerning yields. Some comments have to be made though.

For the aldehyde formation in the **G1** series, when the first two reactions of the series are taken out of the statistics, the average yield increases to 80% and becomes equal to the **G2** reaction. For the phthalimide reaction if one of the reactions is ignored in the statistics in the **G1** series, the yield is increased to 95%. Some statistical outliers have to be expected and unfortunately have a strong influence on the statistics considering the very small pool of data used in some cases. The bromide synthesis, for which a bigger set of data is available, clearly shows a reduced yield for the formation of the second generation. Apart from steric reasons being responsible for the smaller yield, no other reasons are obvious for this observation.

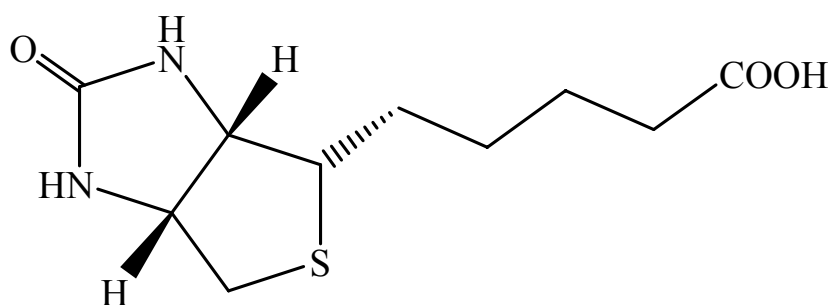


Fig. 3.3.3 Structure of biotin

The first and second generation dendritic wedges were both modified with biotin (fig. 3.3.3). This was achieved by a coupling assisted by N,N' -carbonyldiimidazole as described by Garlick and Giese¹⁸. Notably, the dendritic wedge coupled to the biotin had a very favourable influence on the solubility of biotin so that highly resolved NMR spectra of biotin could be obtained. These syntheses were performed for Prof. Bianca Hermann of the TU in Munich as part of a collaboration. The aim was to study biotin-avidin coupling on a graphite surface. The compounds (**9**) and (**17**) (fig. 3.3.4, 3.3.5) were fully characterised using the standard techniques of NMR, IR, MS and microanalysis.

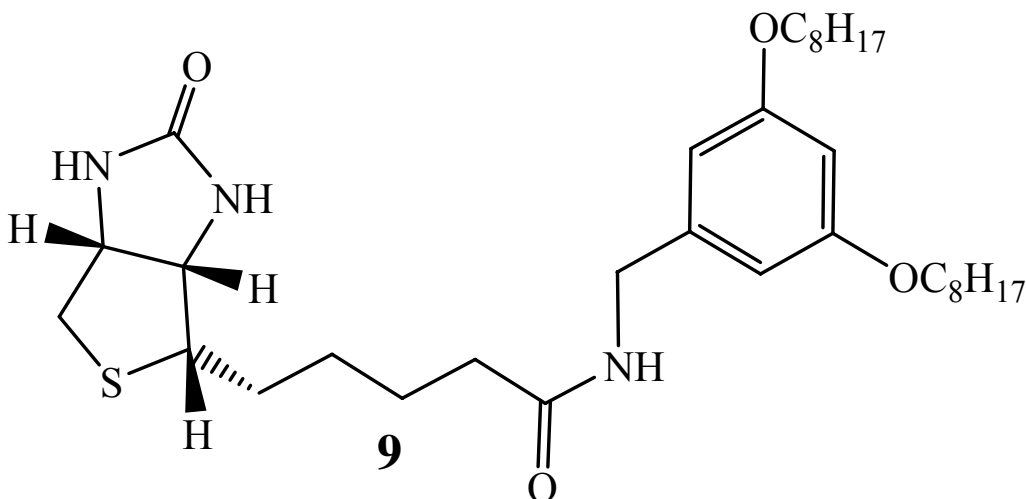


Fig. 3.3.4 Structure of compound (**9**)

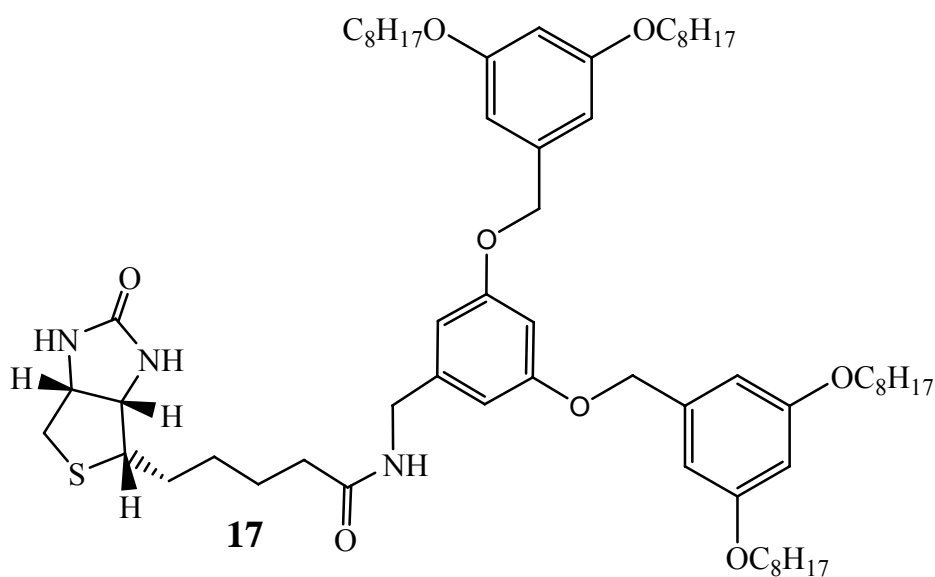


Fig. 3.3.5 Structure of compound (17)

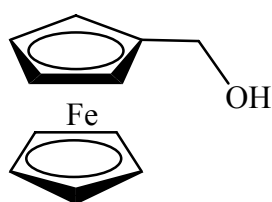


Fig. 3.3.6 Structure of ferrocenemethanol

Also for use by Prof. Hermann, a ferrocene derivative with a dendritic wedge was synthesised. Ferrocenemethanol (fig. 3.3.6) was treated with sodium hydride and then reacted with **G1** bromide. This procedure was repeated for the **G2** derivative.

Again both structures (**10**), (**18**) (fig. 3.3.7 and 3.3.8) were fully characterised with standard of NMR, IR, MS and microanalysis. Due to overlapping peaks in the NMR spectrum, a full assignment was not possible.

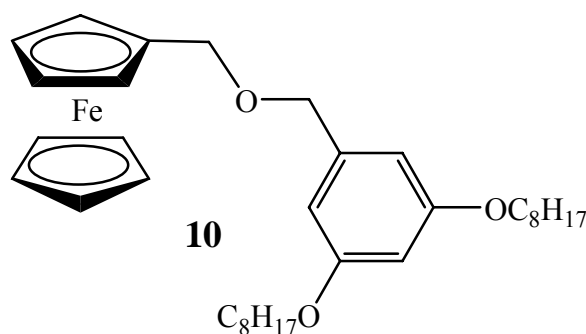


Fig. 3.3.7 Structure of compound (10)

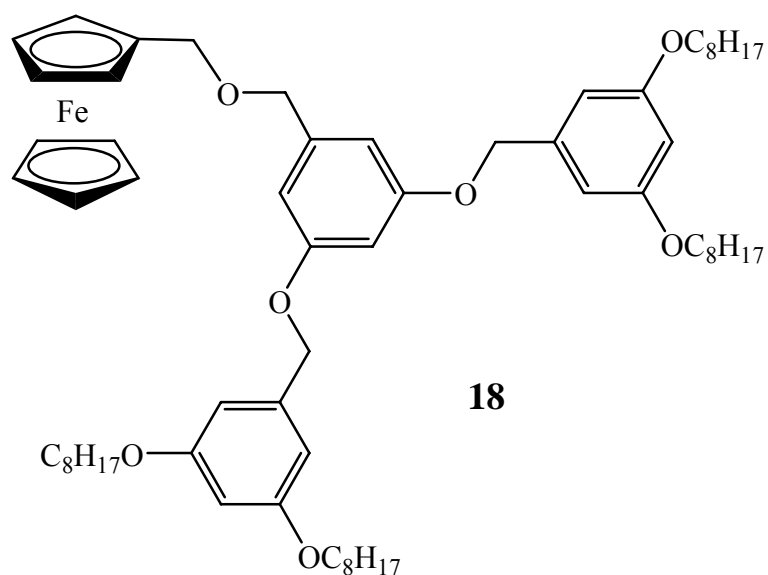


Fig. 3.3.8 Structure of compound (18)

3.4 Dendritic wedge compounds

To gain further insights into the arrangement of the dendritic wedges on the HOPG surface the synthesis of symmetrical molecules with two dendritic wedges was proposed. To offer the possibility at studying the influences of surface modification, the desired molecule was designed to have a central functional group that would allow for an easy, and preferably reversible, modification.

The first synthesis attempted for such a compound was conducted starting from dimethyl 3-oxopentanedioate. The keto group was reduced with sodium borohydrate and the resulting alcohol was then protected as the tetrahydropyran ether (fig 3.4.1). The resulting compound was then treated with lithium aluminium hydride to reduce the ester groups to alcohols.

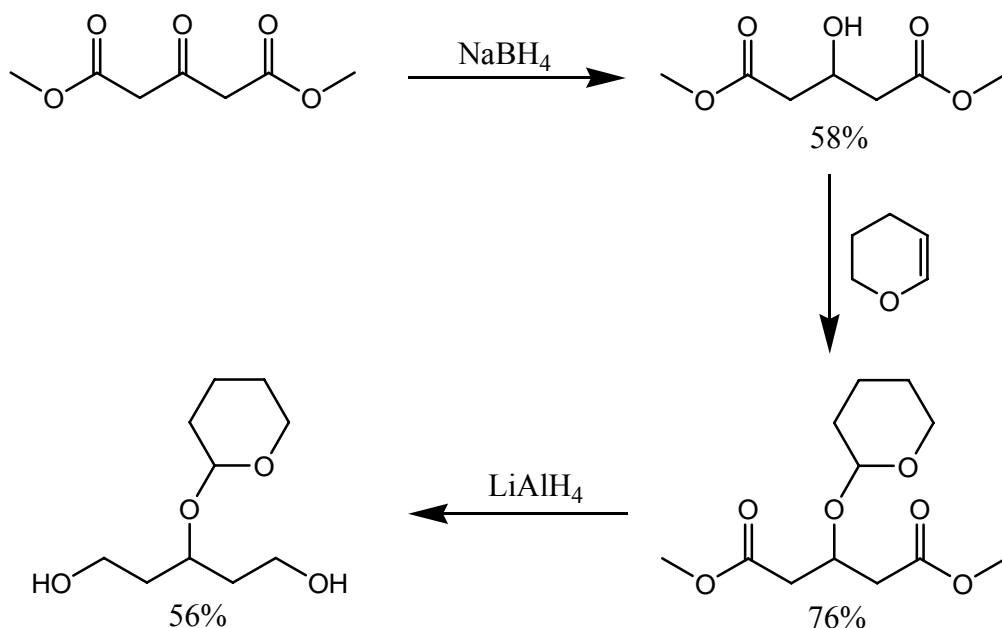


Fig. 3.41 Synthesis of the THP protected diol

Several different methods were tried to couple the dendritic wedges to the alcohol groups were tried but no one showed success. One method was over potassium carbonate as base and the 3,5-bis(2-oxoethyl)benzyl bromide. This method failed due to insufficient base strength of the potassium carbonate. Turning the alcohols over into the sodium alkoxide did not lead to the desired product. By a mechanistically obscure pathway, the dendritic aldehyde was generated and reisolated.

Turning the nucleophilicity and electrophilicity around, the alcohols on the core unit were tosylated and reacted with the sodium 3,5-bis(2-oxoethyl)benzyl alkoxide. This reaction did not yield the desired product due to lack of reactivity of the tosylate since a lot of the reisolated compound was unreacted tosylate.

An attempt to generate the ester from the dendritic acid chloride was also a failure. In this case it is proposed that the formation of the acid chloride failed. A confirmation of this could not be obtained due to the sensitivity of acid chlorides towards hydrolysis. A second attempt at the ester formation by using the coupling reagent N,N' -carbonyldiimidazole showed no positive result. Though that method works well for amide formation, the alcohol group probably lacks nucleophilicity to drive the reaction to completion.

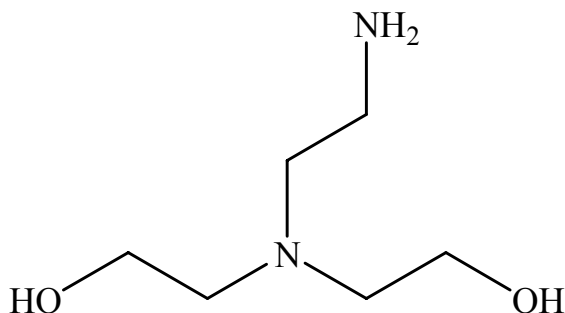


Fig. 3.4.2 Structure of *N,N*-bis(2-hydroxyethyl)ethylenediamine

Due to the lack of positive results, this synthetic pathway was abandoned and a new core unit selected. *N,N*-Bis(2-hydroxyethyl)ethylenediamine (fig. 3.4.2) was selected due to its alcohol groups and the primary amine. The conclusion from some of the failures from the first core unit was that for some reactions, the THP alcohol protection group was too labile and caused some synthetic problems due to severe limitations in the choice of reagents.

The new core unit also did not yield the desired product. Most of the coupling reactions tried with the first core unit were repeated with the new unit and additionally mesylation of the dendritic alcohol was done and that mesylate was then reacted with the alcohol groups of the core unit. This method was only possible because the amine protection group used (*tert.*-butylcarbamate, Boc) is stable under mild acidic conditions.

Because of the lack of useful results with this second synthesis path it was decided to abandon the diol core units and take a completely different approach to this synthetic problem.

The new goal was a didendritic molecule with a functional group in the middle which could then be transformed into a second group better suited for surface modification.

The allylation of the dendritic wedges appeared to be promising followed a Grubbs metathesis to form the central double bond which could be modified by a cyclopropanation reaction. The allylation worked excellent for first and second generation dendritic wedges.

But the Grubbs metathesis was a failure for both generations due a rearrangement of the double bond that happened instead of the planed reaction. M. Arisawa et al.¹⁹ described this competitive reaction (fig. 3.4.3).

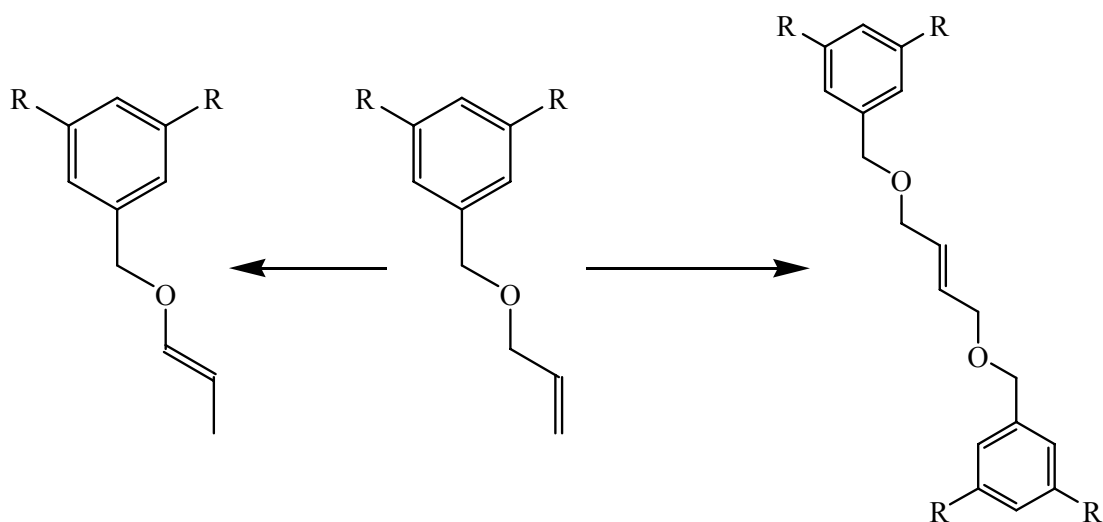


Fig. 3.4.3 The two possible reactions starting from the educt (middle). To the left the rearrangement product, right the desired product

For the first generation dendritic wedge small quantities of product could be isolated. The second generation dendritic wedge showed almost exclusively the rearrangement product. In both cases the yields were too low to justify a continuation of this synthetic plan. Additionally a test reaction of the cyclopropanation with the first generation didendritic wedge confirmed expectations of very low yields raised by the textbook by B. F. Trost²⁰. Consequently this synthetic path was considered not effective.

A completely different approach was then chosen and a synthetic route by Sonogashira coupling reactions was devised. These reactions offer high yields, are very selective and are done under relatively mild conditions. The alkyne groups involved in Sonogashira couplings allow for long rod like parts in the molecule and are also very electron rich which is useful for detection in STM measurements. As starting material, 1-bromo-3,5-dimethoxybenzene was selected.

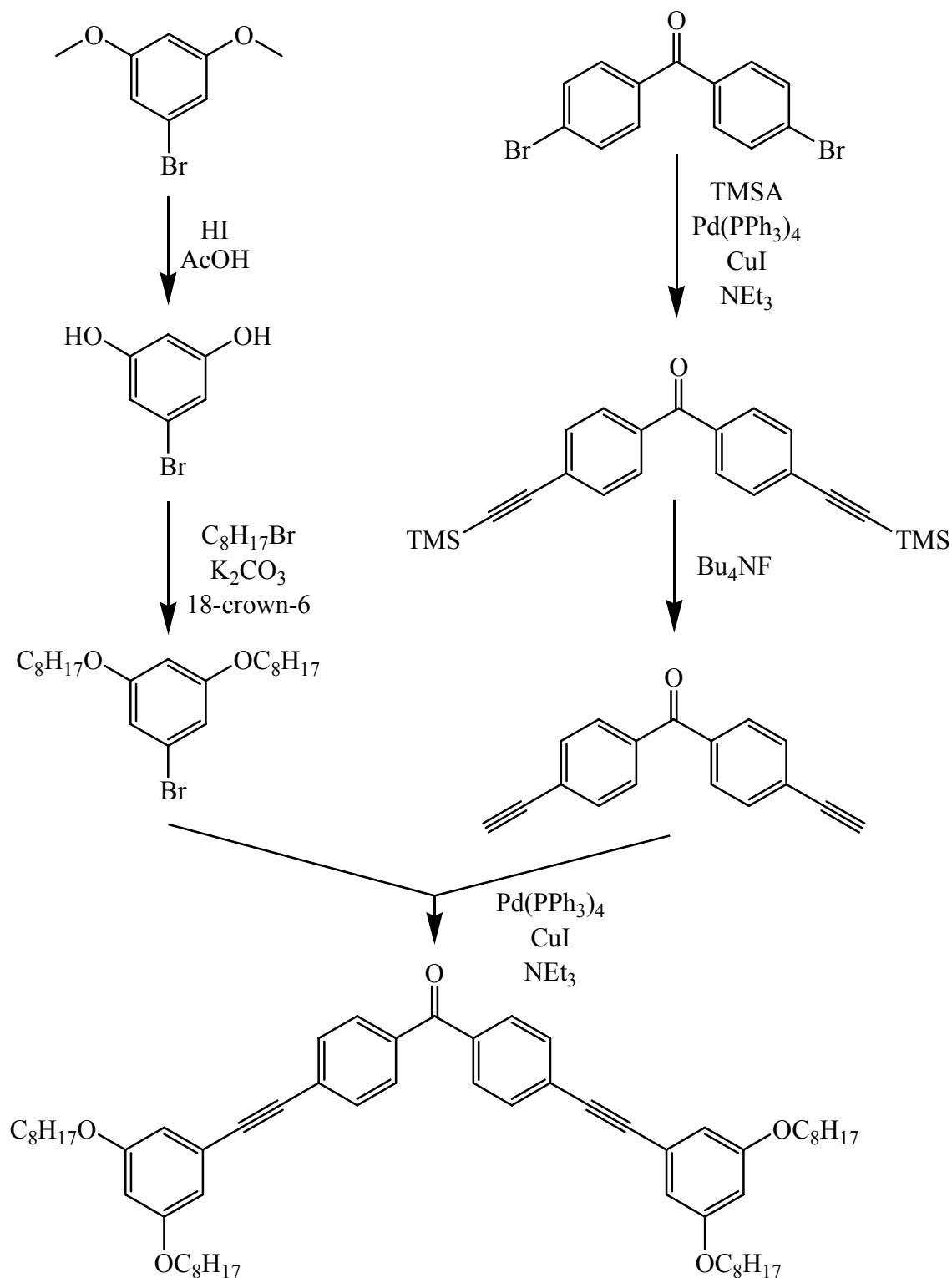


Fig. 3.4.4 Sonogashira synthetic pathway to a didendritic molecule

To do the Sonogashira coupling reactions before the cleavage of the methoxy groups was not possible since the triple bond has shown to be reactive under the harsh conditions needed for the cleavage. The best method for the cleavage of the methoxy groups proved to be concentrated hydroiodic acid and concentrated acetic acid at reflux²¹. The selected core unit

was 4,4'-dibromobenzophenone. A. Avent et al²² did work with similar compounds and also showed that the keto group of the core unit can be turned into the Schiff base allowing for easy modifications. The final synthetic plan is shown in fig. 3.4.4.

Due to most likely steric reasons the last coupling reaction only gave very small yields. This and the high costs for materials (4,4'-dibromobenzophenone, Pd-catalyst) this project was considered to be not economical. Especially if the conclusions about the steric reasons for the low yield are right, expanding this synthesis to the second generation is questionable.

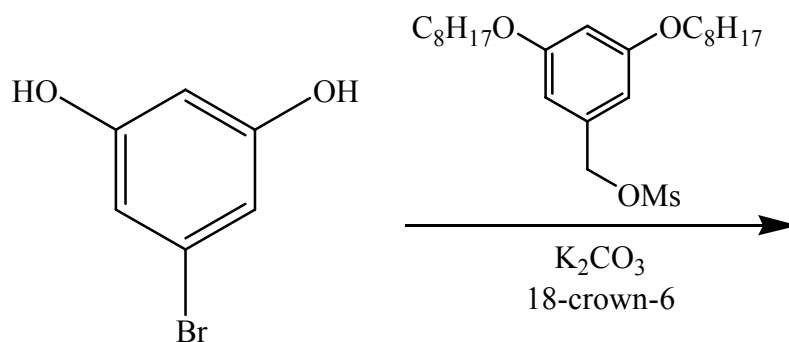


Fig. 3.4.5. Formation of **G2** bromide for the didendritic wedge

The synthesis of the **G2** wedge showed another problem. Due to the reactivity of the bromide, a selfreaction can occur and forms a polymeric product (fig. 3.4.5). This was observed as the main product and only minor amounts of the desired product could be isolated.

3.5 Results and Conclusions

The syntheses of the dendritic wedges are efficient and high yielding. Simple functional group transformations using a wide variety of different functional groups are accessible and are suitable for almost any purpose.

Perhaps the most severe drawback in the convergent synthesis is a relatively high wastage of first generation material in the synthesis of the second generation compound.

C. Hawker and J. M. Fréchet¹ have pointed out the big advantages of the convergent synthesis approach compared to the starburst synthesis of conventional dendrimers.

The starburst synthesis starts with the core unit and assembles the generations from the core out. This method is generally simple and allows reaching high generations and molecular

weight quiet easily. But the drawbacks to these advantages are loss of control and therefore polydiversity due to incomplete reactions. Also very often the purification can pose problems since to drive each generation reaction to completion as far as possible big excess amounts of reagents are used.

The convergent approach devised by Hawker and Fréchet calls for a stepwise, very controlled synthesis of the dendrimer branches or wedges that allows sorting out wedges where the coupling of the next generation was not complete. Also a much smaller excess of reagent in each coupling step is necessary which simplifies purification after each step.

This means a Fréchet dendrimer is generally cleaner and with a very low mass distribution making predictions on the structure much more accurate, reliable and repeatable.

formula	C ₂₄ H ₄₀ O ₄
formula weight	392.58
Z	4
calculated density	1.141 Mg · m ⁻³
F(000)	864
description and size of crystal	colourless plate, 0.11 · 0.22 · 0.32 mm
absorption coefficient	0.075 mm ⁻¹
min/max transmission	0.98 / 0.99
temperature	173K
radiation(wavelength)	Mo K α (λ = 0.71073 Å)
Crystal system, space group	monoclinic, <i>P</i> 2 ₁ / <i>n</i>
a	5.37150(10) Å
b	18.5310(4) Å
c	23.0801(4) Å
α	90°
β	95.6726(12)°
γ	90°
V	2286.13(8) Å ³
min/max Θ	1.412° / 27.476°
number of collected reflections	19344
number of independent reflections	5211 (merging <i>r</i> = 0.029)
number of observed reflections	2674 (<i>I</i> > 2.00 σ (<i>I</i>))
number of refined parameters	253
<i>r</i>	0.0432
<i>r</i> W	0.0656
goodness of fit	1.0037

Table 3.5.1 Crystallographic data for the **G1** ester (**1**)

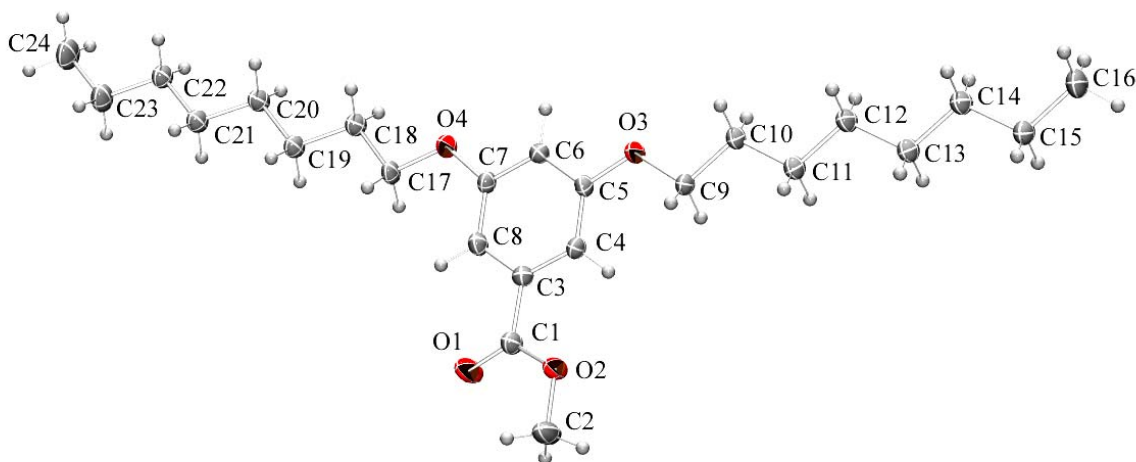


Fig. 3.5.1 ORTEP representation of **G1** ester (**1**) with atom labels

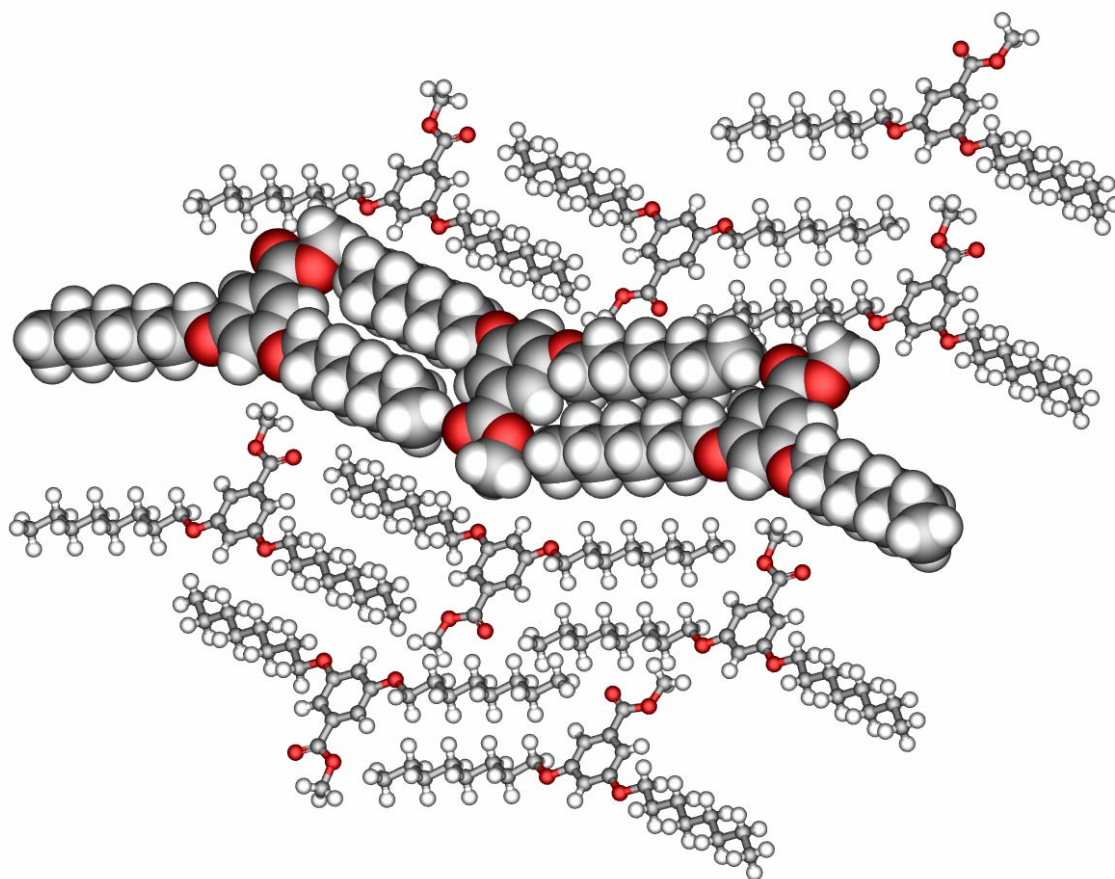


Fig. 3.5.2 Crystal structure of the **G1** ester (**1**). One of the ribbons is in a space filling representation.

For the **G1** ester (**1**) a single crystal structure was obtained. The crystal was grown from a saturated acetone solution. There are some differences compared to the packing of the **G2** amine (**16**) (see fig. 3.5.5 and 3.5.6). The most important difference is that the crystal is not

composed of densely packed planes but of ribbons. In fig. 3.5.3 one of these ribbons is shown in space filling representation. These ribbons are displaced from each other, most likely because of the steric demand of the methyl group of the ester giving a stair like appearance.

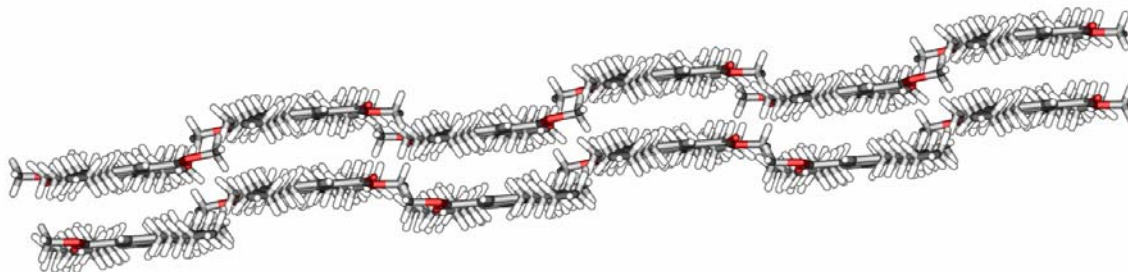


Fig. 3.5.3 *G1 ester (1)*. Sideview onto the ribbons.

formula	$C_{53}H_{84}N_1O_6$
formula weight	831.25
Z	2
calculated density	$1.110 \text{ Mg} \cdot \text{m}^{-3}$
F(000)	914
description and size of crystal	colorless plate, $0.06 \cdot 0.14 \cdot 0.48 \text{ mm}$
absorption coefficient	0.070 mm^{-1}
min/max transmission	0.99 / 1.00
temperature	173K
radiation(wavelength)	Mo $K\alpha$ ($\lambda = 0.71073 \text{ \AA}$)
Crystal system, space group	triclinic, $P - 1$
a	$10.3597(4) \text{ \AA}$
b	$15.6450(5) \text{ \AA}$
c	$16.5620(7) \text{ \AA}$
α	$99.984(2)^\circ$
β	$103.5202(19)^\circ$
γ	$101.540(2)^\circ$
V	$2487.97(17) \text{ \AA}^3$
min/max Θ	$1.365^\circ / 27.507^\circ$
number of collected reflections	21917
number of independent reflections	11397 (merging $r = 0.021$)
number of observed reflections	5423 ($I > 1.50\sigma(I)$)
number of refined parameters	541
r	0.0701
rW	0.1262
goodness of fit	1.107

Table 3.5.2 Crystallographic data for the *G2 amine (16)*

The known functional group library is extended by the amine, further expanding the number of possible modifications. The synthesis of the amine dendritic wedges is straight forward and high yielding. For the **G2** amine a crystal structure was obtained. The material was crystallised from the bulk.

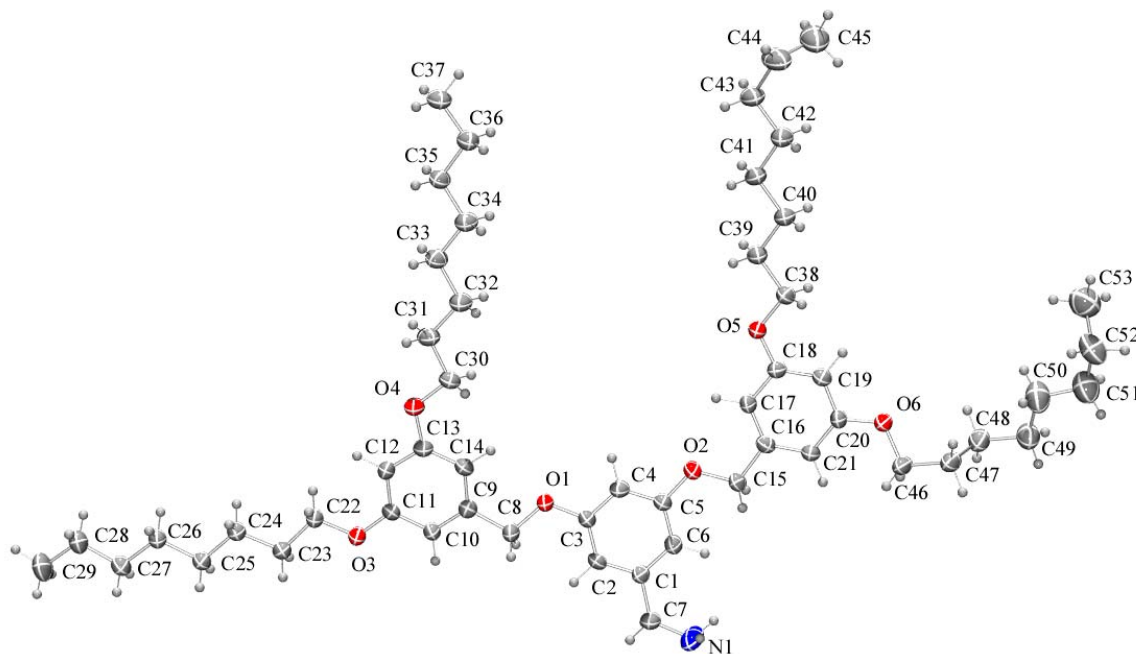


Fig. 3.5.4 ORTEP representation of the **G2** amine with atom labels

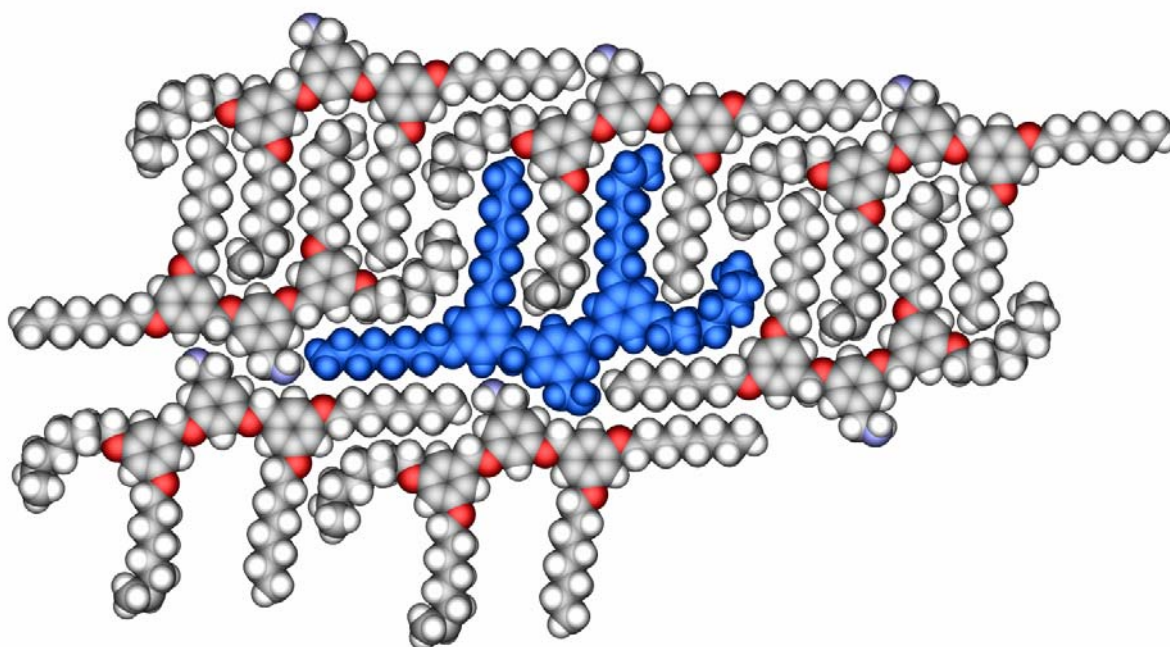
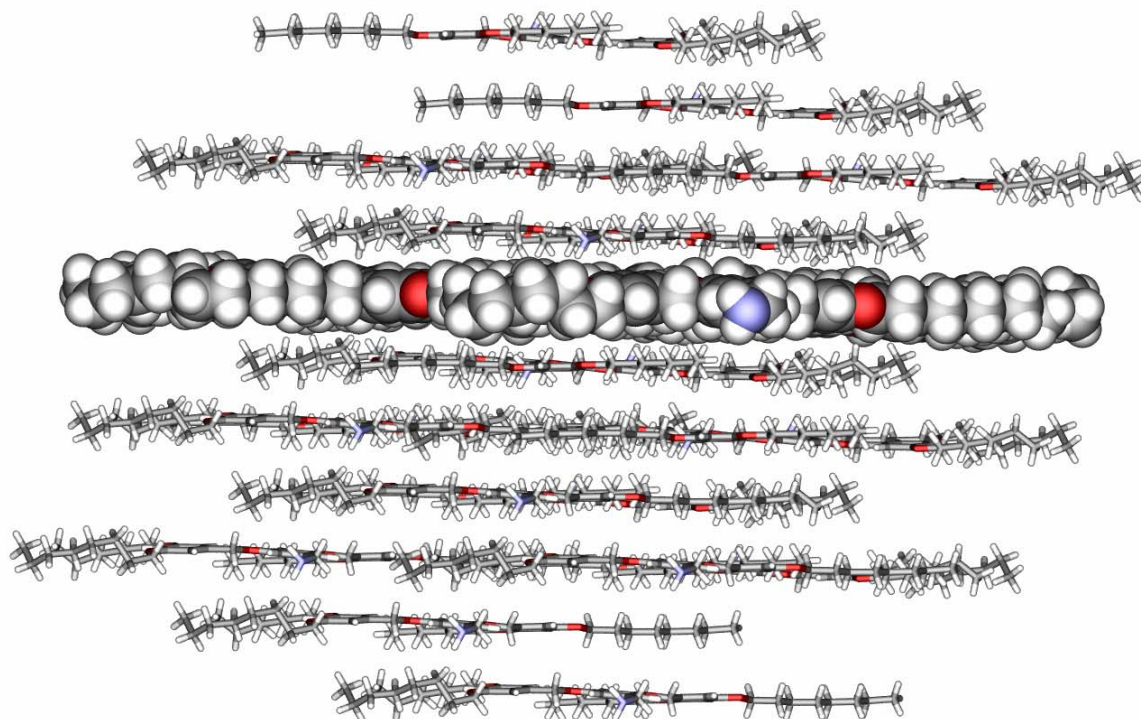


Fig. 3.5.5 Picture out of one plane from the crystal lattice of the **G2** amine. For better visibility one molecule is coloured blue.

Fig. 3.5.5 is an extract from the crystal structure of the **G2** amine compound. The packing within the planes and also between the flat planes (fig. 3.5.6) is very dense. The structure is very similar to the ones obtained by L. Scherer of the **G2** alcohol (**12**) and aldehyde (**14**). In fact all three structures are remarkably similar¹⁰.



*Fig. 3.5.6 Sideview onto the crystal lattice of the **G2** amine. Visible are the different, densely packed planes. For better visibility only one plane is in spacefilling.*

The high similarity of crystal structures of the three different compounds lead us to believe that in these cases the forces governing the arrangement are primarily from London interactions. This is also supported by the observation of structures in the STM that correlated very well with the crystal structures of these compounds. It can be concluded that in these cases the graphite surface is not involved in the formation of a long distance order for these molecules.

In addition to the known crystal structure of the **G2** aldehyde (**14**) a second polymorph was found. This second polymorph is more ordered in respect to the alkyl chains than the previously reported one (fig. 3.5.8).

formula	C ₅₃ H ₈₂ O ₇
formula weight	831.23
Z	2
calculated density	1.099 Mg · m ⁻³
F(000)	912
description and size of crystal	colourless block, 0.07 · 0.11 · 0.23 mm
absorption coefficient	0.071 mm ⁻¹
min/max transmission	0.99 / 1.00
temperature	223K
radiation(wavelength)	Mo K α ($\lambda = 0.71073 \text{ \AA}$)
Crystal system, space group	triclinic, <i>P</i> -1
a [\AA]	10.423(8)
b [\AA]	16.185(15)
c [\AA]	16.326(12)
α [$^\circ$]	102.85(6)
β [$^\circ$]	102.14(7)
γ [$^\circ$]	103.38(7)
V [\AA^3]	2511(4)
min/max Θ	1.603 $^\circ$ / 30.652 $^\circ$
number of collected reflections	38407
number of independent reflections	14932 (merging $r = 0.053$)
number of observed reflections	4402 ($I > 2.0\sigma(I)$)
number of refined parameters	614
r	0.0653
rW	0.2139
goodness of fit	1.1712

Table 3.5.3 Crystallographic data for the new polymorph of the **G2** aldehyde

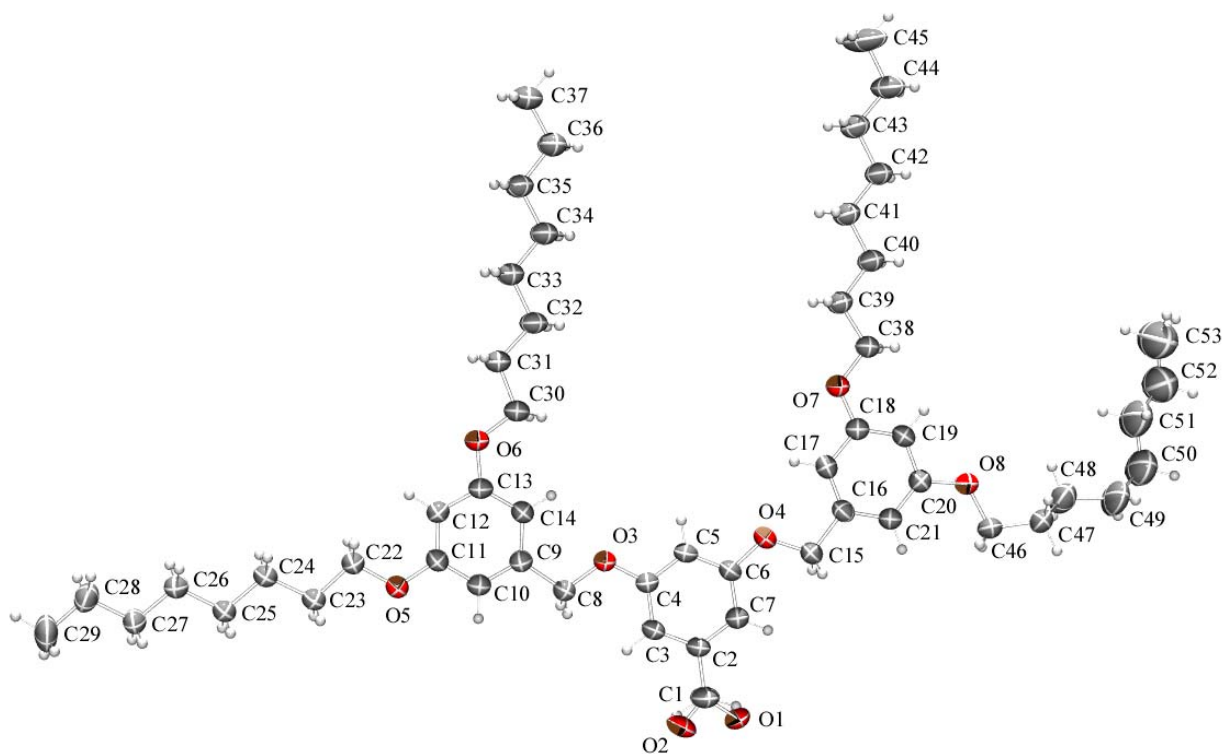


Fig. 3.5.7 ORTEP representation of the new **G2** aldehyde polymorph 2. The chain C46-C53 is disordered and only the major occupancy sites are shown.

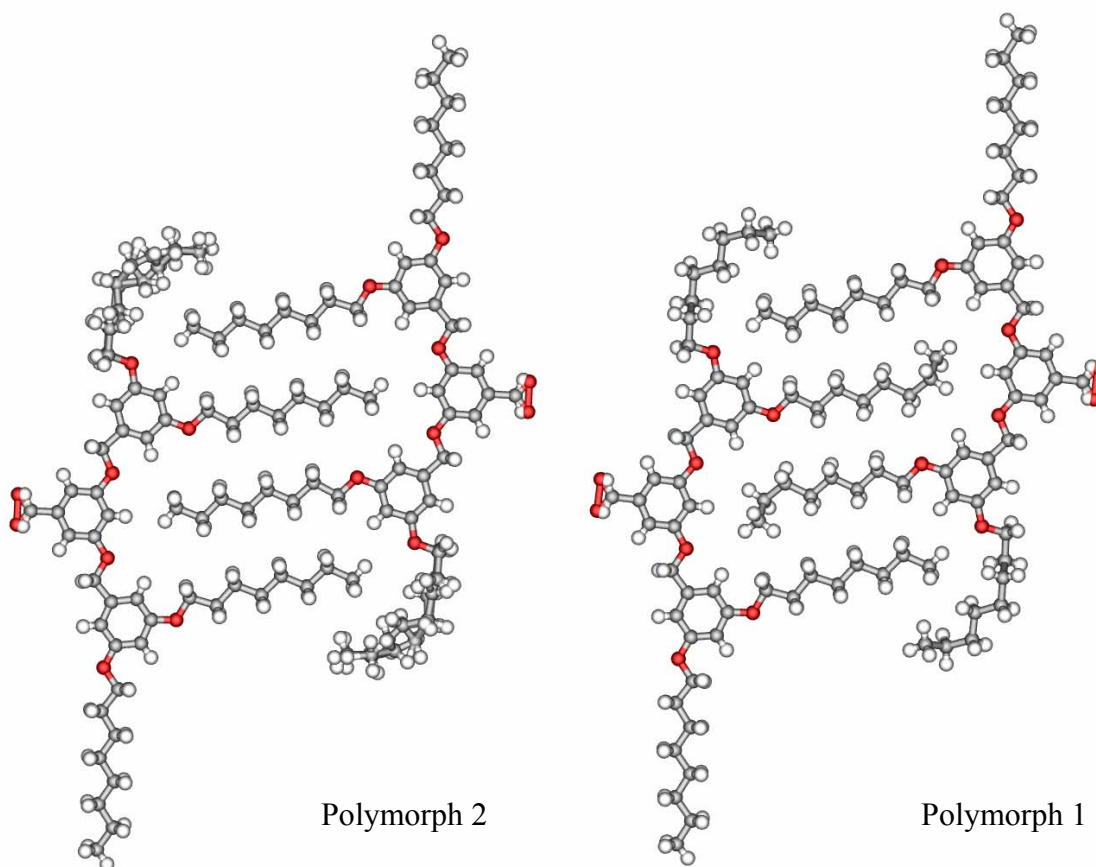


Fig. 3.5.8 The two different polymorphs of the **G2** aldehyde. The new form (left) and the previously reported one¹⁰ (right)

As is visible from fig. 3.5.8 the differences between the two forms are minimal. Basically only the end methyl group of one of the chains has different conformation. Even so, it is remarkable that this small change still has an influence on the crystal unit cell as shown in table 3.5.4.

	Polymorph 2	Polymorph 1	Δ	Δ (%)
Crystal system, space group	triclinic, P -1	triclinic, P -1		
a [Å]	10.423	10.4431	-0.020	-0.19
b [Å]	16.185	15.5189	0.666	4.12
c [Å]	16.326	16.3521	-0.026	-0.16
α [°]	102.85	100.212	2.638	2.56
β [°]	102.14	103.793	-1.653	-1.62
γ [°]	103.38	101.751	1.629	1.58
V [Å ³]	2511	2447.64	63.36	2.52

Table 3.5.4 Structural data for the two polymorphs of the **G2** aldehyde

While the angles, a and c axis are basically the same in both forms, the b axis is stretched out by 4% in the polymorph 2. This leads to a 2.5% increase in unit cell volume.

While the **G2** aldehyde shows no hydrogen bonding between the different planes the **G2** alcohol shows this feature. This is the most likely explanation for the fact the **G2** alcohol, despite the very similar structure to **G2** aldehyde polymorph 1¹⁰, does not show a phase transition like the aldehyde. This means that the switch between the two polymorphs of the **G2** aldehyde very easily blocked.

The coupling of the amine wedge to the biotin worked extremely well for the **G1** and **G2**.

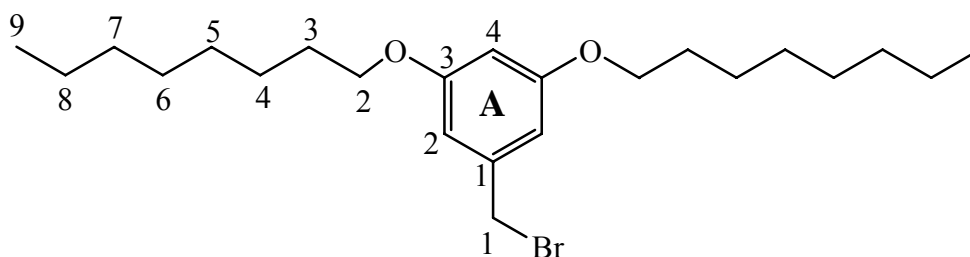
The extension to ferrocene gave a dendritic, charge-free organometallic complex.

The synthesis of the didendritic wedge compounds proved to be surprisingly difficult. Only over the Sonogashira coupling and in low yields for the **G1** compound positive results were observable. This low yields for the final step are hard to explain since the same technique was used by A. Avent et al²² to generate dendritic wedges though his groups compounds were much more rigid and sterically less demanding. The theory is that the long alkyl chains interfere with the palladium catalyst that is also very steric demanding with the four triphenylphosphine groups. This is the only probable explanation for the observed low yields in the final coupling step.

3.6 Experimental section

3.6.1 GI derivatives

3,5-Bis(octyloxy)benzyl bromide¹⁶ (**3**)



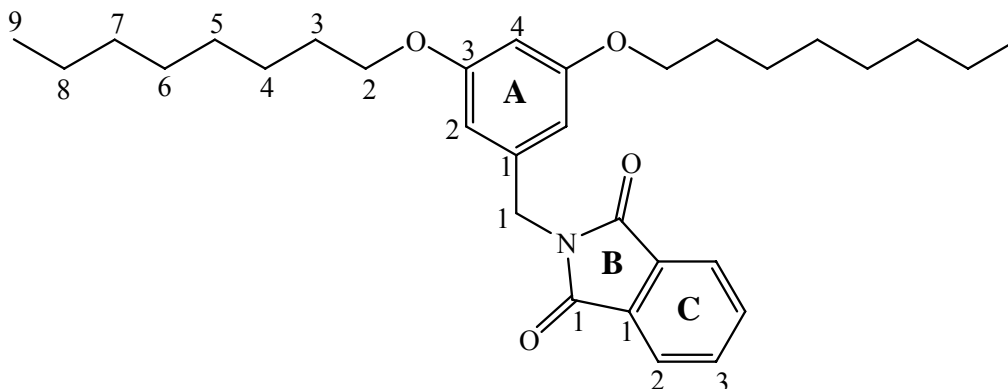
3,5-Bis(octyloxy)benzyl alcohol (**2**) (18.5 g, 50.7 mmol, 1.0 eq) was dissolved in 300 mL of dry CH_2Cl_2 . To this phosphorus tribromide (6.2 mL, 65.9 mmol, 1.3 eq) was added and the round bottomed flask put into the fridge for 4 days.

The reaction mixture was poured into 350 mL of brine and the phases were separated. The organic phase was washed with 150 mL of water. After drying over sodium sulfate, evaporation of the solvent and chromatography (7 x 14 cm, silica, CH_2Cl_2 : hexane 1:1) 18.4 g of a colourless oil were obtained (yield: 85 %).

TLC : R_f (CH_2Cl_2 : Hexane 1:1) : 0.66

$^1\text{H-NMR}$ (250 MHz, CDCl_3) δ / ppm : 6.51 (d, $^4J = 2.0$ Hz, 2H, $\text{H}^{\text{A}2}$); 6.38 (t, $^4J = 2.0$ Hz, 1H, $\text{H}^{\text{A}4}$); 4.41 (s, 2H, H^1); 3.93 (t, $^3J = 7.0$ Hz, 4H, H^2); 1.76 (quintet, $^3J = 7.0$ Hz, 4H, H^3); 1.55 – 1.20 (m, 20H, H^{4-8}); 0.89 (t, $^3J = 6.8$ Hz, 6H, H^9)

N-{3,5-Bis(octyloxy)benzyl}phthalimide¹⁷ (**7**)



3,5-Bis(octyloxy)benzyl bromide (**3**) (203 mg, 609 μmol , 1.0 eq) and potassium phthalimide (114 mg, 615 μmol , 1.0 eq) were dissolved in 10.0 mL dry DMF and heated to 80°C for two hours.

After letting the solution cool down, first 10 mL water then 15 mL of CH_2Cl_2 were added. The phases were separated and the water phase was extracted three times with 20 mL of CH_2Cl_2 . The organic phases were dried over magnesium sulfate. The solvent was evaporated and after chromatography (silica, 3 x 20 cm, CH_2Cl_2 : hexane 1:1) 138 mg of a colourless oil (yield : 59%) were isolated.

TLC : R_f (CH_2Cl_2 : hexane) 0.2

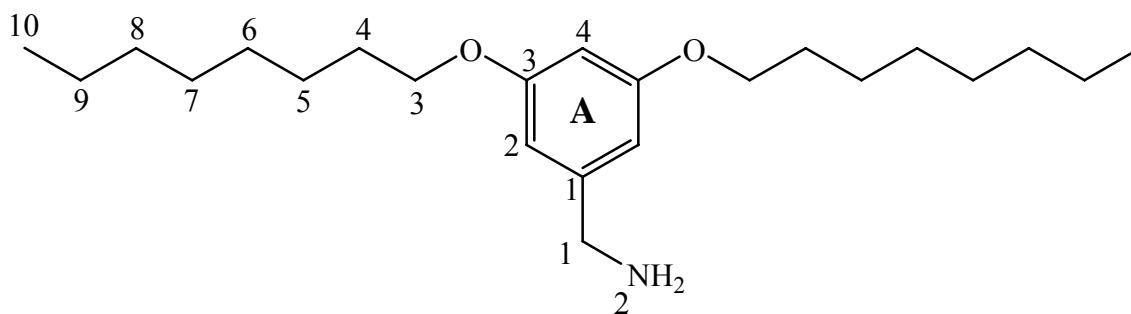
$^1\text{H-NMR}$ (500 MHz, CDCl_3) δ / ppm : 7.84 (AB pattern, 2H, $\text{H}^{\text{C}3}$); 7.70 (AB pattern, 1H, $\text{H}^{\text{C}2}$); 6.54 (d, $^4J = 2.3$ Hz, 2H, $\text{H}^{\text{A}2}$); 6.34 (s, $^4J = 2.3$ Hz, 1H, $\text{H}^{\text{A}4}$); 4.76 (s, 2H, $\text{H}^{\text{B}1}$); 3.90 (t, $^3J = 6.6$ Hz, 4H, $\text{H}^{\text{C}2}$); 1.77 – 1.69 (m, 4H, $\text{H}^{\text{C}3}$); 1.46 – 1.20 (m, 20H, $\text{H}^{\text{A}4-8}$); 0.88 (t, $^3J = 7.0$ Hz, 6H, $\text{H}^{\text{C}9}$).

$^{13}\text{C-NMR}$ (125 MHz, CDCl_3) δ / ppm : 168.0 ($\text{C}^{\text{B}1}$); 160.4 ($\text{C}^{\text{A}3}$); 138.3 ($\text{C}^{\text{C}1}$); 133.9 ($\text{C}^{\text{C}2}$); 132.1 ($\text{C}^{\text{A}1}$); 123.3 ($\text{C}^{\text{C}3}$); 106.8 ($\text{C}^{\text{A}2}$); 100.6 ($\text{C}^{\text{A}4}$); 68.0 ($\text{C}^{\text{B}2}$); 41.7 ($\text{C}^{\text{C}1}$); 31.8 ($\text{C}^{5,6,7\text{ or }8}$); 29.3 ($\text{C}^{\text{C}3}$); 29.2 ($\text{C}^{5,6,7\text{ or }8}$); 26.0 ($\text{C}^{\text{A}4}$); 22.6 ($\text{C}^{5,6,7\text{ or }8}$); 14.1 ($\text{C}^{\text{C}9}$)

Mass (EI 70 eV, ca 200 °C) **m/z** : 493 (48) [M]; 381 (16) [M – C_8H_{16}]; 269 (100) [M – 2 C_8H_{16}]; 251 (13) [M – C_8H_{16} - $\text{C}_8\text{H}_{16}\text{O}$]; 160 (11) [phthalimide- CH_2]

IR ($\tilde{\nu}$ [cm^{-1}]): 2922; 2855; 1771; 1713; 1595; 1466; 1427; 1391; 1346; 1321; 1294; 1167; 1105; 1053; 951; 831; 735; 712; 633

Microanalysis (calculated for $\text{C}_{31}\text{H}_{43}\text{N}_1\text{O}_4$ (493.68 g / mol)): C 75.42, H 8.78, N 2.84; found: C 75.13, H 8.89, N 3.00

3,5-Bis(octyloxy)benzylamine¹⁷ (**8**)

N-{3,5-Bis(octyloxy)benzyl}phthalimide (**7**) (326 mg, 660 μmol , 1.0 eq) was dissolved in 20.0 mL of ethanol. To this solution 0.46 mL of a 80% hydrazine monohydrate solution was added and the solution was refluxed for two and a half hours. During this time a white precipitate emerged. After cooling 34 mL of a 20% potassium hydroxide was added and the precipitate dissolved again. The phases were separated and the water phase was trice extracted with diethyl ether. The combined organic layers were washed twice with water, dried over magnesium sulfate and evaporated to dryness. 227 mg of a slightly yellow oil (yield : 95%) were recovered.

TLC: R_f (CH_2Cl_2 : methanol 10 : 1) = 0.47

m. p. ($^\circ\text{C}$): 50.2 – 59.4 $^\circ\text{C}$

$^1\text{H-NMR}$ (500 MHz, CDCl_3) δ / ppm : 6.45 (d, $^4J = 2.2$ Hz, 2H, $\text{H}^{\text{A}2}$); 6.34 (t, $^4J = 2.2$ Hz, 1H, $\text{H}^{\text{A}4}$); 3.93 (t, $^3J = 6.6$ Hz, 4H, H^3); 3.79 (s, 2H, H^1); 1.76 (tt, $^3J = 6.6$ Hz, $^3J = 6.6$ Hz, 4H, H^4); 1.50 – 1.22 (m, 22H, H^2 , H^{5-9}), 0.89 (t, $^3J = 7.0$ Hz, 6H, H^{10})

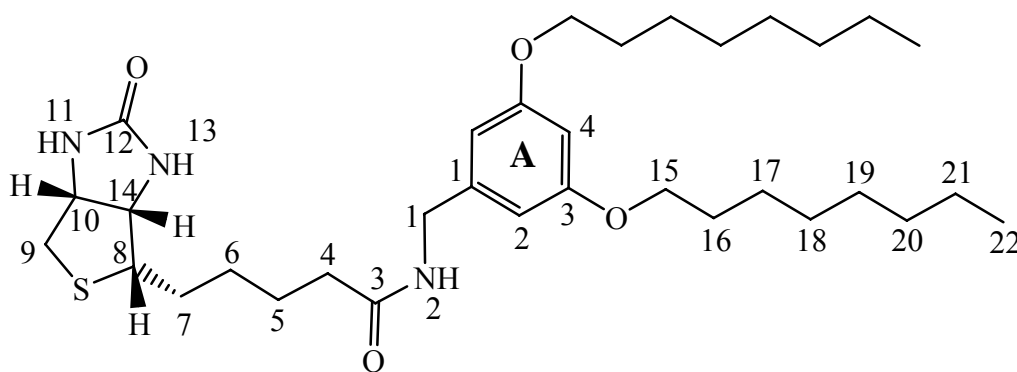
$^{13}\text{C-NMR}$ (125 MHz, CDCl_3) δ / ppm : 160.5 ($\text{C}^{\text{A}3}$); 145.8 ($\text{C}^{\text{A}1}$); 105.2 ($\text{C}^{\text{A}2}$); 99.5 ($\text{C}^{\text{A}4}$); 68.0 (C^3); 46.7 (C^1); 31.8 ($\text{C}^{6,7,8 \text{ or } 9}$); 29.3 (C^4); 29.2 ($\text{C}^{6,7,8 \text{ or } 9}$); 29.2 ($\text{C}^{6,7,8 \text{ or } 9}$); 26.1 (C^5); 22.7 ($\text{C}^{6,7,8 \text{ or } 9}$); 14.1 (C^{10})

Mass (EI 70 eV, ca 200 $^\circ\text{C}$) **m/z** : 363 (100) M; 250 (23) [M – C_8H_{17}]; 234 (23) [M – $\text{C}_8\text{H}_{17}\text{O}$]; 138 (34) [M + H – $2\text{C}_8\text{H}_{17}$]; 122 (59) [M + H – $\text{C}_8\text{H}_{17}\text{O} - \text{C}_8\text{H}_{17}$];

IR ($\tilde{\nu}$ [cm^{-1}]): 3360; 2917; 2870; 2851; 1596; 1588; 1464; 1456; 1448; 1391; 1345; 1327; 1165; 1128; 1066; 1055

Microanalysis (calculated for $\text{C}_{23}\text{H}_{41}\text{NO}_2$ (363.6 g / mol)): C 75.98, H 11.37, N 3.85; found: C 75.39, H 11.17, N

Compound (9)



Biotin (128.6 mg, 526 μmol , 1.0 eq) was dissolved in 2.0 ml DMF by stirring and heating. Then 1,1'-carbonyldiimidazole (102.5 mg, 632 μmol , 1.2 eq) was added. The mixture was then stirred at room temperature for two hours. During this time a white precipitate appeared. 3,5-Bis(octyloxy)benzylamine (**8**) (190 mg, 523 μmol , 1.0 eq) was dissolved in 0.5 mL of DMF and added to the reaction mixture which was then stirred for 16 hours.

The solvent was then evaporated to yield a yellow solid. After chromatography (silica, CH_2Cl_2 : methanol 10:1) 296 mg a white solid could be isolated (yield : 95%).

TLC: R_f (CH_2Cl_2 : methanol 10 : 1) = 0.23

m. p. ($^\circ\text{C}$): 125.8 – 127.5 $^\circ\text{C}$

$^1\text{H-NMR}$ (500 MHz, CDCl_3) δ / ppm : 6.72 (s, 1H, H^{11} or 13); 6.61 (t, $^3J = 5.7$ Hz, 1H, H^2); 6.39 (d, $^4J = 2.2$ Hz, 2H, $\text{H}^{\text{A}2}$); 6.32 (t, $^4J = 2.2$ Hz, 1H, $\text{H}^{\text{A}4}$); 5.36 (s, 1H, H^{11} or 13), 4.42 (dd, $^3J = 7.7$ Hz, $^3J = 4.8$ Hz, 1H, H^{10}); 4.32 (dd, $^3J = 5.6$ Hz, $J = 1.7$ Hz, 2H, H^1); 4.24 (dd, $^3J = 7.8$ Hz, $^3J = 4.9$ Hz, 1H, H^{14}); 3.89 (t, $^3J = 6.6$ Hz, 4H, H^{15}); 3.09 (td, $^3J = 7.4$ Hz, $^3J = 4.7$, 1H, H^8); 2.84 (dd, $^2J = 12.9$, $^3J = 4.9$ Hz, 1H, H^9); 2.63 (d, $^2J = 12.8$ Hz, 1H, H^9); 2.25 – 2.20 (m, 2H, H^5); 1.77 – 1.58 (m, 6H, $\text{H}^{4,6,16}$); 1.48 – 1.28 (m, 22H, $\text{H}^{7,17-21}$), 0.88 (t, $^3J = 7.0$ Hz, 6H, H^{22})

$^{13}\text{C-NMR}$ (125 MHz, CDCl_3) δ / ppm : 173.1 (C^3); 164.0 (C^{12}); 160.5 ($\text{C}^{\text{A}3}$); 140.9 ($\text{C}^{\text{A}1}$); 106.1 ($\text{C}^{\text{A}2}$); 100.0 ($\text{C}^{\text{A}4}$); 68.0 (C^{15}); 61.6 (C^{14}); 60.2 (C^{10}); 55.7 (C^8); 43.4 (C^1); 40.4 (C^9); 36.0 (C^5); 31.8; 29.3; 29.2; 29.2; 28.2; 28.0; 26.0; 25.7; 22.7; 14.1 (C^{22})

Mass (FAB NBA) **m/z** : 590 (100) [$\text{M} + \text{H}$]; 529 (15) [$\text{M} - \text{CO}(\text{NH}_2)_2$]; 362 (28) [$\text{C}_6\text{H}_3(\text{OC}_8\text{H}_{17})_2\text{CH}_2\text{NH}$]; 347 (15) [$\text{C}_6\text{H}_3(\text{OC}_8\text{H}_{17})_2\text{CH}_2$]; 250 (10) [$\text{C}_6\text{H}_3(\text{OC}_8\text{H}_{17})(\text{OH})\text{CH}_2\text{NH}$]; 234 (23) [$\text{C}_6\text{H}_3(\text{OC}_8\text{H}_{17})(\text{O})\text{CH}_2$]; 138 (12) [$\text{C}_6\text{H}_3(\text{C}_8\text{H}_{17})_2(\text{O})_2\text{CH}_2\text{NH}_2$]; 123 (20) [$\text{C}_6\text{H}_3(\text{OH})_2\text{CH}_2$];

IR ($\tilde{\nu}$ [cm^{-1}]): 3239.2; 2923.4; 2854.5; 1705.4; 1699.7; 1641.3; 1594.1; 1553.6; 1532.8; 1456.2; 1385.8; 1354.4; 1322.6; 1264.3; 1165.9; 1059.8

Microanalysis (calculated for $\text{C}_{33}\text{H}_{55}\text{N}_3\text{O}_4\text{S}$ (589.87 g / mol)): C 67.19, H 9.40, N 7.12; found: C 66.65, H 9.40, N 6.92

3,5-Bis(octyloxy)benzoic acid (**6**)



Methyl 3,5-bis(octyloxy)benzoate (**1**) (6.01 g, 15.3 mmol, 1 eq), potassium hydroxide (pellets, 2.62 g, 46.5 mmol, 3.0 eq) and THF (100 mL) were mixed and refluxed for two days. Dilute HCl was added till the pH 3 was reached. The organic phase was separated and dried (magnesium sulfate) and evaporated to dryness. A colourless solid was isolated (5.93 g, 100% yield).

TLC: R_f (CH_2Cl_2 : MeOH 10 : 1) = 0.56

$^1\text{H-NMR}$ (500 MHz, CDCl_3) δ / ppm : 7.23 (s, 2H, $\text{H}^{\text{A}2}$); 6.69 (s, 1H, $\text{H}^{\text{A}4}$); 3.98 (t, $^3J = 6.5$ Hz, 4H, H^2); 1.85 – 1.69 (m, 4H, H^3), 1.52 – 1.20 (m, 20H, H^{4-8}); 0.89 (t, $^3J = 6.5$ Hz, 6H, H^9)

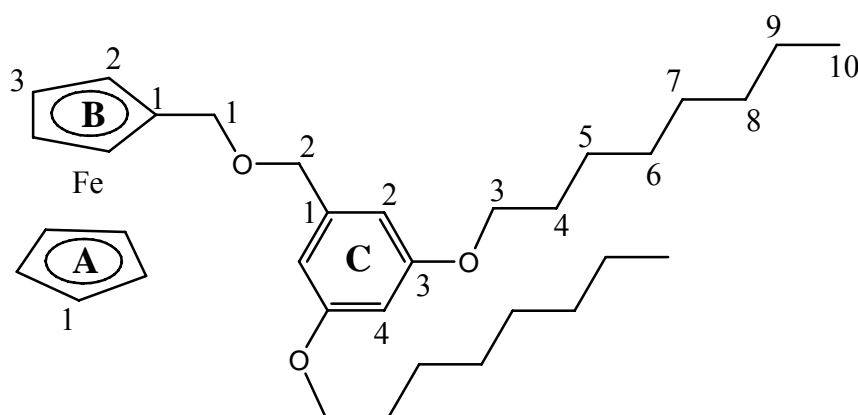
$^{13}\text{C-NMR}$ (125 MHz, CDCl_3) δ / ppm : 171.9 (C^1), 160.2 ($\text{C}^{\text{A}3}$), 131.0 ($\text{C}^{\text{A}1}$), 108.2 ($\text{C}^{\text{A}2}$), 107.5 ($\text{C}^{\text{A}4}$), 68.4 (C^2), 31.9 ($\text{C}^{3,4,5,6,7 \text{ or } 8}$), 29.4 ($\text{C}^{3,4,5,6,7 \text{ or } 8}$), 29.3 ($\text{C}^{3,4,5,6,7 \text{ or } 8}$), 29.2 ($\text{C}^{3,4,5,6,7 \text{ or } 8}$), 26.0 ($\text{C}^{3,4,5,6,7 \text{ or } 8}$), 22.7 ($\text{C}^{3,4,5,6,7 \text{ or } 8}$), 14.1 (C^9)

Mass (EI 70 eV, ca 250°C) **m/z** : 378 (38) [M]; 266 (17) [M – C_8H_{16}]; 154 (100) [M – 2 C_8H_{16}];

IR ($\tilde{\nu}$ [cm^{-1}]): 2957; 2917; 2871; 2851; 1689; 1604; 1481; 1467; 1443; 1420; 1392; 1316; 1268; 1249; 1165; 1131; 1060; 920; 856;

Microanalysis (calculated for (378.55 g / mol)): C 72.98, H 10.12; found: C 72.36, H 10.00

Compound (10)



Ferrocenemethanol (102 mg, 472 μmol , 1.0 eq), sodium hydride (60% in mineral oil) (33.9 mg, 848 μmol , 1.8 eq) were mixed in dry THF (10 mL) under nitrogen. After two hours stirring 3,5-bis(octyloxy)benzyl bromide (**3**) (216 mg, 505 μmol , 1.1 eq) dissolved in dry THF (7 mL) was added and the mixture was refluxed for five days.

The solvent was evaporated and CH_2Cl_2 and water were added. The phases were separated and the water phase extracted with CH_2Cl_2 (2x). The combined organic phases were dried over magnesium sulfate and evaporated to dryness. After chromatography (silica, ethyl acetate : hexane 1 : 9) a yellow oil was obtained (132 mg, 50% yield).

TLC: R_f (ethyl acetate : hexane 1 : 1) = 0.82

$^1\text{H-NMR}$ (500 MHz, C_6D_6) δ / ppm : 6.82 (s, 2H, $\text{H}^{\text{C}2}$); 6.70 (s, 1H, $\text{H}^{\text{C}4}$); 4.52 (s, 2H, H^2); 4.30 (s, 2H, H^1); 4.19 (s, 2H, $\text{H}^{\text{B}2}$ or $\text{B}3$); 3.97 (s, 7H, $\text{H}^{\text{A}1, \text{B}2}$ or $\text{B}3$), 3.76 (t, $^3J = 5.9$ Hz, 4H, H^3); 1.74 – 1.54 (m, 2H, H^4); 1.49 – 1.10 (m, 20H, H^{5-9}); 0.90 (t, $^3J = 6.6$ Hz, 6H, H^{10}).

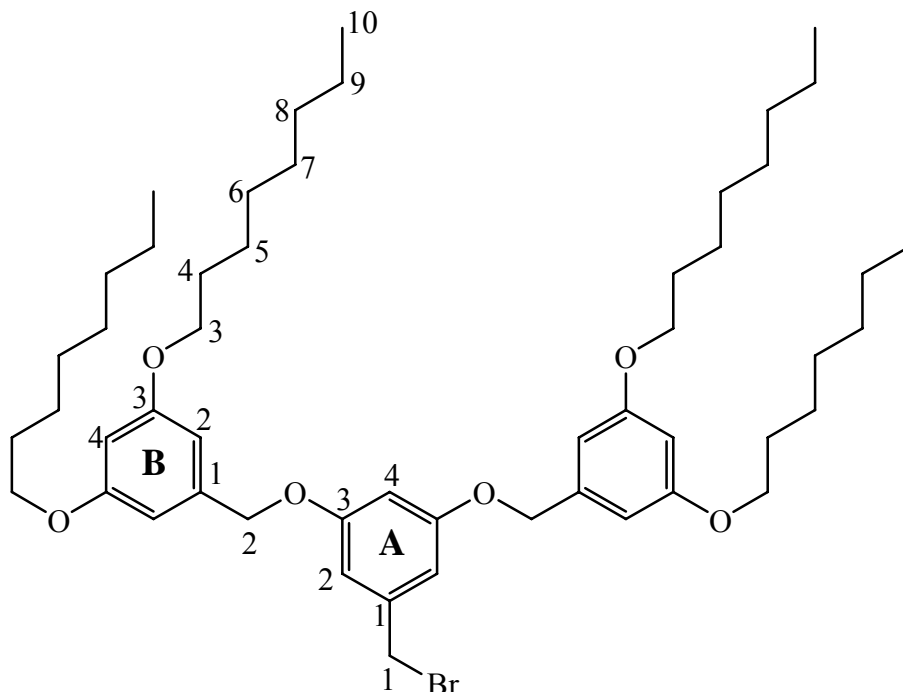
$^{13}\text{C-NMR}$ (125 MHz, C_6D_6) δ / ppm : 161.6 ($\text{C}^{\text{C}3}$); 142.2 ($\text{C}^{\text{C}1}$); 106.5 ($\text{C}^{\text{C}2}$); 101.4 ($\text{C}^{\text{C}4}$); 84.8 ($\text{C}^{\text{B}1}$); 72.4 (C^2); 70.0 ($\text{C}^{\text{B}2}$ or $\text{B}3$); 69.2 ($\text{C}^{\text{A}1}$); 68.9 ($\text{C}^{\text{B}2}$ or $\text{B}3$); 68.8 (C^1); 68.4 (C^3); 32.5 ($\text{C}^{4,5,6,7,8}$ or 9); 30.1 ($\text{C}^{4,5,6,7,8}$ or 9); 30.1 ($\text{C}^{4,5,6,7,8}$ or 9); 30.0 ($\text{C}^{4,5,6,7,8}$ or 9); 26.8 ($\text{C}^{4,5,6,7,8}$ or 9); 23.4 ($\text{C}^{4,5,6,7,8}$ or 9); 14.7 (C^{10})

Mass (FAB NBA + KCl (subtr)) m/z : 562 (100) [M^+]; 199 (6) [$\text{Fe}(\text{C}_5\text{H}_5)(\text{C}_5\text{H}_4\text{CH}_2)$];

IR ($\tilde{\nu}$ [cm^{-1}]): 3096; 2951; 2922; 2854; 1595; 1452; 1378; 1342; 1321; 1291; 1235; 1162; 1105; 1061; 1039; 1022; 1000; 828; 819;

Microanalysis (calculated for $\text{C}_{34}\text{H}_{50}\text{FeO}_3$ (562.61 g / mol)): C 72.58; H 8.96; found : C 72.61; H 9.00

3.6.2 G2 derivatives

3,5-Bis(3,5-dioctyloxybenzyloxy)benzyl bromide (**13**)

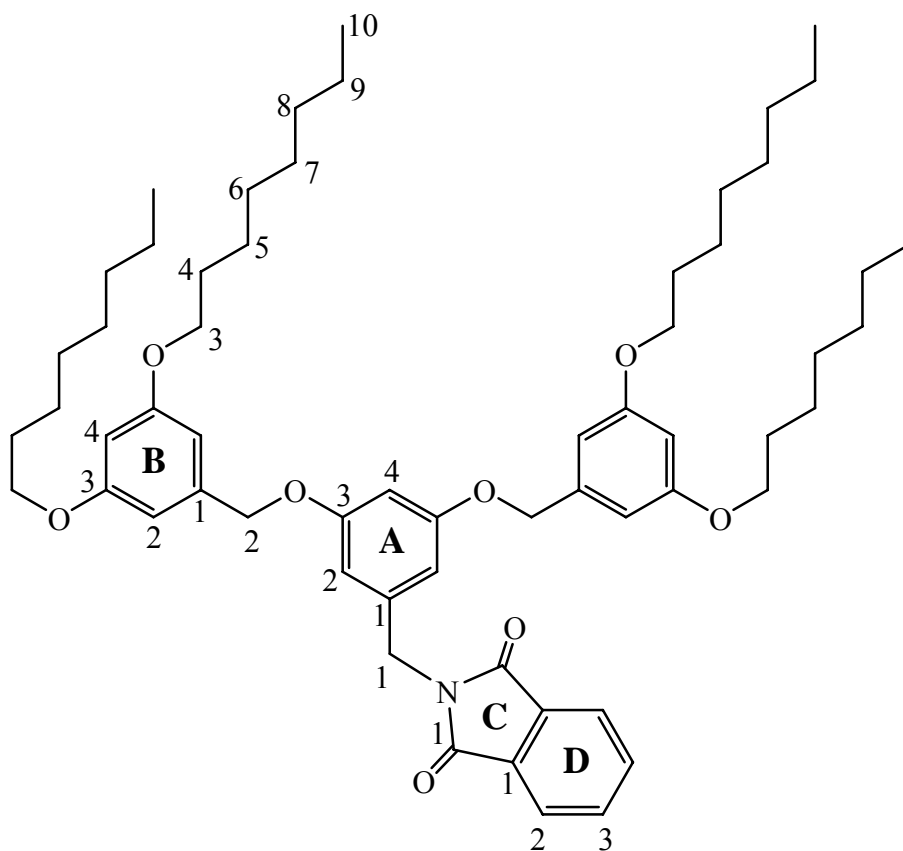
3,5-Bis(3,5-dioctyloxybenzyloxy)benzyl alcohol (**12**) (2.97 g, 3.56 mmol, 1.0 eq) was dissolved in 50 mL CH_2Cl_2 and placed in the fridge. To this phosphorus tribromide (0.35 mL, 3.72 mmol, 1.04 eq) was added and left in the fridge for six days.

The reaction mixture was poured into 500 mL water. To enhance phase separation brine (100 mL) was added and the phases were separated. The organic phase was washed once with brine and dried over magnesium sulfate.

After chromatography (silica, 5 x 10 cm, CH_2Cl_2 : hexane 1:1) 2.46 g product could be isolated (yield : 77%).

TLC : R_f (CH_2Cl_2 : Hexane 1:1) : 0.55

$^1\text{H-NMR}$ (250 MHz, CDCl_3) δ / ppm : 6.62 (d, $^4J = 2.1$ Hz, 2H, $\text{H}^{\text{A}2}$); 6.56 – 6.49 (m, 5H, $\text{H}^{\text{A}4,\text{B}2}$); 6.38 (t, $^4J = 2.1$ Hz, 2H, $\text{H}^{\text{B}4}$); 4.94 (s, 4H, H^2); 4.41 (s, 2H, H^1), 3.93 (t, $^3J = 6.5$ Hz, 8H, H^3); 1.85 – 1.67 (m, 8H, H^4); 1.50 – 1.20 (m, 40H, H^{5-9}); 0.89 (t, $^3J = 6.8$ Hz, 12H, H^{10})

N-{3,5-Bis(3,5-dioctyloxybenzyloxy)benzyl}phthalimide (**15**)

3,5-Bis(3,5-dioctyloxybenzyloxy)benzyl bromide (**13**) (453 mg, 506 μmol , 1.0 eq) and potassium phthalimide (139 mg, 750 μmol , 1.5 eq) were dissolved in 10.0 mL dry DMF and heated to 80°C for two hours.

After letting the solution cool down, first 20 mL water were added. The reaction mixture was extracted three times with 30 ml of CH_2Cl_2 . The organic phases were washed twice with water and dried over magnesium sulfate. After chromatography (silica, 3 x 22 cm, CH_2Cl_2 : hexane 1:1) 462 mg of a colourless viscous oil were isolated (yield 95%).

TLC: R_f (CH_2Cl_2 : hexane 1 : 1) = 0.29

$^1\text{H-NMR}$ (500 MHz, CDCl_3) δ / ppm : 7.85 (AB pattern, 2H, $\text{H}^{\text{D}2}$); 7.71 (AB pattern, 2H, $\text{H}^{\text{D}3}$); 6.65 (d, $^4J = 2.1$ Hz, 2H, $\text{H}^{\text{A}2}$); 6.53 (d, $^4J = 2.1$ Hz, 4H, $\text{H}^{\text{B}2}$); 6.51 (t, $^4J = 2.0$ Hz, 1H, $\text{H}^{\text{A}4}$); 6.38 (t, $^4J = 2.0$ Hz, 2H, $\text{H}^{\text{B}4}$); 4.91 (s, 4H, H^2); 4.78 (s, 2H, H^1); 3.93 (t, $^3J = 6.6$ Hz, 8H, H^3); 1.82 – 1.68 (m, 8H, H^4), 1.50 – 1.20 (m, 40H, H^{5-9}), 0.88 (t, $^3J = 6.5$ Hz, 12H, H^{10})

$^{13}\text{C-NMR}$ (125 MHz, CDCl_3) δ / ppm : 168.0 ($\text{C}^{\text{C}1}$); 160.5 ($\text{C}^{\text{B}3}$); 160.1 ($\text{C}^{\text{A}3}$); 138.8 ($\text{C}^{\text{B}1}$); 138.5 ($\text{C}^{\text{A}1}$); 134.0 ($\text{C}^{\text{D}3}$); 132.1 ($\text{C}^{\text{D}1}$); 123.4 ($\text{C}^{\text{D}2}$); 107.4 ($\text{C}^{\text{A}2}$); 105.8 ($\text{C}^{\text{B}2}$); 101.3 ($\text{C}^{\text{A}4}$);

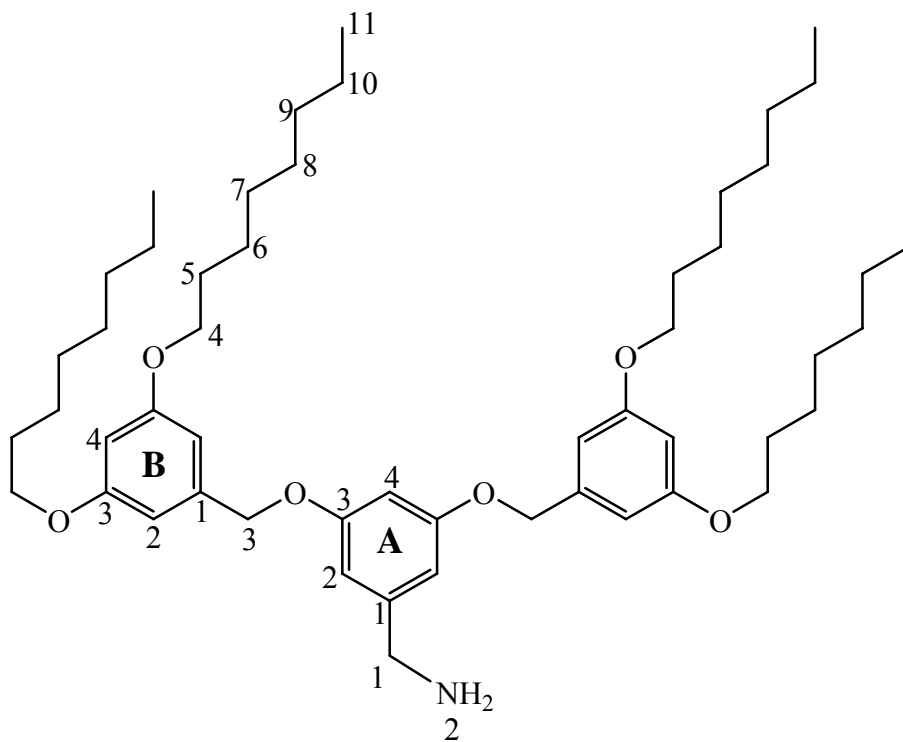
100.9 (C^{B4}); 70.2 (C²); 68.1 (C³); 41.6 (C¹); 31.9 (C^{5,6,7,8 or 9}); 29.4 (C^{5,6,7,8 or 9}); 29.3 (C⁴); 29.3 (C^{5,6,7,8 or 9}); 26.1 (C^{5,6,7,8 or 9}); 22.7 (C^{5,6,7,8 or 9}); 14.2 (C¹⁰)

Mass (FAB NBA + KCl (subtr)) **m/z** : 962 (9) [M⁺]; 347 (13) [C₆H₃(OC₈H₁₇)₂CH₂];

IR ($\tilde{\nu}$ [cm⁻¹]): 2924; 2854; 1774; 1713; 1597; 1458; 1389; 1350; 1165; 1057; 949; 833; 733; 717; 687; 633; 571; 525

Microanalysis (calculated for C₆₁H₈₇N₁O₈ (962.36 g / mol)): C 76.13; H 9.11; N 1.46
found : C 76.18; H 9.09; N 1.48

3,5-Bis(3,5-dioctyloxybenzyloxy)benzylamine (**16**)



N-{3,5-Bis(3,5-dioctyloxybenzyloxy)benzyl}phthalimide (**15**) (1.02 g, 1.06 mmol, 1.0 eq) was dissolved in 30.0 mL of ethanol. To this solution 0.70 mL of an 80% hydrazine monohydrate solution were added and the solution was refluxed for two and a half hours. During this time a white precipitate emerged. After the cool down 50 mL of a 20% sodium hydroxide solution and 50 mL of diethyl ether were added and the precipitate dissolved again. The phases were separated and the water phase was twice extracted with diethyl ether. The combined organic layers were washed twice with water, dried over magnesium sulfate and evaporated to dryness. After chromatography (silica, 3 x 28 cm, CH₂Cl₂ : methanol 10 : 1) 680 mg of a colourless oil were recovered that crystallised at room temperature (yield : 77%).

TLC: R_f (CH_2Cl_2 : methanol 10 : 1) = 0.43

m. p. ($^\circ\text{C}$): 38.1 – 39.9 $^\circ\text{C}$

$^1\text{H-NMR}$ (500 MHz, CDCl_3) δ / ppm : 6.58 (d, $^4J = 2.2$ Hz, 2H, $\text{H}^{\text{A}2}$); 6.55 (d, $^4J = 2.2$ Hz, 4H, $\text{H}^{\text{B}2}$); 6.50 (t, $^4J = 2.1$ Hz, 1H, $\text{H}^{\text{A}4}$); 6.40 (t, $^4J = 2.2$ Hz, 2H, $\text{H}^{\text{B}4}$); 4.94 (s, 4H, H^3); 3.93 (t, $^3J = 6.6$ Hz, 8H, H^4); 3.82 (s, 2H, H^1); 1.76 (tt, $^3J = 6.6$ Hz, $^3J = 6.7$ Hz, 4H, H^5); 1.47 – 1.40 (m, 8H, H^6); 1.37 – 1.23 (m, 32H, H^{7-10}); 0.88 (t, $^3J = 7.0$ Hz, 6H, H^{11})

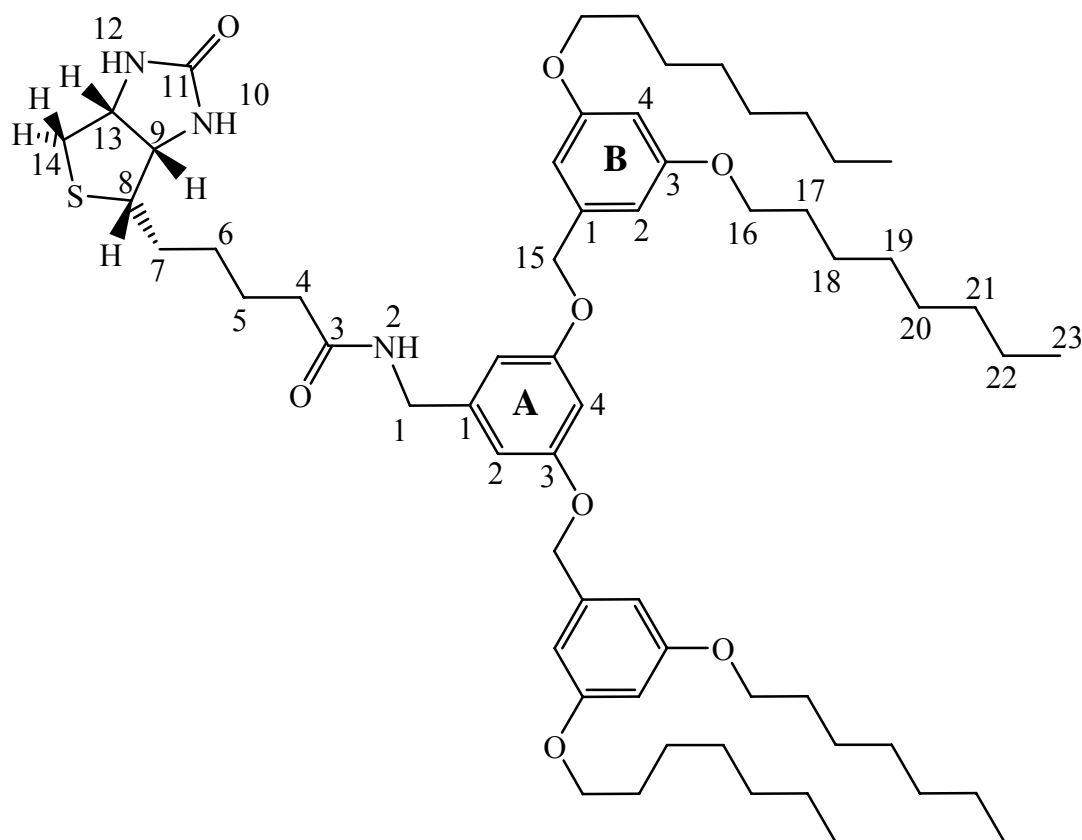
$^{13}\text{C-NMR}$ (125 MHz, CDCl_3) δ / ppm : 160.6 ($\text{C}^{\text{B}3}$); 160.3 ($\text{C}^{\text{A}3}$); 139.1 ($\text{C}^{\text{B}1}$); 106.3 ($\text{C}^{\text{A}2}$); 105.8 ($\text{C}^{\text{B}2}$); 100.9 ($\text{C}^{\text{B}4}$); 100.7 ($\text{C}^{\text{A}4}$); 70.2 (C^2); 68.2 (C^3); 45.5 (C^1); 32.0; 29.5; 29.2; 26.2; 22.8; 14.3

Mass (FAB NBA (subtr)) m/z : 832 (100) [M]; 484 (8) [M – $\text{CH}_2(\text{C}_6\text{H}_3)(\text{OC}_8\text{H}_{17})_2$]

IR ($\tilde{\nu}$ [cm^{-1}]): 2924; 2855; 1597; 1443; 1373; 1319; 1296; 1258; 1165; 1049; 949; 826; 725; 679

Microanalysis (calculated for $\text{C}_{53}\text{H}_{85}\text{NO}_6$ (832.26 g / mol)): C 76.49, H 10.29, N 1.68; found: C 76.45, H 10.17, N 1.68

Compound (17)



Biotin (107 mg, 438 μmol , 1.0 eq) was dissolved in 2.0 ml DMF by stirring and heating. Then 1,1'-Carbonyldiimidazole (84.7 mg, 522 μmol , 1.2 eq) was added. The mixture was then stirred at room temperature for an hour. During this time a white precipitate appeared. 3,5-Bis(3,5-dioctyloxybenzyloxy)benzylamine (**16**) (309 mg, 371 μmol , 0.7 eq) was dissolved in 1.5 mL of DMF and added to the reaction mixture which was then stirred for 18 hours.

The solvent was then evaporated to yield a yellow solid. After chromatography (silica, 3 x 23 cm, CH_2Cl_2 : methanol 10:1) 53.8 mg a white solid could be isolated (yield : 91%).

TLC: R_f (CH_2Cl_2 : methanol 10 : 1) = 0.38

m. p. ($^\circ\text{C}$): 102.5 – 104.8 $^\circ\text{C}$

$^1\text{H-NMR}$ (500 MHz, CDCl_3) δ / ppm : 6.53 (d, $^4J = 2.2$ Hz, 4H, $\text{H}^{\text{B}2}$); 6.51 (d, $^4J = 2.2$ Hz, 2H, $\text{H}^{\text{A}2}$); 6.49 (t, $^4J = 2.2$ Hz, 1H, $\text{H}^{\text{A}4}$); 6.39 (t, $^4J = 2.2$ Hz, 2H, $\text{H}^{\text{B}4}$); 4.90 (s, 4H, $\text{H}^{\text{I}5}$); 4.36 (dd, $^3J = 5.0$ Hz, $^3J = 7.9$ Hz, 1H, $\text{H}^{\text{I}3}$); 4.34 (s, 2H, $\text{H}^{\text{I}1}$); 4.22 (dd, $^3J = 4.6$ Hz, $^3J = 7.8$ Hz, 1H, $\text{H}^{\text{O}9}$); 3.92 (t, $^3J = 6.6$ Hz, 8H, $\text{H}^{\text{I}6}$); 3.06 (dt, $^3J = 4.6$ Hz, $^3J = 7.4$ Hz, 1H, $\text{H}^{\text{O}8}$); 2.79 (dd, $^3J = 4.8$ Hz, $^3J = 12.9$ Hz, 1H, $\text{H}^{\text{I}4}$); 2.61 (d, $^3J = 12.8$ Hz, 1H, $\text{H}^{\text{I}4}$); 2.24 (t, $^3J = 7.5$ Hz, 2H, $\text{H}^{\text{I}4}$); 1.80 – 1.56 (m, 14H, $\text{H}^{\text{I}5-7, 17}$); 1.48 – 1.21 (m, 40H, $\text{H}^{\text{I}18-22}$); 0.88 (t, $^3J = 7.0$ Hz, 12H, $\text{H}^{\text{I}23}$)

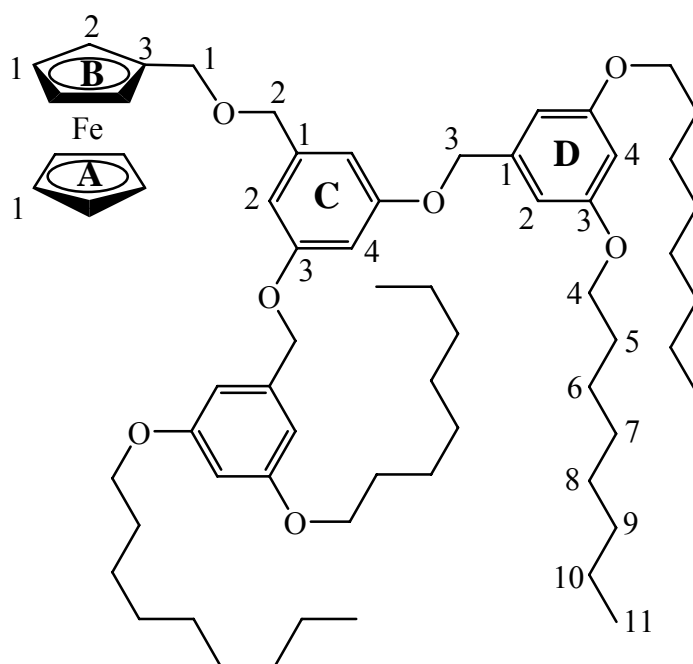
$^{13}\text{C-NMR}$ (125 MHz, CDCl_3) δ / ppm : 173.2 (C^3); 163.8 ($\text{C}^{\text{I}1}$); 160.4 ($\text{C}^{\text{B}3}$); 160.1 ($\text{C}^{\text{A}3}$); 141.0 ($\text{C}^{\text{A}1}$); 138.8 ($\text{C}^{\text{B}1}$); 106.7 ($\text{C}^{\text{A}2}$); 105.8 ($\text{C}^{\text{B}2}$); 100.7 ($\text{C}^{\text{A}4}$); 100.7 ($\text{C}^{\text{B}4}$); 70.1 ($\text{C}^{\text{I}5}$); 68.1 ($\text{C}^{\text{I}6}$); 61.8 ($\text{C}^{\text{O}9}$); 60.3 ($\text{C}^{\text{I}3}$); 55.4 ($\text{C}^{\text{O}8}$); 43.5 ($\text{C}^{\text{I}1}$); 40.3 ($\text{C}^{\text{I}4}$); 35.8 ($\text{C}^{\text{I}5}$); 31.8; 29.4; 29.2; 29.2; 28.1; 27.9; 26.0; 25.6; 22.6; 14.1 ($\text{C}^{\text{I}23}$)

Mass (FAB NBA subtracted) **m/z** : 1058 (12) [M]

IR ($\tilde{\nu}$ [cm^{-1}]): 3402; 3294; 3202; 3071; 2924; 2855; 1705; 1643; 1597; 1528; 1451; 1373; 1327; 1296; 1157; 1050; 949; 826; 718; 679

Microanalysis (calculated for $\text{C}_{33}\text{H}_{55}\text{N}_3\text{O}_4\text{S}$ (1058.55 g / mol)): C 71.48, H 9.43, N 3.97; found: C 71.52, H 9.40, N 3.99

Compound (18)



Ferrocenemethanol (102 mg, 464 μmol , 1.00 eq) was dissolved under nitrogen in THF (5.0 mL). Sodium hydride (60% suspension in mineral oil) (20.4 mg, 510 mmol, 1.10 eq) was added and the reaction was stirred for two hours.

3,5-Bis(3,5-dioctyloxybenzyl) oxybenzyl bromide (**13**) (429 mg, 479 μmol , 1.03 eq) was dissolved under nitrogen in THF (10 mL) and this solution was added to the ferrocenemethanol solution. The combined solutions were refluxed for 8 days.

The solution was evaporated to dryness and water (40 mL) and CH_2Cl_2 (40 mL) were added and the phases were separated. The water phase was extracted with CH_2Cl_2 (2 x 40 mL) and the combined organic phases were dried over magnesium sulfate. After chromatography (silica, ethyl acetate : hexane 1 : 13) a yellow oil (329 mg, 68% yield) was isolated.

TLC: R_f (ethyl acetate : hexane 1 : 13) = 0.50

$^1\text{H-NMR}$ (500 MHz, C_6D_6) δ / ppm : 6.87 (s, 2H, H^{D4}), 6.82 (s, 1H, H^{C4}), 6.75 (s, 4H, H^{D2}), 6.67 (s, 2H, H^{C2}), 4.85 (s, 4H, H^{B3}), 4.45 (s, 2H, H^{A1}), 4.25 (s, 2H, H^{B2}), 4.16 (s, 2H, $\text{H}^{\text{B2 or B3}}$), 3.98 (s, 7H, $\text{H}^{\text{A1, B2 or B3}}$), 3.72 (t, $^3J = 6.3$ Hz, 8H, H^{A4}), 1.73 – 1.55 (m, 8H, H^{B5}), 1.42 – 1.15 (m, 40H, $\text{H}^{\text{B6-10}}$), 0.91 (t, $^3J = 6.9$ Hz, 12H, H^{B11})

$^{13}\text{C-NMR}$ (125 MHz, C_6D_6) δ / ppm : 161.6 (C^{D3}), 161.2 (C^{C3}), 142.4 (C^{D1}), 140.4 (C^{C1}), 107.2 (C^{D4}), 106.3 (C^{D2}), 102.2 (C^{C4}), 101.8 (C^{C2}), 84.7 (C^{B1}), 72.1 (C^{A1}), 70.7 (C^{B3}), 70.0 (C^{B2})

or B³), 69.2 (C^{A1}), 68.9 (C^{B2} or B³), 68.7 (C²), 68.4 (C⁴), 32.6 (C^{5,6,7,8,9} or 10), 30.1 (C^{5,6,7,8,9} or 10), 30.0 (C^{5,6,7,8,9} or 10), 26.8 (C^{5,6,7,8,9} or 10), 23.4 (C^{5,6,7,8,9} or 10), 14.7 (C¹¹)

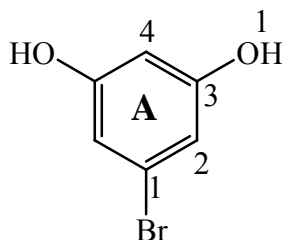
Mass (EI 70 eV, 300 °C) **m/z** : 1030 (40) [M-H]

IR ($\tilde{\nu}$ [cm⁻¹]): 3092, 2921, 2853, 1593, 1452, 1376, 1344, 1323, 1294, 1236, 1160, 1053, 831

Microanalysis (calculated for C₃₃H₅₅N₃O₄S (1031.29 g / mol)): C 74.54, H 9.19; found: C 74.42, H 9.27

3.6.3 Didendritic wedge compounds

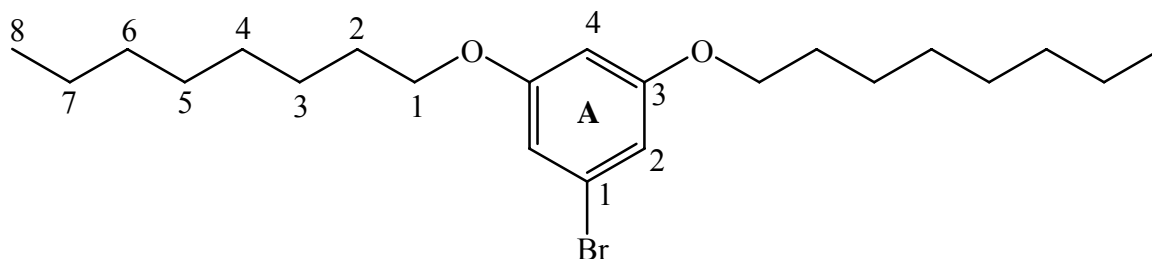
Bromo-3,5-dihydroxybenzene



Bromo-3,5-dimethoxybenzene (4.34 g, 20.0 mmol, 1.00 eq), acetic acid (50 mL) and concentrated hydriodic acid (40 mL) were refluxed for 6 hours. A solution of sodium bisulfite (300 mL, 5%) was added. The aqueous phase was extracted 5 times with diethyl ether. The combined organic phases were washed once with water and dried over sodium sulfate.

After chromatography (silica, 5 x 10 cm, CH₂Cl₂ : MeOH 10 : 1) an oil (3.59 g, 95% yield) was obtained that crystallised at room temperature.

¹H-NMR (250 MHz, CDCl₃) δ / ppm : 6.59 (d, ⁴J = 2.2 Hz, 2H, H²); 6.28 (t, ⁴J = 2.2 Hz, 1H, H⁴)

Bromo-3,5-bis(octyloxy)benzene (**19**)

Bromo-3,5-dihydroxybenzene (5.91 g, 31.3 mmol, 1.0 eq), potassium carbonate (10.8 g, 78.1 mmol, 2.5 eq), 1-bromooctane (16.5 mL, 91.3 mmol, 3.0 eq) and acetone (100 mL) were mixed in nitrogen atmosphere and refluxed for four days.

The mixture was filtered and the solvent evaporated. After chromatography (silica, 5 x 16 cm, CH₂Cl₂ : hexane 1 : 1) a colourless oil (7.07 g, 55% yield) was isolated.

TLC: R_f (hexane) = 0.41

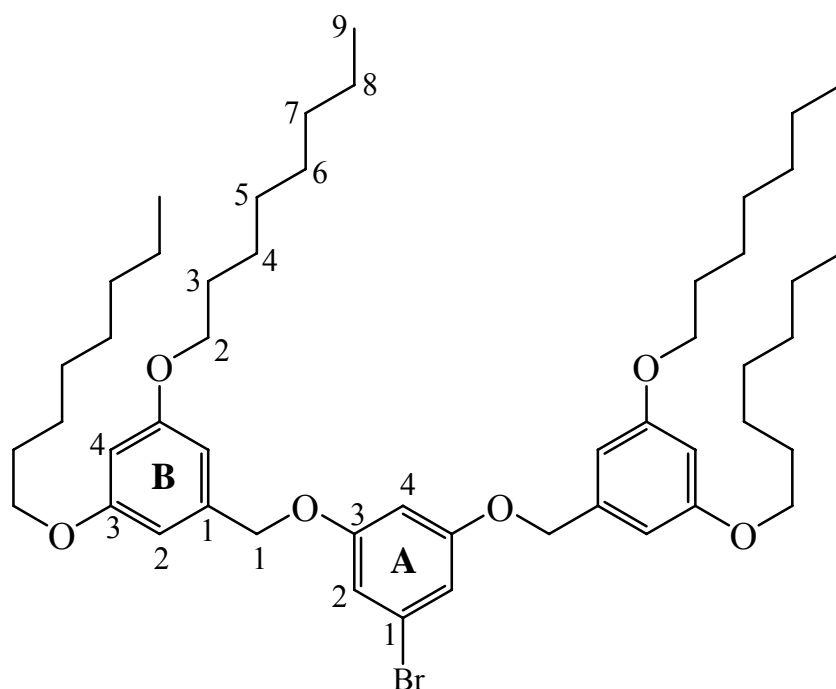
¹H-NMR (500 MHz, CDCl₃) δ / ppm : 6.64 (d, ⁴J = 0.9 Hz, 2H, H^{A2}); 6.37 (s, 1H, H^{A4}); 3.90 (t, ³J = 6.5 Hz, 4H, H¹); 1.80 – 1.70 (m, 4H, H²); 1.47 – 1.23 (m, 28H, H³⁻⁷); 0.89 (t, ³J = 6.64 Hz, 6H, H⁸)

¹³C-NMR (125 MHz, CDCl₃) δ / ppm : 160.8 (C^{A3}); 122.8 (C^{A1}); 110.2 (C^{A2}); 100.6 (C^{A4}); 68.3 (C¹); 31.8 (C^{2,3,4,5,6 or 7}); 29.4 (C^{2,3,4,5,6 or 7}); 29.3 (C^{2,3,4,5,6 or 7}); 29.2 (C^{2,3,4,5,6 or 7}); 26.0 (C^{2,3,4,5,6 or 7}); 22.7 (C^{2,3,4,5,6 or 7}); 14.1 (C⁸)

Mass (EI 70 eV, ca 200°C) **m/z** : 412 (30) [M]; 333 (9) [M – Br]; 300 (11) [M – C₈H₁₆]; 221 (81) [M - Br - C₈H₁₆]; 188 (100) [M - 2 C₈H₁₆];

IR ($\tilde{\nu}$ [cm⁻¹]): 2951; 2923; 2870; 2853; 1595; 1574; 1452; 1437; 1385; 1330; 1309; 1297; 1278; 1162; 1050; 989; 830; 806

Microanalysis (calculated for C₂₂H₃₇BrO₂ (413.43 g / mol)): C 63.91, H 9.02; found: C 63.45, H 9.16

1-Bromo-3,5-bis(octyloxy benzyloxy) benzene (**20**)

1-Bromo-3,5-dihydroxybenzene (846 mg, 4.48 mmol, 1.0 eq), potassium carbonate (1.61 g, 11.6 mmol, 2.6 eq), **G1** mesylate (**5**) (13.7 mmol, 3.0 eq), 18-crown-6 (104 mg, 393 μ mol, 0.1 eq) and acetone (100 mL) were mixed and refluxed for five days.

The mixture was filtered through celite and evaporated to dryness. After chromatography (silica, 5 x 15 cm, CH_2Cl_2 : hexane 1:1) a yellow oil could be isolated (487 mg, 12% yield).

TLC: R_f (ethyl acetate : hexane 1:7) = 0.78

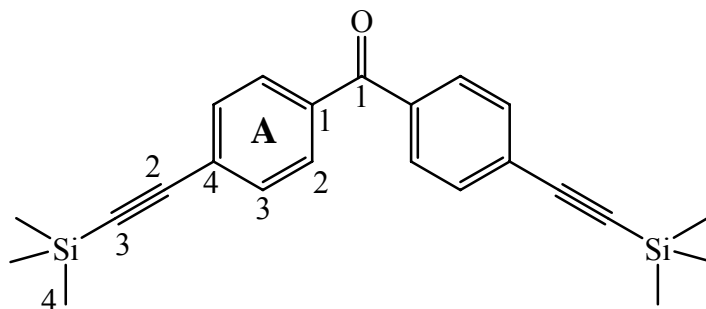
$^1\text{H-NMR}$ (500 MHz, CDCl_3) δ / ppm : 6.76 (s, 2H, $\text{H}^{\text{A}2}$), 6.53 (m, 5H, $\text{H}^{\text{A}4,\text{B}2}$), 6.42 (s, 2H, $\text{H}^{\text{B}4}$), 4.92 (s, 4H, H^1), 3.94 (t, $^3J = 6.5$ Hz, 8H, H^2), 1.84 – 1.71 (m, 8H, H^3), 1.50 – 1.25 (m, 40H, H^{4-8}), 0.90 (t, $^3J = 6.5$ Hz, 12H, H^9)

$^{13}\text{C-NMR}$ (125 MHz, CDCl_3) δ / ppm : 160.6 ($\text{C}^{\text{B}3}$), 160.4 ($\text{C}^{\text{A}3}$), 138.5 ($\text{C}^{\text{B}1}$), 122.9 ($\text{C}^{\text{A}1}$), 111.0 ($\text{C}^{\text{A}2}$), 105.7 ($\text{C}^{\text{B}2}$), 101.4 ($\text{C}^{\text{A}4}$), 100.9 ($\text{C}^{\text{B}4}$), 70.3 (C^1), 68.1 (C^2), 31.89 ($\text{C}^{3,4,5,6,7 \text{ or } 8}$), 29.4 ($\text{C}^{3,4,5,6,7 \text{ or } 8}$), 29.4 ($\text{C}^{3,4,5,6,7 \text{ or } 8}$), 29.3 ($\text{C}^{3,4,5,6,7 \text{ or } 8}$), 26.1 ($\text{C}^{3,4,5,6,7 \text{ or } 8}$), 22.7 ($\text{C}^{3,4,5,6,7 \text{ or } 8}$), 14.2 (C^9)

Mass (EI 70 eV, ca. 300°C) m/z : 880 (34) [M]; 801 (43) [M – Br];

IR ($\tilde{\nu}$ [cm^{-1}]): 2921; 2869; 2854; 1593; 1575; 1452; 1437; 1376; 1347; 1326; 1295; 1164; 1051; 832;

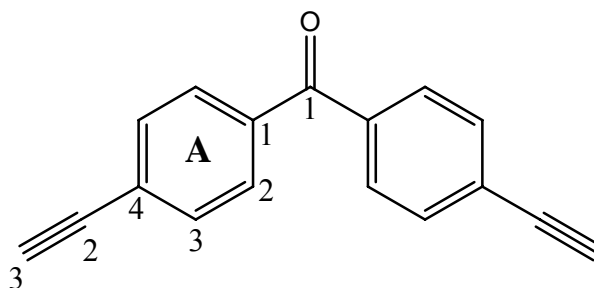
Microanalysis (calculated for $\text{C}_{22}\text{H}_{37}\text{BrO}_2$ (882.11 g / mol)): C 70.80, H 9.26; found: C 70.85, H 9.23

4,4'-Bis(trimethylsilylethynyl)acetophenone (**21**)

4,4'-Dibromobenzophenone (760 mg, 2.24 mmol, 1.00 eq), trimethylsilylacetylene (1.30 mL, 9.13 mmol, 4 eq), palladium tetrakis(triphenyl phosphine (71.1 mg, 61.5 μ mol, 0.03 eq), copper(I) iodide (25.5 mg, 134 μ mol, 0.06 eq), triethylamine (15 mL) and dry toluene (7 mL) were mixed and the solution degassed and placed under nitrogen. The mixture was then heated to 55°C and stirred at that temperature for 16 hours.

The reaction mixture was then filtered through a silica plug and was washed with CH_2Cl_2 . After evaporation to dryness and chromatography (silica, 3 x 15 cm, CH_2Cl_2 : hexane 1 : 4) a white solid was isolated (793 mg, yield : 95%).

$^1\text{H-NMR}$ (250 MHz, CDCl_3) δ / ppm : 7.71 (d, $^3J = 8.5$ Hz, 4H, $\text{H}^{\text{A}2}$), 7.56 (d, $^3J = 8.5$ Hz, 4H, $\text{H}^{\text{A}3}$), 0.27 (s, 9H, $\text{H}^{\text{A}4}$)

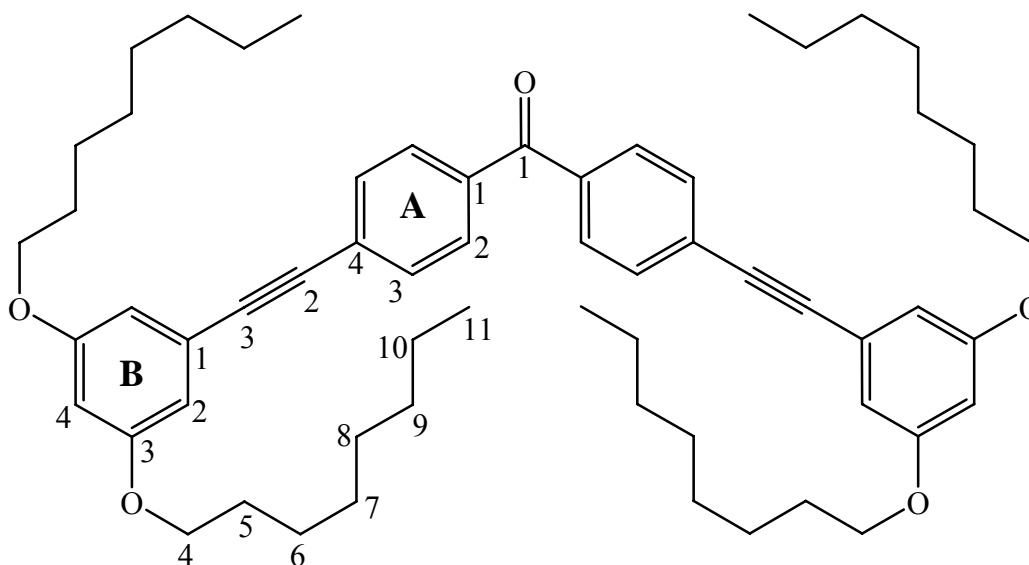
4,4'-Bis(ethynyl)acetophenone (**22**)

4,4'-Bis(trimethylsilylethynyl)acetophenone (**21**) (793 mg, 2.12 mmol, 1.0 eq), CH_2Cl_2 (30 mL), MeOH (30 mL) and tetrabutylammonium fluoride (2.03 g, 7.76 mmol, 3.7 eq) were mixed and stirred at room temperature for 30 minutes.

Water was added and the phases were separated. The organic phase was washed with water (3x) and the combined water phases were the extracted with CH_2Cl_2 . After drying over magnesium sulfate and filtration through a silica plug the solution was evaporated to dryness giving a white, crystalline solid (433 mg, 89% yield).

$^1\text{H-NMR}$ (250 MHz, CDCl_3) δ / ppm : 7.75 (d, $^3J = 8.6$ Hz, 4H, $\text{H}^{\text{A}2}$); 7.60 (d, $^3J = 8.5$ Hz, 4H, $\text{H}^{\text{A}3}$); 3.26 (s, 2H, H^3)

(3,5-Bis(octyloxy)phenylethynyl)acetophenone (**23**)



4,4'-Bis(ethynyl)acetophenone (**22**) (100 mg, 434 μmol , 1.0 eq), palladium tetrakis triphenylphosphine (50.7 mg, 43.8 μmol , 0.1 eq), copper iodide (13.8 mg, 72.4 μmol , 0.17 eq), bromo-3,5-bis(octyloxy)benzene (415 mg, 1.00 mmol, 2.3 eq) triethyl amine (9.0 mL) and toluene (4 mL) were mixed under nitrogen and irradiated in a microwave reactor for 30 minutes and kept at 373 K.

The product was evaporated to dryness. After chromatography (silica, CH_2Cl_2 : hexane 1:1) an orange oil was obtained (54.8 mg, 14% yield).

TLC: R_f (CH_2Cl_2 : hexane 1:1) = 0.41

$^1\text{H-NMR}$ (500 MHz, CDCl_3) δ / ppm : 7.79 (d, $^3J = 8.3$ Hz, 4H, $\text{H}^{\text{A}2}$), 7.63 (d, $^3J = 8.3$ Hz, 4H, $\text{H}^{\text{A}3}$), 6.69 (d, $^4J = 2.2$ Hz, 4H, $\text{H}^{\text{B}2}$), 6.49 (t, $^4J = 2.2$ Hz, 2H, $\text{H}^{\text{B}4}$), 3.95 (t, $^3J = 6.6$ Hz, 8H, H^4), 1.85 – 1.70 (m, 8H, H^5), 1.49 – 1.15 (m, 40H, H^{6-10}), 0.89 (t, $^3J = 6.9$ Hz, 12H, H^{11}).

$^{13}\text{C-NMR}$ (125 MHz, CDCl_3) δ / ppm : 160.2 ($\text{C}^{\text{B}3}$), 136.6 ($\text{C}^{\text{A}1}$), 131.6 ($\text{C}^{\text{A}3}$), 130.0 ($\text{C}^{\text{A}2}$), 127.7 ($\text{C}^{\text{A}4}$), 123.8 ($\text{C}^{\text{B}1}$), 110.0 ($\text{C}^{\text{B}2}$), 103.3 ($\text{C}^{\text{B}4}$), 92.9 (C^3), 88.0 (C^2), 68.3 (C^4), 31.9, 29.7, 29.4, 29.3, 29.2, 26.1, 22.7, 14.1 (C^{11}), Carbonyl C not observed.

Mass (EI 70 eV, ca. 300°C) m/z : 895 (100) [M]

IR ($\tilde{\nu}$ [cm^{-1}]): 2952; 2920; 2869; 2853; 1652; 1597; 1583; 1463; 1431; 1403; 1384; 1354; 1307; 1287; 1270; 1255; 1235; 1167; 1056

Microanalysis (calculated for $\text{C}_{61}\text{H}_{82}\text{O}_5$ (895.31 g / mol)): C 81.83, H 9.23; found: C 80.72; H 9.09

3.7 References

- (1) Hawker, C. J.; Frechet, J. M. J. *J. Am. Chem. Soc.* **1990**, *112*, 7638-7647.
- (2) Elias, H.-G. *Makromoleküle*; 5th ed.; Hüthig & Wepf, 1992; Vol. 2.
- (3) Cyr, D. M.; Venkataraman, B.; Flynn, G. W. *Chem. Mater.* **1996**, *8*, 1600-1615.
- (4) Claypool, C. L.; Faglioni, F.; Goddard, W. A.; Gray, H. B.; Lewis, N. S.; Marcus, R. A. *J. Phys. Chem. B* **1997**, *101*, 5978-5995.
- (5) De Feyter, S.; Gesquiere, A.; Abdel-Mottaleb, M. M.; Grim, P. C. M.; De Schryver, F. C.; Meiners, C.; Sieffert, M.; Valiyaveetil, S.; Mullen, K. *Acc. Chem. Res.* **2000**, *33*, 520-531.
- (6) De Feyter, S.; De Schryver, F. C. *J. Phys. Chem. B* **2005**, *109*, 4290-4302.
- (7) Merz, L.; Guntherodt, H.; Scherer, L. J.; Constable, E. C.; Housecroft, C. E.; Neuburger, M.; Hermann, B. A. *Chem.-Eur. J.* **2005**, *11*, 2307-2318.
- (8) Jones, L.; Atkins, P. *Chemistry - Molecules, Matter, and Change*; 4th ed.; W. H. Freeman, 2000.
- (9) Price, S. L. *Phys. Chem. Chem. Phys.* **2008**, *10*, 1996-2009.
- (10) Constable, E. C.; Haeusler, M.; Hermann, B. A.; Housecroft, C. E.; Neuburger, M.; Schaffner, S.; Scherer, L. J. *CrystEngComm* **2007**, *9*, 176-180.
- (11) Johannes, A. A. W. E.; Shengbin, L.; Steven, De F. *Angew. Chem. Int. Ed.* **2009**, *48*, 7298-7332.
- (12) Rheiner, P. B.; Seebach, D. *Chem-Eur J* **1999**, *5*, 3221-3236.
- (13) Scherer, L. J.; Merz, L.; Constable, E. C.; Housecroft, C. E.; Neuburger, M.; Hermann, B. A. *J. Am. Chem. Soc.* **2005**, *127*, 4033-4041.
- (14) Zhu, J.; Beugelmans, R.; Bourdet, S.; Chastanet, J.; Roussi, G. *J. Org. Chem.* **1995**, *60*, 6389-6396.
- (15) vanNunen, J. L. M.; Folmer, B. F. B.; Nolte, R. J. M. *J. Am. Chem. Soc.* **1997**, *119*, 283-291.
- (16) Rajakumar, P.; Murali, V. *Tetrahedron* **2004**, *60*, 2351-2360.
- (17) Vögtle, F.; Plevoets, M.; Nachtsheim, G.; Worsdorfer, U. *J. Prakt. Chem.* **1998**, *340*, 112-121.
- (18) Garlick, R. K.; Giese, R. W. *J. Biol. Chem.* **1988**, *263*, 210-215.
- (19) Arisawa, M.; Terada, Y.; Nakagawa, M.; Nishida, A. *Angew. Chem. Int. Edit.* **2002**, *41*, 4732-4734.
- (20) Trost, B. M.; Fleming, I.; Semmelhack, M. F. *Comprehensive organic synthesis: selectivity, strategy & efficiency in modern organic chemistry*; Pergamon, 1991; Vol. 4.
- (21) Merz, L.; Hitz, J.; Hubler, U.; Weyermann, P.; Diederich, F.; Murer, P.; Seebach, D.; Widmer, I.; Stohr, M.; Guntherodt, H. J.; Hermann, B. A. *Single Mol* **2002**, *3*, 295-299.
- (22) Avent, A. G.; Birkett, P. R.; Paolucci, F.; Roffia, S.; Taylor, R.; Wachter, N. K. *J. Chem. Soc., Perkin Trans. 2* **2000**, 1409-1414.

4. Pyridine-2-carbaldehyde-2-pyridylhydrazone and its iron(II) complexes

4.1 Introduction

4.1.1 History

The pyridine-2-carbaldehyde-2-pyridylhydrazone ligand (Hpaphy) has been known since the late 1950's. It is easily synthesised as the condensation product of pyridine-2-carbaldehyde and 2-hydrazinopyridine. The synthesis was first reported by F. Lions and K. Martin¹. The authors also noted that when a solution of cobalt(II) bromide in methanol is added to Hpaphy, the cobalt(III) complex with only two counter ions is formed. The final charge was balanced by the loss of one proton from one of the ligands. That complex can be dissolved in hydrobromic acid accompanied by a significant colour change. Upon neutralisation of the acid, the original colour is restored.

In the *Inorganic Chemistry* publication from 1963 the authors, J. F. Geldard and F. Lions², synthesised a series of Hpaphy complexes with different metal ions and also generated the deprotonated compounds. It is noteworthy that the high solubility of the charge free complexes in organic solvents was observed. The authors also reported the increase in solubility in organic solvents when the imine carbon carries an alkyl chain instead of hydrogen. These were the first reported deviations away from the simple Hpaphy ligand.

In a series of two papers^{3,4} stability constants and pK_a values of Hpaphy, Hpaphy complexes and with derivatized Hpaphy complexes were measured. The measurements show clearly that the acidity of the amine proton in the backbone of the ligand is only measurable in complexes.

Other work in the same group⁵ showed that the oxidation that occurred in Co(II) Hpaphy complexes can be suppressed by the use of sterically more demanding Hpaphy ligands that shield the metal core.

Copper can also form square planar complexes as shown by F. Lions et al.⁶.

Interestingly, five coordinate cobalt(II) Hpaphy complexes are known. The crystal structure was reported by M. Gerloch^{7,8}. While three of the five coordination positions are occupied by one Hpaphy ligand, the last two are taken by chlorides. This is remarkable in respect two points. First all of the mentioned above complexes with Hpaphy are with two

Hpaphy ligands per metal centre. Second is that cobalt(II) forms almost exclusively octahedral complexes.

Hpaphy was used by F. Lions, I. G. Dance and J. Lewis⁹ in the preparation of a series on mono-chelate complexes. What makes this paper stand out is the care with which the different forms of cobalt Hpaphy complexes were studied. A similar paper was published by R. A. Walton¹⁰.

The papers by C. F. Bell and D. R. Rose^{11,12,13} are worthwhile mentioning since the authors took great care analysing and characterising the Hpaphy ligand and some of its complexes. Rose and Bell also carefully examined the two possible isomers of Hpaphy. The E-Hpaphy can be considered an analogue of 2,2':6',2''-terpyridine for both compounds offer a tridentate coordination site while Z-Hpaphy can be considered an analogue of 2,2'-bipyridine (fig. 4.1.1 and 4.1.2) for their bidentate coordination sites. The second pyridine ring has only steric influences since the nitrogen is bound in the hydrogen bond to the amine proton.

All four ligands have the common properties that they are planar and conjugated throughout. While this is not surprising for bipy and terpy, it is special in Hpaphy since the secondary amine in the backbone could break the conjugation.

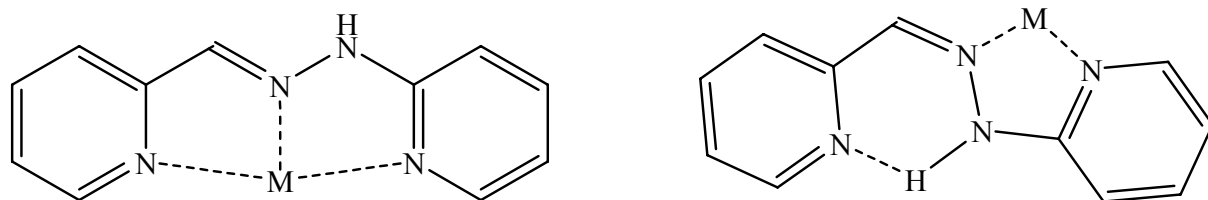


Fig. 4.1.1 E-Hpaphy (left) and Z-Hpaphy (right). Both ligands are shown with their coordination site

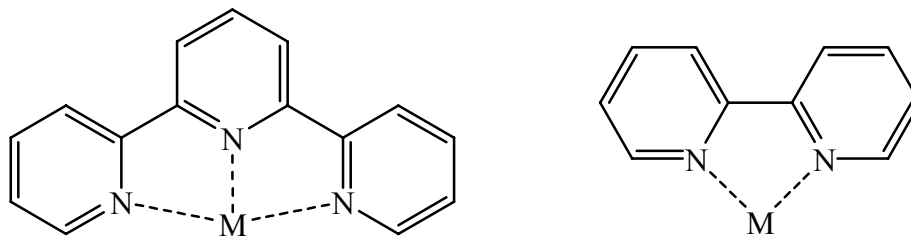


Fig. 4.1.2 2,2':6',2''-terpyridine (terpy) (left) and 2,2'-bipyridine (bipy) (right). Both ligands are shown with their coordination site

While studies show that the conversion of free E-Hpaphy to Z-Hpaphy is possible by heating or irradiation¹² the conversion back for the free ligand seems to be blocked. The conversion of Z-Hpaphy to E-Hpaphy has been observed in iron complexes¹².

As expected, the two different conformations of Hpaphy give rise to very different behaviour. The two forms can easily be distinguished by ¹H-NMR spectroscopic measurements since there is a big shift observable for the H-bridged proton in the Z form compared to the unbridged H in the E form.

The paper by J. G. Dunn and D. A. Edwards¹⁴ has a strong focus on Z-Hpaphy as a bidentate ligand and is therefore not of much interest for this work due to our strong focus on the tridentate iron(II) Hpaphy complexes. Dunn and Edwards^{15,16} continued their work with Hpaphy creating a new series bi and tri dentate Hpaphy complexes with several different metals.

To illustrate the unbroken scientific interest in Hpaphy and its complexes a selection of references concerning Hpaphy has been compiled. While the references above and following are concerned more with general scientific interest, analytical and direct practical applications that were proposed are placed in separate subsections.

G. Anderegg¹⁷ measured the stability constants of Hpaphy complexes with manganese, copper, zinc and cadmium. R. Crichton et al.¹⁸ used Hpaphy to release iron from ferritin to allow for better analysis. L. Constanzo et al.^{19,20} studied the mechanism of photoisomerisation of Hpaphy while A. Mihkelson^{21,22} used Hpaphy to study the interactions of tri dentate ligands with palladium. Butler et al.²³ examined the oxidative cyclization of Hpaphy and some similar compounds in the presence of mercury and lead ions. M. Mohan et al. synthesised a variety of Hpaphy complexes and studied their cell toxicity²⁴. E. Ainscough et al. synthesised some interesting copper Hpaphy complexes and measured the crystal structures²⁵. Remarkable is that in one case the unit cell of one complex possess two metal centres with different geometries.

One of the more recent publication by A. Wood, et al.²⁶ deals with the acidity of the secondary amine proton in E-Hpaphy iron complexes. The shifts in the UV-vis spectra for the protonated (Hpaphy) and deprotonated (paphy) complex are described. Further it is shown that the iron-paphy complexes can be alkylated at the N-position by a variety of electrophiles.

F. Dumitru et al. created with Hpaphy and two other nitrogen containing aromatic ligands a series of homo and heteroleptic zinc complexes and were able to obtain for several of these complexes the crystal structures²⁷.

R. Warr et al.²⁸ used Hpaphy for its simple formation over Schiff base condensation. The usage of a tridentate ligand in the asymmetric inorganic synthesis Warr et al. conducted required mild reaction conditions due to the optically active core that was used to induce the stereoselectivity.

4.1.2 Analytical Applications

Due to the intense colouring of the solutions of some of the Hpaphy complexes, spectroscopic quantitative methods for the determination of metal ions in solution were proposed, for example for palladium²⁹.

The first fully developed analytical method based on Hpaphy is as an agent to bind palladium, followed by the spectroscopic determination of the concentration of the complex. The method developed by A. Cameron and N. Gibson³⁰ showed good results.

A. Cameron and N. Gibson^{31,32} also proposed the usage of paphy/Hpaphy complexes as acid base indicators for titrations. This is only logical due to Hpaphy's ability to lose protons upon complexation and the intense colour change in the protonation/deprotonation event. The authors took great care studying the properties of the indicator constants (in reference to this also see the paper by R. Green et al³³). Bell and Quddus³⁴ proposed the usage of Hpaphy in nephelometric (measuring of light scattering of a solution) and turbidometric (light absorbance of a solution due to clouding) methods. These two methods are not very often used due to the difficulties in obtaining reproducible results. The biggest problem to overcome here is that the suspensions have to form always the same way in respect to particle size. Ryan et al³⁵ conducted some fluorescence studies with Hpaphy and derivatives of Hpaphy focusing on zinc. Although Hpaphy itself did not show any remarkable fluorescence some, of its derivatives certainly would allow for applications in analytics. Based on the work of Quddus and Bell, P. Haddad et al³⁶ did spectroscopic and fluorometric determination of cobalt in solutions after phase extraction with Hpaphy. D. Burns et al.³⁷ used Hpaphy for the determination of cobalt in steel by the spectroscopic analysis of the complex concentration using a fluorescent counter ion. R. Montes et al. used Hpaphy in the development of kinetic methods to determine the concentrations of palladium³⁸ and nitrate³⁹. A. Abu Zuhri et al. did polarography studies on solutions of Hpaphy⁴⁰. H. Ishii et al. used Hpaphy derivatives for the spectroscopic trace analysis of various metals⁴¹ and the equilibria and kinetics of nickel extraction⁴². Surface enhanced Raman spectroscopy was used by M. Hidalgo et al.⁴³ in conjunction with Hpaphy for trace analysis of metals. Complexation of the trace metal is in

this case necessary since single atoms do not possess bond vibrations that can be measured with Raman or infrared spectroscopy.

4.1.3 Practical Applications

Quddus et al.⁴⁴ proposed the usage of Hpaphy for phase extraction of metal ions in solution utilising the strongly changing solubility behaviours when a metal complex of Hpaphy is deprotonated. The wide range of metals used in the study suggests that this method works very well as a general metal ion catcher.

Quddus and Bell⁴⁵ studied the extraction of zinc as Hpaphy complex into organic phases. The general possibility has been shown and proven. Since only zinc had been tested the question about selectivity remains.

Among other similar compounds Hpaphy was tested by A. Todeschini et al.⁴⁶ for analgesic, anti-inflammatory and antiplatelet properties but did not show any activity.

4.1.4 Properties

Hpaphy possesses some interesting features. The ligand can have either a bi- or tridentate coordination mode. In the bidentate form, an internal hydrogen bond is present (fig. 4.1.1). Interconversions between the two forms are possible and have been observed.

The complexes of Hpaphy with different metals show when the ligand is tridentate it gains the ability to lose the N-H proton on the back bone of the ligand upon complexation (fig. 4.1.3).

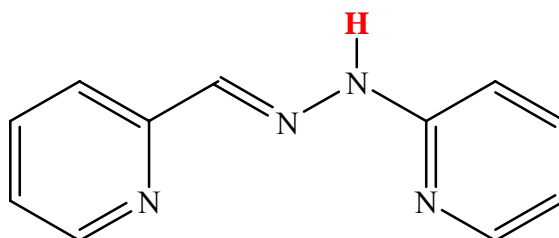


Fig. 4.1.3 Hpaphy with removable proton in red

When the deprotonation occurs, complexes with doubly charged metal ions become overall charge neutral, giving compounds that are usually no longer soluble in water. The charged backbone is stabilised by the resonance forms shown in fig. 4.1.4.

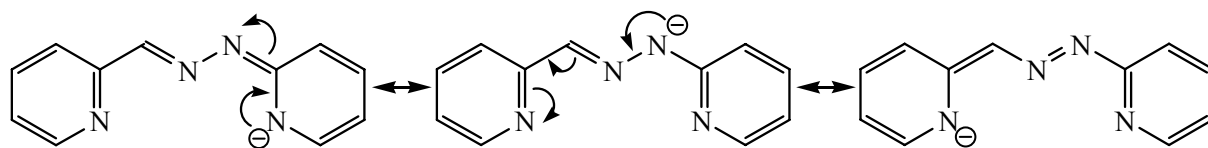


Fig. 4.1.4 The three resonance forms of the paphy ligand

The deprotonation is not possible in the free ligand. For reasons of presentation the metal centre in fig. 4.1.4 was neglected. Deprotonation of the ligand generally leads to an increase of electron density in the nitrogen metal bonds. This can lead to drastically changed chromophoric behaviour of the complex. The best examined example for this is the iron(II) Hpaphy complex that changes from red (protonated state) to dark green in paphy (deprotonated state).

This colour change is due to an increase in σ -donor strength that then increases the electron density on the metal centre claim A. Wood et al²⁶. This theory is supported by the fact that there is no spin change observable going from one form to the other.

This is confirmed by NMR spectroscopy where both forms, the protonated and deprotonated, can be measured without requiring special parameters. This is only possible if the complex is diamagnetic (see fig. 4.1.5).

The orbitals shown in fig. 4.1.6 are the five 3d orbitals of iron(II). In the free iron ion the five 3d orbitals are degenerate (they have the same energy level) when the ion is present in a complex this is no longer true. If along the axis of a coordination system 6 ligands (octahedral coordination sphere) are put close to the iron ion, unfavourable interactions in the d-orbitals closest to the axes ($d_{x^2-y^2}$, d_{z^2}) are the result.

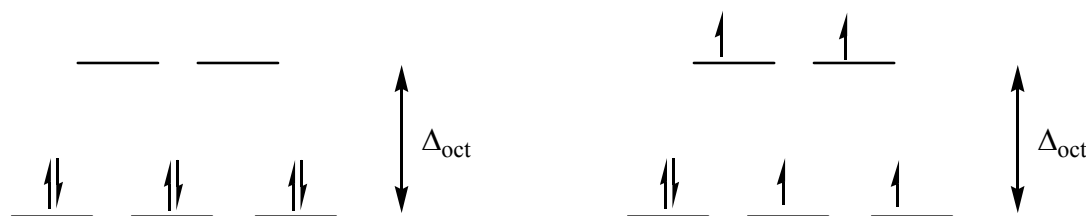


Fig. 4.1.5 The two possible spin states for Fe(II). Left: low spin with all electrons paired.

Right: high spin with unpaired electrons

The distance between the two levels of d-orbitals is called Δ_{oct} . By filling the lower orbitals energy is gained. But at the same time if an orbital has to be filled doubly, the spin pairing energy has to be subtracted from the orbital stabilisation energy. While the spin pairing

energy is constant the orbital stabilisation energy depends strongly on the ligands used to form the complex. If the orbital stabilisation energy is smaller than the spin pairing energy, high spin complexes will result from that combination.

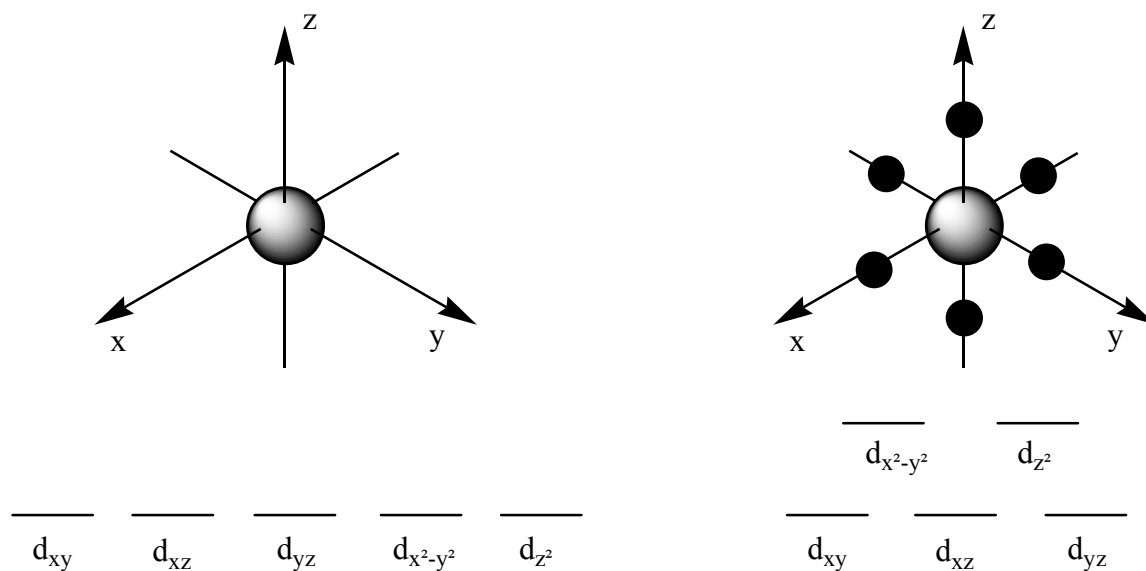


Fig. 4.1.6 Representation of the d-orbitals in the free atom (left) and the octahedral complex (right)

4.1.5 Stereochemistry

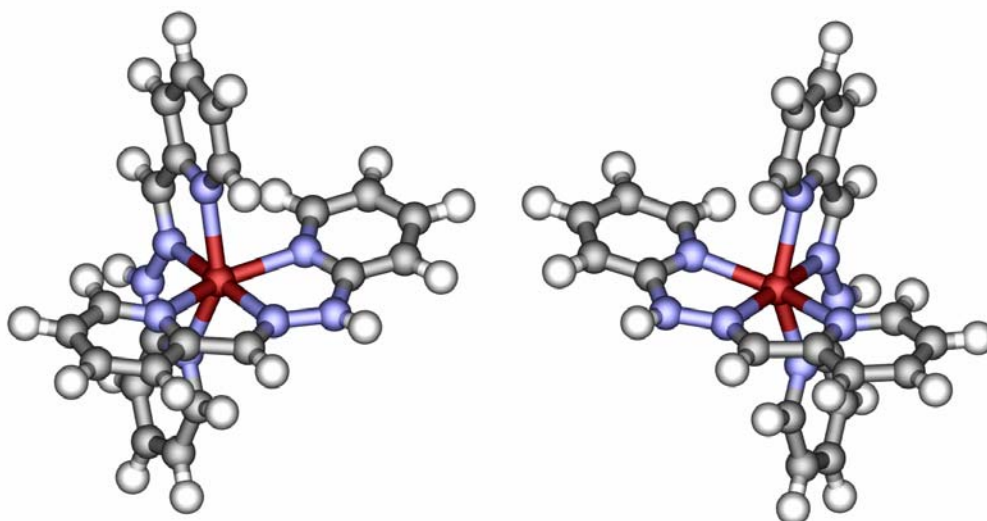


Fig. 4.1.7 The two possible enantiomers of the $[Fe(paphy)_2]$ complex.

Although Hpaphy itself is achiral the complexes of Hpaphy with an octahedral metal ion like Fe^{2+} are enantiomeric. The two possible forms are shown in fig. 4.1.7. The splitting into

enantiomers is the consequence of the asymmetry in the backbone of Hpaphy. The nomenclature to distinguish the two enantiomers can for example be taken from the DNA nomenclature as for example done by Warr et al.²⁸. By looking down the C_2 rotation axis (fig. 4.1.8) we see the two enantiomeric screws. The lefthand screw is anti clockwise and is designated M. The enantiomer on the right is the clockwise screw and designated P. Due to the identical chemical and physical behaviour of the two enantiomers, separation of the two compounds is only possible in a chiral environment.

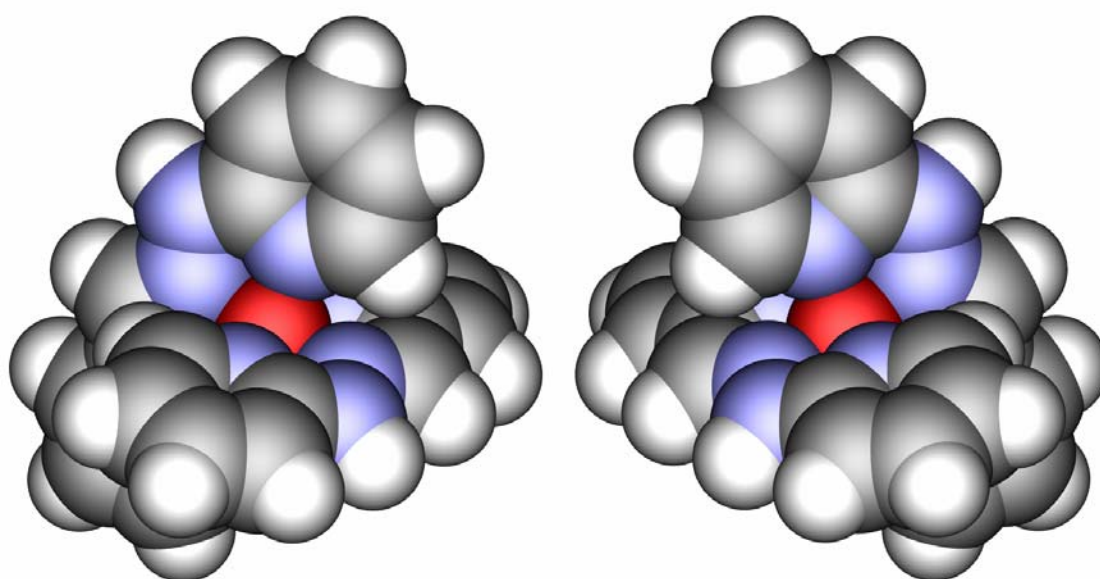


Fig. 4.1.8 Representation of the two possible screws of the octahedral Hpaphy complexes. The C_2 axis is coming straight out of the plane. The left anti clockwise screw is designated M (minus), the right clockwise screw P (plus)

4.1.6 Toxicity

Many publications on the toxicity of hydrazine and some of its derivatives are published. Two such studies are given with reference here to offer an entry into the topic^{47,48}. Especially the publication of A. Siemens, M. Kitzes and M. Berns⁴⁷ contains many references to other studies. In short hydrazine is known to be highly toxic working as a cell toxin. It is also a known carcinogen and mutagen.

Although there are no studies on the toxicity of the Hpaphy ligand it has to be considered that the condensation reaction is reversible and the release of 2-hydrazinopyridine in aqueous

media is likely. The study by B. Mathison, S. Murphy and R. Shank⁴⁸ shows the effects of several hydrazine derivatives on DNA, one of the compounds tested was phenylhydrazine.

Considering the big toxicological effects it is not surprising that the Hpaphy ligand did not succeed in the proposed applications of acid-base indicator, phase extraction reagent or as ligand for colourmetric metal assay even though Hpaphy would be quite well suited for all of the mentioned applications. The non-toxic alternative compounds are generally selected for these applications.

4.1.7 Summary

Compared to, for example, terpy there are surprisingly few published papers on paphy and metal complexes with Hpaphy. Despite the fact that the ligand has been known for a long time, till about now (middle of 2009) only a little over one hundred publications about Hpaphy have been written (data mining conducted with Scifinder).

Apart from the standard work on metal ligands several proposals to what effect paphy could be used have been published. The proposed applications range from the use as acid-base indicator, spectroscopic tool for metal analysis, phase extraction reagent for metals, oxidation reagent for analysis and even in medical applications as cell toxin.

Despite all this work and proposals, large scale usage of Hpaphy in any of these fields never occurred. The probable reasons for this are though that Hpaphy in all of these areas works fine but also suffers serious drawbacks in each of these fields. As acid-base indicator a problem is the insolubility of the charge free species in water as well as the relatively broad range for the colour change due to the two proton exchange for the full conversion.

For the spectroscopic application the biggest problem is most likely the labile protons of the complexes. The spectra of the complexes differ strongly in the protonated and deprotonated state. This makes it necessary to work with buffer solutions to obtain reproducible results.

The phase extraction with Hpaphy works well but the ligand is not reusable since the conditions needed to take the complexed metal out of Hpaphy again are usually harsh enough to irreversibly decompose the ligand itself. This severely limits industrial applications.

Over all these problems the issue of toxicity remains to be addressed. Studies have shown that Hpaphy and derivatives of it can be used as cell toxins and are able to bind to DNA⁴⁹. This is a severe drawback for any other application than medical.

4.2 Aims

The aims were the synthesis of Hpaphy and paphy ligands modified with dendritic wedges. With these ligands iron(II) complexes were made.

4.3 Synthesis

The synthesis described by Lions and Martin¹ works extremely well and is high yielding. As the simple condensation reaction from the pyridine-2-carbaldehyde and 2-hydrazinopyridine, both commercially available, the unmodified Hpaphy ligand is easily available. Only the price of the 2-hydrazinopyridine and its toxicity are issues that need to be addressed.

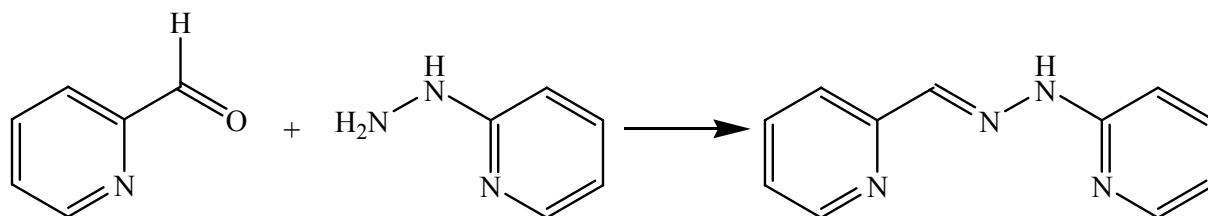


Fig. 4.3.1 Condensations reaction for the synthesis of paphy

Hpaphy was selected for this work for its ability to lose the NH proton upon complexation of a metal, yielding for the homoleptic charge neutral bis paphy complex with a 2+ metal ion. It was expected that the charge neutral iron paphy complexes would have better properties for examination by STM. Due to the lower charge density within the monolayer improved properties for the arrangement on the surface were expected. Another important point is that since the counter ions needed in charged complexes could be eliminated, raising expectations of more predictable arrangements on the surface.

It is noteworthy that within our research group previous work has managed to obtain STM pictures of charged terpy complexes but the counter ions could never be observed.

To be able to work with more symmetrical ligands, two sites on Hpaphy were selected for modification (fig. 4.3.2). The two sites differ very strongly in their chemistry. Site X for example is only available before the condensation reaction by selecting a matching ketone instead of pyridine-2-carbaldehyde. Modifications on the X position are no longer possible once the final ligand has been formed.

The opposite is true for the position Y that can only be modified in the complex form. Upon complexation of a metal, the N-H proton becomes very acidic (for an amine proton) and removal of the proton can be achieved by a simple wash with aqueous sodium hydroxide. Very interesting is the shift in colour upon deprotonation. While the protonated, charged iron complex is red, the deprotonated complex is green. With a doubly charged metal ion like iron(II) an overall charge neutral complex is obtained.

When the charge neutral complex is being reacted with an electrophile like alkyl halogens the Y position gets alkylated. This has been done for example with iodomethane²⁶.

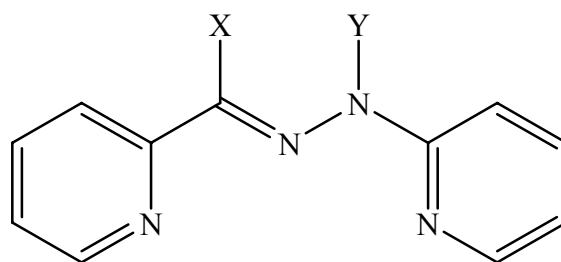


Fig. 4.3.2 Positions X and Y that were selected for modification

The modification of the Y position worked well and with reasonable yields. For that the iron papy complex was simply reacted with the **G1** bromide (**3**) in CH_2Cl_2 . The same was also done with the **G2** bromide wedge (**13**) (fig. 4.3.3).

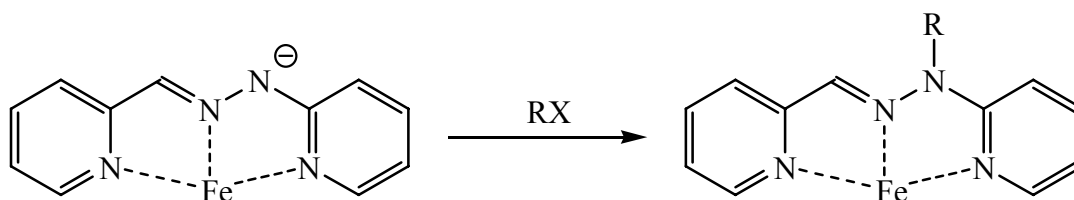


Fig. 4.3.3 Schematic representation for the alkylation of a deprotonated papy complex. RX represents an alkyl halogenid, $\text{X} = \text{Br}, \text{I}$

The modifications on the X position proved to be somewhat more complicated. Several different synthetic routes were examined. The first attempted route was with methyl-2-pyridine ketone which was treated with strong base and then **G1** bromide was added for the ketone to nucleophilic attack. For reasons unknown the desired product could not be isolated. Only small quantities of the bis adduct were isolated (fig. 4.3.4).

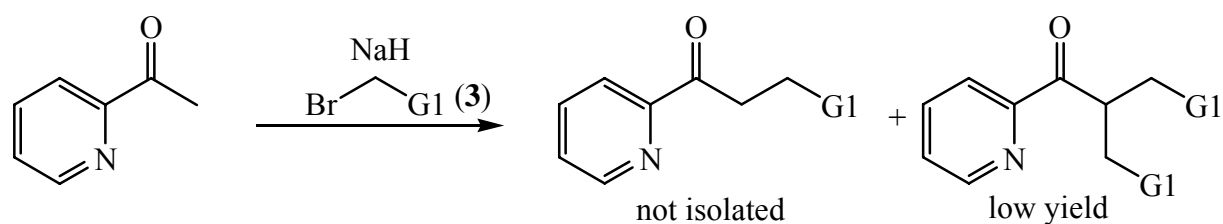


Fig. 4.3.4 Synthetic approach for the synthesis of the desired ketone for Hpaphy synthesis. The desired product (left) could not be isolated.

To prevent the bis alkylation product formation, ethyl picolinoylacetate was used as starting material. This worked and the desired mono alkylation product could be isolated in reasonable yields. The following step of ester cleavage and decarboxylation on the other hand could not be brought to success. Several methods were examined but usually the harsh reaction conditions destroyed the starting material.

The reaction of 2-bromopyridine with first butyl lithium and then propionitrile followed by acidic hydrolysis gave a modest yield of the ethyl-2-pyridine ketone. The reasoning for selecting this starting material was that the ethyl instead of the methyl group could prevent the bis adduct from being formed. A continued test reaction for the formation to the dendritic ketone did not work. Due to the negative results and the introduction of an undesired stereo centre in the ligand with the last reaction this pathway was abandoned.

The attempt over a Wittig reaction starting from 2-(bromomethyl)pyridine hydrobromide followed by an oxidation of the resulting alcohol was workable. To find an oxidation method reactive and mild enough proved to be not a simple task. A modified Oppenauer oxidation⁵⁰ gave the best results. Here the oxidation was propagated by the reduction of 9-fluorenone.

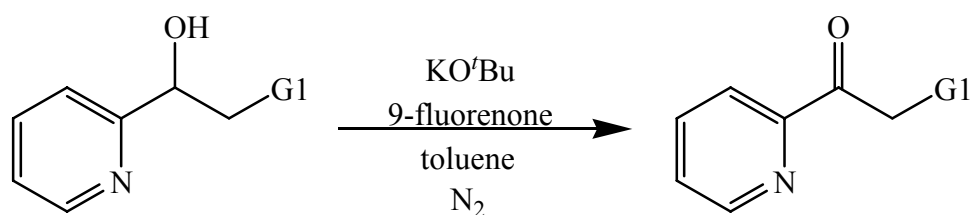


Fig. 4.3.5 Reaction scheme for the modified Oppenauer oxidation

But the general low yields of the reaction steps towards the target molecule, especially for the generation of the Grignard reagent from the dendritic bromide, made the synthesis following this path undesirable.

A better method was found with fewer steps and higher yields. This alternative starts with pyridine-2-carbaldehyde and generates the diphenyl-1-(phenylamino)-1-(2-pyridyl) methylphosphonate (**27**) in combination with diphenylphosphate and aniline⁵¹ (fig. 4.3.6). This product is then reacted with the dendritic wedge aldehyde and base to form an enamine intermediate (fig. 4.3.7) that is then hydrolysed with hydrochloric acid to the desired ketone.

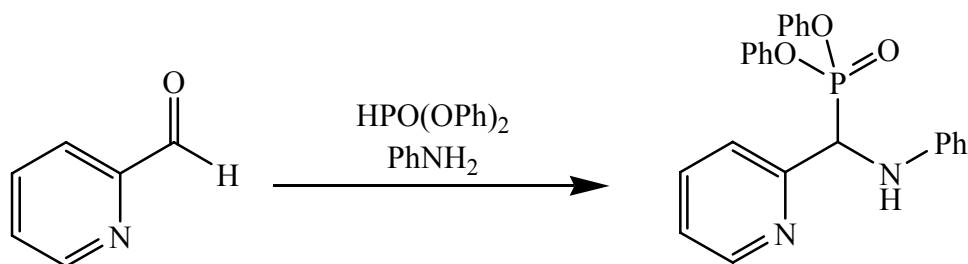


Fig. 4.3.6 reaction scheme for the formation of diphenyl-1-(phenylamino)-1-(2-pyridyl) methylphosphonate

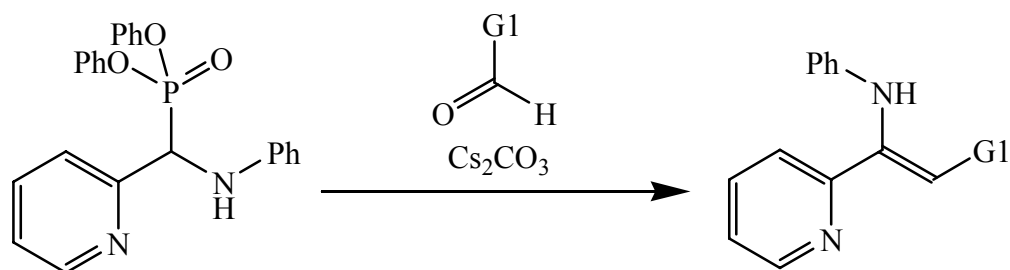


Fig. 4.3.7 Synthesis of the enamine derivative

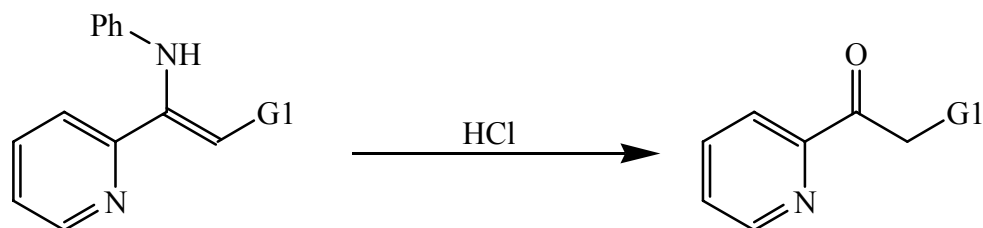


Fig. 4.3.8 Hydrolysis to the ketone with hydrochloric acid

By the simple condensation reaction with 2-hydrazinopyridine, the final Hpaphy ligand was generated. The same path works also for the **G2** wedge. In the condensation step, the yield is only about 50% because of the increasingly favoured formation of the Z-Hpaphy ligand over the E-Hpaphy due to the increased steric demand of the dendritic wedge.

The **G1** and **G2** modified free Hpaphy ligands (**29**), (**32**) were therefore synthesised by this route.

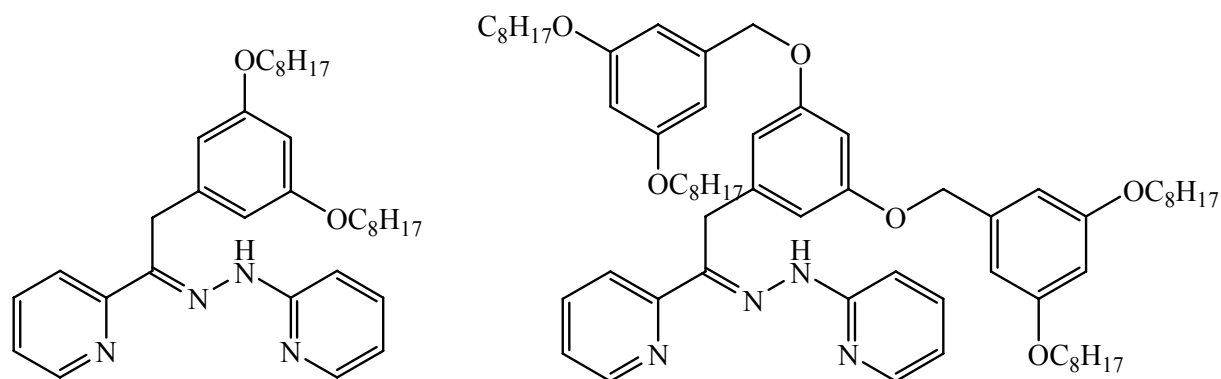


Fig. 4.3.9 Structures of the Hpaphy ligands modified with the first (**29**) (left) and second (**32**) (right) generation dendritic wedges.

These ligands still possess the ability to be deprotonated upon complexation. Due to the labile protons, it was difficult to obtain complexes of these compounds pure. It was observed that the complexes tended to lose a proton in the protonated state or when working with the deprotonated compounds, a proton was added. This posed tremendous problems since the purity of the compounds was essential for the STM measurements. To overcome this problem it was decided to use iodomethane to alkylate the amine position in the complexes. This worked well, and the resulting complexes are stable and showed no change upon treatment with acid or base. While the synthesis worked very well, purification of these compounds proved to be difficult. For the **G2** compound, chromatography gave satisfactory results but the **G1** compounds proved to be impossible to purify. Due to the nature of the compound (viscous oil) some of the best methods for purification could not be applied. These methods include crystallisation and precipitation. Attempts were made to purify the compound by diffusion experiments. An attempt was made at a phase separation between a highly saturated solution of the compound mixture in CH_2Cl_2 . It was tested whether the solution would separate into a pure concentrated phase and a phase containing the impurities. A separation was observed but a $^1\text{H-NMR}$ spectroscopic control showed that the product had not been purified.

Since for all further plans for STM measurements required pure compounds, it was decided to leave the **G1** compound out. To retain a comparison between the **G1** and **G2** complex the unmodified iron paphy complex was directly alkylated with the dendritic wedges. Purification was possible for these two compounds and the pure complexes were characterised with standard methods ($^1\text{H-NMR}$, $^{13}\text{C-NMR}$, IR, mass spectrometry, microanalysis).

4.4 Titration Experiments

For a better understanding of the acid-base equilibria of the $[\text{Fe}(\text{paphy})_2]$ complex system, titration experiments were conducted. Because the changes from protonated to deprotonated or vice versa are accompanied by a strong colour change, the titrations were observed by UV-vis spectroscopy.

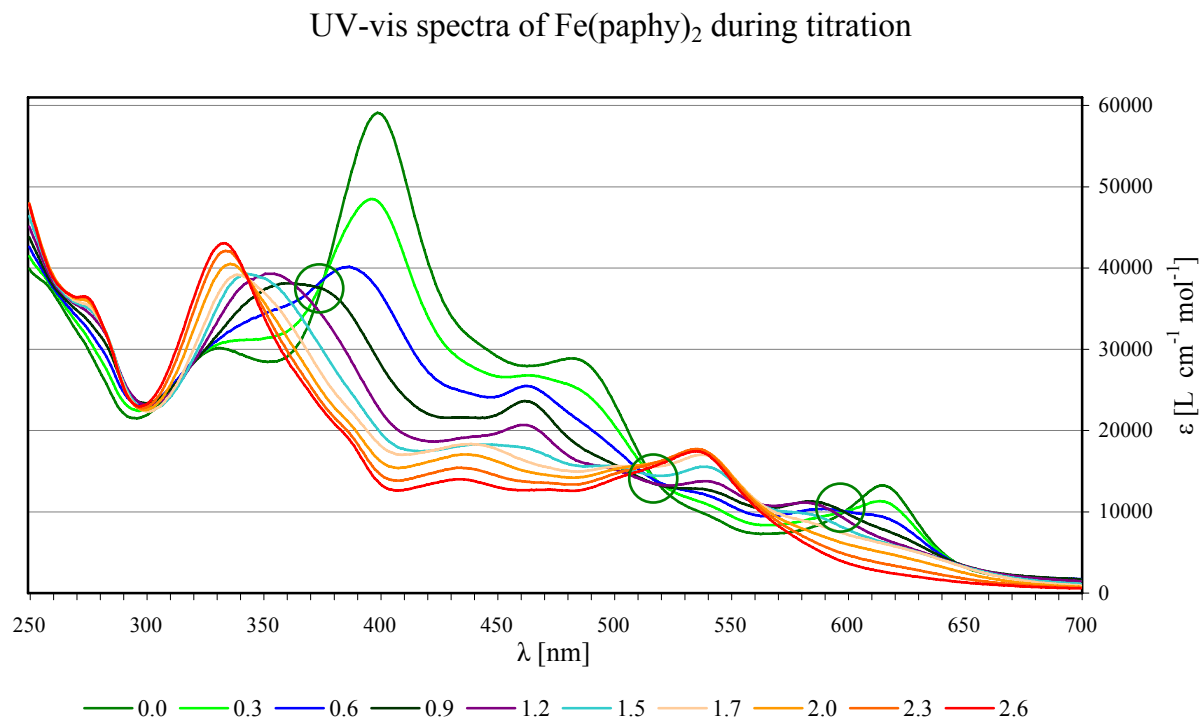


Fig. 4.4.1 UV-vis spectra of $[\text{Fe}(\text{paphy})_2]$ complex during titration. The different curves are standing for acid equivalents. The green circles marking the isosbestic points of the first titration step.

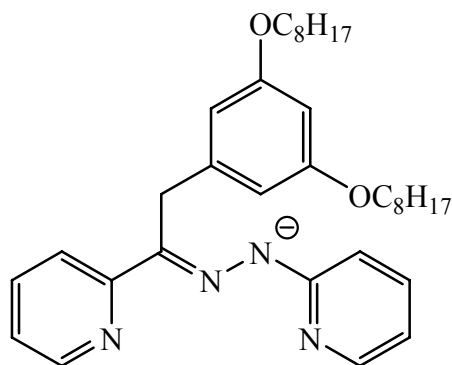


Fig. 4.4.2 The paphy ligand used for the titration experiment. The **G1** dendritic wedge ensures the solubility of the complex in organic solvents.

Fig. 4.4.1 gives the UV-vis spectra of the titration of $[\text{Fe}(\text{paphy})_2]$ with TFA. The isosbestic point at 599 nm is clearly visible. It is very well defined till 0.9 equivalents of acid have been added. With higher concentrations, the point disappears. This shows that till about one equivalent of acid, a simple two component system is being observed. At 517 nm and 373

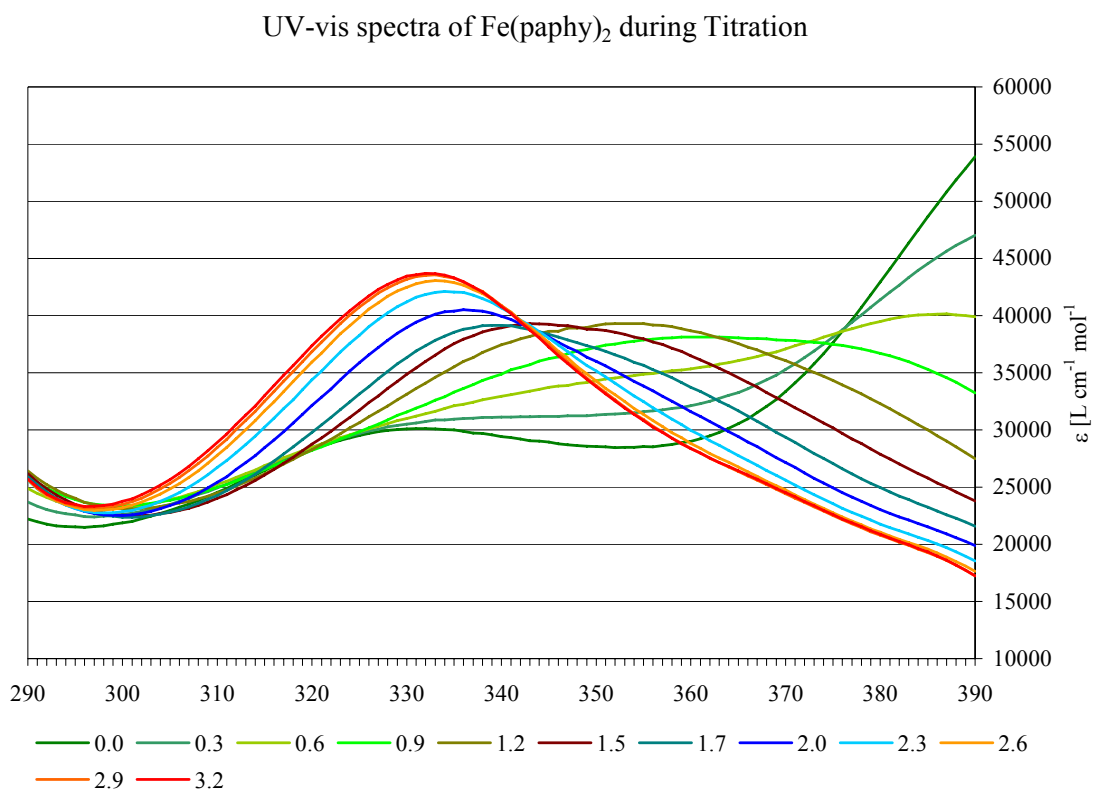


Fig. 4.4.3 Enhancement of the UV-Vis titration spectra of $\text{Fe}(\text{paphy})_2$ with the isosbestic point.

nm, two other isosbestic points are visible for the same four titration curves. These points are not as well defined and sharp as the one at 599 nm but still these two additional points give support for the claim of a simple one to one conversion for the first protonation step. With higher acid concentrations, this system becomes more complex.

A new isosbestic point emerges at 344 nm beginning with 1.2 equivalents of acid. The curve at 1.5 acid equivalents is an outlier that is the only deviant from that new isosbestic point. Very clear from the enhanced view (fig. 4.4.3) is that above two equivalents of acid no significant change in the spectra is observed anymore.

In the deprotonated form, four charge transfer bands are observable at 329 nm, 398 nm, 480 nm, 613 nm. With rising acid concentrations a new species arises with charge transfer bands at 351 nm, 460 nm and 582 nm. This species is most likely the mono protonated complex. This species disappears again with further increased acid concentration. This is most

likely the fully protonated complex which exhibits charge transfer bands at 332 nm, 433 nm and 534 nm.

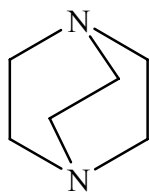


Fig. 4.4.4 Structure of DABCO

An additional titration experiment was conducted starting from the iron Hpaphy complex which was titrated using DABCO. DABCO was selected due to its mediocre base strength (bases that are too strong could lead to ligand decomposition) and its solubility in organic solvents. The pK_a values for $[Fe(Hpaphy)_2]^{2+}$ were determined by Cameron et al.^{31,32} and in these papers the pH for the middle of the colour change is given as 6.4.

UV-vis spectra of $Fe(paphy)_2$ during titration

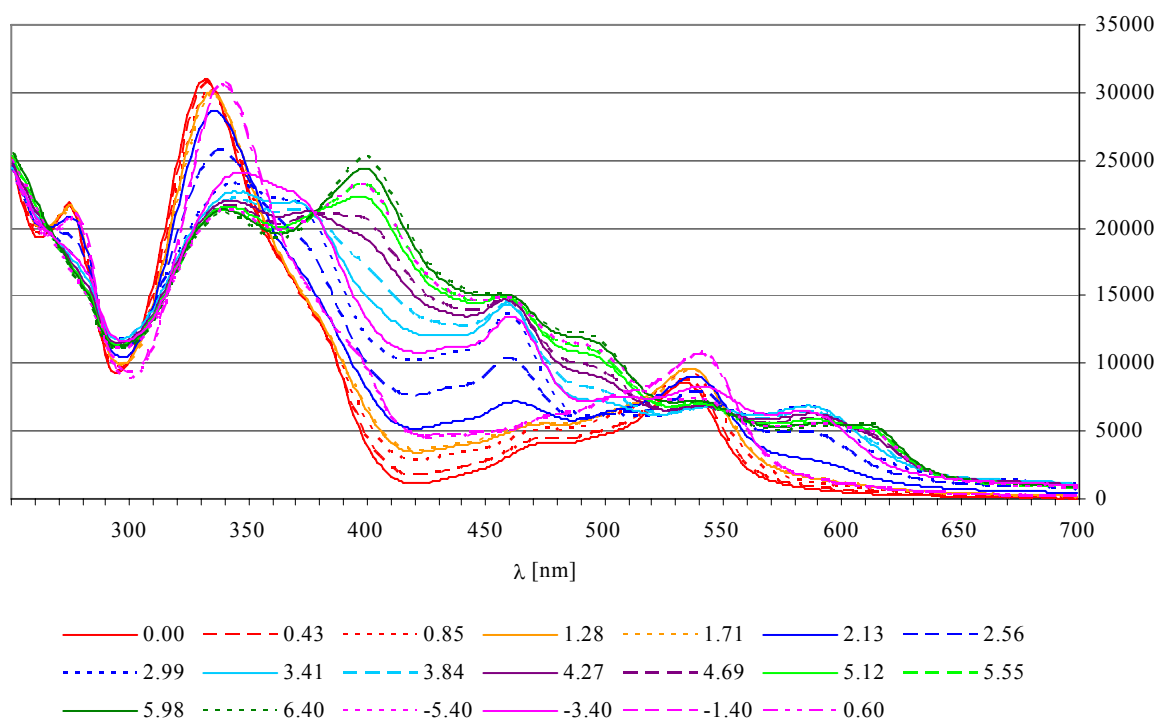


Fig. 4.4.5 Titration experiment of charged $Fe(Hpaphy)_2$ complex with DABCO. The spectra of 0.00 to 6.40 are base equivalents. The last four spectra are for acid equivalents.

The titration of the charged $[Fe(Hpaphy)_2]^{2+}$ complex with DABCO is shown in fig. 4.4.5. As is clearly visible from the curves and comparison with fig. 4.4.1, a full deprotonation could not be achieved with DABCO. The maximum at 397 nm is not nearly as high as in the case when the titration was started with the deprotonated compound (fig. 4.4.1). The system is

highly reversible as shown in fig. 4.4.5. After the addition of 6.4 equivalents of DABCO, TFA was added till all base was neutralised (the last four spectra in fig. 4.4.5). Even though the spectra do not reverse fully to the starting spectra the deviation is assumed to come from the buffering resulting from the neutralisation of the base with the acid.

4.5 Hindered Rotation

Indications have been found that for compounds (25) and (26), the rotation around the bond shown in fig. 4.5.1 (red circle) is hindered on the NMR timescale.

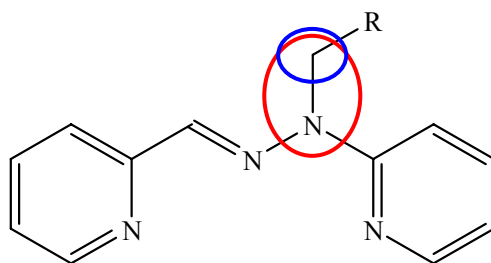


Fig. 4.5.1 Ligand structure for compounds (25) and (26). Complete complex structure is not shown for simplicity.

The indication for the hindered rotation is the splitting of the signal for the CH₂ group (blue circle) in the proton NMR spectra. For compounds with unhindered rotation, a singlet is expected for the CH₂ group. A splitting of the signal into two doublets was observed with a coupling constant of 18 Hz which is typical for geminal coupling. In the spectrum recorded in CDCl₃, the two signals come close together and almost look like a quartet. When the solvent is changed to C₆D₆ it becomes very clear that there are two doublets.

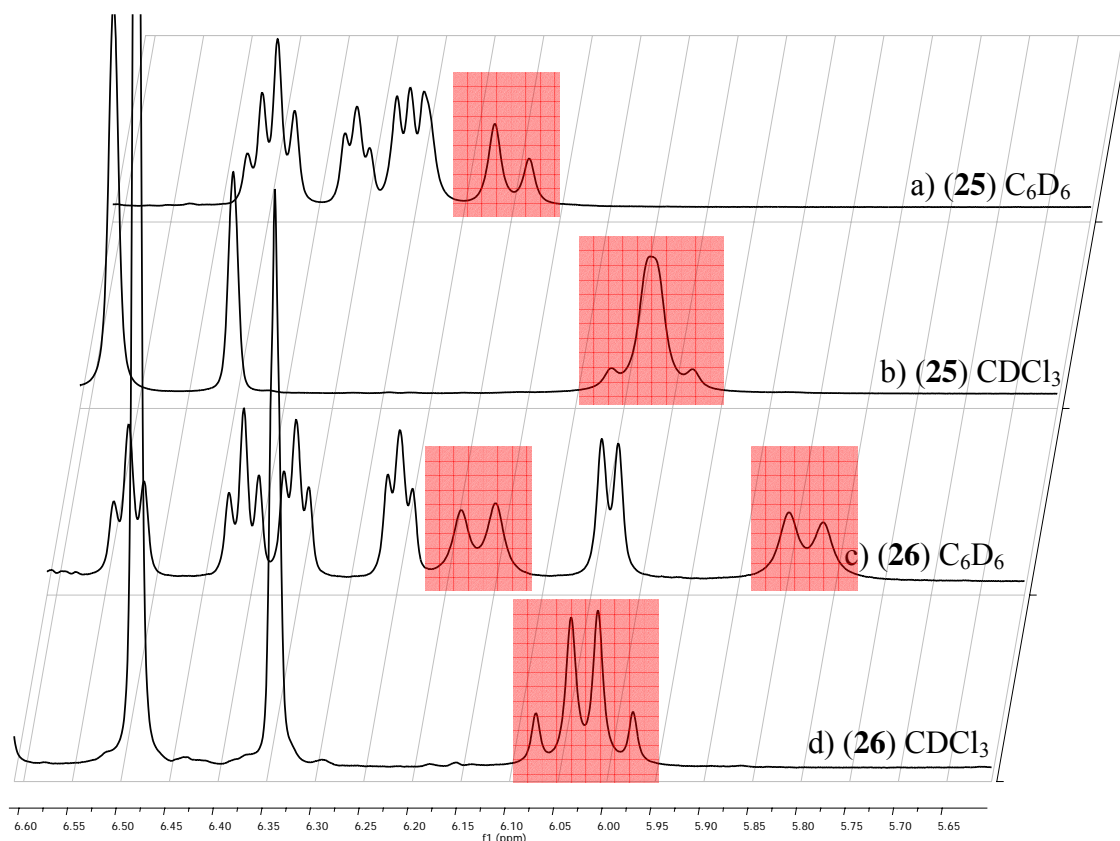


Fig. 4.5.2 ^1H -NMR spectrum extracts for compounds (25) and (26) in CDCl_3 and C_6D_6 . The red boxes marking the signals for the CH_2 group. In spectrum a) only one doublet is visible.

The second one is obscured by other signals.

The reason for the hindered rotation is at present unclear. Low temperature proton NMR measurements were done with compound (33) to see if the bond to the dendritic wedge would also start to express hindered rotation but no observation for that could be made.

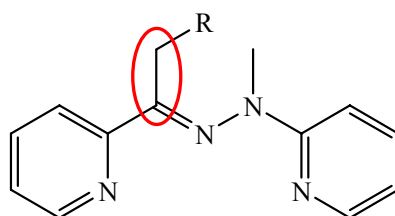


Fig. 4.5.3 Ligand structure of compound (33). No hindered rotation around the marked bond was observable

But it is clear that the different substitution leads to a change in the π -system of the ligand. This is also expressed in the changes in the UV-vis spectra for compounds (25), (26) and (33)

(fig. 4.5.4). While all three spectra are the same for the UV region (> 300 nm); observed differences in that region are simply the result of the **G2** compounds (**26**), (**33**) having more aromatic rings than the **G1** compound (**25**). But significant differences are apparent in the visible region of the spectra. While compound (**33**) shows three charge transfer bands at 340, 480 and 543 nm, compounds (**25**) and (**26**) show four charge transfer bands at 334, 385, 464 and 524 nm.

UV-vis spectra of compounds (**25**), (**26**) and (**33**)

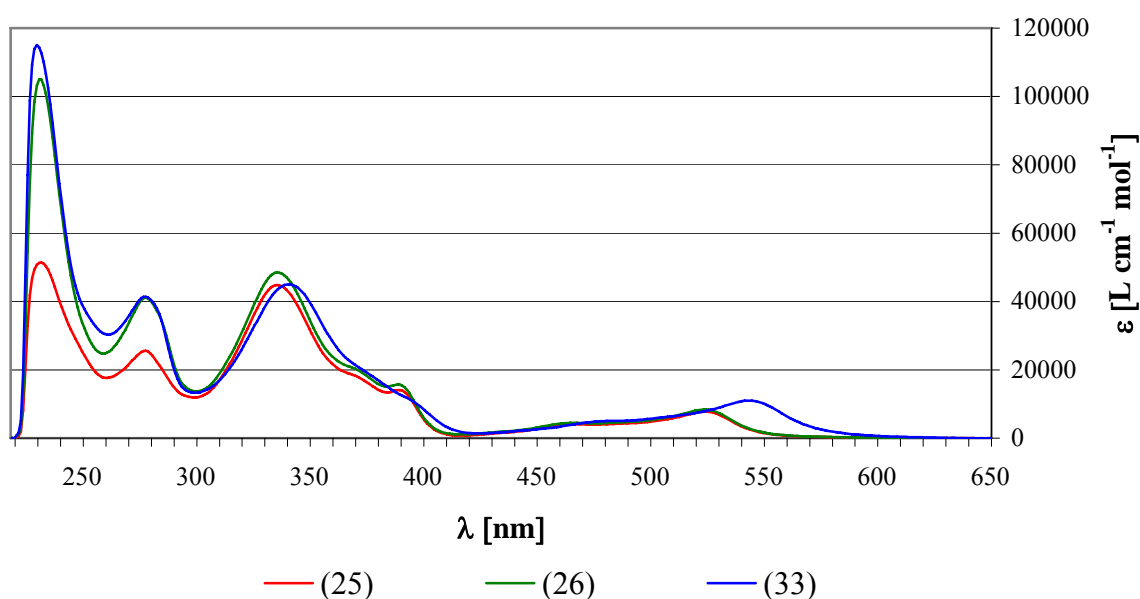


Fig. 4.5.4 UV-vis spectra of compounds (**25**), (**26**) and (**33**).

It has to be noted that the $[\text{Fe}(\text{Hpaphy})_2]^{2+}$ and $[\text{Fe}(\text{paphy})_2]$ complexes possess some interesting properties. While most metal complexes (for example with terpy) show only one charge transfer band in the UV-vis spectra the Hpaphy and paphy complexes show three to four such bands. This might be credited to a separation of the ligand π -system into π^* sub systems like the pyridine and imine π^* systems.

4.6 Conclusions

Hpaphy is a very interesting ligand with many promising features. The simple and easy synthesis from 2-pyridine aldehyde/ketone with the 2-hydrazinopyridine gives opportunities for many different modifications on the pyridine rings as well as the ligand back bone. Since the different positions for modification are available at different stages of the synthesis, this allows for a selective synthetic approach. Longterm storage of the ligand can be problematic due to possible photoisomerisation of the E-Hpaphy to Z-Hpaphy.

With doubly charged metal ions, neutral complexes can be synthesised by deprotonation of the ligands at the amine position. The complexes so obtained are usually very soluble in organic solvents. With a electrophile, the ligands can be alkylated at the deprotonated amine position. This further increases the possibilities for modifications.

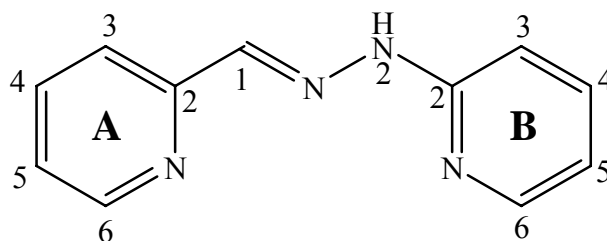
While Hpaphy in general is a stable ligand and also forms stable complexes the ability for deprotonation of the ligand in complexes poses some problems. When in the complex the ligands are deprotonated is that accompanied by an increase in general reactivity. This is problematic since it also reduces the long term stability of the complex. It was observed that the iron(II) paphy complex did undergo a conversion when stored for longer periods. That conversion was not a simple backprotonation of the ligand since it was tried to regenerate the original complex by a basic workup.

To avoid these problems it was decided to only store the N-alkylated complexes.

Once the problems with the iron paphy and Hpaphy complexes have been overcome, especially the purification problems, paphy and Hpaphy give reliable and good results.

4.7 Experimental Section

Pyridine-2-carbaldehyde-2-pyridiylhydrazone (**24**)¹



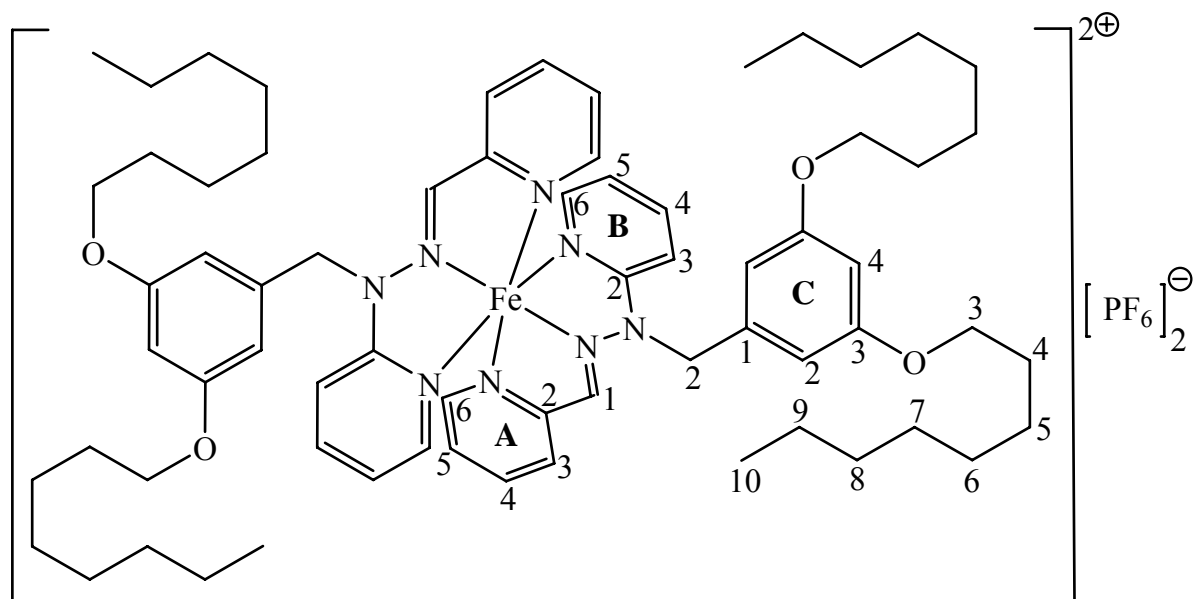
2-Hydrazinopyridine (14.7 g, 135 mmol, 1.00 eq) was dissolved in ethanol (20 mL). Pyridine-2-carboxaldehyde (13.0 mL, 137 mmol 1.01 eq) was added and an exothermic reaction occurred. The reaction mixture changed colour from yellow to red.

Upon cooling, the crude product precipitated and was separated by filtration. After recrystallization from ethanol and drying in vacuo the pure product (23.7 g, 89% yield) was isolated.

¹H-NMR (500 MHz, CDCl₃) δ / ppm : 8.57 (ddd, ³J = 4.9 Hz, ⁴J = 1.7 Hz, ⁵J = 0.9 Hz, 1H, H^{A6}), 8.13 (ddd, ³J = 5.2 Hz, ⁴J = 1.8 Hz, ⁵J = 0.8 Hz, 1H, H^{B6}), 8.01 (s, 1H, H¹), 7.95 (dt, ³J = 8.0 Hz, ^{4,5}J = 1.0 Hz, 1H, H^{A3}), 7.72 (ddd, ³J = 8.1 Hz, ³J = 7.7 Hz, ⁴J = 1.7 Hz, 1H, H^{A4}), 7.66 (ddd, ³J = 8.5 Hz, ³J = 7.2 Hz, ⁴J = 1.8 Hz, 1H, H^{B4}), 7.45 (dt, ³J = 8.5 Hz, ^{4,5}J = 0.9, 1H, H^{B3}), 7.23 (ddd, ³J = 7.5 Hz, ³J = 4.9 Hz, ⁴J = 1.2 Hz, 1H, H^{A5}), 6.83 (ddd, ³J = 7.1 Hz, ³J = 5.2 Hz, ⁴J = 1.0 Hz, 1H, H^{B5}).

¹³C-NMR (125 MHz, CDCl₃) δ / ppm : 155.5 (C^{B2}), 153.7 (C^{A2}), 149.3 (C^{A6}), 145.4 (C^{B6}), 140.8 (C¹), 139.6 (C^{B4}), 137.0 (C^{A4}), 123.6 (C^{A5}), 120.9 (C^{A3}), 116.2 (C^{B5}), 109.0 (C^{B3}).

Compound (25)



Pyridine-2-carbaldehyde-2-pyridylhydrazone (**24**) (171 mg, 863 μmol , 2.07 eq) was dissolved in methanol (15 mL). Ammonium iron(II) sulfate hexahydrate (163 mg, 416 μmol , 1.00 eq) was added and the solution heated to reflux.

After one day the solvent was evaporated and water (20 mL) was added. To this 1 M sodium hydroxide solution (30 mL) was added and the mixture was extracted with CH_2Cl_2 (2 x 40 mL). The combined organic phases were dried over magnesium sulfate and evaporated down to a volume of about 20 mL. To this 3,5-bis(octyloxy)benzyl bromide (**3**) (359 mg, 840 μmol , 2.02 eq) was added and the mixture was stirred for three days.

Ammonium hexafluorophosphate (one spatula tip, approx. 50 mg) and water (40 mL) were added. The phases were separated and the aqueous phase was extracted with CH_2Cl_2 (2 x 50 mL), the combined organic phases were dried over magnesium sulfate and evaporated to dryness. After chromatography (silica, CH_2Cl_2 with 1% methanol) a dark red, viscous oil (185 mg, 31% yield) was isolated.

TLC: R_f (CH_2Cl_2 : methanol 10 : 1) = 0.44

$^1\text{H-NMR}$ (500 MHz, CDCl_3) δ / ppm : 9.28 (s, 1H, H^1), 7.80 (d, $^3J = 7.5$ Hz, 1H, $\text{H}^{\text{A}6}$), 7.67 (t, $^3J = 7.6$ Hz, 1H, $\text{H}^{\text{B}5}$), 7.60 (t, $^3J = 7.4$ Hz, 1H, $\text{H}^{\text{A}5}$), 7.54 (d, $^3J = 4.8$ Hz, 1H, $\text{H}^{\text{B}3}$), 7.50 (d, $^3J = 4.5$ Hz, 1H, $\text{H}^{\text{A}3}$), 7.10 (d, $^3J = 8.3$ Hz, 1H, $\text{H}^{\text{B}6}$), 6.98 (t, $^3J = 5.9$ Hz, 1H, $\text{H}^{\text{A}4}$), 6.85 (t, $^3J = 6.1$ Hz, 1H, $\text{H}^{\text{B}4}$), 6.64 (s, 2H, $\text{H}^{\text{C}2}$), 6.52 (s, 1H, $\text{H}^{\text{C}4}$), 6.09 (m, 2H, H^2), 3.99 (t, $^3J = 6.2$ Hz, 4H, H^3), 1.83 – 1.70 (m, 4H, H^4), 1.54 – 1.16 (m, 20H, H^{5-9}), 0.87 (t, $^3J = 6.5$ Hz, 6H, H^{10})

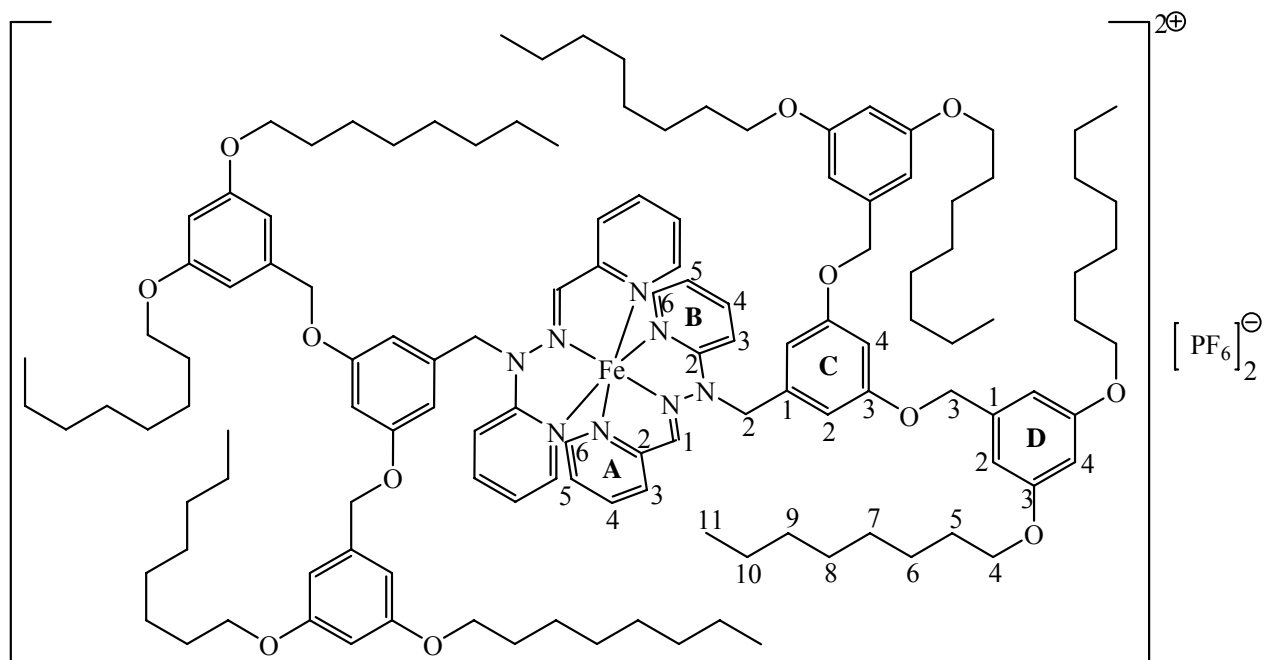
$^{13}\text{C-NMR}$ (125 MHz, CDCl_3) δ / ppm : 161.8 ($\text{C}^{\text{C}3}$), 158.8 ($\text{C}^{\text{A}2}$), 157.9 ($\text{C}^{\text{B}2}$), 152.3 ($\text{C}^{\text{A}3}$), 150.8 ($\text{C}^{\text{B}3}$), 144.2 (C^1), 141.4 ($\text{C}^{\text{B}5}$), 138.5 ($\text{C}^{\text{A}5}$), 134.7 ($\text{C}^{\text{C}1}$), 126.9 ($\text{C}^{\text{A}4}$), 126.4 ($\text{C}^{\text{A}6}$), 121.4 ($\text{C}^{\text{B}4}$), 107.8 ($\text{C}^{\text{B}6}$), 105.7 ($\text{C}^{\text{C}2}$), 101.4 ($\text{C}^{\text{C}4}$), 68.6 (C^3), 50.9 (C^2), 32.0 ($\text{C}^{4,5,6,7,8}$ or 9), 29.6 ($\text{C}^{4,5,6,7,8}$ or 9), 29.5 ($\text{C}^{4,5,6,7,8}$ or 9), 26.3 ($\text{C}^{4,5,6,7,8}$ or 9), 22.9 ($\text{C}^{4,5,6,7,8}$ or 9), 14.3 (C^{10})

Mass (FAB, NBA matrix) m/z : 1289.7 [$\text{M} - \text{PF}_6$] $^+$ (16), 572.8 [$\text{M} - 2\text{PF}_6$] $^{2+}$ (23)

IR ($\tilde{\nu}$ [cm^{-1}]): 3103, 2925, 2853, 1601, 1595, 1576, 1533, 1484, 1464, 1447, 1395, 1343, 1322, 1297, 1259, 1245, 1163, 1117, 1106, 1058, 1031, 962, 821, 762

Microanalysis (calculated for $\text{C}_{68}\text{H}_{96}\text{F}_{12}\text{FeN}_8\text{O}_4\text{P}_2$ (1435.31 g / mol) + 2 CH_2Cl_2): C 52.38; H 6.28; N 6.98; found: C 52.89; H 6.48; N 7.11

Compound (26)



Pyridine-2-carbaldehyde-2-pyridylhydrazone (**24**) (101 mg, 510 μmol , 2.01 eq) was dissolved in methanol (5 mL). Ammonium iron(II) sulfate hexahydrate (99.5 mg, 254 μmol , 1.00 eq) was added and the solution heated to reflux.

After one day, the reaction mixture was diluted with CH_2Cl_2 (30 mL). To this 1 M sodium hydroxide solution (30 mL) was added and the phases were separated. The water phase was extracted with CH_2Cl_2 (2 x 40 mL). The combined organic phases were dried over magnesium sulfate and evaporated to dryness. To this 3,5-bis(3,5-dioctyloxybenzyl)oxybenzyl bromide (**13**) (455 mg, 508 μmol , 2.00 eq) and CH_2Cl_2 (10 mL) were added and the mixture was stirred for three days.

Ammonium hexafluorophosphate (one spatula tip, approx. 50 mg) and water (20 mL) were added. The phases were separated and the aqueous phase was extracted with CH₂Cl₂ (2 x 30 mL), the combined organic phases were dried over magnesium sulfate and evaporated to dryness. After chromatography (silica, ethyl acetate : hexane 1:1) a dark red, viscous oil (138 mg, 23% yield) was isolated.

TLC: R_f (Ethyl acetate : hexane 1: 3) = 0.32

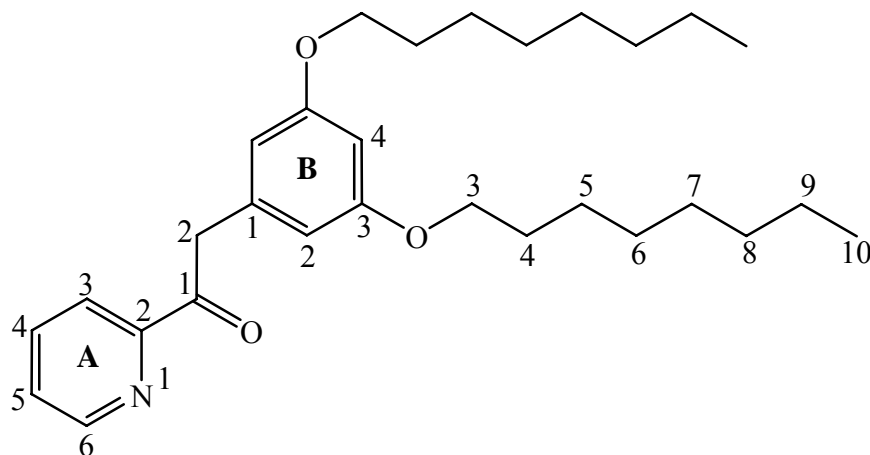
¹H-NMR (500 MHz, CDCl₃) δ / ppm : 9.25 (s, 1H, H¹), 7.78 (d, ³J = 7.9 Hz, 1H, H^{A6}), 7.60 (t, ³J = 8.0 Hz, 1H, H^{B5}), 7.58 – 7.53 (m, 2H, H^{A5,B3}), 7.51 (d, ³J = 5.3 Hz, 1H, H^{A3}), 7.02 – 6.93 (m, 2H, H^{A4,B6}), 6.86 (t, ³J = 6.5 Hz, 1H, H^{B4}), 6.74 (s, 2H, H^{C2}), 6.69 (s, 1H, H^{C4}), 6.55 (s, 4H, H^{D2}), 6.41 (s, 2H, H^{D4}), 6.16 - 6.02 (m, 2H, H²), 5.02 (s, 4H, H³), 3.94 (t, ³J = 6.5 Hz, 8H, H⁴), 1.81 – 1.69 (m, 8H, H⁵), 1.50 – 1.19 (m, 40H, H⁶⁻¹⁰), 0.87 (t, ³J = 6.7 Hz, 12H, H¹¹)

¹³C-NMR (125 MHz, CDCl₃) δ / ppm : 161.4 (C^{C3}), 160.8 (C^{D3}), 158.7 (C^{A2}), 157.8 (C^{B2}), 152.2 (C^{A3}), 150.7 (C^{B3}), 144.3 (C¹), 141.5 (C^{B5}), 138.5 (C^{A5}), 136.4 (C^{C1}), 134.8 (C^{D1}), 127.1 (C^{A4}), 126.5 (C^{A6}), 121.6 (C^{B4}), 107.5 (C^{B6}), 106.2 (C^{D2}), 106.1 (C^{C2}), 102.3 (C^{C4}), 100.9 (C^{D2}), 70.5 (C³), 68.4 (C⁴), 50.3 (C²), 32.0 (C^{5,6,7,8,9 or 10}), 29.6 (C^{5,6,7,8,9 or 10}), 29.5 (C^{5,6,7,8,9 or 10}), 29.5 (C^{5,6,7,8,9 or 10}), 26.3 (C^{5,6,7,8,9 or 10}), 22.9 (C^{5,6,7,8,9 or 10}), 14.3 (C¹¹)

Mass (ESI, CH₂Cl₂ + MeOH) **m/z** : 2227.7 [M – PF₆]⁺, 1041.6 [M – 2 PF₆]²⁺

IR ($\tilde{\nu}$ [cm⁻¹]): 2950, 2925, 2854, 1595, 1533, 1488, 1465, 1447, 1376, 1343, 1324, 1298, 1259, 1159, 1046, 965, 828

Microanalysis (calculated for C₁₂₈H₁₈₄F₁₂FeN₈O₁₂P₂ (2372.65 g / mol) + 1.5 CH₂Cl₂): C 62.21; H 7.54; N 4.48; found: C 62.06; H 7.78; N 4.49

2-(3,5-Bis(octyloxy)phenyl)(2-pyridyl)ethanone (**28**)

Diphenyl-1-(phenylamino)-1-(2-pyridyl) methylphosphonate¹ (**27**) (2.13 g, 5.12 mmol, 1 eq) and 3,5-bis(octyloxy)benzaldehyde (**4**) (2.04 g, 5.63 mmol, 1.1 eq) were dissolved under nitrogen in 25 mL of a THF / ⁱPrOH 4:1 mixture. Cesium carbonate (2.17 g, 6.66 mmol, 1.3 eq) was added in one portion and the reaction mixture was stirred for three days.

Dilute HCl (20 mL, 1.5 M) was added slowly and the reaction stirred for another day. CH₂Cl₂ (50 mL) was added and the phases were separated. The aqueous phase was extracted twice with CH₂Cl₂ and the combined CH₂Cl₂ phases were washed once with a saturated NaHCO₃ solution.

The organic phases were dried over MgSO₄ and evaporated to dryness. Column chromatography (silica, ethyl acetate : hexane 1 : 7) gave (1.58 g, 57% yield) a yellow oil .

TLC: R_f (Silica, ethyl acetate : hexane 1:7) = 0.26

¹H-NMR (500 MHz, CDCl₃) δ / ppm: 8.72 (dd, ³J = 4.7 Hz, ⁴J = 0.6 Hz, 1H, H^{A6}), 8.05 (d, ³J = 7.8 Hz, 1H, H^{A3}), 7.82 (td, ³J = 7.7 Hz, ⁴J = 1.7 Hz, 1H, H^{A4}), 7.47 (ddd, ³J = 7.5 Hz, ³J = 4.8 Hz, ⁴J = 1.1 Hz, 1H, H^{A5}), 6.47 (d, ⁴J = 2.1 Hz, 2H, H^{B2}), 6.33 (t, ⁴J = 2.1 Hz, 1H, H^{B4}), 4.46 (s, 2H, H²), 3.90 (t, ³J = 6.6 Hz, 4H, H³), 1.78 – 1.69 (m, 4H, H⁴), 1.49 – 1.20 (m, 20H, H⁵⁻⁹), 0.88 (t, ³J = 6.9 Hz, 6H, H¹⁰)

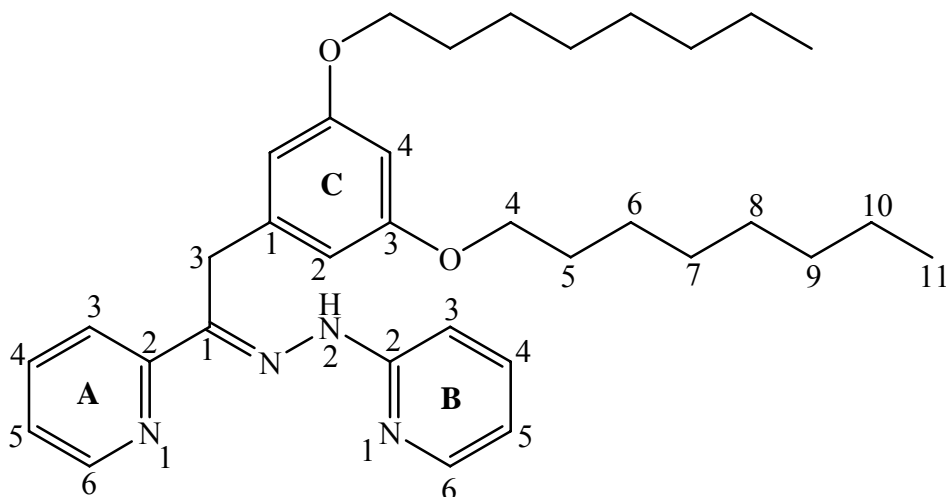
¹³C-NMR (125 MHz, CDCl₃) δ / ppm: 199.0 (C¹), 160.2 (C^{B3}), 153.1 (C^{A2}), 148.9 (C^{A6}), 136.9 (C^{A4}), 136.6 (C^{B1}), 127.1 (C^{A5}), 122.4 (C^{A3}), 108.4 (C^{B2}), 99.8 (C^{B4}), 67.9 (C³), 44.1 (C²), 31.8 (C^{6,7,8 or 9}), 29.3 (C^{6,7,8 or 9}), 29.2 (C^{6,7,8 or 9}), 29.2 (C⁴), 26.0 (C⁵), 22.6 (C^{6,7,8 or 9}), 14.1 (C¹⁰)

Mass (EI 70 eV, 200 °C) m/z : 453.3 [M]⁺ (100), 341.2 [M – C₈H₁₆]⁺ (46)

IR (neat) (ν̄ [cm⁻¹]): 2918, 2847, 1703, 1599, 1462, 1448, 1312, 1161, 1072

Microanalysis (calculated for $C_{29}H_{43}NO_3$ (453.66 g / mol)): C 76.78, H 9.55, N 3.09
found C 77.07, H 9.62, N 3.11

2-(3,5-Bis(octyloxy)phenyl)(2-pyridyl)ethanone-2-pyridylhydrazone (**29**)



2-(3,5-Bis(octyloxy)phenyl)(2-pyridyl)ethanone (**28**) (399 mg, 880 μ mol, 1 eq) and 2-hydrazinopyridine (105 mg, 960 μ mol, 1.1 eq) were dissolved in 20 mL ethanol and refluxed for seven days. The solution was evaporated to dryness and purified by column chromatography (silica, ethyl acetate : hexane 1:1). A yellow oil could be isolated (248 μ mol, 52% yield). TLC is not a good indicator for the column due to extensive streaking on TLC plates.

1H -NMR (500 MHz, $CDCl_3$) δ / ppm: 8.58 (d, $^3J = 4.3$ Hz, 1H, H^{A6}), 8.41 (s, 1H, H^2), 8.23 (d, $^3J = 8.1$ Hz, 1H, H^{A3}), 8.11 (d, $^3J = 4.9$ Hz, 1H, H^{B6}), 7.71 (td, $^3J = 7.9$ Hz, $^4J = 1.7$ Hz, 1H, H^{A4}), 7.61 (td, $^3J = 8.5$ Hz, $^4J = 1.6$ Hz, 1H, H^{B4}), 7.41 (d, $^3J = 8.4$ Hz, 1H, H^{B3}), 7.21 (ddd, $^3J = 7.4$ Hz, $^3J = 4.8$ Hz, $^4J = 0.8$ Hz, 1H, H^{A5}), 6.78 (ddd, $^3J = 6.9$ Hz, $^3J = 4.9$ Hz, $^4J = 0.6$ Hz, 1H, H^{B5}), 6.40 (d, $^4J = 1.9$ Hz, 2H, H^{C2}), 6.28 (t, $^4J = 1.9$ Hz, 1H, H^{C4}), 4.38 (s, 2H, H^3), 3.86 (t, $^3J = 6.6$ Hz, 4H, H^4), 1.74 – 1.67 (m, 4H, H^5), 1.43 – 1.20 (m, 20H, H^{6-10}), 0.88 (t, $^3J = 6.9$ Hz, 6H, H^{11})

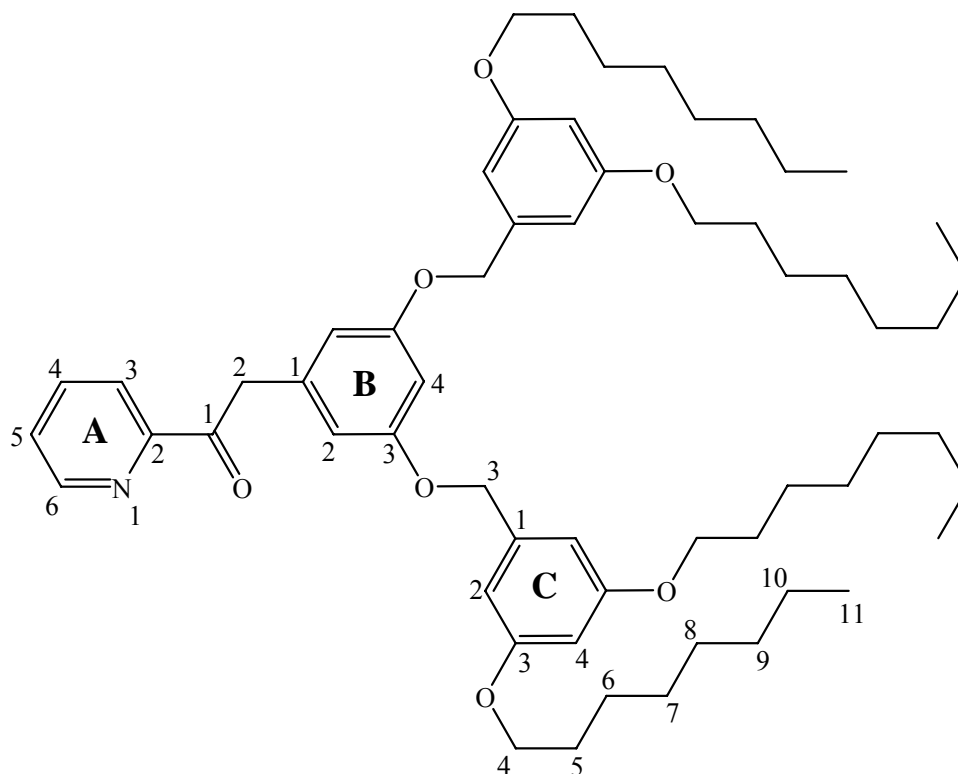
^{13}C -NMR (125 MHz, $CDCl_3$) δ / ppm: 160.8 (C^{C3}), 156.5 (C^{B2}), 155.9 (C^{A2}), 148.7 (C^{A6}), 147.7 (C^{B6}), 145.3 (C^1), 138.0 (C^{B4}), 137.8 (C^{C1}), 136.1 (C^{A4}), 122.8 (C^{A5}), 120.2 (C^{A3}), 116.4 (C^{B5}), 107.8 (C^{B3}), 106.8 (C^{C2}), 99.5 (C^{C4}), 68.0 (C^4), 31.9 ($C^{6,7,8,9}$ or 10), 30.5 (C^3), 29.4 ($C^{6,7,8,9}$ or 10), 29.3 ($C^{6,7,8,9}$ or 10), 29.3 (C^5), 26.1 (C^6), 22.7 ($C^{6,7,8,9}$ or 10), 14.2 (C^{11})

Mass (FAB, NBA matrix) m/z : 545.4 $[M+H]^+$ (82)

IR (neat) ($\tilde{\nu}$ [cm^{-1}]): 3304, 2920, 2854, 1591, 1572, 1512, 1468, 1445, 1423, 1290, 1159, 1140, 1059

Microanalysis (calculated for $\text{C}_{34}\text{H}_{48}\text{N}_4\text{O}_2$ (544.78 g / mol) + $\frac{1}{2} \text{H}_2\text{O}$): C 73.74, H 8.92, N 10.12 found C 73.84, H 8.55, N 10.08

2-(3,5-Bis(3,5-dioctyloxybenzyloxy)phenyl)(2-pyridyl)ethanone (**31**)



Diphenyl-1-(phenylamino)-1-(2-pyridyl) methylphosphonate (**27**) (950 mg, 2.28 mmol, 1.13 eq) and 3,5-bis(3,5-dioctyloxybenzyloxy)benzaldehyde (1.68 g, 2.02 mmol, 1 eq) were dissolved under nitrogen in 5 mL of a THF / *i*PrOH 4:1 mixture. Cesium carbonate (925 mg, 2.83 mmol, 1.40 eq) was added in one portion and the reaction was stirred for one day.

Dilute HCl (15 mL, 1.5 M) was added slowly and the reaction mixture was stirred for another day. Saturated NaHCO_3 was added followed by CH_2Cl_2 . The phases were separated and the aqueous phase was extracted with CH_2Cl_2 . The combined organic phases were dried over MgSO_4 and evaporated to dryness. Column chromatography (silica, ethyl acetate : hexane 1 : 7) gave a yellow oil (1.03 g, 55% yield).

TLC: R_f (Silica, ethyl acetate : hexane 1:7) = 0.26

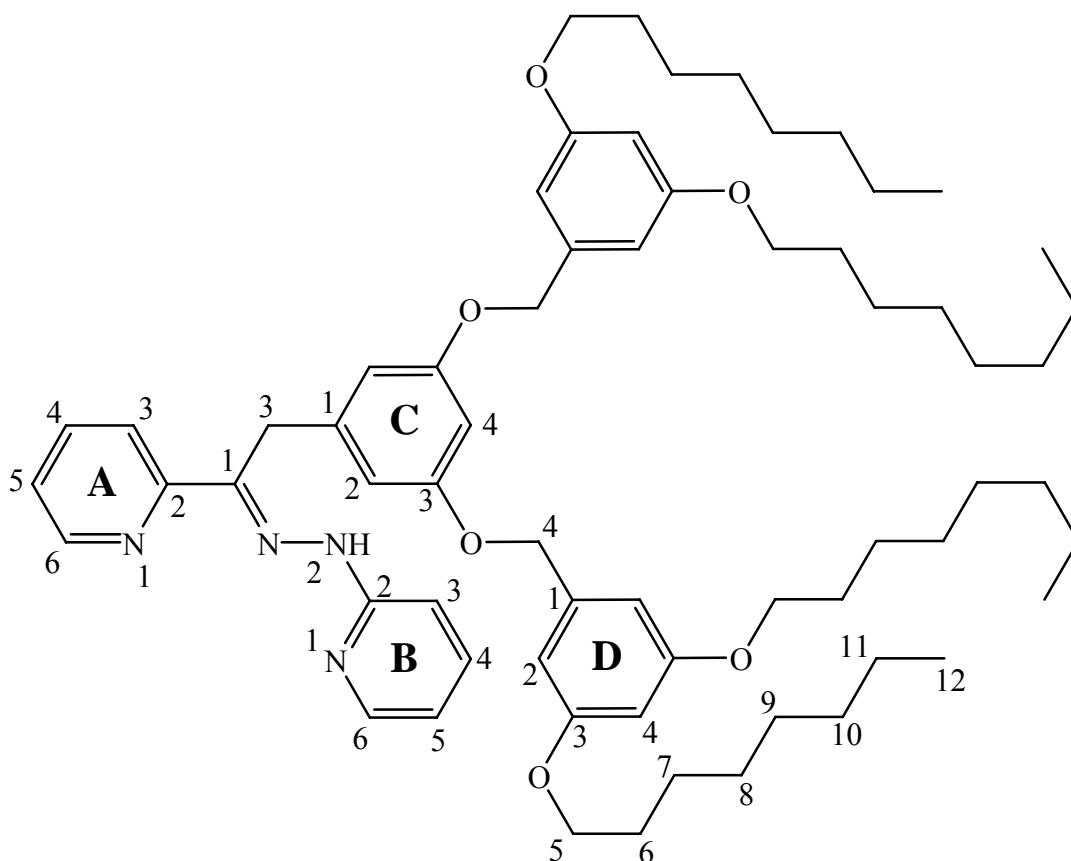
¹H-NMR (500 MHz, CDCl₃) δ / ppm: 8.70 (d, ³J = 4.1 Hz, 1H, H^{A6}), 8.05 (d, ³J = 7.8 Hz, 1H, H^{A3}), 7.82 (td, ³J = 7.7 Hz, ⁴J = 1.7 Hz, 1H, H^{A4}), 7.47 (ddd, ³J = 7.4 Hz, ³J = 4.8 Hz, ⁴J = 1.0 Hz, 1H, H^{A5}), 6.59 (d, ⁴J = 2.1 Hz, 2H, H^{B2}), 6.54 (d, ⁴J = 2.1 Hz, 4H, H^{C2}), 6.50 (t, ⁴J = 2.1 Hz, 1H, H^{B4}), 6.39 (t, ⁴J = 2.0 Hz, 2H, H^{C4}), 4.92 (s, 4H, H³), 4.48 (s, 2H, H²), 3.93 (t, ³J = 6.6 Hz, 9H, H⁴), 1.79 – 1.72 (m, 8H, H⁵), 1.49 – 1.22 (m, 40H, H⁶⁻¹⁰), 0.88 (t, ³J = 6.9 Hz, 12H, H¹¹)

¹³C-NMR (125 MHz, CDCl₃) δ / ppm: 198.9 (C¹), 160.4 (C^{C3}), 159.9 (C^{B3}), 153.0 (C^{A2}), 148.9 (C^{A6}), 139.0 (C^{C1}), 136.9 (C^{A4}), 136.9 (C^{B1}), 127.2 (C^{A5}), 122.4 (C^{A3}), 109.1 (C^{B2}), 105.7 (C^{C2}), 100.8 (C^{C4}), 100.6 (C^{B4}), 70.1 (C³), 68.0 (C⁴), 44.1 (C²), 31.8 (C^{5,6,7,8,9 or 10}), 29.4 (C^{5,6,7,8,9 or 10}), 29.2 (C^{5,6,7,8,9 or 10}), 29.2 (C^{5,6,7,8,9 or 10}), 26.0 (C^{5,6,7,8,9 or 10}), 22.7 (C^{5,6,7,8,9 or 10}), 14.1 (C¹¹)

Mass (EI 70 eV, 300 °C) **m/z** : 921.6 [M]⁺ (12)

IR (neat) ($\tilde{\nu}$ [cm⁻¹]): 2920, 2852, 1686, 1591, 1462, 1452, 1381, 1292, 1171, 1144, 1045

Microanalysis (calculated for C₅₉H₈₇NO₇ (922.32 g / mol)): C 76.83, H 9.51, N 1.52
found C 76.40, H 9.44, N 1.48

2-(3,5-Bis(3,5-bis(octyloxy)benzyl)-oxyphenyl)-(2-pyridyl)-ethanone-2'-pyridylhydrazone (**32**)

2-(3,5-Bis(3,5-dioctyloxybenzyl)-oxyphenyl)-(2-pyridyl)-ethanone (1.03g, 1.12 mmol, 1 eq) and 2-hydrazinopyridine (227 mg, 2.08 mmol, 1.8 eq) were dissolved in 15 mL THF and 10 ml methanol. The mixture was refluxed for five days. The solution was evaporated to dryness followed by chromatography (silica, ethyl acetate : hexane 1 : 3). TLC is not a good indicator for the column due to extensive streaking on TLC plates.

A yellow oil could be isolated (629 mg, 55% yield).

¹H-NMR (500 MHz, CDCl₃) δ / ppm: 8.57 (d, ³J = 4.5 Hz, 1H, H^{A6}), 8.42 (s, 1H, H²), 8.22 (d, ³J = 8.1 Hz, 1H, H^{A3}), 8.11 (d, ³J = 4.7 Hz, 1H, H^{B6}), 7.71 (t, ³J = 7.7 Hz, 1H, H^{A4}), 7.62 (t, ³J = 7.7 Hz, 1H, H^{B4}), 7.41 (d, ³J = 8.4 Hz, 1H, H^{B3}), 7.21 (dd, ³J = 5.5 Hz, ³J = 6.7 Hz, 1H, H^{A5}), 6.79 (dd, ³J = 5.6 Hz, ³J = 6.5 Hz, 1H, H^{B5}), 6.56 – 6.48 (m, 6H, H^{C2,D2}), 6.45 (s, 1H, H^{C4}), 6.38 (s, 2H, H^{D4}), 4.88 (s, 4H, H⁴), 4.39 (s, 2H, H³), 3.91 (t, ³J = 6.6 Hz, 8H, H⁵), 1.81 – 1.69 (m, 8H, H⁶), 1.50 – 1.20 (m, 40H, H⁷⁻¹¹), 0.89 (t, ³J = 6.7 Hz, 12H, H¹²)

¹³C-NMR (125 MHz, CDCl₃) δ / ppm: 160.4 (C^{D3}), 160.4 (C^{C3}), 156.4 (C^{B2}), 155.7 (C^{A2}), 148.6 (C^{A6}), 147.6 (C^{B6}), 145.1 (C¹), 138.9 (C^{D1}), 138.0 (C^{B1}), 137.9 (C^{B4}), 136.0 (C^{A4}), 122.7 (C^{A5}), 120.2 (C^{A3}), 116.3 (C^{B5}), 107.7 (C^{B3}), 107.4 (C^{C2}), 105.8 (C^{D2}), 100.9 (C^{D4}), 100.1

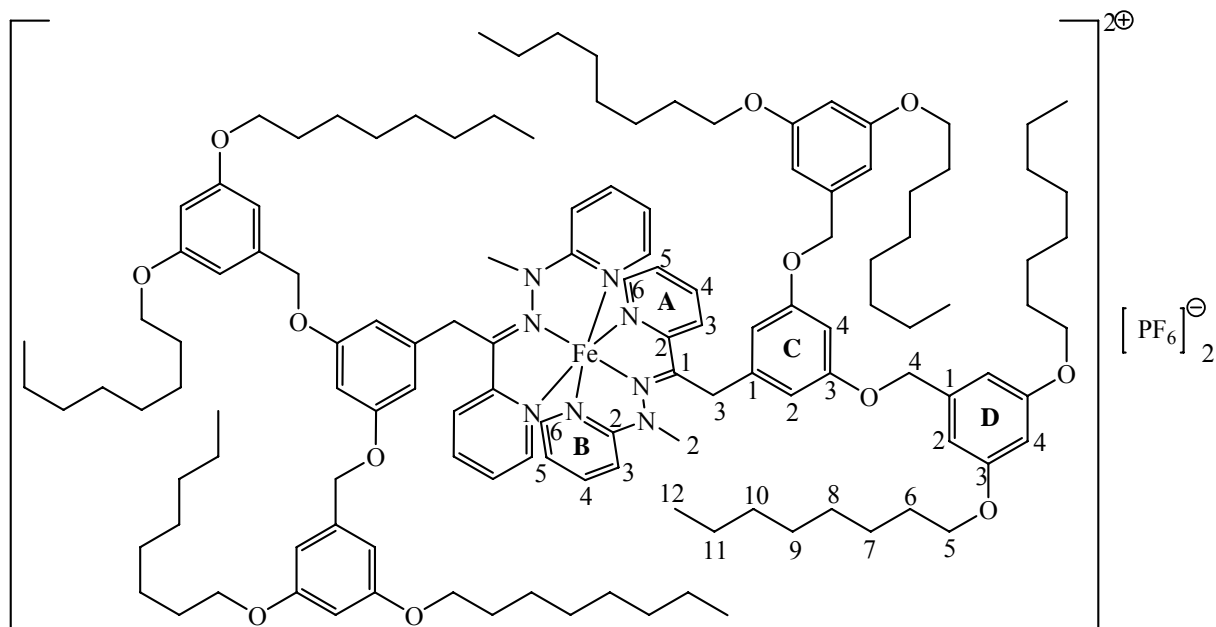
(C^{C4}), 70.1 (C⁴), 68.0 (C⁵), 31.8 (C^{6,7,8,9,10 or 11}), 30.3 (C³), 29.3 (C^{6,7,8,9,10 or 11}), 29.3 (C^{6,7,8,9,10 or 11}), 29.2 (C^{6,7,8,9,10 or 11}), 26.0 (C^{6,7,8,9,10 or 11}), 22.6 (C^{6,7,8,9,10 or 11}), 14.1 (C¹²)

Mass (FAB, NBA matrix) **m/z** : 1013.7 [M+H]⁺ (15)

IR (neat) ($\tilde{\nu}$ [cm⁻¹]): 3317, 2920, 2851, 1589, 1572, 1510, 1460, 1443, 1423, 1371, 1350, 1328, 1292, 1244, 1205, 1163, 1138, 1053

Microanalysis (calculated for C₆₄H₉₂N₄O₆ (1013.45 g / mol)): C 75.85, H 9.15, N 5.53
found C 76.19, H 8.98, N 5.46

Compound (33)



2-(3,5-Bis(3,5-bis(octyloxy)benzyl)-oxyphenyl)-(2-pyridyl)-ethanone-2'-pyridylhydrazone (32) (100 mg, 98.7 μ mol, 2.00 eq), ammonium iron(II) sulfate hexahydrate (19.4 mg, 49.5 μ mol, 1.00 eq), THF (4 mL) and methanol (4.0 mL) were refluxed for one day.

The solvents were removed and CH₂Cl₂ (10 mL) was added. To this 20 mL 1M sodium hydroxide solution was added and the phases were separated. The aqueous phase was extracted with CH₂Cl₂ (2 x 10 mL) and the combined organic phases were dried over magnesium sulfate. The solvent was then evaporated. To this iodomethane (5.0 mL) was added and the mixture was refluxed for three days. It was then stirred at room temperature for 7 days then the iodomethane was removed by evaporation. After chromatography (silica, MeCN : sat. KNO₃ sol. 40 : 1) and a wash with water and ammonium hexafluorophosphate a red, viscous oil (50.1 mg, 42% yield) was isolated.

¹H-NMR (500 MHz, CD₃CN) δ / ppm: 7.75 (d, $^3J = 8.1$ Hz, 1H, H^{A6}), 7.70 (t, $^3J = 7.9$ Hz, 1H, H^{B5}), 7.63 (t, $^3J = 7.8$ Hz, 1H, H^{A5}), 7.57 (d, $^3J = 5.4$ Hz, 1H, H^{A3}), 7.44 (d, $^3J = 5.6$ Hz, 1H, H^{B3}), 7.09 – 7.03 (m, 2H, H^{A4,B6}), 6.82 (t, $^3J = 6.5$ Hz, 1H, H^{B4}), 6.66 (s, 1H, H^{C4}), 6.63 (s, 2H, H^{C2}), 6.42 (d, $^4J = 1.5$ Hz, 4H, H^{D2}), 6.34 (s, 2H, H^{D4}), 5.10 (s, 2H, H³), 4.99 (s, 4H, H⁴), 4.28 (s, 3H, H²), 3.86 (t, $^3J = 6.5$ Hz, 8H, H⁵), 1.72 – 1.61 (m, 8H, H⁶), 1.45 – 1.18 (m, 40H, H⁷⁻¹¹), 0.86 (t, $^3J = 6.7$ Hz, 12H, H¹²)

¹³C-NMR (125 MHz, CD₃CN) δ / ppm: 162.6 (C^{B2}), 161.9 (C^{C3}), 161.1 (C^{D3}), 158.0 (C^{A2}), 152.4 (C^{A3}), 149.3 (C^{B3}), 142.3, 140.6 (C^{B5}), 138.7 (C^{A5}), 126.8 (C^{A4}), 125.0 (C^{A6}), 120.8 (C^{B4}), 111.2, 109.7 (C^{B6}), 107.6 (C^{C2}), 105.3 (C^{D2}), 100.9 (C^{C4}), 99.9 (C^{D4}), 69.3 (C⁴), 67.5 (C⁵), 44.7 (C²), 35.9 (C³), 32.9 (C^{6,7,8,9,10 or 11}), 30.4 (C^{6,7,8,9,10 or 11}), 30.4 (C^{6,7,8,9,10 or 11}), 30.3 (C^{6,7,8,9,10 or 11}), 27.1 (C^{6,7,8,9,10 or 11}), 23.8 (C^{6,7,8,9,10 or 11}), 14.8 (C¹²)

Mass (ESI) m/z : 2255.7 [M – PF₆]⁺, 1055.6 [M – 2 PF₆]²⁺

IR (neat) ($\tilde{\nu}$ [cm⁻¹]): 2923, 2853, 1591, 1536, 1476, 1461, 1452, 1436, 1376, 1341, 1314, 1295, 1215, 1159, 1104, 1047, 987, 949, 830

Microanalysis (calculated for C₁₃₀H₁₈₈F₁₂FeN₈O₁₂P₂ (2400.7 g / mol) 0.5 CH₂Cl₂): C 64.15, H 7.80, N 4.59 found C 64.38, H 8.04, N 4.61

4.8 References

- (1) Lions, F.; Martin, K. V. *J. Am. Chem. Soc.* **1958**, *80*, 3858-3865.
- (2) Geldard, J. F.; Lions, F. *Inorg. Chem.* **1963**, *2*, 270-282.
- (3) Green, R. W.; Hallman, P. S.; Lions, F. *Inorg. Chem.* **1964**, *3*, 1541-1544.
- (4) Green, R. W.; Hallman, P. S.; Lions, F. *Inorg. Chem.* **1964**, *3*, 376-381.
- (5) Chiswell, B.; Lions, F.; Geldard, J. F.; Phillip, A. T. *Inorg. Chem.* **1964**, *3*, 1272-1277.
- (6) Geldard, J. F.; Lions, F. *Inorg. Chem.* **1965**, *4*, 414-417.
- (7) Gerloch, M. *J. Chem. Soc. A* **1966**, 1317-1325.
- (8) Dance, I. G.; Gerloch, M.; Lewis, J.; Stephens, F. S.; Lions, F. *Nature* **1966**, *210*, 298.
- (9) Lions, F.; Dance, I. G.; Lewis, J. *J. Chem. Soc. A* **1967**, 565-572.
- (10) Walton, R. A. *J. Chem. Soc. A* **1967**, 1485-1489.
- (11) Bell, C. F.; Rose, D. R. *Inorg. Chem.* **1968**, *7*, 325-329.
- (12) Bell, C. F.; Rose, D. R. *J. Chem. Soc. A* **1969**, 819-822.
- (13) Bell, C. F.; Rose, D. R. *Inorg. Chem.* **1969**, *8*, 161-163.
- (14) Dunn, J. G.; Edwards, D. A. *Inorg. Nucl. Chem. Lett.* **1969**, *5*, 539-43.
- (15) Dunn, J. G.; Edwards, D. A. *J. Chem. Soc. A* **1971**, 988-994.
- (16) Dunn, J. G.; Edwards, D. A. *J. Organomet. Chem.* **1973**, *61*, 323-328.
- (17) Anderegg, G. *Helv. Chim. Acta* **1971**, *54*, 509-512.
- (18) Crichton, R. R.; Roman, F.; Roland, F. *J. Inorg. Biochem.* **1980**, *13*, 305-316.
- (19) Costanzo, L. L.; Chiacchio, U.; Giuffrida, S. *J. Photochem.* **1980**, *13*, 83-87.

- (20) Costanzo, L. L.; Chiacchio, U.; Giuffrida, S.; Condorelli, G. *J. Photochem.* **1980**, *14*, 125-132.
- (21) Mihkelson, A. E. *J. Inorg. Nucl. Chem.* **1981**, *43*, 123-126.
- (22) Mihkelson, A. E. *J. Inorg. Nucl. Chem.* **1981**, *43*, 127-136.
- (23) Butler, R. N.; Johnston, S. M. *J. Chem. Soc. Perk T 1* **1984**, 2109-2116.
- (24) Mohan, M.; Gupta, M. P.; Chandra, L.; Jha, N. K. *Inorg. Chim. Acta* **1988**, *151*, 61-68.
- (25) Ainscough, E. W.; Brodie, A. M.; Ingham, S. L.; Waters, J. M. *Inorg. Chim. Acta* **1996**, *249*, 47-55.
- (26) Wood, A.; Aris, W.; Brook, D. J. R. *Inorg. Chem.* **2004**, *43*, 8355-8360.
- (27) Dumitru, F.; Petit, E.; van der Lee, A.; Barboiu, M. *Eur. J. Inorg. Chem.* **2005**, 4255-4262.
- (28) Warr, R. J.; Willis, A. C.; Wild, S. B. *Inorg. Chem.* **2006**, *45*, 8618-8627.
- (29) Bell, C. F.; Rose, D. R. *Talanta* **1965**, *12*, 696-700.
- (30) Cameron, A. J.; Gibson, N. A. *Anal. Chim. Acta* **1968**, *40*, 413-419.
- (31) Cameron, A. J.; Gibson, N. A. *Anal. Chim. Acta* **1970**, *51*, 249-256.
- (32) Cameron, A. J.; Gibson, N. A. *Anal. Chim. Acta* **1970**, *51*, 257-263.
- (33) Greene, T. W.; Wuts, P. G. M. *Protective groups in organic synthesis*; 3rd ed.; John Wiley: New York, 1999.
- (34) Bell, C. F.; Quddus, M. A. *Anal. Chim. Acta* **1970**, *52*, 313-321.
- (35) Ryan, D. E.; Winpe, M.; Snape, F. *Anal. Chim. Acta* **1972**, *58*, 101-106.
- (36) Haddad, P. R.; Alexander, P. W.; Smythe, L. E. *Talanta* **1976**, *23*, 275-281.
- (37) Burns, D. T.; Hanprasopwattana, P.; Kheawpintong, S. *Anal. Chim. Acta* **1983**, *151*, 245-249.
- (38) Montes, R.; Laserna, J. J. *Analyst* **1985**, *110*, 1339-1341.
- (39) Montes, R.; Laserna, J. J. *Talanta* **1987**, *34*, 1021-1026.
- (40) Zuhri, A. Z. A.; Shalabi, J. S. *J. Chem. Soc. Perk T 2* **1985**, 499-502.
- (41) Ishii, H.; Odashima, T.; Hashimoto, T. *Anal. Sci.* **1987**, *3*, 347-352.
- (42) Ishii, H.; Odashima, T.; Hashimoto, T. *Anal. Sci.* **1988**, *4*, 73-76.
- (43) Hidalgo, M.; Montes, R.; Laserna, J. J.; Ruperez, A. *Anal. Chim. Acta* **1996**, *318*, 229-237.
- (44) Quddus, M. A.; Bell, C. F. *Anal. Chim. Acta* **1968**, *42*, 503-513.
- (45) Quddus, M. A.; Bell, C. F. *J. Inorg. Nucl. Chem.* **1971**, *33*, 2001-2007.
- (46) Todeschini, A. R.; de Miranda, A. L. P.; da Silva, K. C. M.; Parrini, S. C.; Barreiro, E. J. *Eur. J. Med. Chem.* **1998**, *33*, 189-199.
- (47) Siemens, A. E.; Kitzes, M. C.; Berns, M. W. *Toxicol. Appl. Pharmacol.* **1980**, *55*, 378-392.
- (48) Mathison, B. H.; Murphy, S. E.; Shank, R. C. *Toxicol. Appl. Pharmacol.* **1994**, *127*, 91-98.
- (49) Cory, J. G.; Downes, D. L.; Cory, A. H.; Schaper, K. J.; Seydel, J. K. *Anticancer Res.* **1994**, *14*, 875-879.
- (50) Warnhoff, E. W.; Reynolds-Warnhoff, P. *J. Org. Chem.* **1963**, *28*, 1431-3.
- (51) Journet, M.; Cai, D. W.; Larsen, R. D.; Reider, P. J. *Tetrahedron Lett.* **1998**, *39*, 1717-1720.

5. Monolayer formation and STM analysis

5.1 Introduction

5.1.1 History

Scanning Tunneling Microscopy (STM) is a technique only developed at the beginning of the 1980s¹. A comprehensive history about the development has been compiled by G. Binnig and H. Rohrer².

The importance of their discovery and the following development of the STM instrument can be seen in the award of the Nobel Prize in Physics to Binnig and Rohrer received 1986.

STM found broad acceptance very rapidly in the physical and chemical community. STM is one of the few methods that allows observations on a sub molecular level, often even with atomic resolution. Especially for materials and surface chemistry, STM proved to be groundbreaking. This is due to the ability to observe single molecules or even atoms which have a different behaviour than the bulk material³. Standard analysing methods like nuclear magnetic resonance (NMR), infrared (IR) or UV-vis spectroscopy allow only for the observation of the bulk material with many molecules and with averaged behaviour.

Understanding of molecular behaviour, electron transport and intermolecular interactions is very important. Today's silicon-based electronics will soon face the limit of miniaturisation of what is possible with the current fabrication methods^{3,4}. Molecular electronics would be a possible alternative. Still much basic research has to be conducted before the actual development of molecular electronics. Some of the problems are self-assembly, electron transport and the quantum mechanical behaviour of single molecules³.

STM is also an important tool for supramolecular chemistry⁵. With the growing interest in molecular networks based on intermolecular interactions, the direct observation on surfaces of such networks is an important tool. Such supramolecular networks are under extensive investigation for the storage of hydrogen⁵. Even the actual manipulation of molecules is possible with the STM tip³.

The published work on STM is too extensive to give more than just a glimpse into the topic. For further reading the above mentioned review articles provide a good starting point. Also the book *Scanning Probe Microscopies*⁶ from Samorì provides a good overview and many references.

5.1.2 Working principle

The basic principle of STM is very simple. Between a substrate and a tip that is without contact to the substrate, a voltage is applied. The observed tunneling current is dependent on several variables as distance between tip and substrate, the applied voltage and of course the electron density and density of the states on the substrate.

For STM measurements, the voltage and the tip-substrate distance is usually kept constant and the tunnelling current is measured. Differences in tunneling current are usually represented as contrast in the measurements. The mechanisms leading to the contrast are not completely understood and different models are being discussed, but the local density of states seems to be of big importance^{6,7}.

The observed tunneling current depends also strongly on the orbitals and so on the electron density on the substrate⁸. Other factors also have a big influence, with the electron density of monolayers also depending on the topography of the monolayer.

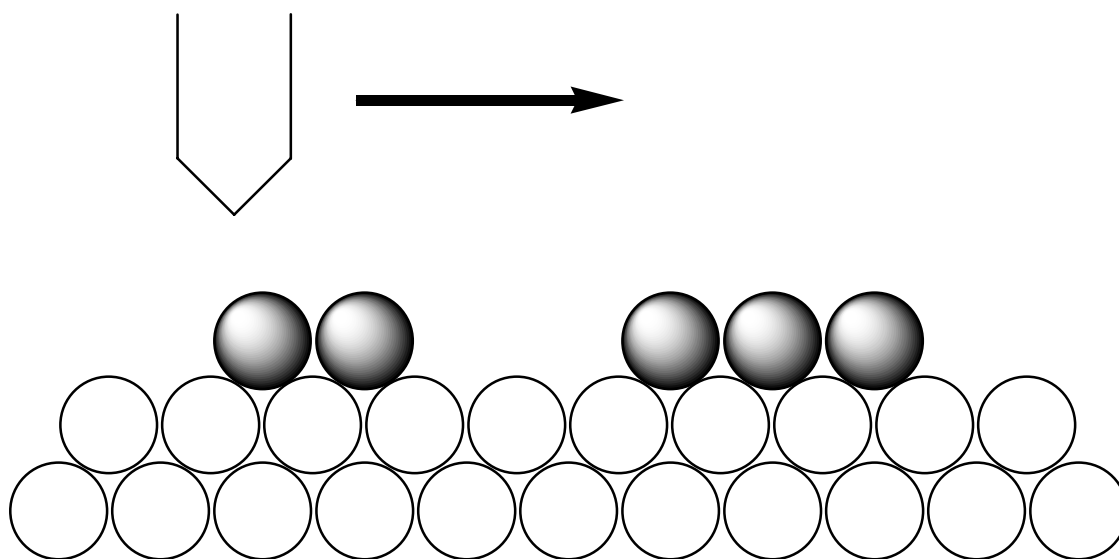


Fig. 5.1.2.1 Schematic representation of an STM measurement. On the substrate (white balls) lies the analyte (grey balls). The STM tip is moved at a constant height above the surface. The closer the tip is to the surface, the stronger is the tunnelling current.

Fig. 5.1.2.1 gives a schematic view of an STM measurement. The measurement of the tunnelling current is a very sensitive method. Not only the height difference between the substrate and analyte is observable, but also the height difference inside the monolayer, represented by the different balls. An exhaustive review on the theoretical side of STM

measurements has been written by Blanco, Flores and Pérez⁷. In addition, modelling is of great assistance in understanding the substrate-analyte-tip interactions and the resulting pictures. An interesting review written by Faglioni et al.⁹ deals with problems in modelling and also compares the models of different functional groups with the actual measurement.

Since their beginning, STM techniques have greatly advanced. New techniques like scanning electrochemical microscopy and scanning probe microscopy have been added to the available methods. Different measurement parameters allow for a wide variety of conditions, from high vacuum and near 0 K, the parameters can be varied up to ambient temperature and in air.

Since an atomically flat substrate surface is paramount for STM measurements the number of possible substrates is limited. One of the most commonly used is gold. This is often the substrate of choice, since the high affinity of sulfur for gold allows simple surface modification strategies. If, for example, thiols are brought in contact with a gold surface they will be bound to it. This relation makes gold a very suitable substrate for the investigation of sulfur containing materials and also almost guarantees that the measurements will return useful data.

Other often used substrates for STM are silver and graphite. The focus here will be laid on graphite substrates since this was the substrate of choice for this work. Graphite substrates are made of highly ordered pyrolytic graphite (HOPG). This artificial polymorph of carbon is basically a big single crystalline block of graphite resulting in very few step edges and very regular planes. To renew the substrate surface of the graphite the top layer can be easily stripped away.

It is known that long alkyl chains are able to adsorb on HOPG surfaces. The adsorption energy is surprisingly high with almost 1 kJ/mol per methylene unit⁸. Another contributing factor to the stabilisation energy of the adsorbed monolayers is the intermolecular Van-der-Waals or London forces. Needless to say that only the total free energy is measurable, and not the partial contributions of the two forces to the total energy. Theoretical studies exist on these topics but the lack of empirical data makes it difficult to judge the quality of the obtained data (also see chapter 3).

5.2 Aims

All the molecules synthesised (see chapter 3 and 4) are carrying alkyl chains. It was expected that these molecules would form monolayers on HOPG as previous work has

shown¹⁰⁻¹². The aim of this work was to gain better insights into the mechanisms and energies determining the final arrangement of the monolayers on the HOPG substrate. Empirical proof for the existence of ordered monolayers exists¹² as well for some 2,2':6',2''-terpyridine ligands modified with dendritic wedges.

5.3 Procedures and Techniques

5.3.1 General information

The STM measurements were conducted on a Nanoscope model MMAFM-2 from Digital Instruments. The measurements were conducted with a bias voltage of -700 mV in reference to the tip and a current set point of 8 pA. The z-limit (distance from surface) was set to 300 nm. The measurements were conducted in air at ambient temperature.

The HOPG was bought from SPI supplies. The platinum-iridium wire 90:10 0.5 mm diameter was bought from Chemie Brunschwig AG.



Fig. 5.3.1.1 Picture of the STM instrument

5.3.2 Substrate preparation

Substrate preparation is relatively simple for highly ordered pyrolytic graphite (HOPG). The top layer of the substrate is simply removed with sticky tape giving a fresh and atomical flat surface. It can occur that the cleaving procedure only removes parts of the top graphite layer leading to many step edges. If this happens the procedure has to be repeated till satisfactory results have been achieved.

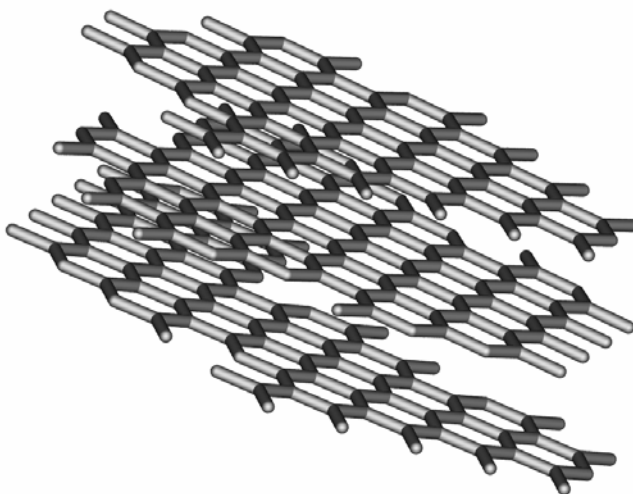


Fig. 5.3.2.1 Structure of graphite. The sheets of carbon are nicely visible

When these layers are stripped more than one plane can be severed. This is due to defects in the lattice and where the graphite block has structural weak points that could lead to a break between the layers. Once a sufficiently plane surface has been generated, the cleanness of the surface can be confirmed by eye. If a compound is deposited to form a monolayer for example the glossy black surface changes its optical properties.

5.3.3 Tip preparation

The tips used for the measurements are made from a platinum-iridium 90:10 alloy. For the generation of good and sharp tips for the STM it is important to more pull the wire apart than cut it. This is best achieved with a wire cutter. A wire cutter allows one to grab hold of the wire and generates at the same time a weak spot in the wire where it is most likely to rupture.

A careful measure of the applied force is necessary to prevent the wire from being simply cut. This technique needs some training.

Using the wire cutter simply for cutting, the tip would be squashed. The ideal tip for STM would be with exactly one atom at the apex. A squashed tip from simple cutting would be almost guaranteed to be dull and not sharp enough. By using force to pull the wire apart much better results are obtained.

5.3.4 Sample preparation

For the monolayer preparation there are two main methods

- (i) solution casting of the monolayer with measurements at the air-solid interface and
- (ii) measurements at the solid-liquid interface.

For the solution casting, a solution of the compound to be analysed is made in a volatile solvent and that solution is then applied to a freshly cleaved HOPG surface. Upon evaporation of the solvent regions of monolayer of the compound is left on the surface. That sample is then directly used for the STM analysis.

The measurements at the liquid-solid interface are done in a similar way as a solution of the compound in a non-volatile solvent is prepared. The most commonly used solvent for this type of measurement is 1-phenyloctane. A drop of the solution is then applied to a freshly cleaved HOPG surface. If the solvent shows a stronger affinity for the substrate than the analyte no monolayer will be formed. Coadsorption of analyte and solvent have been observed and were reported¹³.

The platinum-iridium tip is then, in both cases, lowered close to the surface without touching it. Due to the sensitivity of the method, the final approach to the surface has to be performed by the STM instrument. In theory the STM instrument would be able to perform the complete approach but practical considerations make this choice not advisable. Due to the slow approach by the STM machine it can take very long to reach the measuring position if the tip is very far from the surface when the approach is started. Usually the tip is approached manually and with assistance of a strong magnifying glass to about 0.5 mm from the surface.

5.3.5 Data analysis

Data analysis was performed with a shell extension for PV-Wave, SXM. This program was designed and written at the University of Basel. Other software used was WSxM. This is freeware available on the internet. Further information can be found in the Ph.D. thesis of L. Scherer¹⁴.

5.4 Practical considerations during measurements

5.4.1 Artefacts

Substrate defects

Despite all efforts, no graphite plane is without defects. The most commonly observed defects are step edges. At step edges two different planes in the graphite lattice are visible.

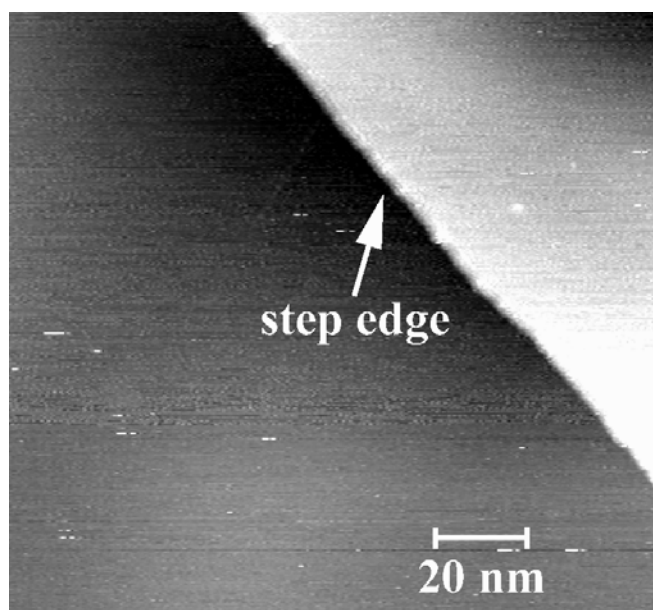


Fig. 5.4.1.1 Example of a step edge in HOPG. The darker half is the lower plane while the brighter one is the upper plane.

Bad tips

One of the more important factors producing artefacts is a bad tip. This includes a whole series of defects. Generally bad tips just give bad picture quality. The most common defect of a tip is lack of sharpness. Blunt tips lead to bad resolution in the STM images. This can mean

that the structure of a monolayer can still be resolved but finer details are lost. This is the case for tips that are just a little too blunt. If a tip is even blunter than this, then even the overall monolayer structure resolved might not be resolved.

Another problem from producing the tip can be a double pointed tip. Then two points exist that have a similar distance from the surface, signals from both tips are obtained. This can lead to unpredictable results.

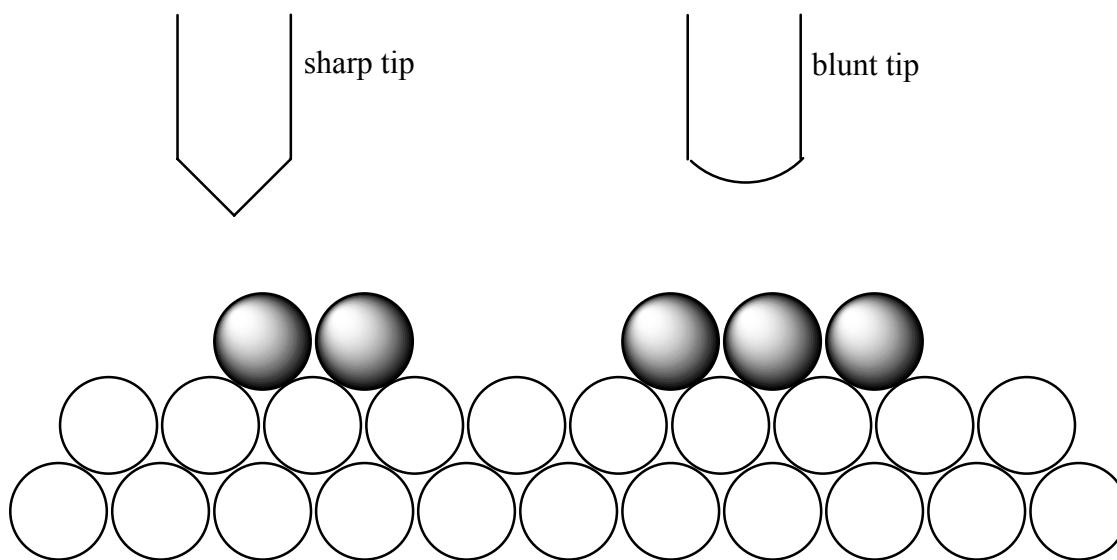


Fig. 5.4.1.2 Difference between a sharp and a blunt tip. While the sharp tip allows for fine resolution not only between the substrate and analyte but also differences within the analyte, the blunt tip is not able to record differences within the analyte.

Moiré Patterns

Moiré patterns have their origin in the fine grating generated by the scanning procedure. If the scanning grid and the grid generated by the analyte are close together a Moiré pattern is generated. Fig. 5.4.1.3 gives a schematic view on the problem. If this happens, a frequency change in the measurement can help, because this changes the distances between the measuring points. Fig. 5.4.1.4 shows a Moiré pattern most likely caused by an interference with the graphite substrate.

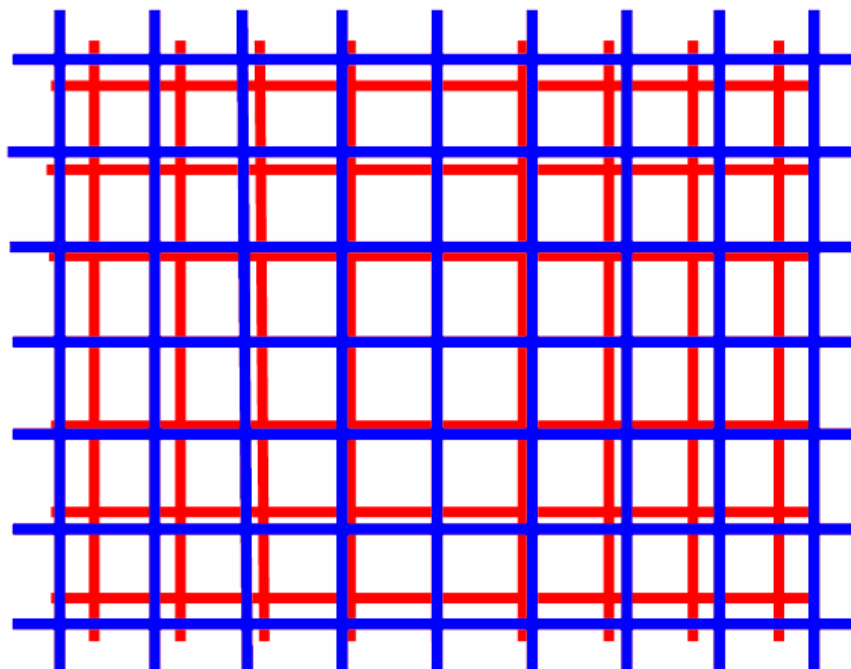


Fig. 5.4.1.3 Schematic representation of the cause for a Moiré pattern. The two grids have very similar distances (frequencies). Starting from the centre that shows the strongest overlap (resonance) the overlap becomes less. If the grid would continue the overlap would eventually reach a maximum again.

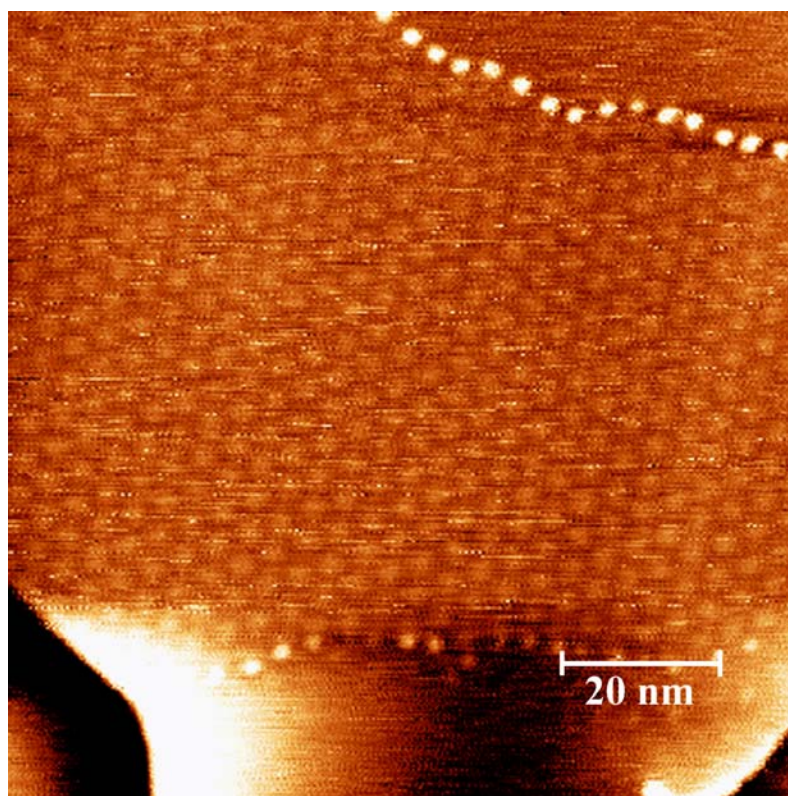


Fig. 5.4.1.4 Example for a Moiré pattern. Most likely produced by the graphite (100 x 100 nm)

Missing Analyte

It can happen that despite optical confirmation of the presence of the analyte on the substrate, no STM pictures can be obtained of a monolayer. This is usually the case when no ordered monolayer is formed. The adsorption bond of the analyte with the substrate surface is intentionally reversible. That way defects in the monolayer can be repaired by desorption and readsorption. This means that the analyte substrate interaction is relatively weak. If no ordered monolayer is formed, the thermal movement of the analyte will be too big to allow imaging because the ordered monolayers have a greatly stabilizing effect on the single molecule by locking it in place. Without this stabilizing factor, the strong electric field of the tip can simply push the unordered molecules away with the obvious consequences for imaging.

5.4.2 Plane group assignment

When doing single crystal analysis of a compound, a space group is assigned to the crystal structure giving information about the symmetry operations with the unit cell. As pointed out in chapter 3, the STM measurements give two dimensional crystallographic data on monolayers. Since these monolayers are in the ideal case, flat on the surface instead of a 3-dimensional conformation, plane groups can be assigned. This ideal case would mean that the molecules within the unit cell are clearly identified. Should only the aromatic systems be properly resolved a tentative plane group assignment is still possible but has to be looked at very carefully.

Compounds can form monolayers and not be lying flat on the surface. So the structures observed by STM might be three dimensional, but the obtained data carries only two dimensional data. Should this be the case, plane group assignment is in principle no longer reasonable because it is not possible to express a three dimensional structure in two dimensions. But regular unit cell might be visible and symmetry operations possible. In these cases tentative plane group is again possible.

5.5 Results

5.5.1 STM

N-{3,5-Bis(octyloxy)benzyl}phthalimide (**7**)

Highly resolved images of monolayers of *N*-{3,5-bis(octyloxy)benzyl}phthalimide could be obtained. The monolayers resulted from solution casting from hexane.

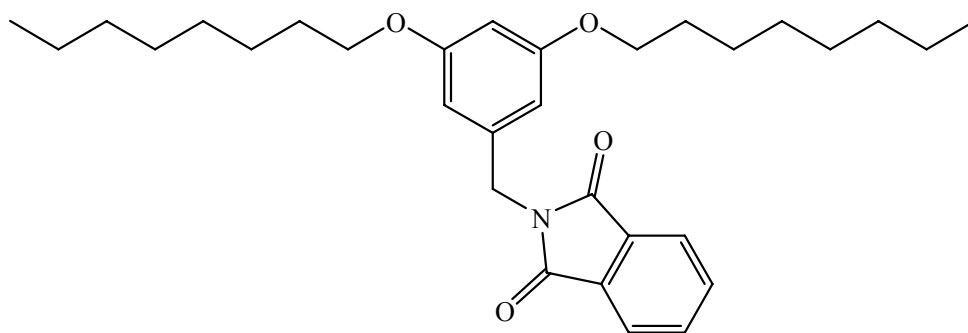


Fig. 5.5.1.1 Structure of *N*-{3,5-bis(octyloxy)benzyl}phthalimide (**7**)

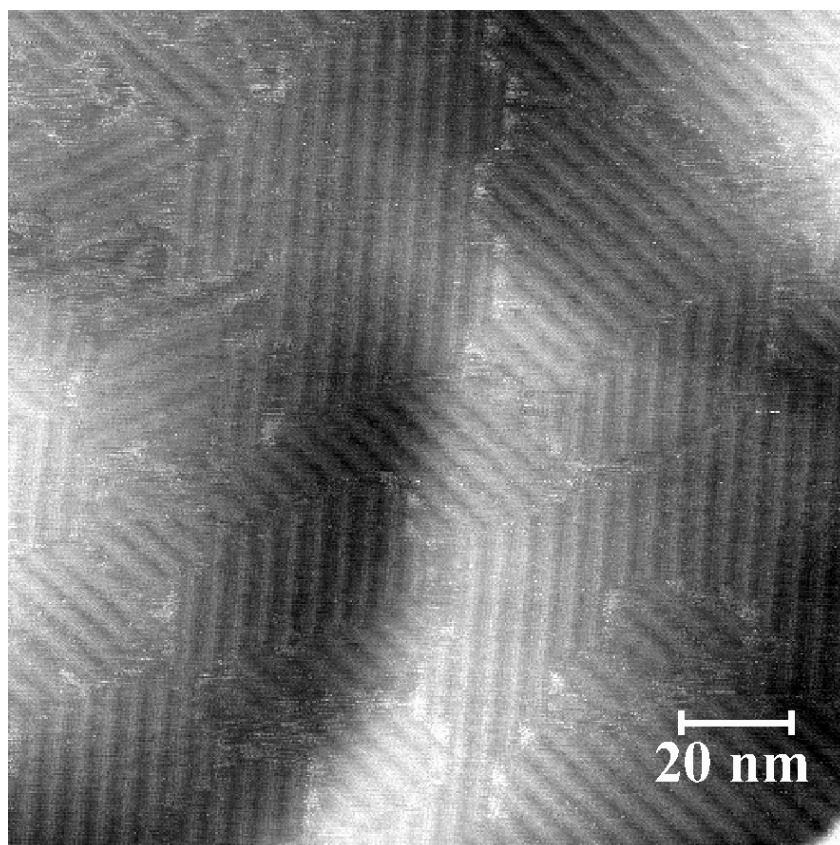


Fig. 5.5.1.2 STM image of (**7**). Monolayer prepared by solution casting. (150 x 150 nm)

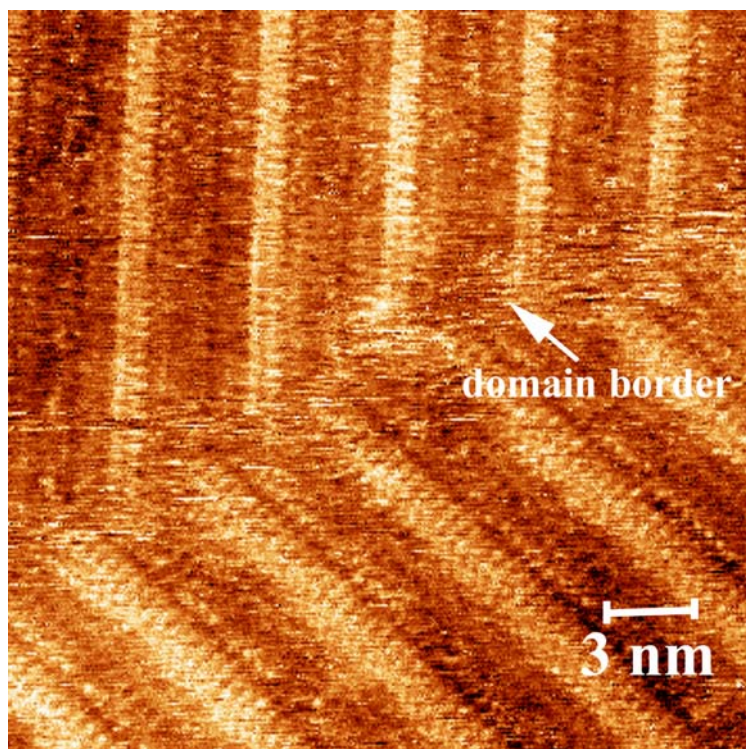


Fig. 5.5.1.3 STM picture of (7). Shown is a domain border with the graphite substrate showing through along the border (25x25nm).

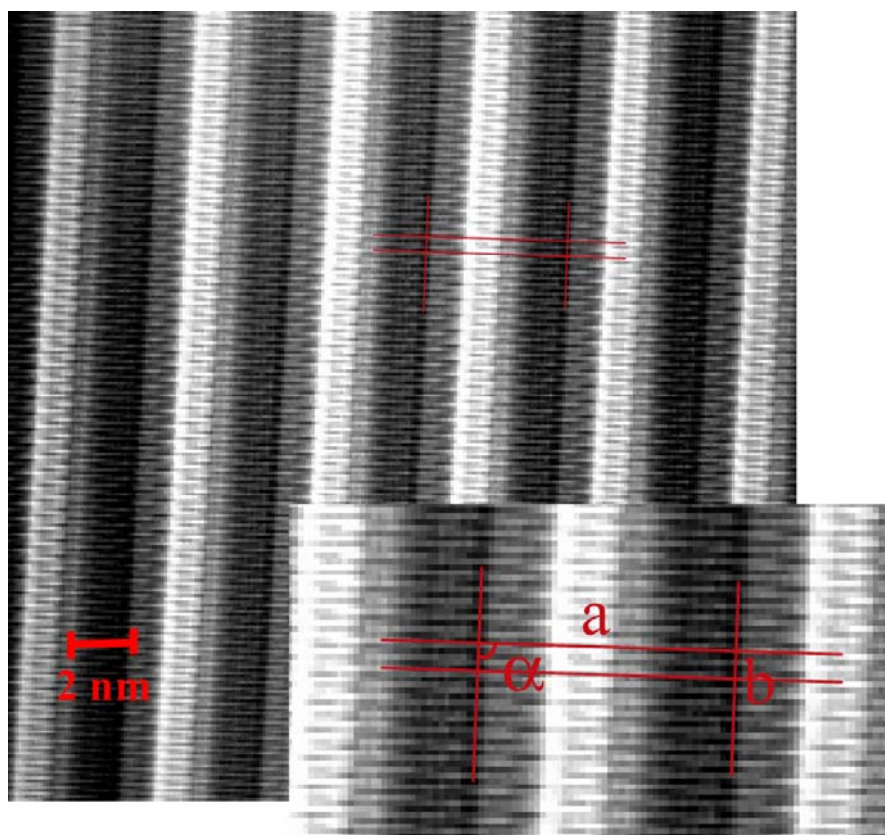


Fig. 5.5.1.4 Filtered and averaged STM picture of (7). (25 x 25 nm). The unit cell is marked with the red frame

a	4410 pm
b	490 pm
α	90°

Table 5.5.1.1 Unit cell data for Compound (7)

The measured dimensions from the unit cell as obtained from fig. 5.5.1.4 are 490 by 4410 pm and the angle α of 90°. The plane group was tentatively determined to be $p1^{15}$.

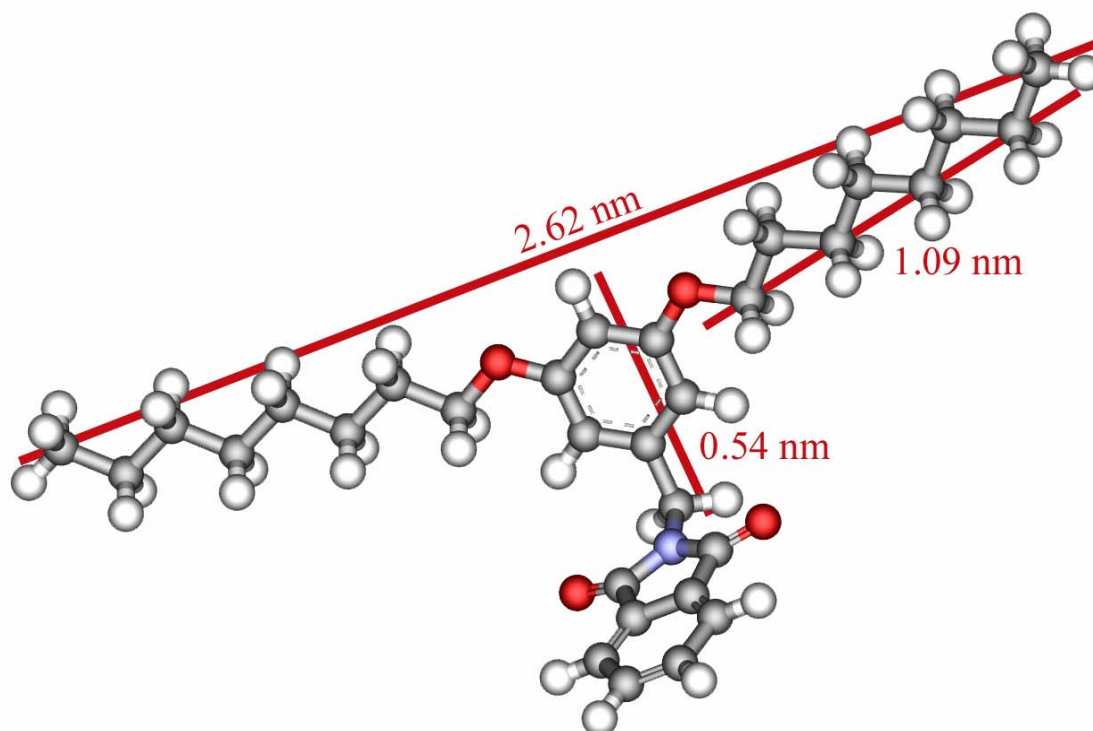


Fig. 5.5.1.5 SpartanTM representation of (7). Structure optimised in SpartanTM (MM) and the measured distances given

When looking at the averaged picture of the monolayer (fig. 5.5.1.4) it is obvious that the molecule can not be lying completely flat on the surface of the substrate. The dimensions of the unit cell with 490 pm by 4.41 nm simply do not allow the accommodation of the molecule lying flat on the surface. This has the consequence that no definite proposal for the arrangement on the surface and in the monolayer is possible. But it appears that not even the aromatic ring of the dendritic part is lying flat on the surface.

2-(3,5-Bis(3,5-bis(octyloxy)benzyl)oxyphenyl)-2-(2-pyridyl)ethanone-2'-pyridylhydrazone
(32)

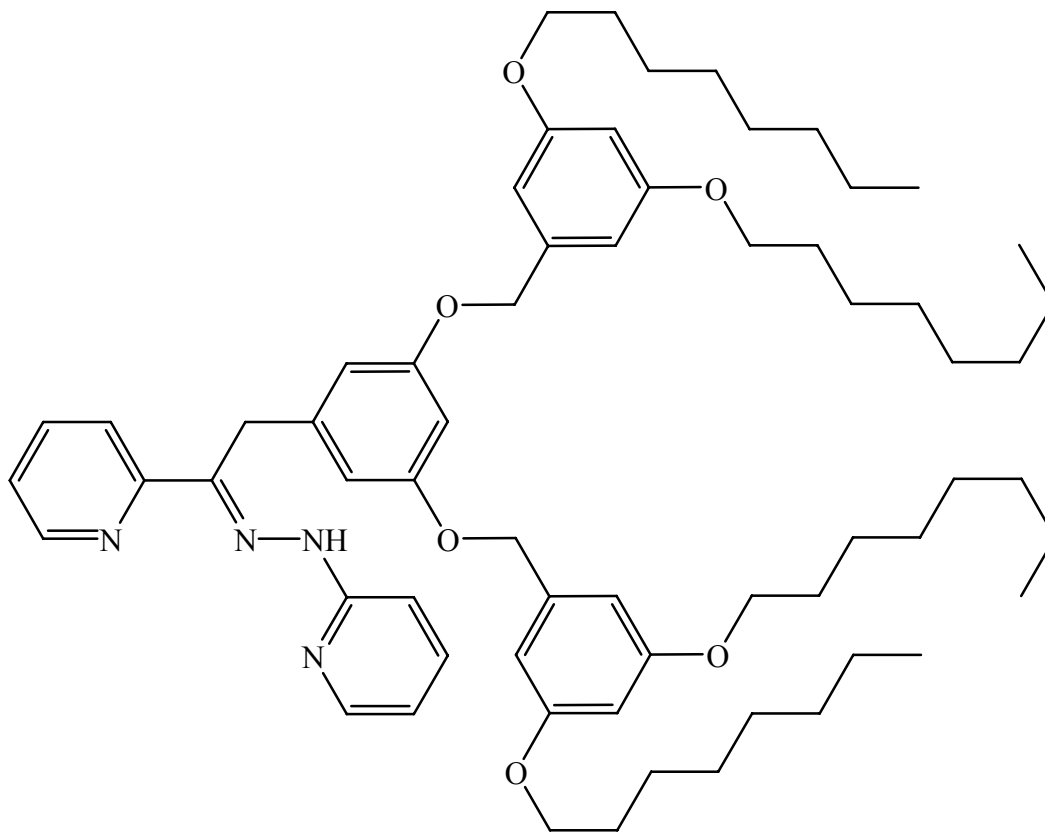


Fig. 5.5.1.6 Structure of 2-(3,5-Bis(3,5-bis(octyloxy)benzyl)oxyphenyl)-2-(2-pyridyl)ethanone-2'-pyridylhydrazone (32)

From measurements of (32) at the liquid-solid interface of 1-phenyloctane small patchy domains of monolayer could be observed. The fact that only very small domains could be obtained is remarkable in itself. Usually monolayers generated at the liquid-solid interface are large and homogenous. That this is not the case, is an indication that the formation of monolayers for this compound is not very favourable.

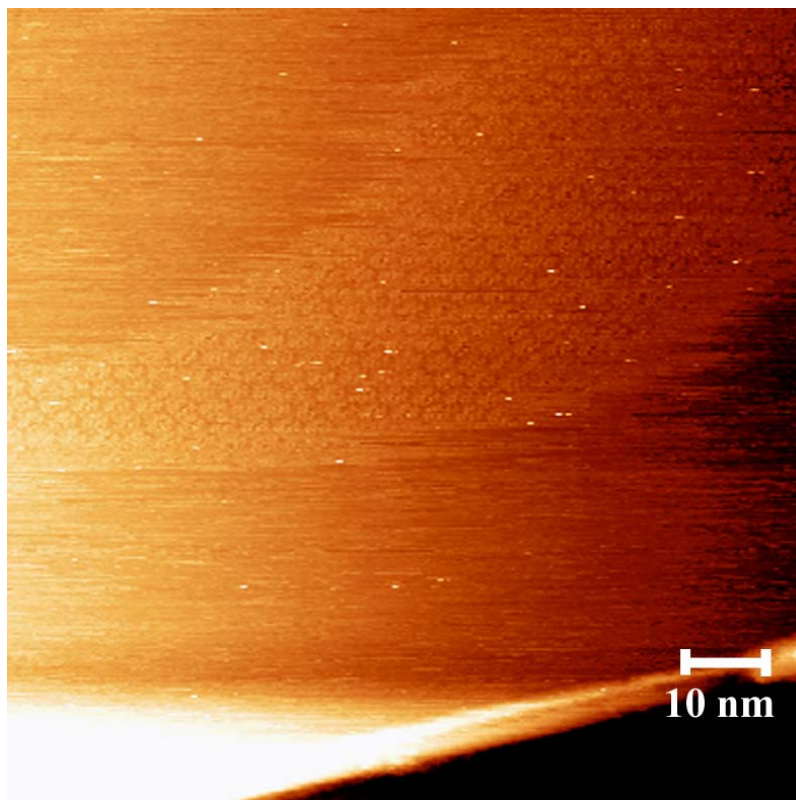


Fig. 5.5.1.7 STM picture of a domain of (32) (100 x 100 nm)

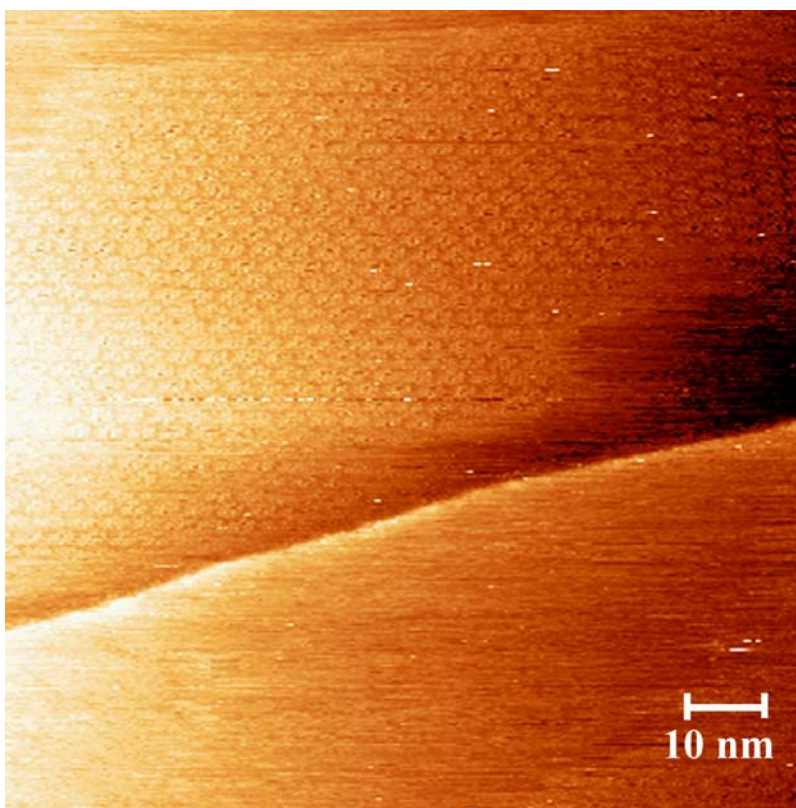


Fig. 5.5.1.8 STM picture of a domain of (32) (100 x 100 nm)

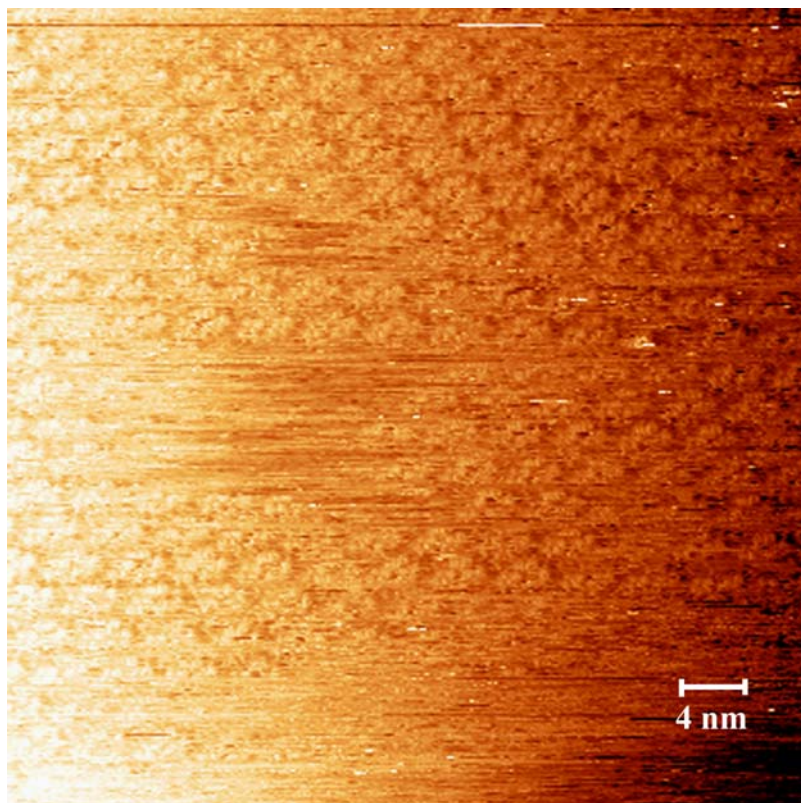


Fig. 5.5.1.9 STM picture of a domain of (32) (50 x 50 nm)

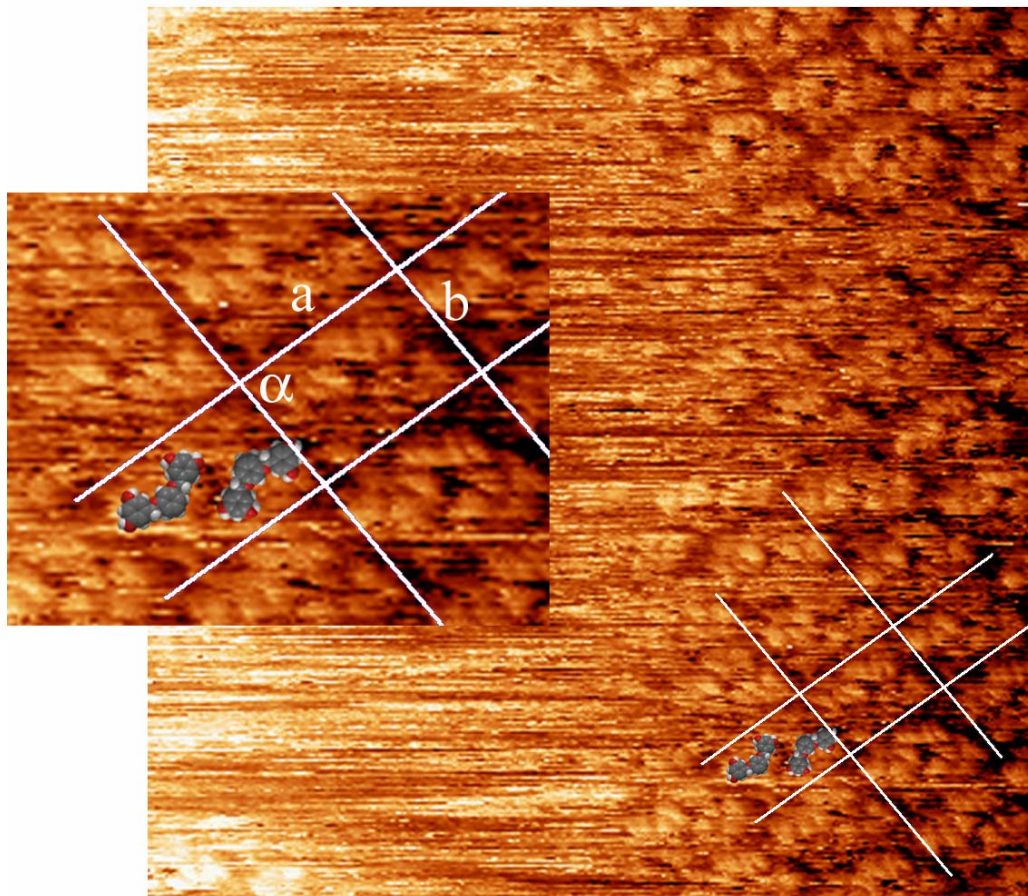


Fig. 5.5.1.10 STM picture of (32) (25 x 25 nm). Unit cell marked.

a	3.27 nm
b	2.17 nm
α	86.1°

Table 5.5.1.2 Unit cell data for (32)

The dimensions of the unit cell of the monolayer of (32) were measured to be 3.27 nm and 2.17 nm with α 86.1°. The plane group was tentatively determined to be p2¹⁵. It is assumed that only the dendritic part of the molecule is lying on the surface. This is a reasonable hypothesis since the ligand part of the molecule has a steric demand that make the assumption that the molecule is lying flat on the surface unlikely. Some irregularities are observable in the structure of the monolayer that makes the fitting of the molecules difficult. These irregularities are probably the result of the loose ligand part of the molecules interacting with the tip.

5.6 Langmuir-Blodgett technique

5.6.1 Introduction

Some of the pioneers in surface chemistry were Irving Langmuir and Katherine B. Blodgett. Although many researchers did work on surface chemistry, Langmuir and Blodgett developed many standard technologies still used today. Langmuir was awarded the Nobel Prize in 1932 for his work¹⁶.

The Langmuir-Blodgett trough (LB trough) is still the most commonly used tool developed by Langmuir and Blodgett. In the LB trough, compounds are floated on a water surface. Movable barriers are then used to compress the molecules into an ordered monolayer (fig. 5.6.1.1).

LB work is usually conducted with amphiphilic molecules that have a hydrophilic and a lipophilic part. The surface tension of water allows these compounds to float on the surface. When the compound is first put onto the surface without pressure the molecules distribute themselves on the available surface rapidly with maximal distance between them forming a monolayer. They are in a state that is quite similar to the gas phase in normal matter¹⁷. When the barriers are closed and the area available to the molecules is reduced, a long-range

ordering is induced. The molecules are entering a condensed phase. This phase can be compared to the liquid state in normal matter (fig. 5.6.1.1 b)). When the compression is continued a homogenous long-range ordering is forced, with the hydrophilic parts pointing to the water surface and the lipophilic parts maximising their interactions.

After at that point, further compression of the LB film usually leads to collapse of the LB film. This is usually an irreversible process.

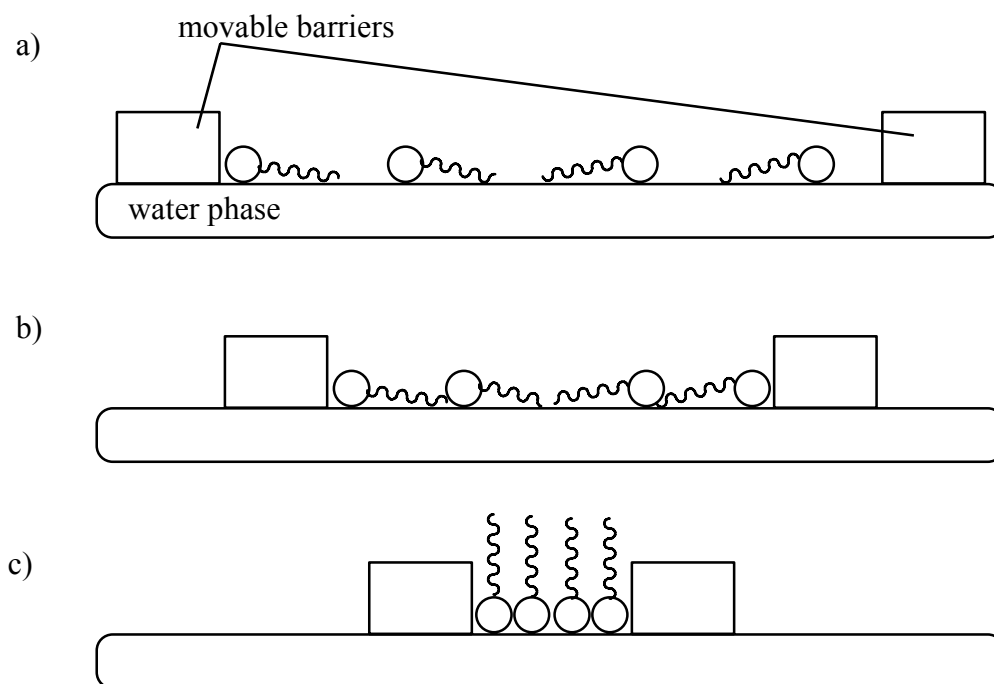


Fig. 5.6.1.1 schematic representation of the three phases in LB films. a) gasous phase b) liquid phase c) solid phase

While in state a) (fig. 5.6.1.1) the surface distributed molecules still have a lot of room around them, and their influence on the surface pressure is only marginal. As the monolayer is compressed, the surface pressure starts to change. During a LB measurement, the surface pressure vs. mean molecular area is monitored. The resulting curve is called an isotherm.

An excellent introduction into the LB methods is *Langmuir-Blodgett Films*¹⁸ from Petty.

5.6.2 Aims

Compounds **(25)**, **(26)** and **(33)** were tested with LB measurements. This is because by using the usual solution casting methods to generate monolayers and measurements at the liquid-solid interface no ordered monolayers were observed and no useful STM measurements were obtained. To test if the compounds could generate ordered monolayers, the LB technique was used.

5.6.3 Methods and Procedures

The LB measurements were performed by Agnieszka Jagoda and Serena Belegriou. The instruments used were a Langmuir Teflon trough from KSV Inc., Finland (area 420 cm²) equipped with a Brewster Angle Microscope (BAM) from Nanofilm, Goettingen in Germany. It is equipped with a Nd:YAG laser (λ 532 nm).

For deposition experiments the mini-LB trough from KSV Inc., Finland (area 242 cm²) was used.

For the measurements the compounds were dissolved in chloroform. Small quantities of these solutions were then dispersed on the water surface of the LB trough. By closing the movable barriers of the trough the monolayers are compressed.

By measuring the surface pressure, the moment of the monolayer collapse can be determined.

5.6.4 Results

Compound (25)

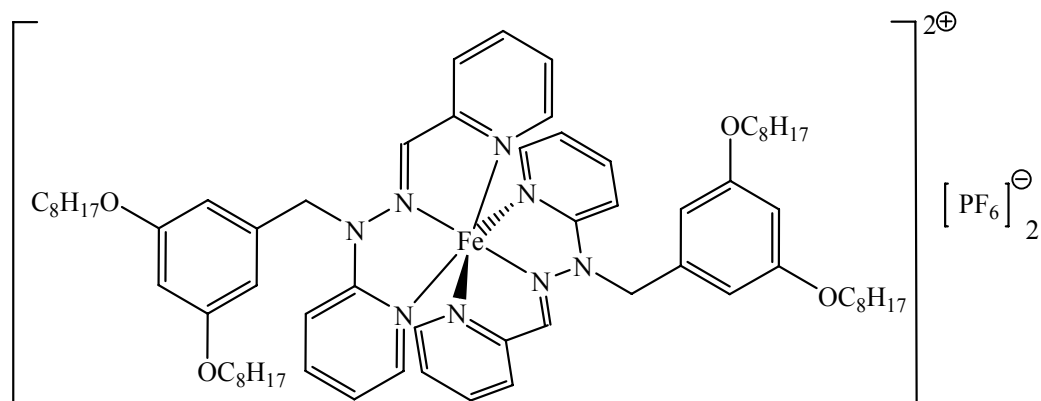


Fig. 5.6.4.1 Structure of (25)

It was expected that compound (25) would give observable monolayers. Since no STM pictures of a monolayer of (25) could be obtained, LB measurements were conducted to see if the compound would even form monolayers.

The compound showed a reproducible isotherm shown in fig. 5.6.4.2. The isotherm shows the three classical phases.

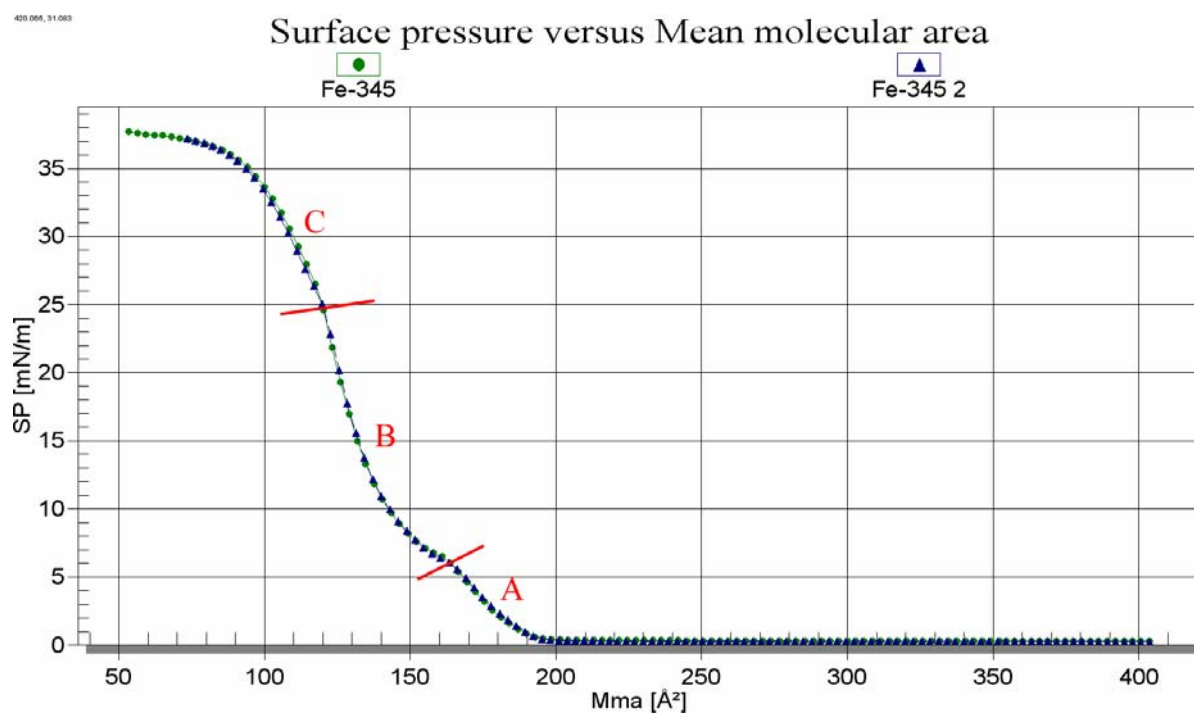


Fig. 5.6.4.2 Isotherm of (25) with the three phases visible. A) gasous phase B) liquid phase C) solid phase

Surprisingly (**25**) formed aggregates during the compression. Pictures of these aggregates were obtained by the BAM (fig. 5.6.4.3 to 5.6.4.5). Their leaf-like structure is very remarkable and the reasons for their formation are unknown. What can be said is that they form during the liquid phase (B) in fig. 5.6.4.2).

If the assumption is correct that phase B) is still the liquid phase, the point where phase B) changes to phase C) the molecules should in theory still be lying flat on the subphase but in the densest possible matter. This would mean that the mean molecular area is about 120 \AA^2 .

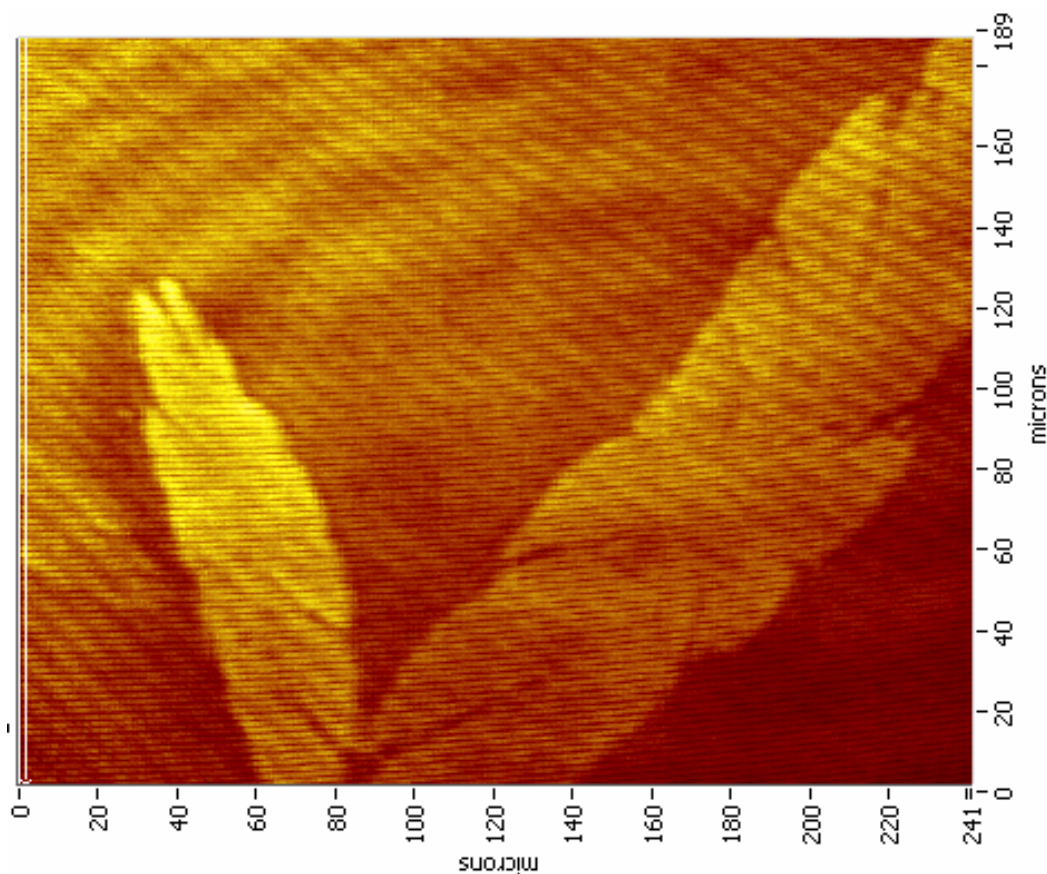


Fig. 5.6.4.3 BAM pictures of leaf like structures of (25)

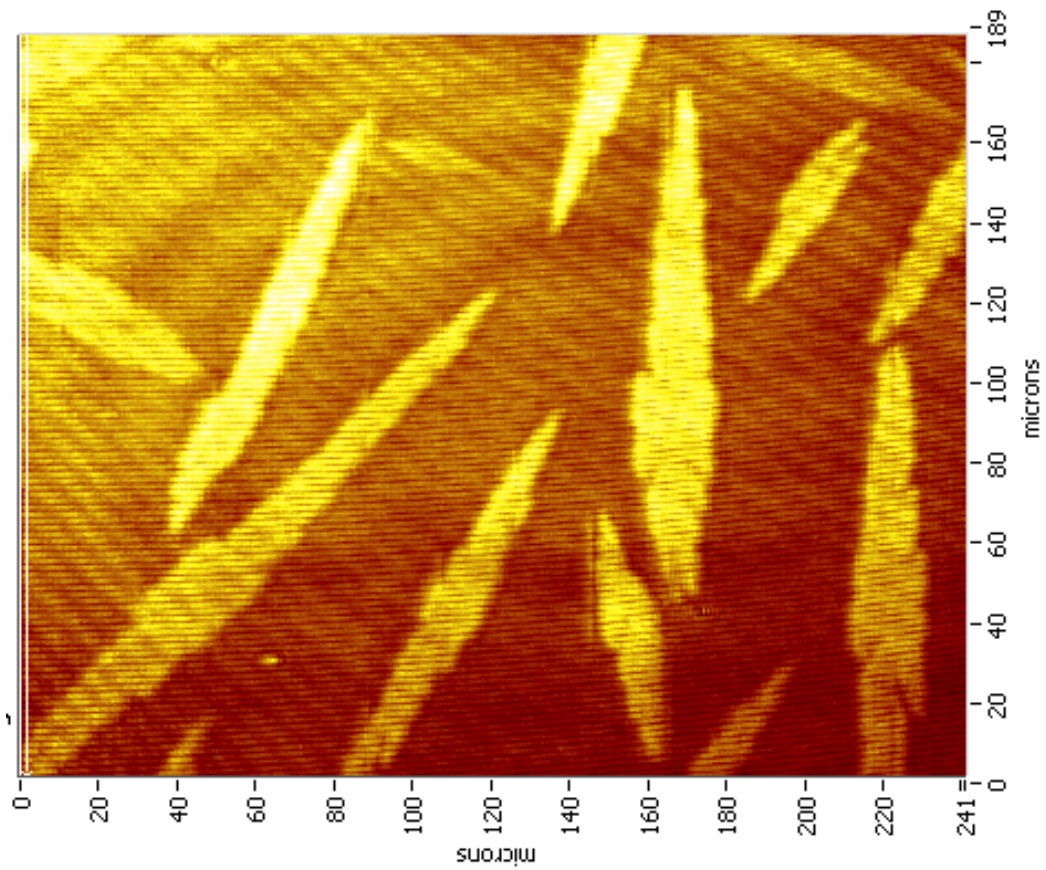


Fig. 5.6.4.4 BAM pictures of leaf like structures of (25)

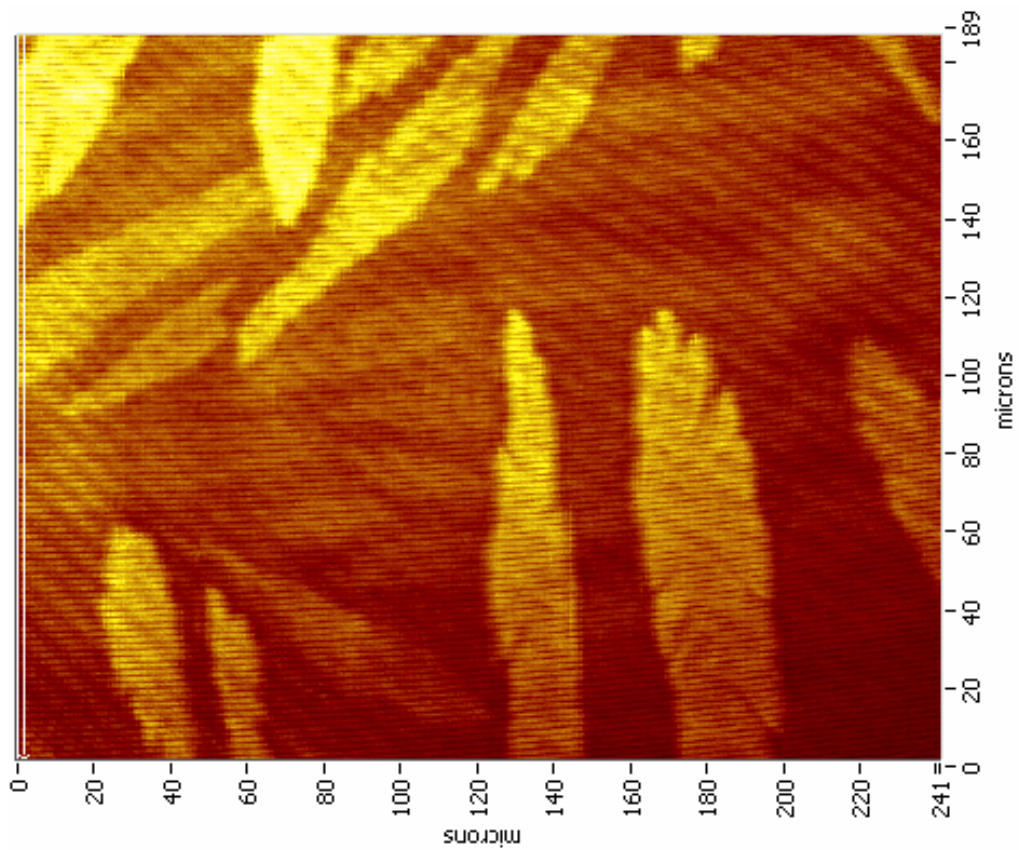
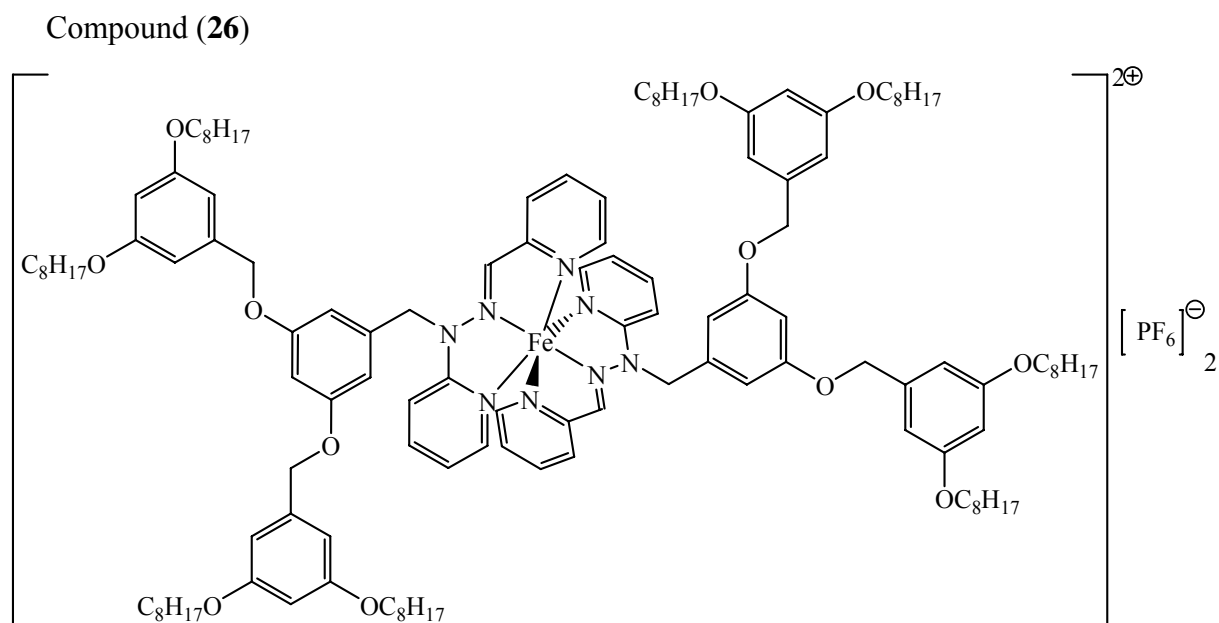
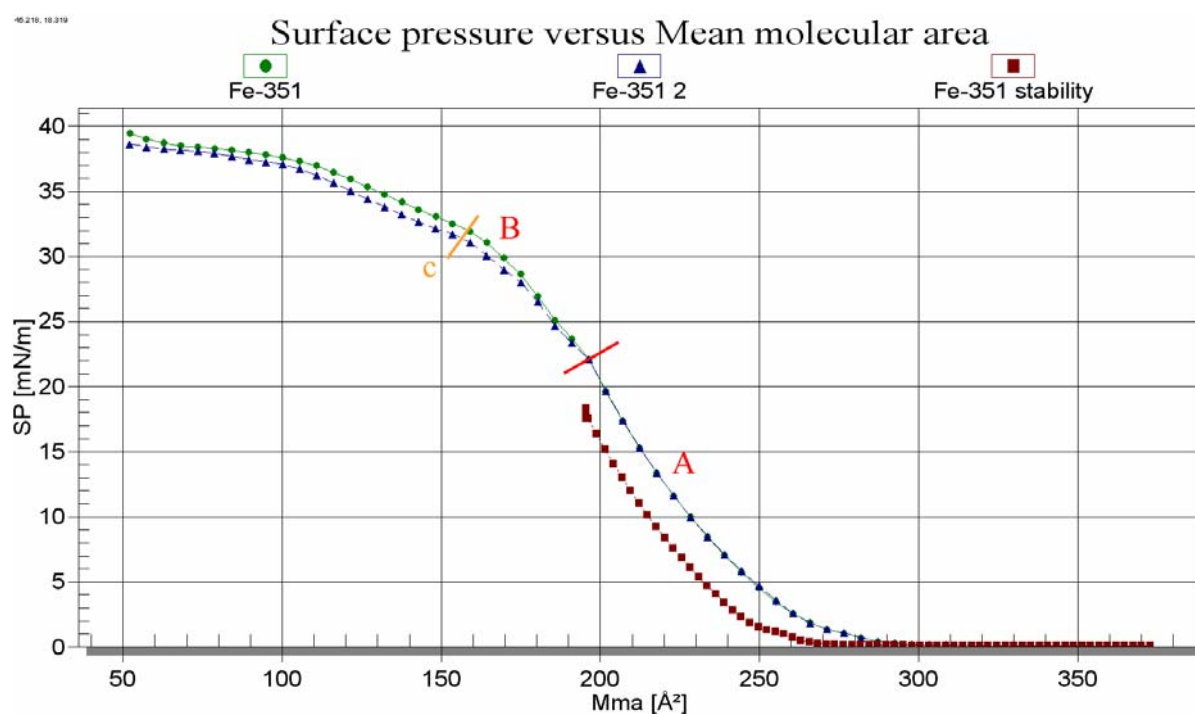


Fig. 5.6.4.5 BAM picture of leaf like structures of (25)



Compound (26) was another promising candidate for STM analysis. Like compound (25) no STM images were obtained. With LB measurements it was tested to see if (26) is able to form monolayers.



The obtained isotherm (fig. 5.6.4.7) shows a different picture to that of compound (25). Phase A) is assumed to be the gaseous phase and shows a highly reproducible behaviour. In phase B) which most likely is the liquid phase deviations between the different measurements

are observable. This is most likely the result of the second generation dendritic wedge attached to the complex core. The increased complexity of the G2 wedge creates bigger disorder and so changing the kinetics for the ordering process.

Phase B) seems to be divided into at least three other phases. This makes it difficult to estimate when the liquid phase ends which would be necessary to give the mean molecular area. If we place the phase transition at point c (orange marking) the mean molecular area is about 160 \AA^2 .

BAM pictures were also obtained. They do not show interesting features like those of (25). At low pressures the incomplete surface coverage is observable. Once the first stage of the compression is complete and the surface completely covered no more features are observed on the surface.

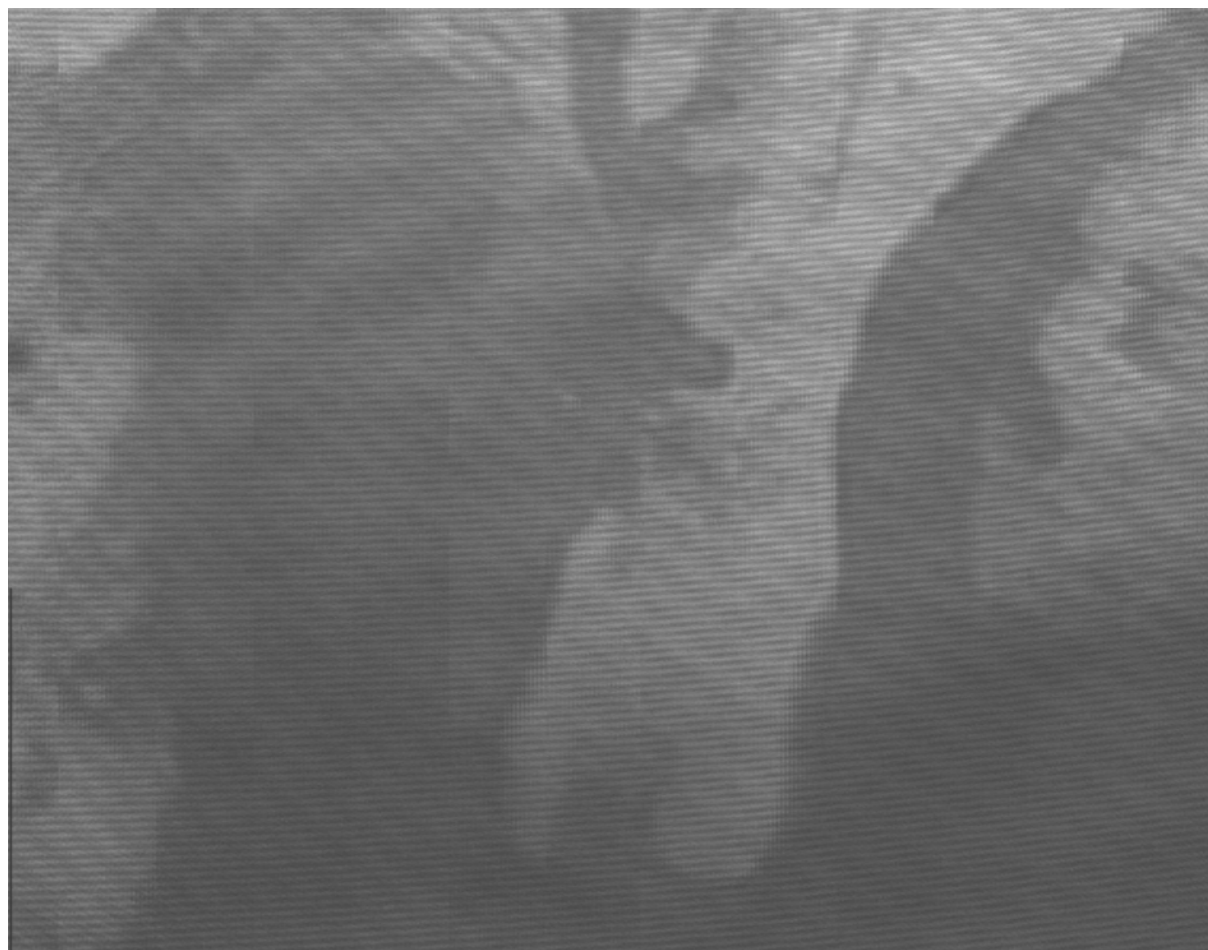


Fig. 5.6.4.8 BAM pictures of (26) at 0 surface pressure

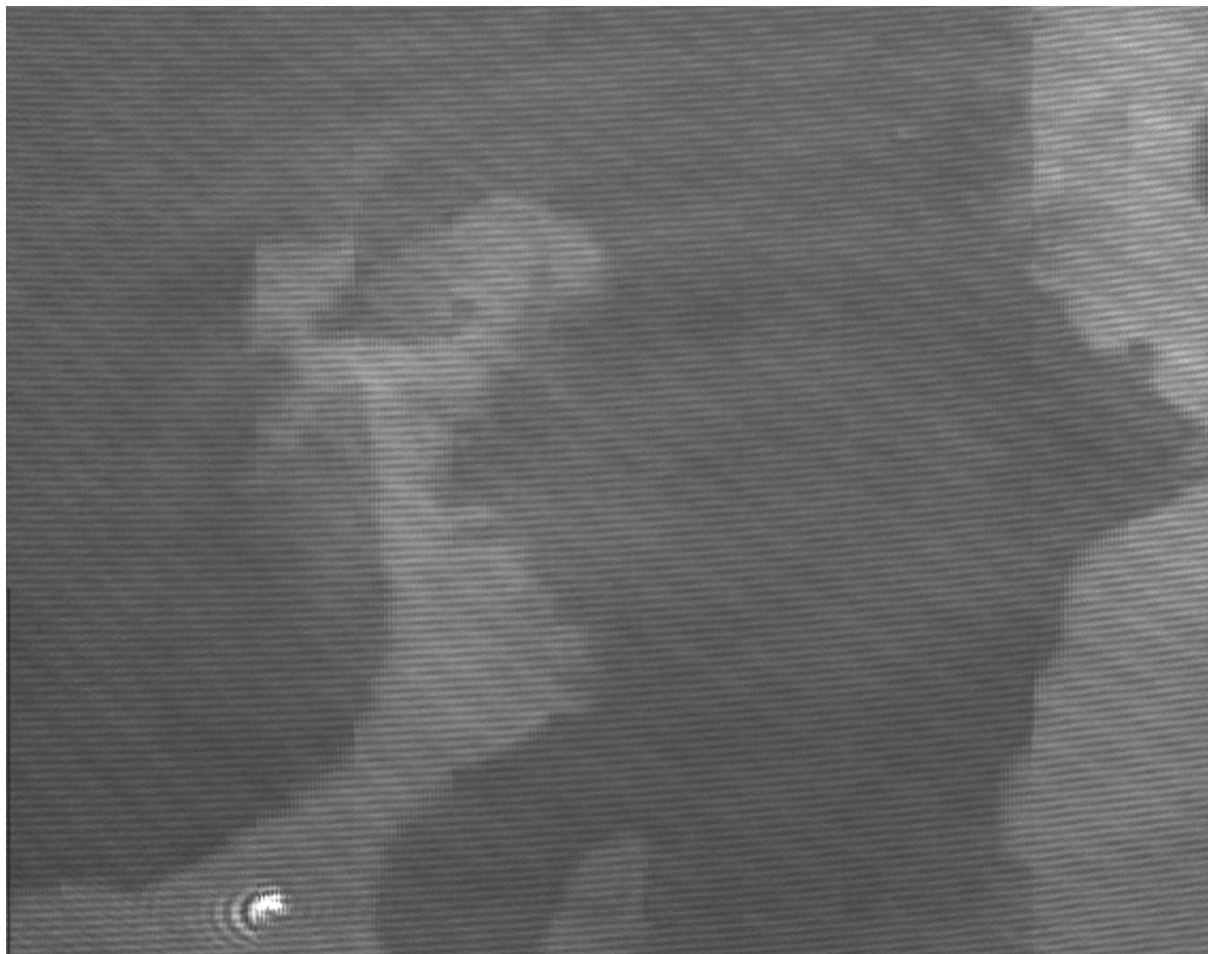


Fig. 5.6.4.9 BAM pictures of (26) at 0 surface pressure

Compound (33)

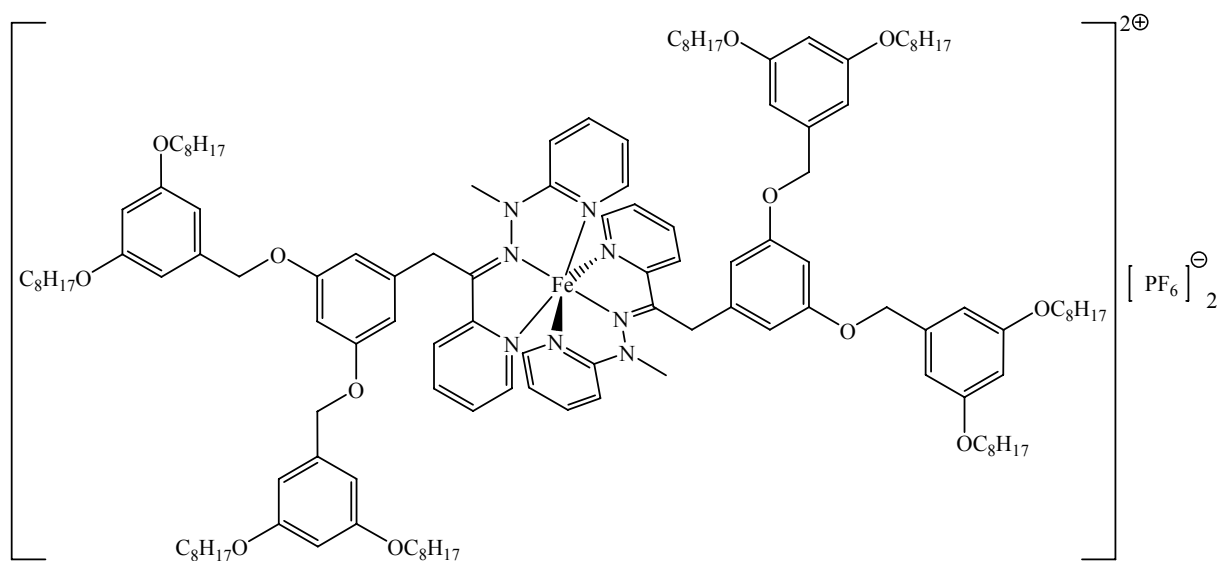


Fig. 5.6.4.10 Structure of (33)

A variation on the structure of (26) is seen in compound (33). Although very similar, some differences between the compounds were observed like the hindered rotation around the bond between the ligand backbone and the dendritic part for (26) (see chapter 4).

The obtained isotherm is quite different to the one of compound (26), although the mean molecular area was expected to be similar. Comparison of the isotherms of (26) (fig. 5.6.4.7) and (33) (fig. 5.6.4.11) reveal that they are quite similar but also show some differences. The most interesting fact is that the first phase transition point for (26) is at about 198 \AA^2 while (33) shows that transition at about 183 \AA^2 . For two so similar compounds, this is a significant difference.

The behaviour after the first phase transition is also different. Compound (33) shows after the first phase transition no other clear defined point while (26) shows two other inflections in the isotherm. Since no other inflections are observable, an estimation of the mean molecular area is more difficult to obtain.

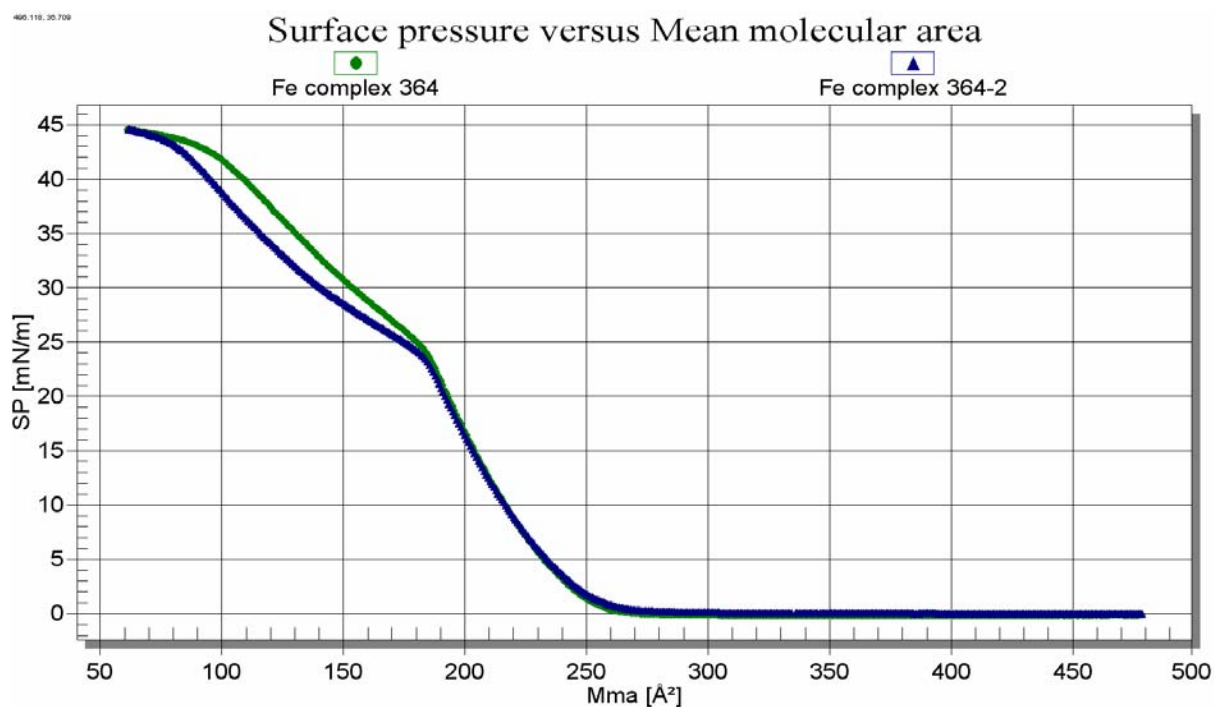


Fig. 5.6.4.11 Isotherm of compound (33)

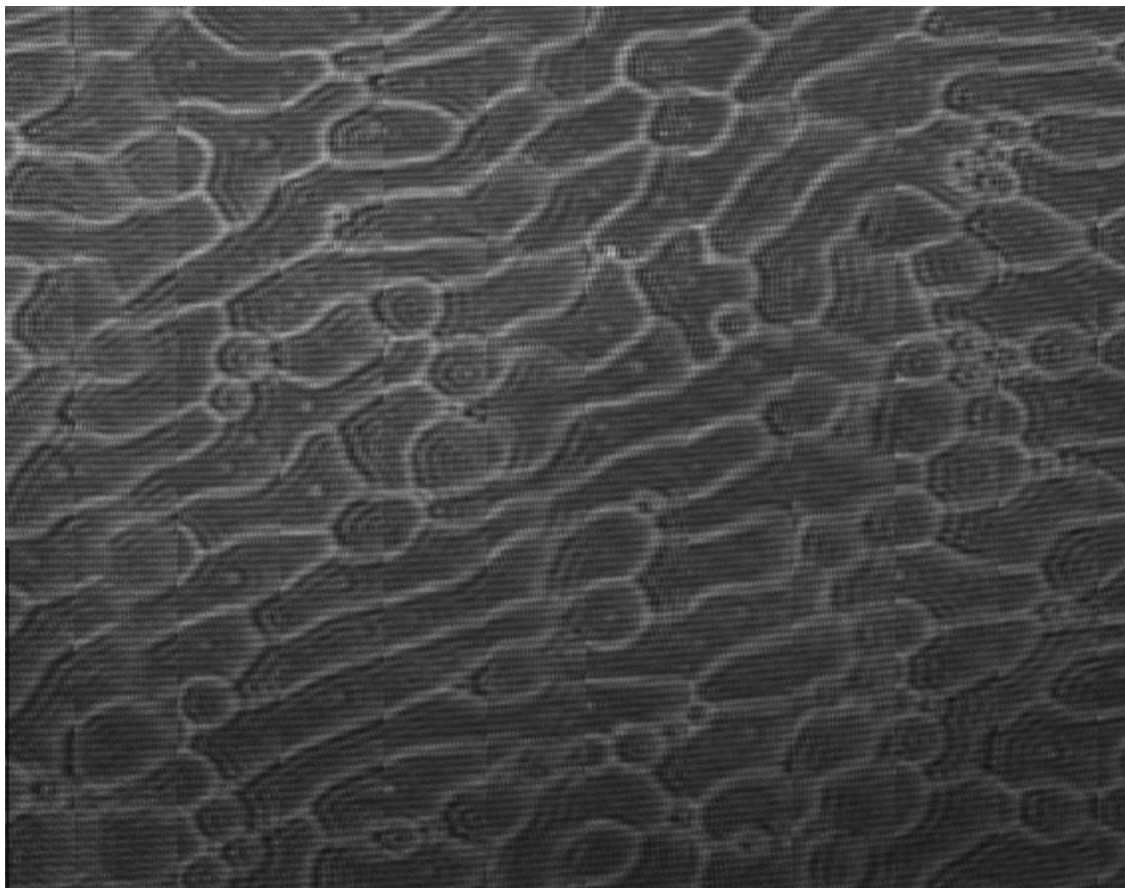


Fig. 5.6.4.12 BAM picture of (33) at 0 surface pressure

5.6.5 LB deposition

Compound **(33)** was selected for a deposition experiment on graphite for further analysis by STM. This was done due to the more regular isotherm of the compound.

Two possible deposition methods were available, LB upstroke or LB downstroke. For the downstroke the plate begins above the subphase and is slowly lowered through the monolayer into the subphase, for the upstroke it is the other way round. The upstroke method was selected to not disturb the deposited monolayer by the subphase. For both cases it is important that the plate is only pulled once through the monolayer to prevent the deposition of dual or multilayers on the plate.

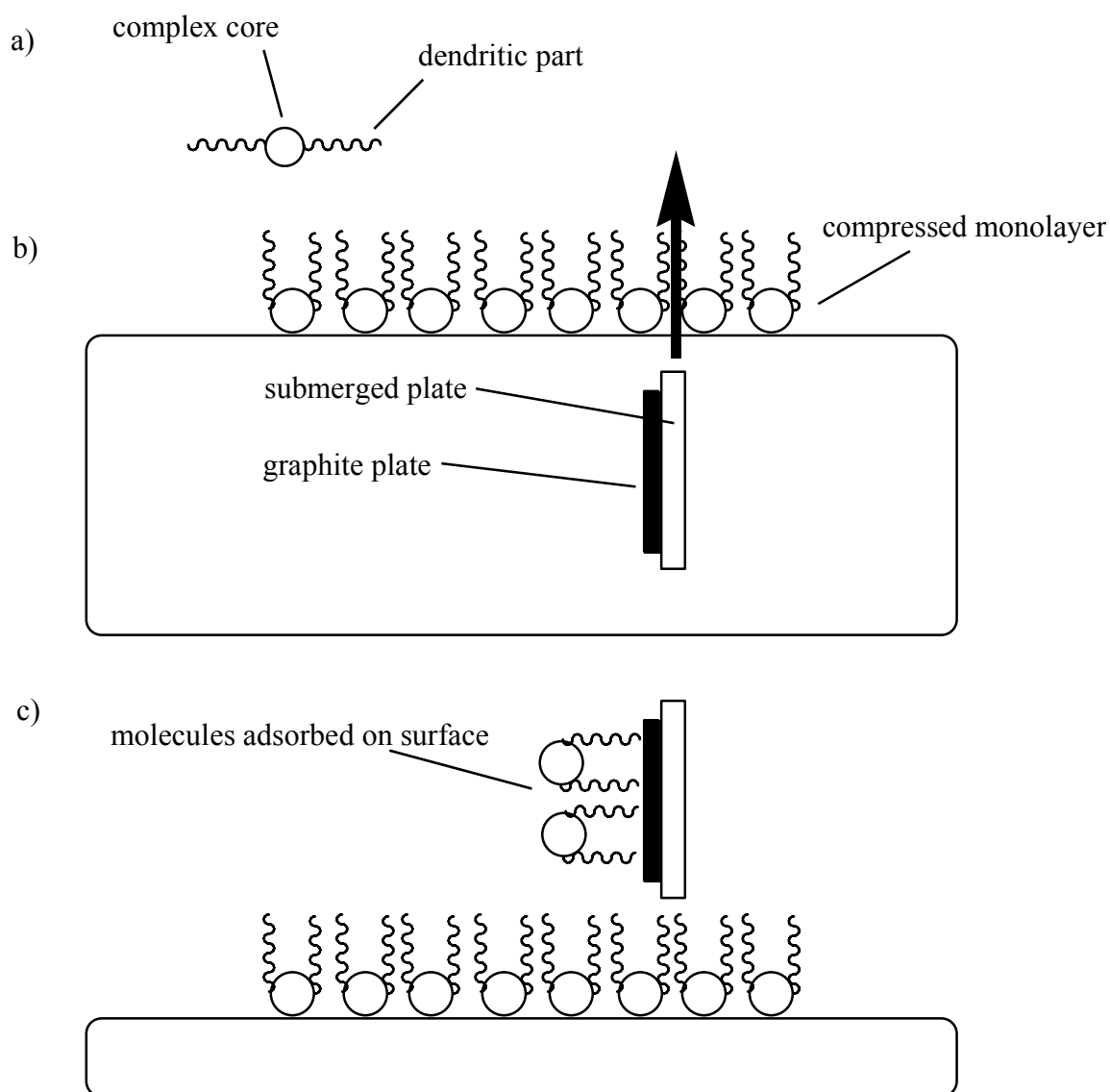


Fig. 5.6.5.1 Schematic representation of the LB upstroke deposition method. a) schematic representation of (33). b) before the deposition experiment c) after

The deposition was conducted in the LB upstroke method on a HOPG plate (fig. 5.6.5.1). The monolayer was compressed to 22 mN/m and the barriers were stopped. After a stabilisation period of 15 minutes the plate was slowly raised above the subphase with the speed of 0.5 mm/min.

The plate was then directly measured by STM.

5.6.6 STM Measurements

Pictures of an ordered monolayer of (33) were obtained. The pictures are not high enough resolved to allow for structural analysis. This is not very surprising due to the structure of the compound as well as the deposition method. If the assumption is correct that the paphy complex core is oriented to the water subphase and the dendritic parts aligned along each other then the deposition on the surface should expose the dendritic core with the dendritic parts below it (see fig. 5.6.5.1).

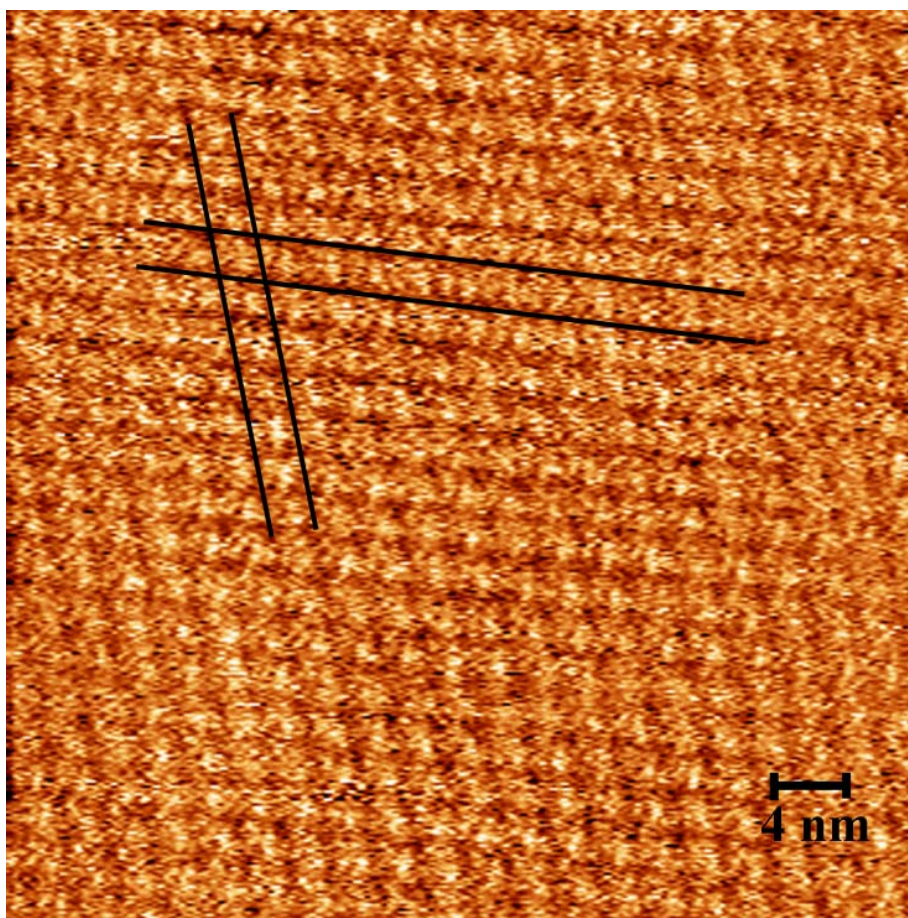


Fig. 5.6.6.1 STM Picture of LB deposited monolayer of (33) (50x50 nm)

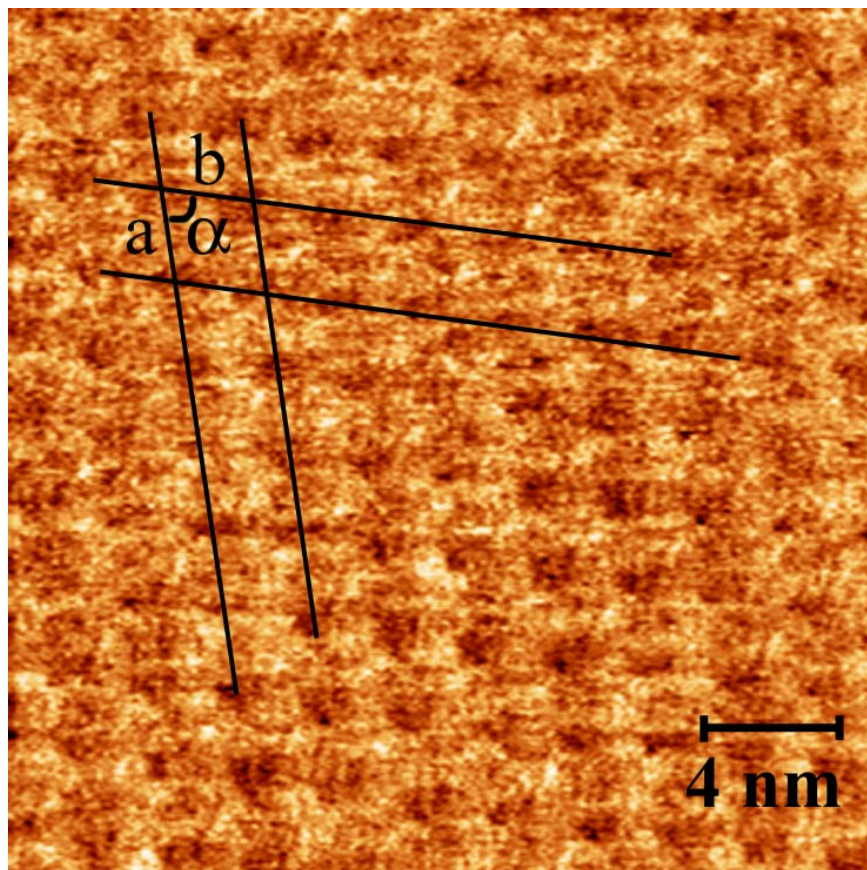


Fig. 5.6.6.2 STM Picture of LB deposited monolayer of (33) (25x25 nm)

The unit cell is marked in fig. 5.6.6.1 and 5.6.6.2. The dimensions are 2.52 by 2.40 nm with the angle α 73.6°. The tentatively assigned plane group is P-1 but this is very questionable since there are actually two different enantiomers that compound (33) is composed of (see chapter 4).

a	2.40
b	2.52
α	73.6°

Fig. 5.6.6.1 Table for the unit cell data of (33)

The size calculation for the dimensions of the complex core give a diameter of about 860 pm for the top view as shown in fig. 5.6.6.3. It was assumed that the imine carbons with the dendritic wedges are closer to the surface. This model is represented in fig. 5.6.6.4.

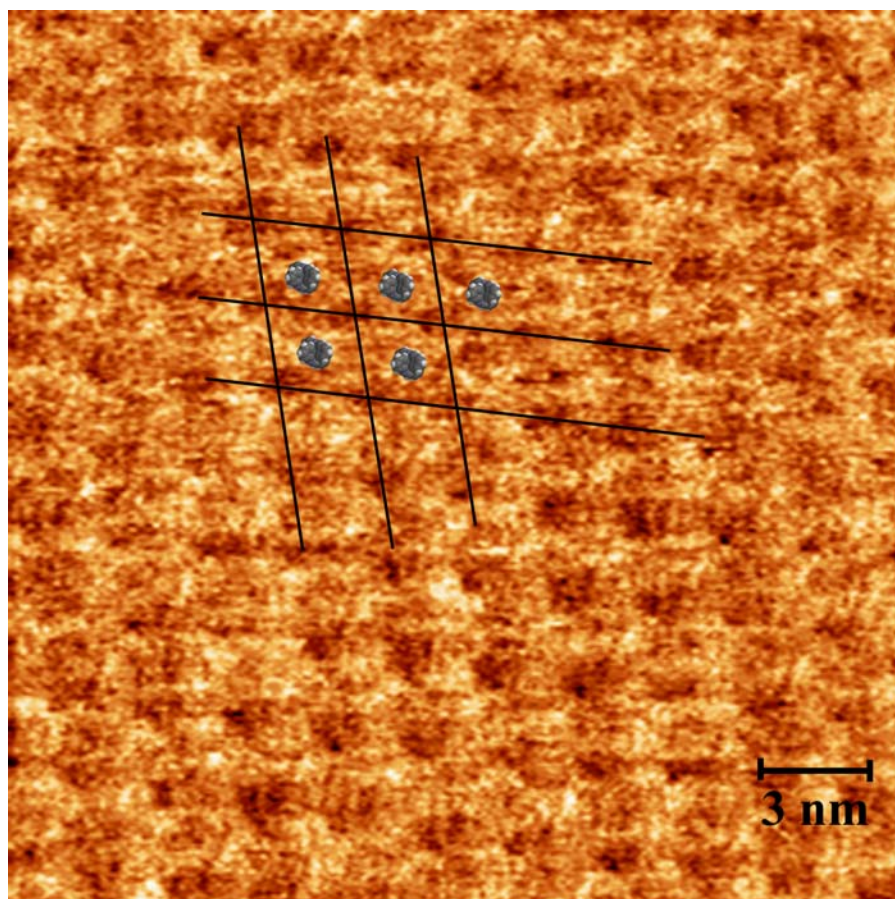


Fig. 5.6.6.3 STM picture of the monolayer of (33) (25x25 nm). The complex core fitted to the bright centres.

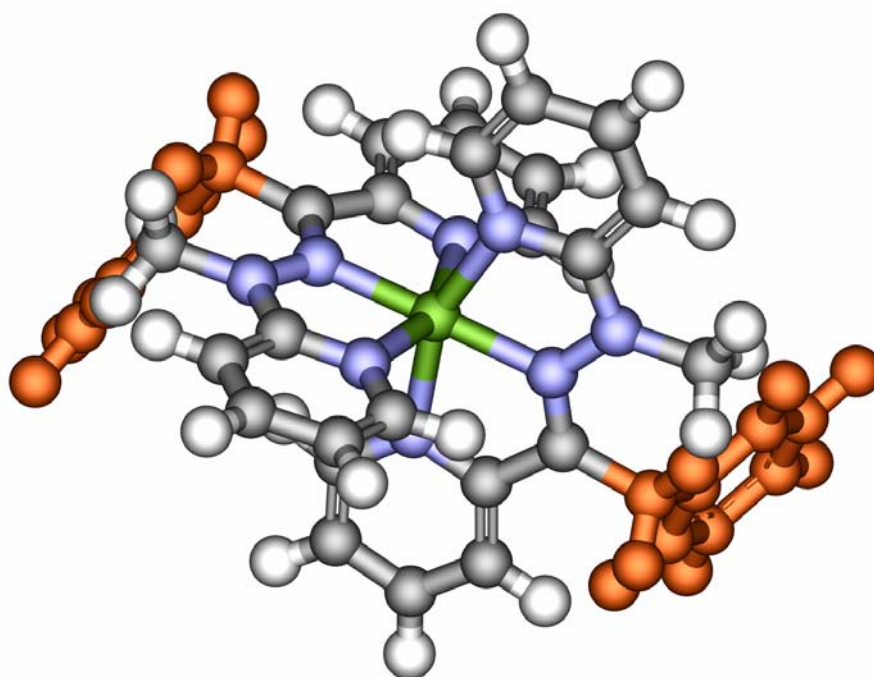


Fig. 5.6.6.4 Model of the complex core of (33) shown with the central aromatic ring of the dendritic wedge (shown in orange)

The size of the complex core fits well with the bright spots in the STM image. Of the exact alignment of the anchoring dendritic wedges no definite comments can be made. This has also the consequence that the exact rotation of the complex core on the substrate is unknown.

5.7 Conclusions

STM is a proven method for obtaining structural information on the molecular and even sub molecular level. In excellent condition even atomic resolution is possible. Very good results can be achieved by permanently adsorbing the compounds on the substrate. As pointed out previously, for this work a different setup was selected. By using HOPG and compounds modified with long alkyl chains, an intentionally relatively weak analyte-substrate interaction was selected. The argument for this is that the weak interaction would allow defects in the monolayer to fix themselves by desorption and re-adsorption. A disadvantage of weakly interacting systems is that thermal motion might lead to a gas-like monolayer. Besides the thermal movement the electric field of the STM tip might push the molecules away.

The ability to form ordered monolayers is directly associated with the complexity of the structure of the compound. This principle is demonstrated in this work by the inability of several compounds to form observable monolayers in HOPG. The ability of very similar but simpler structures to form monolayers is amply demonstrated; these compounds are even in many cases precursors to the compounds in this work. It was concluded that the structures are too complex to form monolayers by themselves. So an alternate system was required to help the formation of monolayers along. LB methods were selected and are showing promising results. A conducted deposition experiment gave an observable monolayer that was analysed by STM.

In conclusion it can be said the usually applied methods of solution casting and measurements at the liquid-solid interface have their limitations of what is possible with the formation of monolayers. By extending the methods with LB techniques new possibilities open up.

5.8 References

- (1) Binning, G.; Rohrer, H.; Gerber, C.; Weibel, E. *Phys. Rev. Lett.* **1982**, *49*, 57-61.
- (2) Binnig, G.; Rohrer, H. *Reviews of Modern Physics* **1987**, *59*, 615-625.
- (3) Kroger, J.; Neel, N.; Limot, L. *J. Phys.: Condens. Matter* **2008**, *20*, -.
- (4) Grill, L. *J. Phys.: Condens. Matter* **2008**, *20*, 1-19.
- (5) Johannes, A. A. W. E.; Shengbin, L.; Steven, De F. *Angew. Chem., Int. Ed.* **2009**, *48*, 7298-7332.
- (6) Samori, P. *Scanning probe microscopies beyond imaging manipulation of molecules and nanostructures*; WILEY-VCH: Weinheim, 2006.
- (7) Blanco, J. M.; Flores, F.; Perez, R. *Prog. Surf. Sci.* **2006**, *81*, 403-443.
- (8) Claypool, C. L.; Faglioni, F.; Goddard, W. A.; Gray, H. B.; Lewis, N. S.; Marcus, R. A. *J. Phys. Chem. B* **1997**, *101*, 5978-5995.
- (9) Faglioni, F.; Claypool, C. L.; Lewis, N. S.; Goddard, W. A. *J. Phys. Chem. B* **1997**, *101*, 5996-6020.
- (10) Cyr, D. M.; Venkataraman, B.; Flynn, G. W. *Chem. Mater.* **1996**, *8*, 1600-1615.
- (11) De Feyter, S.; De Schryver, F. C. *J. Phys. Chem. B* **2005**, *109*, 4290-4302.
- (12) Scherer, L. J.; Merz, L.; Constable, E. C.; Housecroft, C. E.; Neuburger, M.; Hermann, B. A. *J. Am. Chem. Soc.* **2005**, *127*, 4033-4041.
- (13) De Feyter, S.; Gesquiere, A.; Abdel-Mottaleb, M. M.; Grim, P. C. M.; De Schryver, F. C.; Meiners, C.; Sieffert, M.; Valiyaveetil, S.; Mullen, K. *Acc. Chem. Res.* **2000**, *33*, 520-531.
- (14) Scherer, L. J. *Ph. D. Thesis*, University of Basel, **2006**.
- (15) *International Tables for Crystallography*; 4th ed., 1995; Vol. A - Spacegroup Symmetry
- (16) Talham, D. R.; Yamamoto, T.; Meisel, M. W. *J. Phys.: Condens. Matter* **2008**, *20*.
- (17) *KSV 2000 Instruction Manual*; KSV instruments Ltd: Helsinki, Finland, 2001.
- (18) Petty, M. C. *Langmuir-Blodgett films - An introduction*; Cambridge University Press, 1996.

6. Conclusions

The syntheses of the functional dendritic wedges are reliable and efficient up to the second generation. With the numerous functional group modifications available many different reactions can be conducted making the wedges very versatile. Interestingly, despite their increased complexity the **G2** derivatives of the wedges are often solid at room temperature, allowing them to be crystallized. Two new crystal structures of **G2** derivatives could be obtained, one being of the **G2** amine (**16**) which was a new structure and the second of **G2** aldehyde (**14**), of which a new polymorph was found through a change in crystallization conditions.

The modifications of the paphy ligand were successfully conducted. Two different modifications were achieved on the backbone of paphy. Strategies were developed allowing the different modifications to be made at different stages of the synthesis allowing, for selective synthesis.

The properties of the paphy ligand and its iron(II) complexes were examined, mainly with UV-vis spectroscopy. The iron complexes of paphy show a drastically increased acidity of the amine proton on the ligand backbone. Deprotonation and protonation are accompanied by a strong colour change. This was examined in titration experiments.

The paphy ligands modified with dendritic wedges and the iron complexes were tested for monolayer formation and subsequent STM analysis. For the free ligand small patches of monolayers were obtained but careful analysis led to the conclusion that these molecules are not lying flat on the surface, making only the dendritic wedge visible under STM. For the iron(II) complexes neither solution casting nor keeping the analyte in solution yielded monolayers on HOPG.

Langmuir-Blodgett (LB) methods were examined as an alternative for monolayer formation. The iron(II) complexes behaved more irregularly than expected, showing only at the beginning of the measurements a reproducible behaviour. Compound (**33**) showed the most regular behaviour and was therefore selected for a LB deposition experiment. After a LB upstroke deposition experiment, a monolayer could be observed under STM. An analysis of the data lead again to the belief that the monolayer was not lying flat on the surface, a fact not really surprising considering the steric demand of the complex centre and the LB method used for the monolayer formation. Nonetheless the LB method offers a valuable alternative in the monolayer formation for steric difficult systems.

Appendix – Crystallographic Data

Crystal Data and Details of the Structure Determination for
Methyl 3,5-bis(octyloxy)benzoate
 $P 21/n$ $R = 0.04$

Crystal Data

Formula	$C_{24}H_{40}O_4$
Formula Weight	392.58
Crystal System	Monoclinic
Space group	$P 21/n$ (No. 14)
a, b, c [Å]	5.3715(1) 18.5310(4) 23.0801(4)
α, β, γ [°]	90 95.6726(12) 90
V [Å ³]	2286.13(8)
Z	4
D(calc) [g/cm ³]	1.141
Mu(Mo K_{α}) [/mm]	0.075
F(000)	864
Crystal Size [mm]	0.11 x 0.22 x 0.32

Data Collection

Temperature (K)	173
Radiation [Å]	Mo K_{α} 0.71073
Theta Min-Max [°]	1.4, 27.5
Dataset	-6: 6 ; -24: 24 ; -29: 29
Tot., Uniq. Data, R(int)	19344, 5211, 0.029
Observed data [I > 2.0 sigma(I)]	2674

Refinement

N_{ref}, N_{par}	2674, 253
R, wR2, S	0.0432, 0.0656, 1.00
$w = (MAX(F_0^2, 0) + 2F_C^2)/3$	
Max. and Av. Shift/Error	0.00, 0.00
Min. and Max. Resd. Dens. [e/ Å ³]	-0.20, 0.24

Bond Distances [Å]

O1	C1	1.204(3)
O2	C1	1.333(2)
O2	C2	1.441(2)
O3	C5	1.367(2)
O3	C9	1.438(2)
O4	C7	1.371(2)
O4	C17	1.435(2)
C1	C3	1.497(3)
C3	C4	1.394(3)
C3	C8	1.390(3)
C4	C5	1.392(3)
C5	C6	1.386(3)
C6	C7	1.393(2)
C7	C8	1.392(3)
C9	C10	1.506(3)
C10	C11	1.522(2)
C11	C12	1.520(3)
C12	C13	1.527(3)
C13	C14	1.520(3)
C14	C15	1.521(3)
C15	C16	1.520(3)
C17	C18	1.509(3)
C18	C19	1.525(3)
C19	C20	1.526(3)
C20	C21	1.521(3)
C21	C22	1.527(3)
C22	C23	1.512(3)
C23	C24	1.521(3)

Bond Angles [°]

C1	O2	C2	116.83(15)
C5	O3	C9	118.03(14)
C7	O4	C17	117.87(14)
O1	C1	O2	123.77(17)
O1	C1	C3	124.03(19)
O2	C1	C3	112.20(17)
C1	C3	C4	120.58(18)
C1	C3	C8	117.43(18)
C4	C3	C8	121.99(17)
C3	C4	C5	118.34(18)
O3	C5	C4	124.08(18)
O3	C5	C6	115.27(16)
C4	C5	C6	120.64(18)
C5	C6	C7	120.12(17)
O4	C7	C6	115.25(16)
O4	C7	C8	124.42(16)
C6	C7	C8	120.33(17)
C3	C8	C7	118.57(18)
O3	C9	C10	107.73(14)
C9	C10	C11	112.14(15)
C10	C11	C12	112.76(15)
C11	C12	C13	113.56(15)
C12	C13	C14	113.69(16)
C13	C14	C15	113.77(17)
C14	C15	C16	112.80(17)
O4	C17	C18	107.59(15)
C17	C18	C19	111.79(16)
C18	C19	C20	113.50(16)
C19	C20	C21	113.34(16)
C20	C21	C22	114.21(17)
C21	C22	C23	112.99(17)
C22	C23	C24	113.26(18)

Crystal Data and Details of the Structure Determination for
 3,5-Bis(3,5-dioctyloxybenzyloxy)benzaldehyde (Polymorph 2)
P-1 *R* = 0.07

Crystal Data

Formula	C ₅₃ H ₈₂ O ₇
Formula Weight	831.23
Crystal System	Triclinic
Space group	<i>P</i> -1 (No. 2)
a, b, c [Å]	10.3926(5) 16.1928(8) 16.3589(7)
α, β, γ [°]	103.076(2) 102.323(2) 103.409(3)
V [Å ³]	2503.7(2)
Z	2
D(calc) [g/cm ³]	1.103
Mu(Mo K _α) [/mm]	0.071
F(000)	912
Crystal Size [mm]	0.07 x 0.11 x 0.23

Data Collection

Temperature (K)	223
Radiation [Å]	Mo K _α 0.71073
Theta Min-Max [°]	1.6, 29.6
Dataset	-14: 14 ; -22: 22 ; -22: 22
Tot., Uniq. Data, R(int)	67547, 14037, 0.033
Observed data [I > 0.0 sigma(I)]	9686

Refinement

N _{ref} , N _{par}	7646, 614
R, wR2, S	0.0745, 0.1574, 1.18
w = 0.120 0.326E-01	
Max. and Av. Shift/Error	0.00, 0.00
Min. and Max. Resd. Dens. [e/ Å ³]	-0.23, 0.31

Bond Distances [Å]

O1	C1	1.121(4)	C13	C14	1.379(3)
O2	C1	1.065(6)	C15	C16	1.511(3)
O3	C8	1.423(2)	C16	C17	1.372(3)
O3	C4	1.369(2)	C16	C21	1.393(3)
O4	C15	1.422(2)	C17	C18	1.405(3)
O4	C6	1.368(3)	C18	C19	1.367(3)
O5	C22	1.428(2)	C19	C20	1.392(3)
O5	C11	1.368(2)	C20	C21	1.383(3)
O6	C13	1.370(2)	C22	C23	1.505(3)
O6	C30	1.425(3)	C23	C24	1.522(3)
O7	C18	1.369(2)	C24	C25	1.516(3)
O7	C38	1.431(3)	C25	C26	1.523(3)
O8	C46	1.449(3)	C26	C27	1.516(3)
O8	C56	1.461(8)	C27	C28	1.520(3)
O8	C20	1.364(3)	C28	C29	1.515(4)
C1	C2	1.475(3)	C30	C31	1.514(3)
C2	C7	1.389(3)	C31	C32	1.513(3)
C2	C3	1.388(3)	C32	C33	1.533(3)
C3	C4	1.386(3)	C33	C34	1.513(3)
C4	C5	1.384(3)	C34	C35	1.519(3)
C5	C6	1.380(3)	C35	C36	1.515(3)
C6	C7	1.385(3)	C36	C37	1.518(3)
C8	C9	1.506(3)	C38	C39	1.506(3)
C9	C10	1.378(3)	C39	C40	1.522(3)
C9	C14	1.400(3)	C40	C41	1.517(3)
C10	C11	1.389(3)	C41	C42	1.512(3)
C11	C12	1.380(3)	C42	C43	1.516(3)
C12	C13	1.389(3)	C43	C44	1.513(4)
C44	C45	1.507(4)			
C46	C47	1.490(5)			
C47	C48	1.507(7)			
C48	C49	1.506(8)			
C49	C50	1.434(11)			
C50	C51	1.466(9)			
C51	C52	1.413(10)			
C52	C53	1.406(8)			
C53	C62	1.449(11)			
C56	C57	1.491(10)			
C57	C58	1.459(11)			
C58	C59	1.498(16)			
C59	C60	1.446(13)			
C60	C61	1.478(13)			
C61	C62	1.476(15)			

Bond Angles [°]

C4	O3	C8	117.04(14)	C10	C11	C12	120.34(19)
C6	O4	C15	118.10(15)	C11	C12	C13	118.92(18)
C11	O5	C22	117.53(15)	O6	C13	C12	113.11(17)
C13	O6	C30	120.69(16)	O6	C13	C14	124.93(19)
C18	O7	C38	116.53(16)	C12	C13	C14	121.96(18)
C20	O8	C46	118.8(2)	C9	C14	C13	118.16(19)
C20	O8	C56	115.8(3)	O4	C15	C16	108.82(15)
O1	C1	C2	131.0(3)	C15	C16	C17	121.37(18)
O2	C1	C2	132.3(3)	C15	C16	C21	117.59(17)
C1	C2	C3	119.0(2)	C17	C16	C21	121.03(19)
C1	C2	C7	119.11(19)	C16	C17	C18	119.00(19)
C3	C2	C7	121.85(18)	O7	C18	C17	115.34(17)
C2	C3	C4	118.99(19)	O7	C18	C19	123.94(19)
O3	C4	C3	124.79(18)	C17	C18	C19	120.72(18)
O3	C4	C5	115.48(16)	C18	C19	C20	119.48(19)
C3	C4	C5	119.73(17)	O8	C20	C19	114.15(19)
C4	C5	C6	120.55(18)	O8	C20	C21	125.06(18)
O4	C6	C5	114.57(17)	C19	C20	C21	120.78(19)
O4	C6	C7	124.62(18)	C16	C21	C20	118.98(18)
C5	C6	C7	120.80(19)	O5	C22	C23	108.15(15)
C2	C7	C6	118.07(18)	C22	C23	C24	111.23(16)
O3	C8	C9	109.65(15)	C23	C24	C25	113.78(16)
C8	C9	C10	116.92(17)	C24	C25	C26	112.67(16)
C8	C9	C14	122.47(18)	C25	C26	C27	113.71(16)
C10	C9	C14	120.61(18)	C26	C27	C28	113.75(17)
C9	C10	C11	120.03(18)	C27	C28	C29	112.86(19)
O5	C11	C10	115.77(17)	O6	C30	C31	104.70(16)
O5	C11	C12	123.90(17)	C30	C31	C32	115.36(18)
C31	C32	C33	110.92(18)	C43	C44	C45	112.9(2)
C32	C33	C34	114.75(18)	O8	C46	C47	109.3(3)
C33	C34	C35	112.50(18)	C46	C47	C48	118.3(4)
C34	C35	C36	114.07(19)	C47	C48	C49	113.5(5)
C35	C36	C37	112.7(2)	C48	C49	C50	121.6(6)
O7	C38	C39	109.19(17)	C49	C50	C51	115.6(6)
C38	C39	C40	109.88(17)	C50	C51	C52	123.3(6)
C39	C40	C41	113.92(18)	C51	C52	C53	116.2(6)
C40	C41	C42	112.20(18)	O8	C56	C57	108.6(5)
C41	C42	C43	113.70(18)	C56	C57	C58	113.6(6)
C42	C43	C44	112.14(19)	C57	C58	C59	116.3(9)
C58	C59	C60	113.3(8)	C59	C60	C61	121.8(8)
C60	C61	C62	107.8(8)				

Crystal Data and Details of the Structure Determination
 3,5-Bis(3,5-dioctyloxybenzyloxy)benzylamine
P-1 R = 0.06

Crystal Data

Formula	C ₅₃ H ₈₅ NO ₆
Formula Weight	832.26
Crystal System	Triclinic
Space group	<i>P</i> -1 (No. 2)
a, b, c [Å]	10.3597(4) 15.6450(5) 16.5620(7)
α, β, γ [°]	99.984(2) 103.5202(19) 101.540(2)
V [Å ³]	2487.96(17)
Z	2
D(calc) [g/cm ³]	1.111
Mu(Mo K _α) [/mm]	0.071
F(000)	916
Crystal Size [mm]	0.06 x 0.14 x 0.48

Data Collection

Temperature (K)	173
Radiation [Å]	Mo K _α 0.71073
Theta Min-Max [°]	1.4, 27.5
Dataset	-13: 13 ; -20: 20 ; -21: 21
Tot., Uniq. Data, R(int)	21917, 11397, 0.021
Observed data [I > 2.0 sigma(I)]	4912

Refinement

N _{ref} , N _{par}	5886, 541
R, wR2, S	0.0605, 0.1162, 1.10
w = .75	1.03
Max. and Av. Shift/Error	0.00, 0.00
Min. and Max. Resd. Dens. [e/Å ³]	-0.31, 0.55

Bond Distances [Å]

O1	C3	1.371(3)	C18	C19	1.384(3)
O1	C8	1.429(3)	C19	C20	1.394(3)
O2	C5	1.378(3)	C20	C21	1.385(3)
O2	C15	1.422(3)	C22	C23	1.507(4)
O3	C11	1.371(3)	C23	C24	1.514(4)
O3	C22	1.426(3)	C24	C25	1.517(3)
O4	C13	1.372(3)	C25	C26	1.525(4)
O4	C30	1.424(4)	C26	C27	1.519(4)
O5	C18	1.369(3)	C27	C28	1.513(4)
O5	C38	1.436(4)	C28	C29	1.520(5)
O6	C20	1.364(3)	C30	C31	1.510(4)
O6	C46	1.429(4)	C31	C32	1.523(5)
N1	C7	1.397(4)	C32	C33	1.527(4)
C1	C7	1.521(4)	C33	C34	1.515(4)
C1	C2	1.394(3)	C34	C35	1.522(4)
C1	C6	1.392(3)	C35	C36	1.522(4)
C2	C3	1.383(3)	C36	C37	1.515(4)
C3	C4	1.390(3)	C38	C39	1.519(4)
C4	C5	1.379(3)	C39	C40	1.521(4)
C5	C6	1.383(3)	C40	C41	1.531(4)
C8	C9	1.516(4)	C41	C42	1.529(4)
C9	C10	1.384(3)	C42	C43	1.520(4)
C9	C14	1.390(3)	C43	C44	1.554(5)
C10	C11	1.394(3)	C44	C45	1.438(6)
C11	C12	1.388(3)	C46	C47	1.518(4)
C12	C13	1.386(4)	C47	C48	1.515(4)
C13	C14	1.387(4)	C48	C49	1.524(4)
C15	C16	1.512(3)	C49	C50	1.521(6)
C16	C17	1.379(3)	C50	C51	1.490(6)
C16	C21	1.398(3)	C51	C52	1.516(7)
C17	C18	1.404(3)	C52	C53	1.516(7)

Bond Angles [°]

C3	O1	C8	116.93(19)	C17	C16	C21	120.8(2)
C5	O2	C15	117.14(19)	C16	C17	C18	119.2(2)
C11	O3	C22	116.79(19)	O5	C18	C19	123.6(2)
C13	O4	C30	119.3(2)	O5	C18	C17	115.8(2)
C18	O5	C38	116.57(19)	C17	C18	C19	120.6(2)
C20	O6	C46	118.0(2)	C18	C19	C20	119.5(2)
H1	N1	H2	98.00	O6	C20	C19	114.3(2)
C7	N1	H1	117.00	C19	C20	C21	120.5(2)
C7	N1	H2	117.00	O6	C20	C21	125.2(2)
C2	C1	C6	119.8(2)	C16	C21	C20	119.4(2)
C2	C1	C7	117.8(2)	O3	C22	C23	109.4(2)
C6	C1	C7	122.5(2)	C22	C23	C24	110.9(2)
C1	C2	C3	119.6(2)	C23	C24	C25	114.5(2)
C2	C3	C4	120.6(2)	C24	C25	C26	111.9(2)
O1	C3	C4	115.4(2)	C25	C26	C27	115.5(2)
O1	C3	C2	124.0(2)	C26	C27	C28	113.1(2)
C3	C4	C5	119.6(2)	C27	C28	C29	113.9(3)
C4	C5	C6	120.5(2)	O4	C30	C31	105.2(2)
O2	C5	C6	124.5(2)	C30	C31	C32	114.6(3)
O2	C5	C4	115.0(2)	C31	C32	C33	110.8(3)
C1	C6	C5	120.0(2)	C32	C33	C34	114.5(2)
N1	C7	C1	121.0(3)	C33	C34	C35	111.6(2)
O1	C8	C9	108.84(19)	C34	C35	C36	114.3(2)
C10	C9	C14	121.6(2)	C35	C36	C37	112.2(2)
C8	C9	C10	116.6(2)	O5	C38	C39	107.8(2)
C8	C9	C14	121.7(2)	C38	C39	C40	111.2(2)
C9	C10	C11	119.1(2)	C39	C40	C41	111.9(2)
O3	C11	C10	116.1(2)	C40	C41	C42	113.4(2)
O3	C11	C12	123.4(2)	C41	C42	C43	112.7(2)
C10	C11	C12	120.5(2)	C42	C43	C44	113.8(3)
C11	C12	C13	119.0(2)	C43	C44	C45	114.3(3)
C12	C13	C14	121.8(2)	O6	C46	C47	107.6(2)
O4	C13	C14	124.6(3)	C46	C47	C48	113.4(2)
O4	C13	C12	113.6(2)	C47	C48	C49	114.6(3)
C9	C14	C13	118.0(2)	C48	C49	C50	112.5(3)
O2	C15	C16	110.1(2)	C49	C50	C51	116.8(4)
C15	C16	C17	122.6(2)	C50	C51	C52	113.4(4)
C15	C16	C21	116.6(2)	C51	C52	C53	116.7(4)

Curriculum Vitae

Vorname, Name : Marc Häusler
Email : marc.haeusler@stud.unibas.ch
Zivilstand : ledig

Studium

Okt. 2000 - Mär. 2005 Diplomstudium der Chemie an der Universität Basel;
Abschluss mit Diplom Mär. 2005

Diplomarbeit : "Metallomacrocycles based on
Bis(2,2':6',2"-terpyridine)-D-threitol ligands"
bei Prof. Dr. E. C. Constable

Wahlfach : Informatik

Dez. 2005 Beginn der Doktorarbeit unter Prof. Dr. E. C. Constable

Berufserfahrung

Juli – Nov. 2005 Praktikum bei Novartis in der Abteilung von M. Mutz

Schulbildung

Jul.1995 - Dez. 1999 Gymnasium Münchenstein BL, Typus C
Feb. 2000 - Jul. 2000 Sprachaufenthalt in Australien; Besuch des TAFE
International Education Centre in Liverpool; Abschluss mit
Certificate III in English for TAFE

Sprachkenntnisse

Deutsch : Muttersprache
Englisch : Fliessend in Wort und Schrift
Französisch : Kenntnisse in Wort und Schrift

Publikationen

(1) Constable, E. C.; Haeusler, M.; Hermann, B. A.; Housecroft, C. E.; Neuburger, M.; Schaffner, S.; Scherer, L. J. *CrystEngComm* **2007**, 9, 176-180.